## Title

Mechanistic Studies of Silsesquioxane Silanol Organocatalysis and Development of Carbene Insertion into Si–H Bonds for Silicon-Stereogenic Silanes and Functionalized Silsesquioxanes



## Author

Jagannathan, Jake Ravi

## Publication Date

2021

Peer reviewed|Thesis/dissertation

# Mechanistic Studies of Silsesquioxane Silanol Organocatalysis and Development of Carbene Insertion into Si–H Bonds for Silicon-Stereogenic Silanes and Functionalized Silsesquioxanes

By

JAKE RAVI JAGANNATHAN

DISSERTATION

Submitted in partial satisfaction of the requirements for the degree of

DOCTOR OF PHILOSOPHY

in

CHEMISTRY

in the

OFFICE OF GRADUATE STUDIES

of the

UNIVERSITY OF CALIFORNIA

DAVIS

Approved:

_____

Annaliese K. Franz (Chair)

_____

Mark J. Mascal

_____

Dean J. Tantillo

## Table of Contents

**Acknowledgements**

I want first to thank my family. My mom and two brothers, Robby and Zach, have always been there for me, pushed me to follow my passion ever since I was little, and for the occasional reality check when I get lost. I would not have been able to accomplish all that I have without your constant love and support. Matt, thank you for coming into all our lives and brightening our days with amazing food and nothing but love. Linda, you've been my second mom ever since I was little and your love is inspiring. I truly am privileged to have such beautiful people in my life.

I want to thank my Ph.D. advisor, Dr. Annaliese K. Franz. I realized I didn't know chemistry until I joined your lab. Your enthusiasm and energy day in and day out inspired me to improve as a scientist and as an individual. Thank you for hours, if not days, of discussion, career advice, and the occasional reality check. I've learned so many lessons beyond chemistry that I will take into the next step of my career and feel confident in my success. I would also like to thank my undergraduate advisor, Dr. James Fletcher, for his training and guidance at Creighton University, which inspired me to pursue my Ph.D. Also, I'd like to thank Dr. Bradley Parsons at Creighton University for being a fantastic professor and mentor.

I want to thank my dissertation committee, Professor Dean Tantillo and Professor Mark Mascal, for the helpful discussion. Thank you to Dr. Jim Fettinger for your assistance with X-ray analysis and useful discussion. Thank you to Dr. Jeff Walton and Dr. Ping Yu for helpful with NMR spectroscopy. Thank you to Dr. William Jewel for all the help with mass spectrometry over the years.

I want to thank the entire Franz lab, past and present, for constant support. It was fun to share in accomplishments, complain about the hard times, and help each other improve as scientists. A special thank you to Dr. Kayla Diemoz for teaching me kinetics and how to get them zults. Brittney, thanks for being a great safety officer and an awesome source of annulation information. Julia, your NMR expertise was a godsend, and your passion to mentor undergraduates was inspiring. Thank you to Jacob Dalton for always having time to talk about chiral silicon. Linnea, thank you for all the times I would bug you about hydrosilylations. Thank you to Yun-Pu and Teresa for being outstanding members of the X-team. I've had the privilege of working with gifted undergraduates Karina Targos, Nadia Hirbawi, Shaoming Sun, and Jonah Brown, and I am

grateful for the experiences. Thank you to Andrew Burch for introducing me to Tour de Davis and Cody for being a constant source of joy and excitement.

A big thank you goes to Angel Cobo for not only being one of my best friends in graduate school but in life. I loved the hours of discussion about research, complaining about how hard it is and what we want to do when we're done. We survived a pandemic, and I would not have been able to do it without you. Another big thank you to Austin Kelly for not only being a great mentor but also a friend. You invited me into your family, and now I'm the Godfatha (*cotton in the mouth*). Your wife Kate is an absolute delight and one of the kindest people I've ever met.

I've made some incredible friends here in graduate school that have been a constant source of support. Savannah, thank you for always being there for me even when I wasn't there for myself. You are a fantastic friend. Rob, thanks for being an amazing roommate and source of awesome music to groove to. Leo, thanks for being one of the chilliest roommates ever and teaching me inorganic chemistry. Ben, JJ, and Vanessa, thank you for being great friends and for the countless moments of laughter through the years.

I've had great friends outside of academia who have supported me throughout the entire endeavor. Eric and Bobby, thank you for hyping me up whenever I come to visit. Sabrina, your realism is at times hilarious, and your love for the Bay Area brings out mine. Elliott, thank you for teaching me how to fish and telling me what species of tree we're currently looking at. And finally, a big thank you to Karla Sison. Thank you for coming into my life and sweeping me off my feet.

**Abstract**

Organosilicon chemistry is underdeveloped and warrants focus both in synthesis and applications. This dissertation includes a mechanistic analysis of incompletely condensed polyhedral oligomeric silsesquioxane H-bond-donor catalysis in a C–C bond-forming reaction and metal-catalyzed carbene insertion to produce silicon-stereogenic silanes and silsesquioxane nano building blocks. The introduction discusses the properties and applications of silanols, previous methods to access silicon-stereogenic molecules and silsesquioxane-based materials, modern kinetic analysis methods, and carbene insertion into Si–H bonds. Previous literature examples are included for context.

Chapter one details a $^{19}F$ NMR kinetic study of silsesquioxane H-bonding catalysis in a C–C bond-forming reaction using modern kinetic analysis. A comparison of the catalytic activity to previously studied organosilanols is included. The effect of catalyst concentration on the overall mechanism of the transformation is described. Binding studies using $^{1}H$ NMR spectroscopy were used to investigate H-bonding ability and investigate the effect of concentration.

Chapter two presents the development of Rh(II)-catalyzed diarylcarbene insertion into Si–H bonds to produce silicon-stereogenic silanes. Novel prochiral silanes and diazo compounds were synthesized to investigate their effects on enantioselectivity. The effect of a prochiral diazo compound on enantioselectivity was explored. A brief mechanistic study provided insight into structural effects on diazo compound stability. Further transformations of insertion products were explored.

Chapter three describes the development of Rh(II)-catalyzed aryl(ester) carbene insertion into Si–H bonds of silsesquioxane-based silanes. Aryl(ester) and aryl(amide) diazo compounds were tested against POSSs with one, three, and eight Si–H bonds. Novel diazo compounds were synthesized containing fluorinated groups and BODIPY fluorophores. Further transformations of insertion products were explored.

**List of Symbols and Abbreviations**

| | |
|---|---|
| Å | Angstrom |
| Ar | Aryl |
| BODIPY | Borondipyrromethene |
| COE | Cyclooctene |
| CSP-HPLC | Chiral Stationary Phase High Performance Liquid Chromatography |
| D | Diffusion constant |
| DBU | 1,8-Diazabicyclo(5.4.0)undec-7-ene |
| o-DCB | 1,2-Dichlorobenzene |
| DCE | Dichloroethane |
| DMAP | 4-Dimethylaminopyridine |
| DMF | N,N-Dimethylformamide |
| DMSO | Dimethylsulfoxide |
| DOSY | Diffusion ordered spectroscopy |
| dr | Diastereomeric ratio |
| equiv | Equivalents |
| eq | Equation |
| er | Enantiomeric ratio |
| ESI-MS | Electrospray Ionization-Mass Spectrometry |
| Et | Ethyl |
| EtOAc | Ethyl acetate |
| g | Grams |
| h | Hours |
| HPLC | High Pressure Liquid Chromatography |
| HRMS | High Resolution Mass Spectrometry |
| *i*Pr | Isopropyl |
| *i*Bu | Isobutyl |
| $K_a$ | Association constant |
| $K_{dim}$ | Dimerization constant |
| $k_{obs}$ | Observed rate constant |
| $k_{rel}$ | Relative rate |

| | |
|---|---|
| ln | Natural logarithm |
| LRMS | Low Resolution Mass Spectrometry |
| MALDI | Matrix-Assisted Laser Desorption Ionization |
| M | Molar |
| Me | Methyl |
| MeOH | Methanol |
| Mes | Mesityl carboxylate |
| mg | Milligrams |
| MHz | Megahertz |
| min | Minutes |
| mL | Milliliters |
| μL | Microliters |
| mM | Millimolar |
| mmol | Millimole |
| mol | Mole |
| MS | Molecular sieves |
| MW | Molecular weight |
| m/z | Mass-to-charge ratio |
| *n*Bu$_4$NCl | Tetrabutylammonium Chloride |
| NMR | Nuclear magnetic resonance |
| Np | 1-Naphthyl |
| Np$^F$ | 4-Fluoro-1-naphthyl |
| NS | 4-Trifluoromethyl-*trans*-β-nitrostyrene |
| OTf | Trifluoromethylsulfonate |
| P | Product |
| Ph | Phenyl |
| PhMe | Toluene |
| p$K_a$ | Acid dissociation constant |
| ppm | Parts per million |
| POSS | Polyhedral oligomeric silsesquioxane |
| RDS | Rate determining step |

| | |
|---|---|
| RPKA | Reaction Progress Kinetic Analysis |
| rt | Room temperature |
| SM | Starting Material |
| TADDOL | α,α,α',α'-tetraaryl-2,2-disubstituted 1,3-dioxolane-4,5-dimethanol |
| TBTU | 2-(1H-benzotriazole-1-yl)-1,1,3,3-tetramethylaminium tetrafluoroborate |
| *t*-Bu | *tert*-Butyl |
| TCFH | *N,N,N′,N′*-Tetramethylchloroformamidinium hexafluorophosphate |
| TDE | 1-Tetradecene |
| TFAA | Trifluoroacetic anhydride |
| THF | Tetrahydrofuran |
| TLC | Thin Layer Chromatography |
| TMS | Trimethylsilyl |
| Troc | 2,2,2-Trichlorethoxycarbonyl |
| TsCl | Tosyl chloride |
| VTNA | Variable Time Normalization Analysis |
| Δ | Change in indicated quantity |
| δ | Chemical shift |

# Introduction

This chapter presents a summary of organosilicon chemistry relevant to the research in this dissertation. Properties and applications of organosilanols and silica gel are discussed. Strategies towards silicon-stereogenic molecules and silsesquioxane nanomaterials are presented. Modern kinetic analysis methods, including reaction progress kinetic analysis (RPKA) and variable time normalization analysis (VTNA), are introduced.

## 0.1: Overview of Developing Synthetic Methodology to Access Novel Organosilicon Molecules

In the Franz research group, there has been a focus on developing novel synthetic methodology to incorporate silicon into organic molecules. Silicon is the second most abundant element in the Earth's crust, providing a sustainable source for synthetic design.[1] The incorporation of silicon into an organic compound can alter its chemical and physical properties relative to the carbon analog. Compounds **0.1**,[2] **0.2**,[3] and **0.3**[4] are examples of organosilicon molecules previously studied where the properties of silicon improve activity for the designed function. Focuses in the Franz group include silicon-based catalysts,[4] ligands,[5] drug candidates,[6] and nanobuilding blocks.

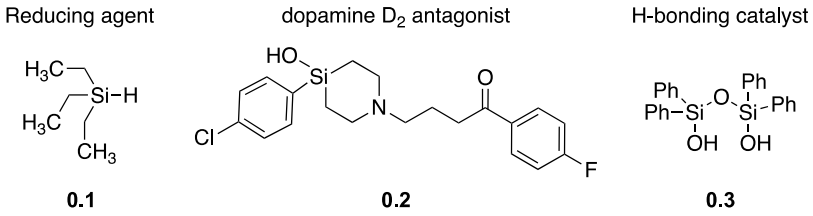


**Figure 0.1.** Examples of organosilicon compounds previously studied

Similar to carbon, silicon can exist in enantiomeric forms with four unique substituents bonded (Figure 0.2). Silicon-stereogenic molecules have been known for over 100 years.[7] Despite the similarities between carbon and silicon, there is a large discrepancy in the enantioselective methods known.[8] The development of enantioselective methodology to generate silicon-centered chirality can have broad applications, as does carbon-centered chirality. The Franz group is interested in applications of silicon-centered chirality in drug design,[9] ligand design,[5,10] and silicon-based materials.

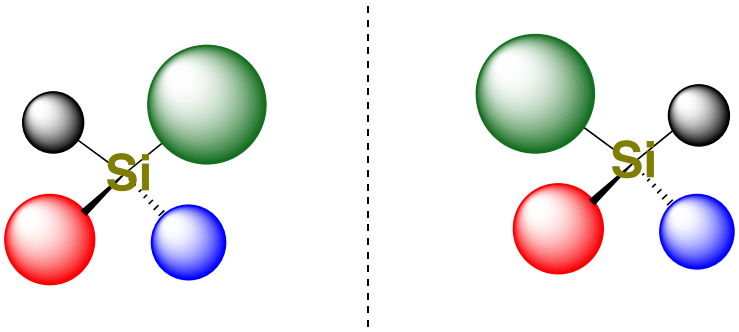


**Figure 0.2.** Enantiomers of tetravalent silicon.

Silicon is commonly used in the form of siloxanes and can be found in polymers[11] and materials.[12] Siloxane networks vary from oligomeric structures such as **0.4**,[13] polymeric forms with surrounding organic functionality (**0.5**),[14] or random structures (**0.6**) (Figure 0.3).[15] The combination of inorganic siloxanes and surrounding organic functionality leads to hybrid materials, often with unique properties.[16] Applications of siloxane polymers and materials are diverse and range from lubricants[17] to explosives.[18] Beyond small molecules, the development of organosilicon methodology can be applied to silicon-based materials and polymers.

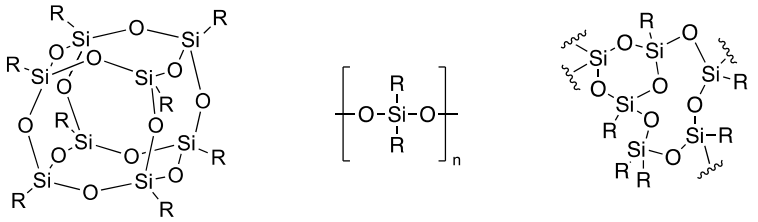


**Figure 0.3.** Examples of siloxane-containing structures with potential for development.

## 0.2: Properties of Organosilanols

Organosilanols, the silicon equivalent of an alcohol, are well-studied in the chemical literature dating to 1871 with Ladenburg's seminal publication on the synthesis of triethylsilanol from triethylchlorosilane.[19,20] The increased electropositivity of silicon compared to carbon (1.7 vs. 2.5) causes hyperconjugation effects from oxygen lone pairs to Si–C σ* orbitals (Figure 0.4).[21,22] Silanols are more acidic as a result, as seen with the difference in p$K_a$ between triphenylmethanol **0.7** (p$K_a$ = 17.0) and triphenylsilanol **0.8** (p$K_a$ = 16.6).[23,24] Silanols are stronger H-bond donors than alcohols as a result.[22]

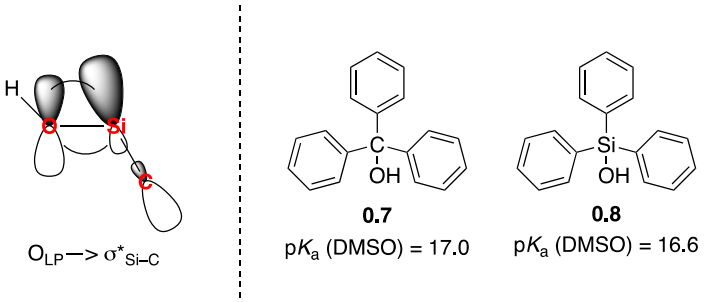


**Figure 0.4.** The acidity of silanols compared to alcohols.

The use of silicon allows for access to H-bonding arrangements that are unstable with carbon-based systems. Silanones are less stable than silanediols due to poor *p* orbital overlap between silicon and oxygen (Figure 0.5).[25,26] Organic substituents can be modified with sterically demanding groups to limit siloxane formation. Molecules such as **0.13**, **0.14**, and **0.15** are stable with potential for intramolecular or intermolecular H-bonding, affecting acidity and activity (Figure 0.5).[27]

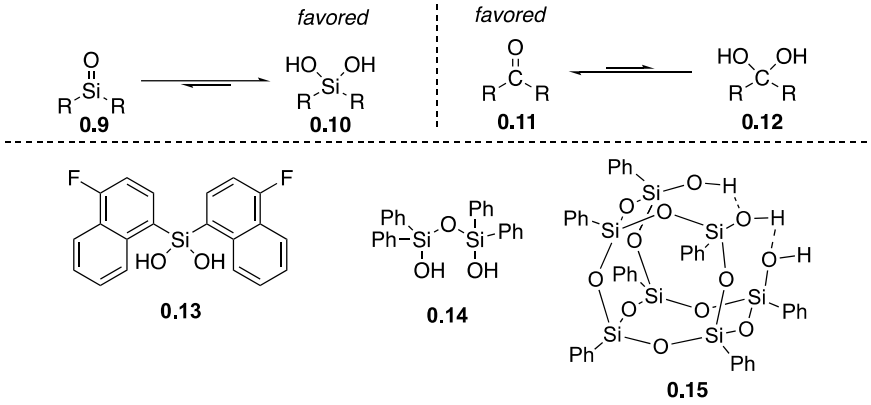


**Figure 0.5.** Access to unique silanol arrangements inaccessible with carbon analogs.

## 0.3: On the Importance of Studying Organosilanols

The unique properties of silanols make them attractive targets as H-bonding catalysts. In 2011, the Franz lab reported the first example of silanediol catalysis of a Diels-Alder reaction of Rawal's diene **0.16** and methacrolein **0.17** to yield product **0.18** (Figure 0.6).[28] Active catalysts include **0.19** containing electron-withdrawing groups and 1,3-disiloxanediol **0.14**. Both catalysts provided 55% yield of product **0.18**. Both Franz and Matson later demonstrated that organosilanols catalyzed the addition of silyl ketene acetals to isoquinolines[29,30] and the addition of indole to

nitrostyrene.[31,32] Kinetic studies by Franz highlight that silanols provide higher rates of catalysis compared to well-known scaffolds, such as thioureas.[4]

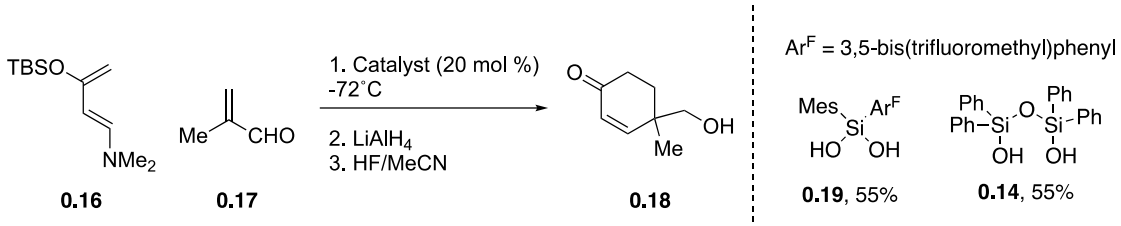


**Figure 0.6.** Franz's silanol-catalyzed [4+2] cycloaddition of Rawal's diene **0.16** and methacrolein **0.17**.

The study of small molecule organosilanols can provide insight into the H-bonding present on silica surfaces (Figure 0.7).[33] The bulk properties of silica gel are well-known, but studies of silica surfaces are generally limited due to insolubility.[34] The properties of a silica surface are determined by the surface silanols, including isolated, geminal, or vicinal arrangements.[35] By studying the hydrogen-bonding ability of discrete small molecule organosilanols, such as triaryl silanol **0.20**, 1,3-disiloxanediol **0.14**, and silsesquioxane **0.15**, information about interactions on silica surfaces can be learned.

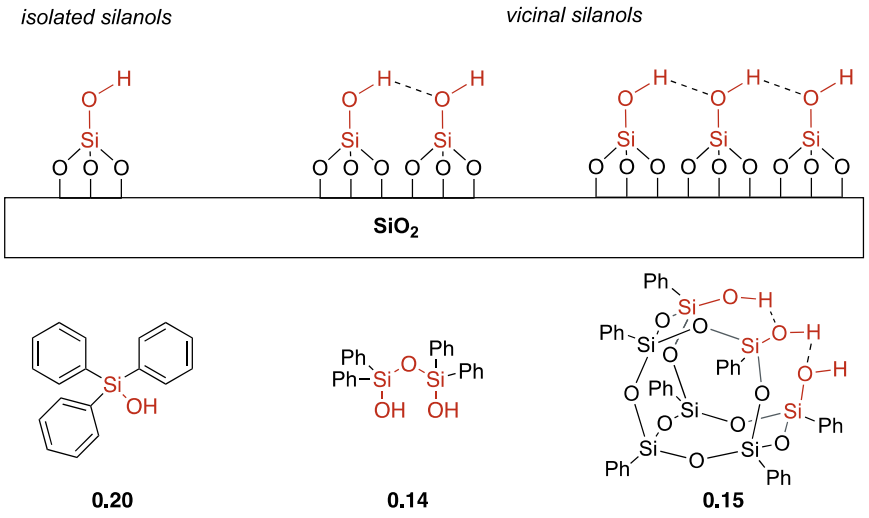


**Figure 0.7.** Organosilanols as soluble model compounds for silica surfaces.

## 0.4 Applications of Silica gel in Materials Science and Catalysis

Silica gel is commonly used for the synthesis of functionalized materials with controlled structure and morphology. The attractive aspects of silica-based materials include cost, thermal

and chemical stability, low environmental and biological toxicity, and diversity of synthetic methods.[36] The applications of silica-based materials include adsorption/separations, optical coatings, and environmental remediation efforts.[37] The resultant morphologies accessible include rods, sheets, spheres with tunable pore size (Figure 0.8A).[38] The surfaces of silica gels can be doped with metals, small molecules, or biomolecules to access hybrid materials. Hybrid silica-based materials have been used in explosives, drug delivery, and tissue engineering.[39,40] Silica gel is also used to immobilize catalysts, resulting in increased thermal stability and recyclability compared to unmodified counterparts.[41] The porous structure of silica gel is useful for heterogeneous reactions where increased surface area results in higher activity.[42] The silanols serve as sites for installation of catalytic groups. Precatalysts can react with silanols to access immobilized catalysts or silanols can be capped with linkers containing catalytic moieties or ligands for coordination (Figure 0.8B). Immobilized silica-gel based catalysts are have been used in industry for polyolefin synthesis and fluid catalytic cracking.[42–44]

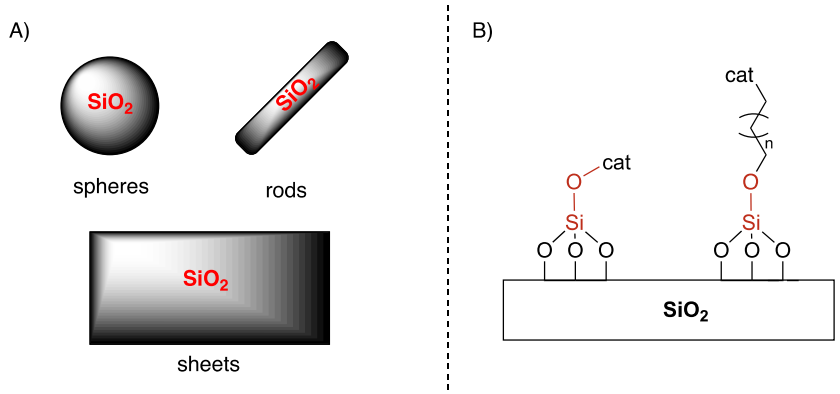


**Figure 0.8.** A) Accessible morphologies of silica-gel based materials B) Strategies for immobilized catalysts onto silica gel.

Silica gel has also been used as a solid acid catalyst extensively due to its facile recycling and thermal stability, with several examples shown below (Figure 0.9). The silanols present on silica surfaces are the catalytically active moiety. Shumalia and coworkers reported that silica gel catalyzed additions of nitrogen heterocycles to electron-poor alkenes.[45] The reaction of nitrostyrene **0.21** and indole **0.22** yielded product **0.23** in 92% yield at room temperature in 30 minutes. Comerford and coworkers reported silica gel-catalyzed amide bond formation of carboxylic acids and amines.[46] The reaction between acid **0.24** and aniline **0.25** produced amide **0.26** in 54% yield after 24 h at 110˚C. Jin and coworkers reported epoxide ring-opening with concomitant sulfur to oxygen acetal migration.[47] Epoxide **0.27** with thiol **0.28** produced product

**0.29** in 85% yield after 14 hours at room temperature. Silica gel has also been used for alkylations of phenols[48] and epoxide ring openings with nitrogen-containing heterocycles.[49] Studies of orgnaosilanol catalysis can provide insight into the active structures present on the surface of silica gel.

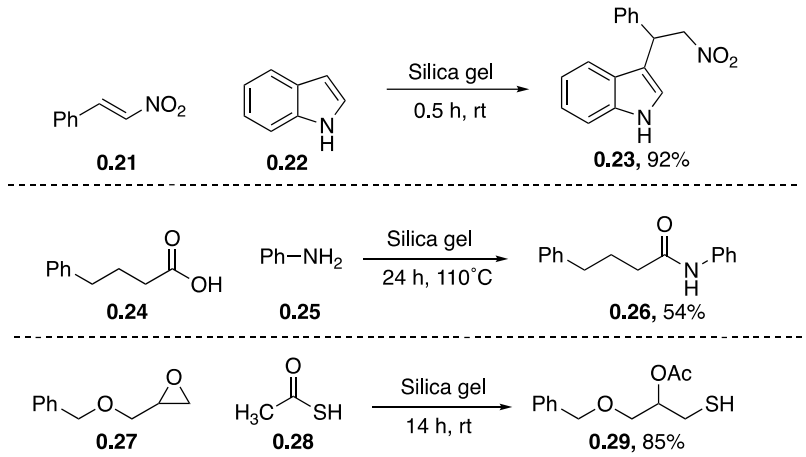


**Figure 0.9.** Some previous examples of silica gel-catalyzed transformations.

## 0.5: Concentration Effects on Small Molecule H-bonding Ability

With small molecule H-bond donor catalysts, aggregation can occur with increased concentration.[50] The resultant conformations can have varied H-bonding strength which can affect rates of catalysis or the mechanism. A common effect with increased concentration of organocatalysts with both donor and acceptor sites is self-association into dimeric species (Figure 0.10).[51] Several classes of organocatalysts are known to self-associate in solution, including organosilanols,[31] thioureas[52], and phosphoric acids[53]. Several examples will be explained below.

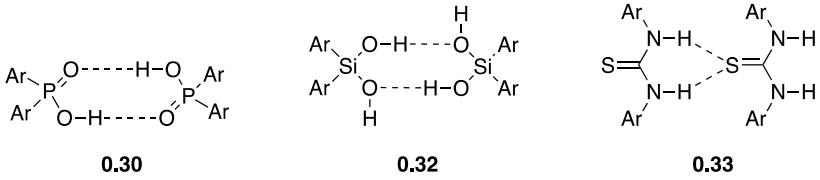


**Figure 0.10.** Self-association of organocatalysts with H-bond donor and acceptor sites.

Silanediols have been previous studied as catalysts,[31] anion receptors,[54] and protease inhibitors.[55] A previous Franz lab member, Dr. Ngon Tran, studied silanediol H-bonding and observed self-association into dimeric species, supported by $^{1}$H NMR DOSY studies (Figure

0.11).[31,56] The formation of self-associated species increased with concentration or by reducing the temperature. A theoretical study of **0.34** by Dr. Tran indicated that self-association to **0.34•0.34** increased acidity of free silanols (p$K_a$ = 10.5) when compared to monomeric **0.34** (p$K_a$ = 11.5) (Figure 0.11).[24] Binding studies of **0.19** with DMF using $^1$H NMR spectroscopy confirm silanediols' increased H-bonding ability with higher concentration. The calculated association constant to DMF increased from 90 ± 4 $M^{-1}$ to 1431 ± 50 $M^{-1}$ with increased concentration from 0.01 M to 0.4 M in $C_6D_6$ (Figure 0.11). In the reaction of nitrostyrene **0.21** and indole **0.22**, yield of product **0.23** increased to 91% with increased concentration to 2.0 M or reducing reaction temperature to 4 ˚C. Overall, the data indicates silanediols are more active H-bond donors when self-associated into dimeric species.

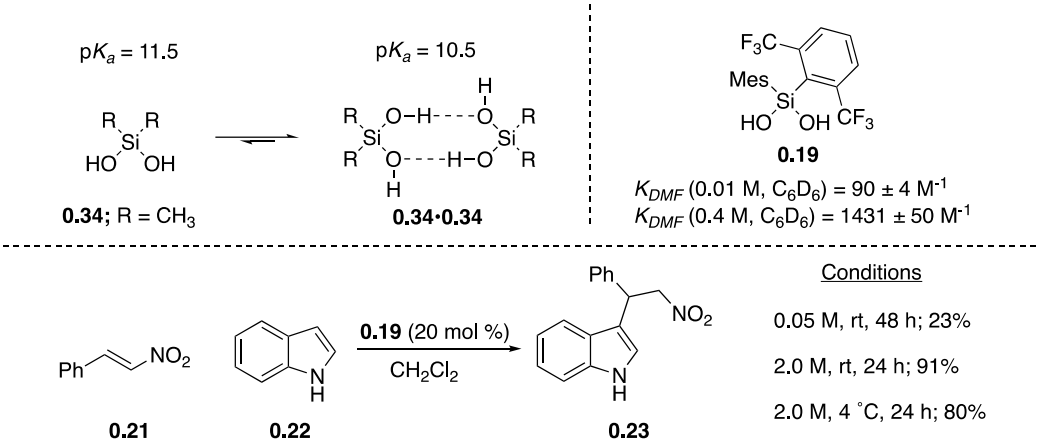


**Figure 0.11.** Concentration effects on silanediol H-bonding with Lewis bases.

Thioureas are potent small-molecule H-bonding catalysts that have been examined for several enantioselective transformations, including multicomponent reactions,[57] conjugate additions,[58] and the addition of silyl ketene acetals to α-chloroethers.[59] Jacobsen and coworkers investigated the reaction with chloroether **0.35** and silyl ether **0.36** using thiourea **0.38** and it is proposed to proceed through an anion-binding mechanism involving two thioureas bound to chloride (**0.39**) (Figure 0.12).[60] The authors performed a kinetic analysis to understand the mechanism of catalysis. When the thiourea **0.38** concentration was below 0.1 M, the catalyst exhibited second-order rate dependence. When the thiourea **0.38** concentration was above 0.1 M, first-order rate dependence was observed (Figure 0.12). Thiourea **0.38** is known to self-associate in solution to **0.38•0.38**. The authors attribute the change in catalyst order to concentration-dependent resting states between monomeric **0.38** and self-associated species **0.38•0.38**. Thioureas

are near one another at high concentrations due to self-association, so the rate dependence is on the concentration of self-associated species. At low concentrations, thioureas must associate before catalysis, leading to second-order rate dependence.

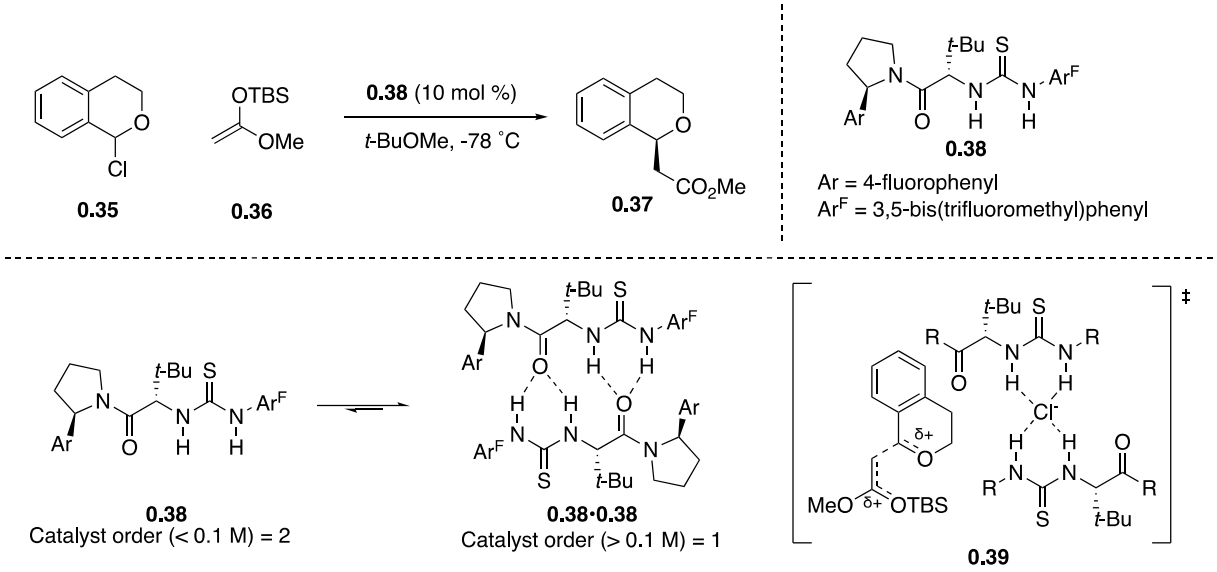


**Figure 0.12.** Jacobsen's addition of silyl-ketene acetals to α-chloroethers using thiourea **0.38**.

## 0.6 Background on Polyhedral Oligomeric Silsesquioxanes (POSS)

Polyhedral oligomeric silsesquioxanes (POSSs) are a class of inorganic-organic hybrid compounds described by the chemical formula $(RSiO_{1.5})_a(H_2O)_{0.5b}$, where R is a hydrogen atom or an organic group and *a* is an integer larger than zero.[61] POSSs are classified into two categories based on the value of *b*: completely condensed POSSs (where $b = 0$) and incompletely condensed POSSs ($b = 1, 2, 3$, etc.). Prismatic POSSs have been the subject of most studies, but ladder[62] and randomly assorted oligomeric siloxanes are known.[63]

Synthesis of POSSs vary depending on the identity of the organic substituent.[64] POSSs are accessed from trichloro or trialkoxy silanes with strong acid or base (Figure 0.13).[65] Hydrolysis of silanes **0.41** yields silanetriol **0.42**, a common intermediate that condenses with additional triols to assemble the siloxane core **0.4**.[66] Controlling the hydrolytic condensation equilibrium is not generalizable and is a current limitation of POSS methodology.[67] Factors that affect this equilibrium include temperature, solvent, pH, concentration, and added water.[68] However, several POSSs are commercially available.[69] Silanol-containing POSSs can react with chlorosilanes and base to access novel structures capable of further functionalization. Additionally, synthetic organic

chemistry can be performed about the organic groups.[70] The combination of inorganic siloxane chemistry from silanols and organic chemistry from the R groups enable versatile applications ranging from silica surface model compounds[71] to additives for healing wounds.[72]

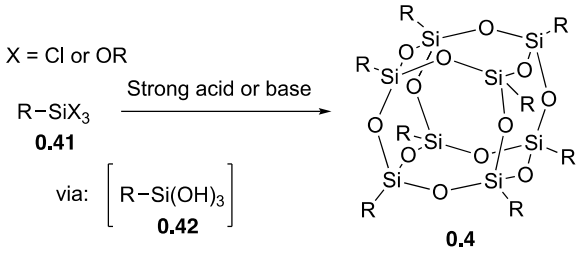


**Figure 0.13.** Synthesis of POSS from alkoxy or chlorosilanes.

Incompletely condensed POSSs have been extensively studied for their structural similarities to vicinal silanols on the surface of silica gel (Figure 0.14).[71,73] Their solubility in organic solvents enables detailed structural investigations that can be difficult to study in bulk silica gel.[35] Discrete silanol configurations can be synthesized to develop structure-activity relationships. POSS **0.43-0.45** are examples of compounds studied to examine H-bonding,[74] acidity,[70] silylation[73], and metal coordination.[75]

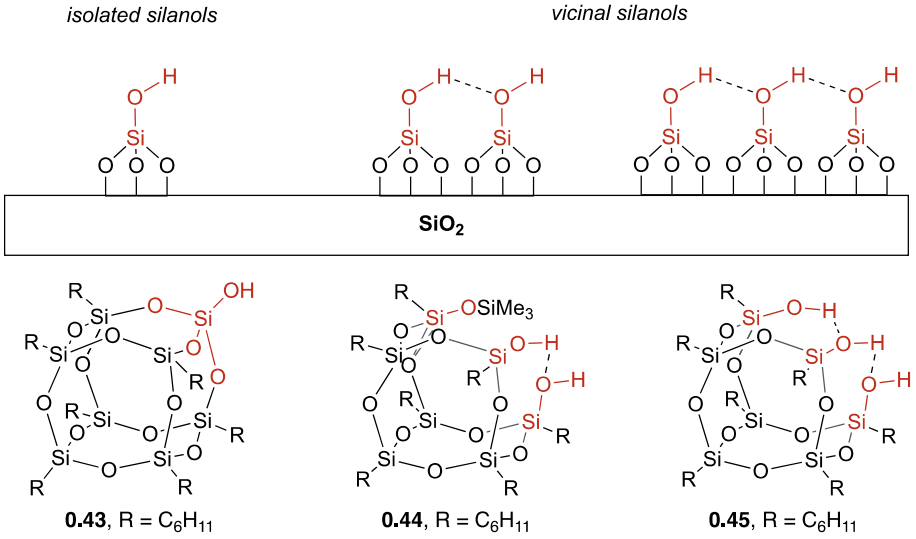


**Figure 0.14.** Previously studied POSS compounds for silica surface modeling studies.

Polyhedral oligomeric silsesquioxane triols (POSS-triols) are organosilanols that have been studied to characterize H-bonding arrangements in solution. Kondo and coworkers investigated POSS-triol **0.46** and observed two modes of H-bonding: intermolecular H-bonding

with Lewis bases and self-association into dimeric species **0.46•0.46** (Figure 0.15).[76] The authors noted that binding studies needed to be conducted at a sufficiently low concentration (0.005 M) so that self-association would not interfere with H-bonding with Lewis bases. The strength of H-bonds to Lewis bases was comparable to previous work with 1,3-disloxanediols[77] and silanediols,[54] suggesting that there are potential applications of POSS-triols as H-bonding catalysts. Prior to work in the Franz lab, no studies had been performed with POSS-triols as H-bond donor catalysts.

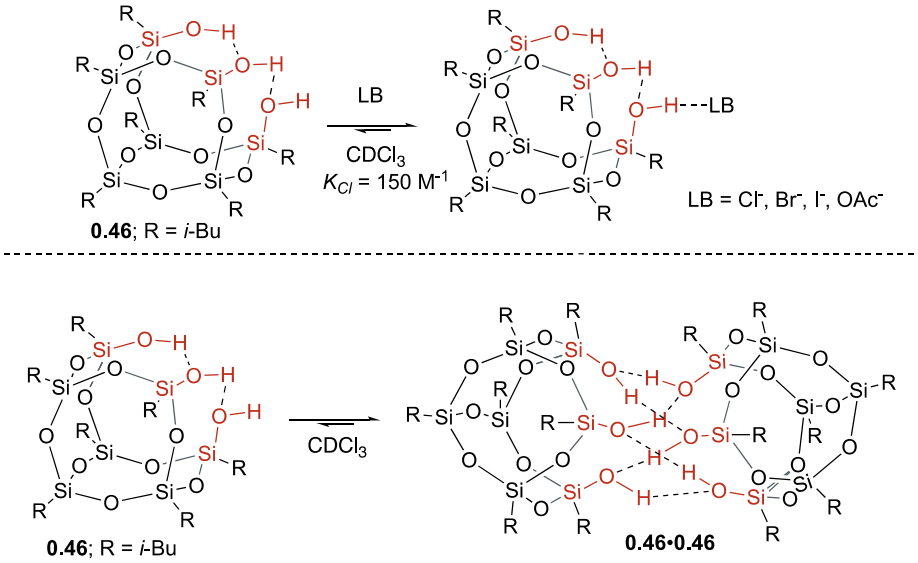


**Figure 0.15.** Kondo's investigation into POSS-triol H-bonding in solution.

Completely condensed POSSs have been used extensively to synthesize hybrid materials.[78,79] The inorganic siloxane core has been noted to increase thermal and chemical stability due to the strength of Si–O–Si bonds.[80,81] The organic groups surrounding POSS enable facile processing and functionalization. Additionally, their discrete size and uniformity make them attractive platforms for design (Figure 0.16).[82] Several strategies have been applied to incorporate completely condensed POSSs into materials with diverse applications.[83] POSSs physically blended with polymers have been shown to provide enhanced stiffness and stability with applications in low dielectric constant materials.[84] Alternative strategies focus on covalent linkages with the surrounding organic groups. Several different forms of connectivity can be accessed based on the cubic shape. Pendant connectivity of POSSs to a polymer has been used for solid-state batteries with increased thermal stability.[85] End-to-end connectivity of POSSs with a covalent linker has been used for hybrid-hydrogels for drug delivery systems.[86] Cross-linked structures of POSSs have been used for liquid crystal polymers for self-assembly.[87]

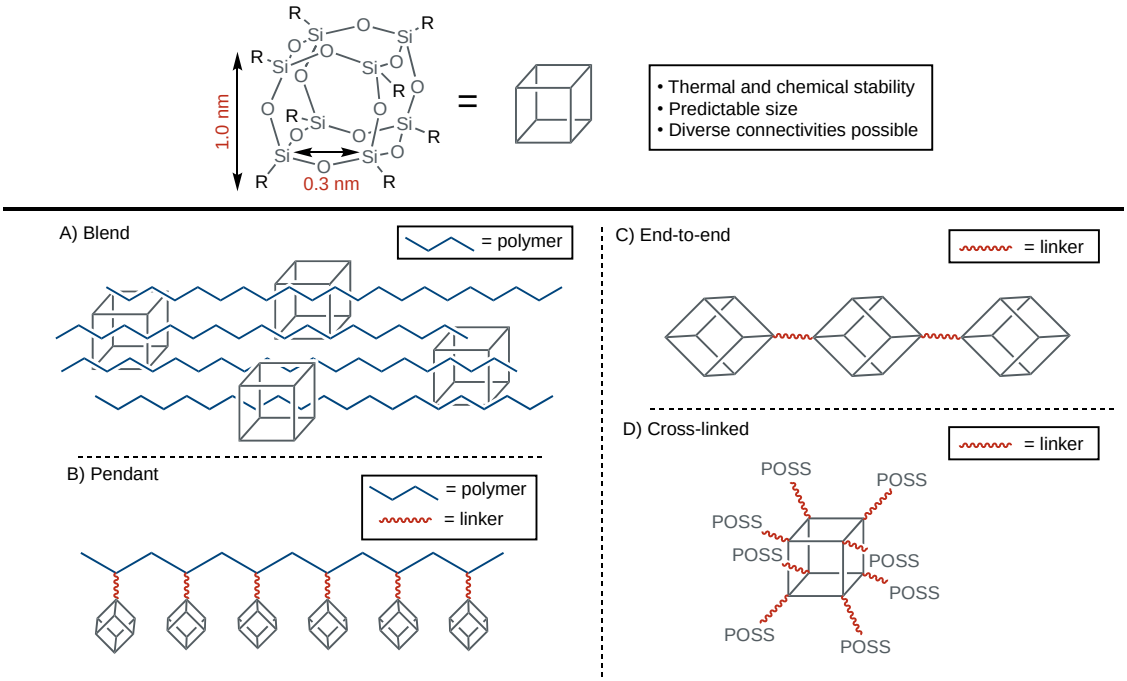


**Figure 0.16.** Strategies for incorporation of POSS into materials and polymers.

## 0.7: Modern Kinetic Analysis Methods

Kinetic analysis of catalytic transformations is an invaluable tool for guided approaches toward designing new catalysts, understanding structure-activity relationships and elucidating reaction mechanisms. However, a barrier of kinetic analysis is the general difficulty of relating mathematical expressions to the system in study. Several modern analysis techniques have enabled facile extraction of kinetic information using reaction profiles, including reaction progress kinetic analysis (RPKA)[88,89] and variable time normalization analysis (VTNA).[90–93] These techniques leverage the visual capacity of human beings and limit the complexity of mathematics required to extract useful kinetic information.

Developed by Professor Donna Blackmond, RPKA is a protocol that uses the difference in concentrations between two substrates for experimental design.[88,89] Applied to a theoretical reaction of A and B catalyzed to make C (Eq 0.1), RPKA relies on the difference between $[A]_o$ and $[B]_o$, known as the "*excess*" (or [xs]) (Eq 0.2).[88,89] This value is constant throughout the entire reaction. The value of [xs] can be minor so that synthetically relevant concentrations are probed, overcoming the need for pseudo-first-order conditions. When varying [xs] between trials while keeping $[A]_o$ constant (known as a "*different excess"* experiment), the order can be determined in

B after manipulation of calculated rate data into graphical rate laws (Figure 0.17). Overlap of trials will be observed when the order in the reagent is successfully determined. A minimum of two trials are needed, but additional trials can be completed to expand the concentrations studied. Reciprocal experiments that determine the order in A (where $[B]_o$ is held constant) can be performed to support the conclusion. This can be applied to reagents and (co)catalysts to determine the overall rate expression.

$$A + B \longrightarrow C \qquad \text{(Eq 0.1)}$$

$$[xs] = [A]_o - [B]_o = [A] - [B] \qquad \text{(Eq 0.2)}$$

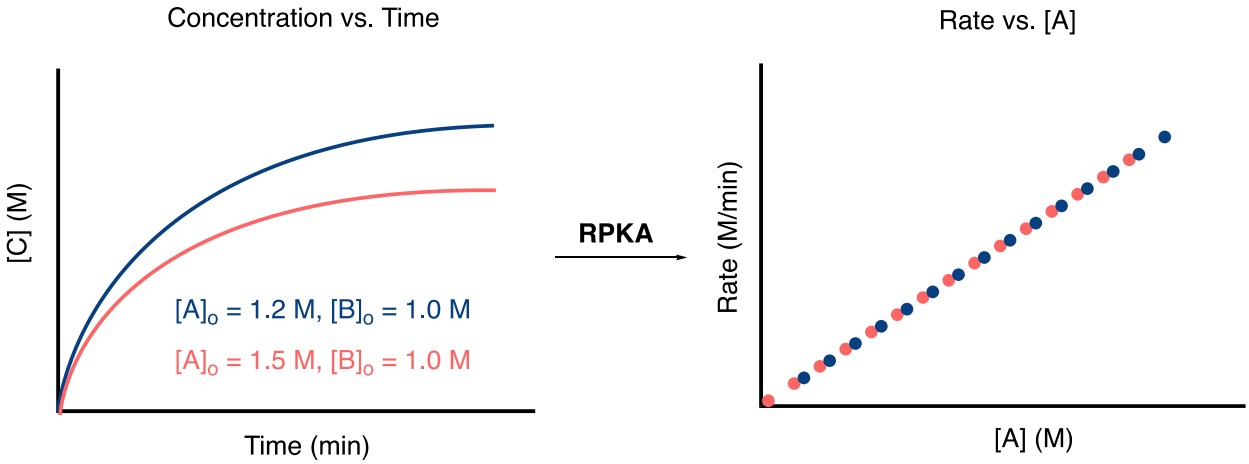


**Figure 0.17.** Example of a "*different excess*" experiment using RPKA indicating first order in A.

The RPKA protocol can be used to probe for catalyst decomposition or product inhibition. Multiple trials can be performed with identical [xs] (known as a "*same excess*" experiment) but different initial concentrations (Figure 0.18).[88,89] At some point in the reaction, the concentrations of both trials will be identical and can be overlayed. The critical difference between trials is the presence of the product and the number of catalyst turnovers. If trials do not overlap, it indicates catalysis is slowing down from product inhibition or catalyst decomposition. Another trial with product present can distinguish between product inhibition or catalyst decomposition.

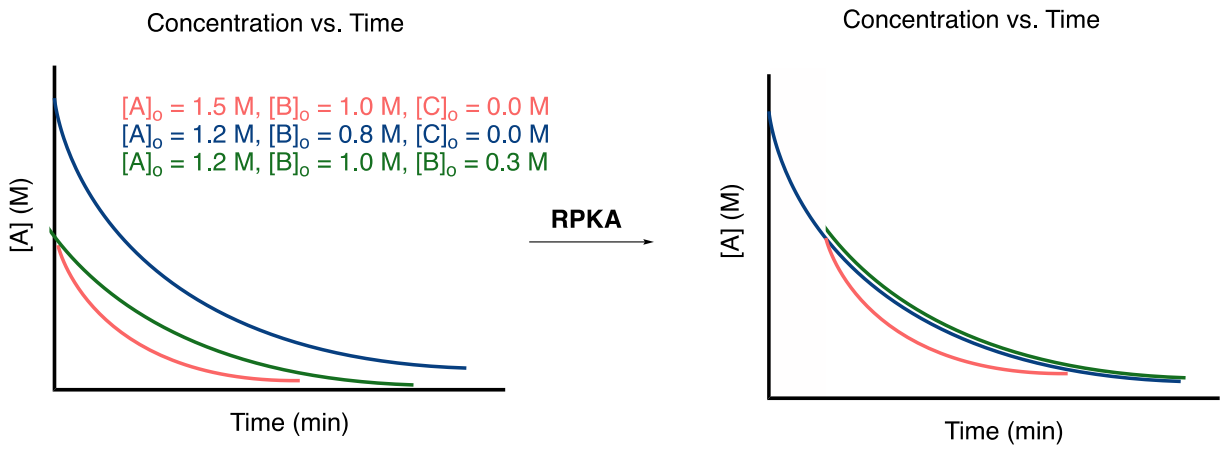


**Figure 0.18.** Example of a "*same excess*" experiment using RPKA depicting product inhibition.

Developed by Professor Jordi Bures, VTNA complements the RPKA protocol because it uses concentration profiles directly.[90,91] Techniques such as NMR, IR, UV, and GC introduce errors in measurements when manipulated to rate data, affecting the accuracy of conclusions. Using the "*different excess*" protocol from RPKA, VTNA effectively integrates out the effect of concentration on rate by exponentiating the time integral (approximated with the trapezoid rule) to a value of *a* (Eq. 0.3). Trials with "*different excess*" will overlay when the correct value of *a* is chosen, indicating the order in the reagent (Figure 0.19). Like RPKA, VTNA can be applied to reagents and (co)catalysts, and is useful for the determination of non-integer catalyst orders.

$$\int_{t=0}^{t=n}[A]^a dt = \sum_{i=1}^{n}\left(\frac{[A]_i+[A]_{i-1}}{2}\right)^a (t_i - t_{i-1}) \qquad \text{(Eq 0.3)}$$

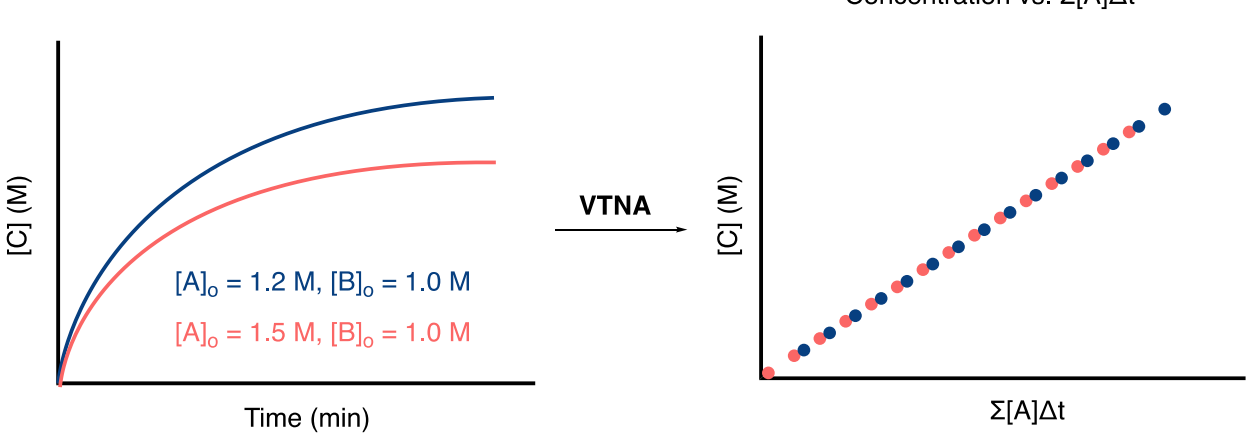


**Figure 0.19.** Example of a "*different excess*" experiment using VTNA indicating first order in A.

## 0.8: Transition-metal Catalyzed Desymmetrization of Prochiral Silanes for the Synthesis of Silicon-stereogenic Molecules

Like carbon, silicon can be chiral with four unique substituents bonded. Stereogenic silicon molecules have been known for over 100 years and have led to the development of an entire field of research.[7] Methods to produce stereogenic carbon compounds use prochiral $sp^2$ intermediates such as alkenes,[94] carbonyls,[95] and carbocations[96] to form chiral $sp^3$ centers. However, the synthesis of enantioenriched silicon requires alternative strategies due to the instability of $sp^2$ silicon centers (Figure 0.20, **0.47**).[97] Instead, the strategy involves enantioselective differentiation of two identical groups of an $sp^3$ silicon center (**0.48**) using a desymmetrization agent.[98,99] Compared to kinetic resolution, desymmetrization allows for theoretical yields of 100% thereby increasing atom economy.

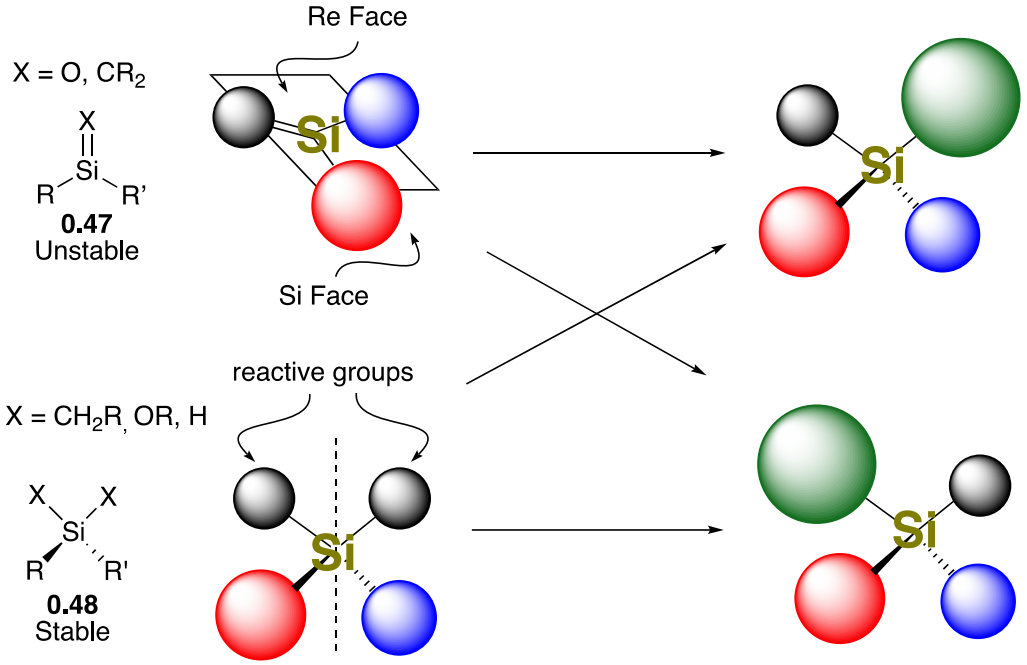


**Figure 0.20.** Desymmetrization of $sp^3$ silicon centers for the synthesis of silicon-stereogenic molecules.

Transition metal-catalyzed desymmetrization of Si–H bonds represents a modular approach to access silicon-stereogenic molecules.[100,101] Prochiral silanes are stable molecules and are capable of structural diversity about the organic groups. Several transformations with Si–H bonds are known, including arylation,[102] hydrosilylation, alcoholysis,[103] and carbene insertion[104,105], which provide a diverse set of metal/ligand combinations for optimization. The remaining Si–H bond can be used for additional transformations to access complex substrates. The

mechanism of desymmetrization occurs in two possible modes: A) Desymmetrization of **0.49** to produce a silicon-stereogenic metal hydride **0.50** followed by coupling to produce **0.51** or **0.52**, or B) Diazo compound **0.53** reacts with the catalyst to form metal carbenoid **0.54** followed by desymmetrization of **0.49** to produce silane **0.55** (Figure 0.21).[106] No metal hydride species form in mechanism B. Most catalysts capable of oxidative addition into Si–H bonds occur through mechanism A, which includes hydrosilylation, arylation, and alcoholysis. Carbene insertion into Si–H bonds occurs through mechanism B. An example of mechanism A will be discussed below and carbene insertion into Si–H bonds is discussed in a separate section of this introduction.

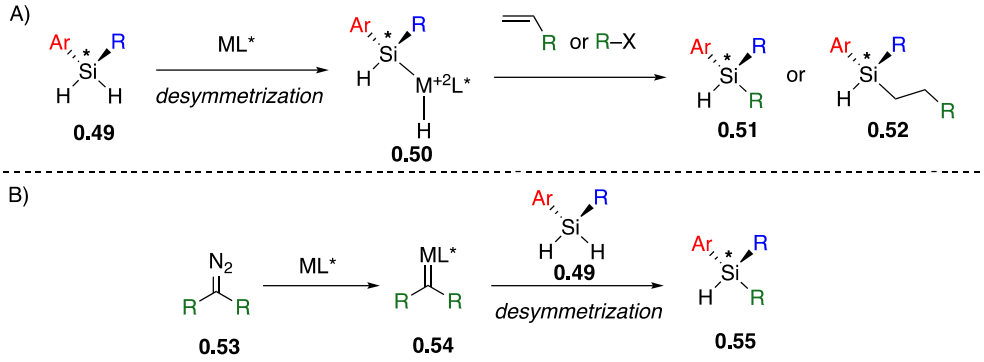


**Figure 0.21.** Mechanisms of desymmetrization of prochiral silanes to produce silicon-stereogenic silanes.

In 2017, Nishihara and coworkers reported the desymmetrization of prochiral silanes **0.56a-f** with aryl iodides **0.57a-c** using a chiral palladium catalyst to produce silanes **0.59a-f** (Figure 0.22).[102] TADDOL-derived ligand **0.58** provided the highest enantioselectivity of ligands tested, forming silane **0.59a** in 57% yield and 80:20 er. Increased steric bulk provided higher enantioselectivity to 85:15 er (**0.59b** and **0.59c**) with reduced yield (64% and 40%, respectively). Substitution of the methyl group to a cyclohexyl group provided slightly increased enantioselectivity (**0.59d**, 82:18 er) and yield was comparable (62%). The authors demonstrated two couplings on a single substrate to access **0.59e** (35%, >99:1er), albeit in low diastereoselectivity (76:24 dr). The proposed mechanism, supported by DFT calculations, involves Si–H desymmetrization followed by base-promoted σ-bond metathesis to furnish silane products. The authors demonstrated additional couplings with the remaining Si–H bond to produce silane **0.59f** in 45% yield and 85:15 er.

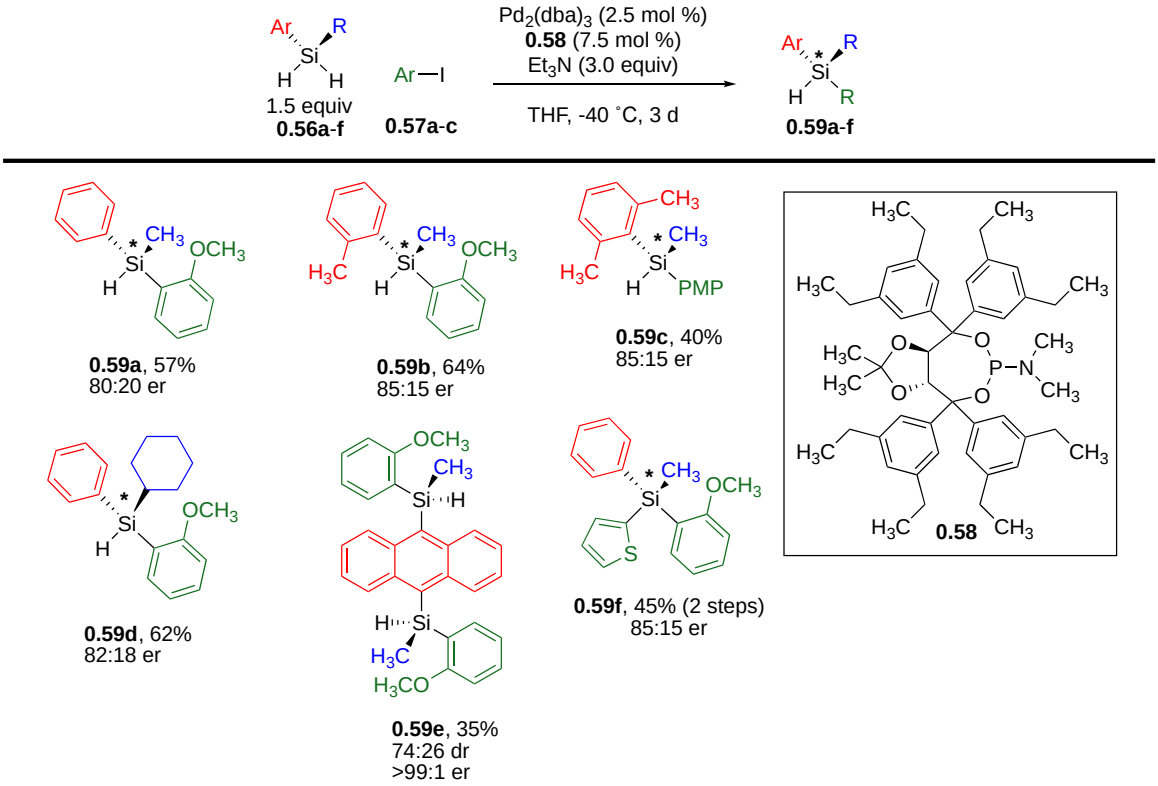


**Figure 0.22.** Nishihara's Pd-catalyzed arylation of prochiral silanes.

## 0.9: Carbene Insertion Into Si–H bonds

Carbene insertion into Si–H bonds is a powerful transformation that forms new Si–C and C–H bonds using transition metals as catalysts.[107] Carbenes are formed *in situ* from diazo compounds **0.53** after the loss of $N_2$ with assistance from the metal center (Figure 0.23).[108] The subsequent metal carbenoid **0.54** can insert into an Si–H bond of **0.61** with the potential to set two stereocenters in a single step in silane **0.62**. An asynchronous, concerted mechanism is proposed where hydride transfer precedes Si–C bond formation.[109,110] Several metals are known to catalyze carbene insertion into Si–H bonds, including Rh(II),[111] Cu(I)[112] and Ag(I).[113] The use of chiral ligands enables enantioselective processes. Compared to C–H bonds, Si–H bonds are more reactive to carbene insertion, supported by competition experiments.[114]

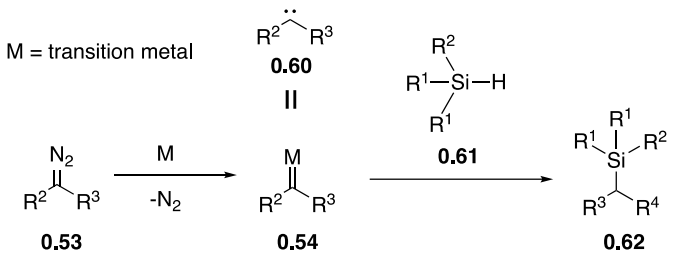


**Figure 0.23.** Overview of carbene insertion into Si–H bonds.

The reactivity of carbenes is tuned by the attached R groups and classified into three main categories: ester carbene (**0.63**), aryl(ester) carbenes (**0.64**), and diarylcarbenes (**0.65**).[115,116] Alternative classifications commonly used in literature are acceptor, donor/acceptor, and donor/donor, respectively. The use of electron-donating groups such as aryl rings, alkenes, or alkyl groups increases the stability of the metal carbenoid and leads to higher selectivity with reduced reactivity. The use of electron-withdrawing groups such as esters or nitriles increases the reactivity of the metal carbene and the stability of the diazo compound.[108] To date, aryl(ester) carbenes are the subject of most studies with silanes due to both electron-donating and electron-withdrawing effects that increase selectivity and promote reactivity, respectively.[107] The use of diarylcarbenes represents a current synthetic challenge due to the stabilization from the donor groups. However, the increased stability could lead to more selective insertion reactions.

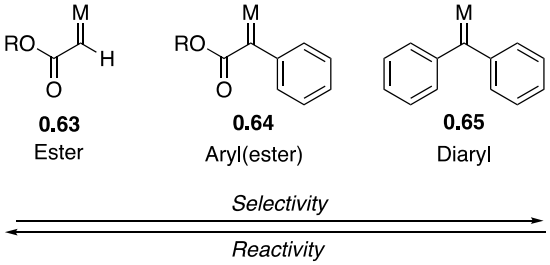


**Figure 0.21.** Reactivity and selectivity of metal carbenoids.

## 0.10: Overview of Dissertation

Chapter one describes a $^{19}F$ NMR kinetic study of incompletely condensed polyhedral oligomeric silsesquioxane H-bond-donor catalysis in a Friedel-Crafts addition reaction. Catalyst concentration-dependent kinetics were observed, attributed to off-cycle self-association into dimeric species, which is supported by $^{1}H$ NMR DOSY experiments. NMR binding studies were

performed to investigate the effect of catalyst concentration on H-bonding ability, showing reduced activity at higher concentrations. Catalytic cycles detailing concentration-dependent resting states are proposed.

Chapter two presents the development of Rh(II)-catalyzed diarylcarbene insertion into Si–H bonds to produce silicon-stereogenic silanes. Novel prochiral silanes and diazo compounds were synthesized to explore structure-activity relationships. The effect of a prochiral diazo compound on enantioselectivity was explored. A mechanistic study highlighted structural effects on diazo compound stability and probed the rate-determining step. Further transformations of insertion products were explored.

Chapter three details the development of Rh(II)-catalyzed aryl(ester) carbene insertion into Si–H bonds of silsesquioxane-based silanes. Aryl(ester) and aryl(amide) diazo compounds were tested against POSSs with one, three, and eight Si–H bonds. Novel diazo compounds were synthesized containing fluorinated groups and BODIPY fluorophores. Further transformations of insertion products were explored.

## 0.11: References


(1) Jaroniec, M. Silicon beyond the Valley. *Nat. Chem.* **2009**, *1* (2), 166. https://doi.org/10.1038/nchem.173.

(2) Nagai, Y. HYDROSILANES AS REDUCING AGENTS. A REVIEW. *Org. Prep. Proced. Int.* **1980**, *12* (1–2), 13–48. https://doi.org/10.1080/00304948009355421.

(3) Tacke, R.; Heinrich, T.; Bertermann, R.; Burschka, C.; Hamacher, A.; Kassack, M. U. Sila-Haloperidol: A Silicon Analogue of the Dopamine (D2) Receptor Antagonist Haloperidol. *Organometallics* **2004**, *23* (19), 4468–4477. https://doi.org/10.1021/om040067l.

(4) Diemoz, K. M.; Hein, J. E.; Wilson, S. O.; Fettinger, J. C.; Franz, A. K. Reaction Progress Kinetics Analysis of 1,3-Disiloxanediols as Hydrogen-Bonding Catalysts. *J. Org. Chem.* **2017**, *82* (13), 6738–6747. https://doi.org/10.1021/acs.joc.7b00875.

(5) Diemoz, K. M. Design, Synthesis, and Investigation of Siloxanol Hydrogen-Bonding Catalysts and Chiral Silanol Ligands, University of California, Davis, 2018.

(6) Franz, A. K.; Wilson, S. O. Organosilicon Molecules with Medicinal Applications. *J. Med. Chem.* **2013**, *56*, 388–405. https://doi.org/10.1021/jm3010114.

(7) Kipping, F. S. XXII.—Organic Derivatives of Silicon. Part II. The Synthesis of Benzylethylpropylsilicol, Its Sulphonation, and the Resolution of the Dl-Sulphonic Derivative into Its Optically Active Components. *J. Chem. Soc. Trans.* **1907**, *91* (0), 209–240. https://doi.org/10.1039/CT9079100209.

(8) Igawa, K.; Tomooka, K. Chiral Silicon Molecules. *Organosilicon Chemistry*. November 11, 2019, pp 495–532. https://doi.org/doi:10.1002/9783527814787.ch14.

(9) Aleman, J.; Cabrera, S. Applications of Asymmetric Organocatalysis in Medicinal

Chemistry. *Chem. Soc. Rev.* **2013**, *42* (2), 774–793. https://doi.org/10.1039/c2cs35380f.
(10) Kelly, A. T. Synthesis of Siloxanol Containing Compounds and Studies Toward Enantioenriched Variants, University of California, Davis.
(11) Blanco, I. Polysiloxanes in Theranostics and Drug Delivery: A Review. *Polymers (Basel).* **2018**, *10* (7), 755. https://doi.org/10.3390/polym10070755.
(12) Chee, W. W. L.; Donovan, T. E. Polyvinyl Siloxane Impression Materials: A Review of Properties and Techniques. *J. Prosthet. Dent.* **1992**, *68* (5), 728–732. https://doi.org/https://doi.org/10.1016/0022-3913(92)90192-D.
(13) Zhou, H.; Ye, Q.; Xu, J. Polyhedral Oligomeric Silsesquioxane-Based Hybrid Materials and Their Applications. *Mater. Chem. Front.* **2017**, *1* (2), 212–230. https://doi.org/10.1039/C6QM00062B.
(14) Mark, J. E. Overview of Siloxane Polymers. *ACS Symp. Ser.* **1999**, *729*, 1–10. https://doi.org/10.1021/bk-2000-0729.ch001.
(15) Babonneau, F. Hybrid Siloxane-Oxide Materials via Sol-Gel Processing: Structural Characterization. *Polyhedron* **1994**, *13* (8), 1123–1130. https://doi.org/https://doi.org/10.1016/S0277-5387(00)80249-1.
(16) Kim, Y. H.; Lee, I.; Lee, H.; Kang, S. M.; Lee, Y.; Kim, S.; Bae, B. S. Sol–Gel Synthesized Siloxane Hybrid Materials for Display and Optoelectronic Applications. *J. Sol-Gel Sci. Technol.* **2021**. https://doi.org/10.1007/s10971-021-05491-4.
(17) Zaman, Q.; Zia, K. M.; Zuber, M.; Mabkhot, Y. N.; Almalki, F.; Hadda, T. Ben. A Comprehensive Review on Synthesis, Characterization, and Applications of Polydimethylsiloxane and Copolymers. *Int. J. Plast. Technol.* **2019**, *23* (2), 261–282. https://doi.org/10.1007/s12588-019-09259-y.
(18) Zalewski, K.; Chyłek, Z.; Trzciński, W. A. A Review of Polysiloxanes in Terms of Their Application in Explosives. *Polymers* . 2021. https://doi.org/10.3390/polym13071080.
(19) Ladenburg, A. Organic Chemistry; On the Silicoheptyl Series. *J. Chem. Soc.* **1872**, *25* (0), 133–156. https://doi.org/10.1039/JS8722500133.
(20) Chandrasekhar, V.; Boomishankar, R.; Nagendran, S. Recent Developments in the Synthesis and Structure of Organosilanols. *Chem. Rev. (Washington, DC, United States)* **2004**, *104* (12), 5847–5910.
(21) Allred, A. L. Electronegativity Values from Thermochemical Data. *J. Inorg. Nucl. Chem.* **1961**, *17* (3), 215–221. https://doi.org/https://doi.org/10.1016/0022-1902(61)80142-5.
(22) West, R.; Baney, R. H. Hydrogen Bonding Studies. II.1 The Acidity and Basicity of Silanols Compared to Alcohols2. *J. Am. Chem. Soc.* **1959**, *81* (23), 6145–6148. https://doi.org/10.1021/ja01532a011.
(23) Damrauer, R.; Simon, R.; Krempp, M. Effect of Substituents on the Gas-Phase Acidity of Silanols. *J. Am. Chem. Soc.* **1991**, *113* (12), 4431–4435.
(24) Liu, M.; Tran, N. T.; Franz, A. K.; Lee, J. K. Gas-Phase Acidity Studies of Dual Hydrogen-Bonding Organic Silanols and Organocatalysts. *J. Org. Chem.* **2011**, *76* (17), 7186–7194. https://doi.org/10.1021/jo201214x.
(25) Kapp, J.; Remko, M.; Schleyer, P. von R. H2XO and (CH3)2XO Compounds (X = C, Si, Ge, Sn, Pb): Double Bonds vs Carbene-Like StructuresCan the Metal Compounds Exist at All? *J. Am. Chem. Soc.* **1996**, *118* (24), 5745–5751. https://doi.org/10.1021/ja953846p.
(26) Kudo, T.; Nagase, S. Theoretical Study on the Dimerization of Silanone and the Properties of the Polymeric Products (H2SiO)n (n = 2, 3, and 4). Comparison with Dimers (H2SiS)2 and (H2CO)2. *J. Am. Chem. Soc.* **1985**, *107* (9), 2589–2595.

https://doi.org/10.1021/ja00295a003.
(27) Huque, F. T. T.; Platts, J. A. The Effect of Intramolecular Interactions on Hydrogen Bond Acidity. *Org. Biomol. Chem.* **2003**, *1* (8), 1419–1424. https://doi.org/10.1039/B300598D.
(28) Tran, N. T.; Min, T.; Franz, A. K. Silanediol Hydrogen Bonding Activation of Carbonyl Compounds. *Chemistry (Easton).* **2011**, *17* (36), 9897–9900. https://doi.org/10.1002/chem.201101492.
(29) Diemoz, K. M.; Wilson, S. O.; Franz, A. K. Synthesis of Structurally Varied 1,3-Disiloxanediols and Their Activity as Anion-Binding Catalysts. *Chemistry (Easton).* **2016**, *22* (51), 18349–18353. https://doi.org/10.1002/chem.201604103.
(30) Schafer, A. G.; Wieting, J. M.; Fisher, T. J.; Mattson, A. E. Chiral Silanediols in Anion-Binding Catalysis. *Angew. Chemie Int. Ed.* **2013**, *52* (43), 11321–11324. https://doi.org/https://doi.org/10.1002/anie.201305496.
(31) Tran, N. T.; Wilson, S. O.; Franz, A. K. Cooperative Hydrogen-Bonding Effects in Silanediol Catalysis. *Org. Lett.* **2012**, *14* (1), 186–189. https://doi.org/10.1021/ol202971m.
(32) Schafer, A. G.; Wieting, J. M.; Mattson, A. E. Silanediols: A New Class of Hydrogen Bond Donor Catalysts. *Org. Lett.* **2011**, *13* (19), 5228–5231. https://doi.org/10.1021/ol2021115.
(33) Roder, A.; Kob, W.; Binder, K. Structure and Dynamics of Amorphous Silica Surfaces. *J. Chem. Phys.* **2001**, *114* (17), 7602–7614. https://doi.org/10.1063/1.1360257.
(34) Zhu, H. Y.; Zhao, X. S.; Lu, G. Q.; Do, D. D. Improved Comparison Plot Method for Pore Structure Characterization of MCM-41. *Langmuir* **1996**, *12* (26), 6513–6517. https://doi.org/10.1021/la960541v.
(35) Duchateau, R.; Dijkstra, T. W.; van Santen, R. A.; Yap, G. P. Silsesquioxane Models for Silica Surface Silanol Sites with Adjacent Siloxide Functionalites and Olefin Polymerization Catalysts Thereof. *Chemistry (Easton).* **2004**, *10* (16), 3979–3990. https://doi.org/10.1002/chem.200400206.
(36) Narayan, R.; Nayak, U. Y.; Raichur, A. M.; Garg, S. Mesoporous Silica Nanoparticles: A Comprehensive Review on Synthesis and Recent Advances. *Pharmaceutics* **2018**, *10* (3), 1–49. https://doi.org/10.3390/pharmaceutics10030118.
(37) Ciriminna, R.; Fidalgo, A.; Pandarus, V.; Béland, F.; Ilharco, L. M.; Pagliaro, M. The Sol–Gel Route to Advanced Silica-Based Materials and Recent Applications. *Chem. Rev.* **2013**, *113* (8), 6592–6620. https://doi.org/10.1021/cr300399c.
(38) Lofgreen, J. E.; Ozin, G. A. Controlling Morphology and Porosity to Improve Performance of Molecularly Imprinted Sol–Gel Silica. *Chem. Soc. Rev.* **2014**, *43* (3), 911–933. https://doi.org/10.1039/C3CS60276A.
(39) Vallet-Regí, M.; Balas, F. Silica Materials for Medical Applications. *Open Biomed. Eng. J.* **2008**, *2* (1), 1–9. https://doi.org/10.2174/1874120700802010001.
(40) Biessikirski, A.; Barański, K.; Pytlik, M.; Kuterasiński, Ł.; Biegańska, J.; Słowiński, K. Application of Silicon Dioxide as the Inert Component or Oxide Component Enhancer in Anfo. *Energies* **2021**, *14* (8), 1–12. https://doi.org/10.3390/en14082152.
(41) Shinde, P. S.; Suryawanshi, P. S.; Patil, K. K.; Belekar, V. M.; Sankpal, S. A.; Delekar, S. D.; Jadhav, S. A. A Brief Overview of Recent Progress in Porous Silica as Catalyst Supports. *J. Compos. Sci.* **2021**, *5* (3), 1–17. https://doi.org/10.3390/jcs5030075.
(42) Erigoni, A.; Diaz, U. Porous Silica-Based Organic-Inorganic Hybrid Catalysts: A Review. *Catalysts* **2021**, *11* (1), 1–39. https://doi.org/10.3390/catal11010079.
(43) Pullukat, T. J.; Hoff, R. E. Silica-Based Ziegler-Natta Catalysts: A Patent Review. *Catal.*

*Rev. - Sci. Eng.* **1999**, *41* (3–4), 389–428. https://doi.org/10.1081/CR-100101172.
(44) Holland, B. T.; Subramani, V.; Gangwal, S. K. Utilizing Colloidal Silica and Aluminum-Doped Colloidal Silica as a Binder in FCC Catalysts: Effects on Porosity, Acidity, and Microactivity. *Ind. Eng. Chem. Res.* **2007**, *46* (13), 4486–4496. https://doi.org/10.1021/ie0702734.
(45) Shumaila, A. M. A.; Kusurkar, R. S. Silica Gel, an Effective Catalyst for the Reaction of Electron-Deficient Nitro-Olefins with Nitrogen Heterocycles. *Synth. Commun.* **2010**, *40* (19), 2935–2940. https://doi.org/10.1080/00397910903340694.
(46) Comerford, J. W.; Clark, J. H.; Macquarrie, D. J.; Breeden, S. W. Clean, Reusable and Low Cost Heterogeneous Catalyst for Amide Synthesis. *Chem. Commun.* **2009**, No. 18, 2562–2564. https://doi.org/10.1039/B901581G.
(47) Jin, Y.; Li, J.; Peng, L.; Gao, C. Discovery of Neat Silica Gel as a Catalyst: An Example of S → O Acetyl Migration Reaction. *Chem. Commun.* **2015**, *51* (84), 15390–15393. https://doi.org/10.1039/C5CC05396J.
(48) Kamitori, Y.; Hojo, M.; Masuda, R.; Izumi, T.; Tsukamoto, S. Silica Gel as an Effective Catalyst for the Alkylation of Phenols and Some Heterocyclic Aromatic Compounds. *J. Org. Chem.* **1984**, *49* (22), 4161–4165. https://doi.org/10.1021/jo00196a012.
(49) Kotsuki, H.; Hayashida, K.; Shimanouchi, T.; Nishizawa, H. High-Pressure Organic Chemistry. 19. High-Pressure-Promoted, Silica Gel-Catalyzed Reaction of Epoxides with Nitrogen Heterocycles1,. *J. Org. Chem.* **1996**, *61* (3), 984–990. https://doi.org/10.1021/jo951106t.
(50) Doyle, A. G.; Jacobsen, E. N. Small-Molecule H-Bond Donors in Asymmetric Catalysis. *Chem. Rev.* **2007**, *107* (12), 5713–5743. https://doi.org/10.1021/cr068373r.
(51) Sherrington, D. C.; Taskinen, K. A. Self-Assembly in Synthetic Macromolecular Systems Multiple Hydrogen Bonding Interactions. *Chem. Soc. Rev.* **2001**, *30* (2), 83–93. https://doi.org/10.1039/B008033K.
(52) Scheerder, J.; Engbersen, J. F. J.; Casnati, A.; Ungaro, R.; Reinhoudt, D. N. Complexation of Halide Anions and Tricarboxylate Anions by Neutral Urea-Derivatized p-Tert-Butylcalix[6]Arenes. *J. Org. Chem.* **1995**, *60* (20), 6448–6454. https://doi.org/10.1021/jo00125a035.
(53) DeFord, J.; Chu, F.; Anslyn, E. V. Dimerization Constants for Phosphoric Acid Diesters. *Tetrahedron Lett.* **1996**, *37* (12), 1925–1928. https://doi.org/https://doi.org/10.1016/0040-4039(96)00184-0.
(54) Kondo, S.-I.; Harada, T.; Tanaka, R.; Unno, M. Anion Recognition by a Silanediol-Based Receptor. *Org. Lett.* **2006**, *8* (20), 4621–4624.
(55) Sieburth, S. M.; Chen, C.-A. Silanediol Protease Inhibitors: From Conception to Validation. *European J. Org. Chem.* **2006**, No. 2, 311–322.
(56) Tran, N. T.; Wilson, S. O.; Franz, A. K. Supramolecular Hydrogen-Bonding Assembly of Silanediols with Bifunctional Heterocycles. *Chem. Commun.* **2014**, *50* (28), 3738–3740. https://doi.org/10.1039/c4cc00672k.
(57) Parvin, T.; Yadav, R.; Choudhury, L. H. Recent Applications of Thiourea-Based Organocatalysts in Asymmetric Multicomponent Reactions (AMCRs). *Org. Biomol. Chem.* **2020**, *18* (29), 5513–5532. https://doi.org/10.1039/D0OB00595A.
(58) Serdyuk, O. V; Heckel, C. M.; Tsogoeva, S. B. Bifunctional Primary Amine-Thioureas in Asymmetric Organocatalysis. *Org. Biomol. Chem.* **2013**, *11* (41), 7051–7071. https://doi.org/10.1039/C3OB41403E.

(59) Ford, D. D.; Lehnherr, D.; Kennedy, C. R.; Jacobsen, E. N. On- and Off-Cycle Catalyst Cooperativity in Anion-Binding Catalysis. *J. Am. Chem. Soc.* **2016**, *138* (25), 7860–7863. https://doi.org/10.1021/jacs.6b04686.
(60) Kennedy, C. R.; Lehnherr, D.; Rajapaksa, N. S.; Ford, D. D.; Park, Y.; Jacobsen, E. N. Mechanism-Guided Development of a Highly Active Bis-Thiourea Catalyst for Anion-Abstraction Catalysis. *J. Am. Chem. Soc.* **2016**. https://doi.org/10.1021/jacs.6b09205.
(61) Pescarmona, P. P.; Aprile, C.; Swaminathan, S. Silsesquioxanes and Their Use as Precursors for Catalysts and as Model Compounds. In *New and Future Developments in Catalysis*; 2013; pp 385–422. https://doi.org/10.1016/b978-0-444-53876-5.00018-0.
(62) Han, X.; Zhang, X.; Guo, Y.; Liu, X.; Zhao, X.; Zhou, H.; Zhang, S.; Zhao, T. Synergistic Effects of Ladder and Cage Structured Phosphorus-Containing POSS with Tetrabutyl Titanate on Flame Retardancy of Vinyl Epoxy Resins. *Polymers* . 2021. https://doi.org/10.3390/polym13091363.
(63) Blanco, I. The Rediscovery of POSS: A Molecule Rather than a Filler. *Polymers (Basel).* **2018**, *10* (8). https://doi.org/10.3390/polym10080904.
(64) Quadrelli, E. A.; Basset, J.-M. On Silsesquioxanes' Accuracy as Molecular Models for Silica-Grafted Complexes in Heterogeneous Catalysis. *Coord. Chem. Rev.* **2010**, *254* (5–6), 707–728. https://doi.org/10.1016/j.ccr.2009.09.031.
(65) Feher, F. J.; Budzichowski, T. A. Silasesquioxanes as Ligands in Inorganic and Organometallic Chemistry. *Polyhedron* **1995**, *14* (22), 3239–3253. https://doi.org/https://doi.org/10.1016/0277-5387(95)85009-0.
(66) Liu, S.; Guo, R.; Li, C.; Lu, C.; Yang, G.; Wang, F.; Nie, J.; Ma, C.; Gao, M. POSS Hybrid Hydrogels: A Brief Review of Synthesis, Properties and Applications. *Eur. Polym. J.* **2021**, *143*, 110180. https://doi.org/https://doi.org/10.1016/j.eurpolymj.2020.110180.
(67) J. Feher, F.; Soulivong, D.; Nguyen, F. Practical Methods for Synthesizing Four Incompletely Condensed Silsesquioxanes from a Single R8Si8O12 Framework. *Chem. Commun.* **1998**, No. 12, 1279–1280. https://doi.org/10.1039/A802670J.
(68) Baney, R. H.; Itoh, M.; Sakakibara, A.; Suzuki, T. Silsesquioxanes. *Chem. Rev.* **1995**, *95* (5), 1409–1430. https://doi.org/10.1021/cr00037a012.
(69) Hybrid Plastics.Com. Several POSS including XX and XX are available for.
(70) Skowronska-Ptasinska, M. D.; Duchateau, R.; van Santen, R. A.; Yap, G. P. A. Methyl Aluminosilsesquioxanes, Models for Lewis Acidic Silica-Grafted Methyl Aluminum Species. *Organometallics* **2001**, *20* (16), 3519–3530. https://doi.org/10.1021/om0102596.
(71) Feher, F. J.; Newman, D. A.; Walzer, J. F. Silsesquioxanes as Models for Silica Surfaces. *J. Am. Chem. Soc.* **1989**, *111* (5), 1741–1748. https://doi.org/10.1021/ja00187a028.
(72) Lichtenhan, J. D.; Hildebrandt, D. A.; Lancaster, L. J. The Thrombogenic Activity of POSS Silanols. *Dalt. Trans.* **2017**, *46* (27), 8788–8796. https://doi.org/10.1039/C7DT00487G.
(73) Feher, F. J.; Newman, D. A. Enhanced Silylation Reactivity of a Model for Silica Surfaces. *J. Am. Chem. Soc.* **1990**, *112* (5), 1931–1936. https://doi.org/10.1021/ja00161a044.
(74) Dijkstra, T. W.; Duchateau, R.; Van Santen, R. A.; Meetsma, A.; Yap, G. P. Silsesquioxane Models for Geminal Silica Surface Silanol Sites. A Spectroscopic Investigation of Different Types of Silanols. *J. Am. Chem. Soc.* **2002**, *124* (33), 9856–9864. https://doi.org/10.1021/ja0122243.
(75) Dutchateau, R. Incompletely Condensed Silsesquioxanes: Versatile Tools in Developing

Silica-Supported Solefin Polymerization Catalusts. *Chem. Rev.* **2001**, *102*, 3525–3542.
(76) Liu, H.; Kondo, S.; Tanaka, R.; Oku, H.; Unno, M. A Spectroscopic Investigation of Incompletely Condensed Polyhedral Oligomeric Silsesquioxanes (POSS-Mono-Ol, POSS-Diol and POSS-Triol): Hydrogen-Bonded Interaction and Host–Guest Complex. *J. Organomet. Chem.* **2008**, *693* (7), 1301–1308. https://doi.org/10.1016/j.jorganchem.2008.01.027.
(77) Kondo, S. ichi; Okada, N.; Tanaka, R.; Yamamura, M.; Unno, M. Anion Recognition by 1,3-Disiloxane-1,1,3,3-Tetraols in Organic Solvents. *Tetrahedron Lett.* **2009**, *50* (23), 2754–2757. https://doi.org/10.1016/j.tetlet.2009.03.134.
(78) Tunstall-Garcia, H.; Charles, B. L.; Evans, R. C. The Role of Polyhedral Oligomeric Silsesquioxanes in Optical Applications. *Adv. Photonics Res.* **2021**, *2* (6), 2000196. https://doi.org/https://doi.org/10.1002/adpr.202000196.
(79) Tanaka, K.; Chujo, Y. Advanced Functional Materials Based on Polyhedral Oligomeric Silsesquioxane (POSS). *J. Mater. Chem.* **2012**, *22* (5), 1733–1746. https://doi.org/10.1039/C1JM14231C.
(80) Seidi, F.; Jouyandeh, M.; Taghizadeh, A.; Taghizadeh, M.; Habibzadeh, S.; Jin, Y.; Xiao, H.; Zarrintaj, P.; Saeb, M. R. Polyhedral Oligomeric Silsesquioxane/Epoxy Coatings: A Review. *Surf. Innov.* **2021**, *9* (1), 3–16. https://doi.org/10.1680/jsuin.20.00037.
(81) Weinhold, F.; West, R. Hyperconjugative Interactions in Permethylated Siloxanes and Ethers: The Nature of the SiO Bond. *J. Am. Chem. Soc.* **2013**, *135* (15), 5762–5767. https://doi.org/10.1021/ja312222k.
(82) Li, Z.; Kong, J.; Wang, F.; He, C. Polyhedral Oligomeric Silsesquioxanes (POSSs): An Important Building Block for Organic Optoelectronic Materials. *J. Mater. Chem. C* **2017**, *5* (22), 5283–5298. https://doi.org/10.1039/c7tc01327b.
(83) Esker, A. R.; Yu, H. Langmuir Monolayers of Siloxanes and Silsesquioxanes. In *Silicone Surface Science*; Owen, M. J., Dvornic, P. R., Eds.; Springer Netherlands: Dordrecht, 2012; pp 195–228. https://doi.org/10.1007/978-94-007-3876-8_7.
(84) Sharma, B.; Verma, R.; Baur, C.; Bykova, J.; Mabry, J. M.; Smith, D. W. Ultra Low Dielectric, Self-Cleansing and Highly Oleophobic POSS-PFCP Aryl Ether Polymer Composites. *J. Mater. Chem. C* **2013**, *1* (43), 7222–7227. https://doi.org/10.1039/C3TC31161A.
(85) Kim, D.-G.; Shim, J.; Lee, J. H.; Kwon, S.-J.; Baik, J.-H.; Lee, J.-C. Preparation of Solid-State Composite Electrolytes Based on Organic/Inorganic Hybrid Star-Shaped Polymer and PEG-Functionalized POSS for All-Solid-State Lithium Battery Applications. *Polymer (Guildf).* **2013**, *54* (21), 5812–5820. https://doi.org/https://doi.org/10.1016/j.polymer.2013.08.049.
(86) Blanco, I. Polyhedral Oligomeric Silsesquioxanes (POSS)s in Medicine. *J. Nanomedicine* **2018**, *1* (1), 1–3. https://doi.org/10.33582/2578-8760/1002.
(87) Hou, P. P.; Gu, K. H.; Zhu, Y. F.; Zhang, Z. Y.; Wang, Q.; Pan, H. B.; Yang, S.; Shen, Z.; Fan, X. H. Synthesis and Sub-10 Nm Supramolecular Self-Assembly of a Nanohybrid with a Polynorbornene Main Chain and Side-Chain POSS Moieties. *RSC Adv.* **2015**, *5* (86), 70163–70171. https://doi.org/10.1039/c5ra12152c.
(88) Blackmond, D. G. Kinetic Profiling of Catalytic Organic Reactions as a Mechanistic Tool. *J. Am. Chem. Soc.* **2015**, *137* (34), 10852–10866. https://doi.org/10.1021/jacs.5b05841.
(89) Blackmond, D. G. Reaction Progress Kinetic Analysis: A Powerful Methodology for Mechanistic Studies of Complex Catalytic Reactions. *Angew. Chemie - Int. Ed.* **2005**, *44*

(28), 4302–4320. https://doi.org/10.1002/anie.200462544.
(90) Bures, J. Variable Time Normalization Analysis: General Graphical Elucidation of Reaction Orders from Concentration Profiles. *Angew. Chemie, Int. Ed. English* **2016**, *55* (52), 16084–16087. https://doi.org/10.1002/anie.201609757.
(91) Bures, J. A Simple Graphical Method to Determine the Order in Catalyst. *Angew. Chemie, Int. Ed. English* **2016**, *55* (6), 2028–2031. https://doi.org/10.1002/anie.201508983.
(92) Martínez-Carrión, A.; Howlett, M. G.; Alamillo-Ferrer, C.; Clayton, A. D.; Bourne, R. A.; Codina, A.; Vidal-Ferran, A.; Adams, R. W.; Burés, J. Kinetic Treatments for Catalyst Activation and Deactivation Processes Based on Variable Time Normalization Analysis. *Angew. Chemie - Int. Ed.* **2019**, *58* (30), 10189–10193. https://doi.org/10.1002/anie.201903878.
(93) Burés, J. What Is the Order of a Reaction? *Top. Catal.* **2017**, *60* (8), 631–633. https://doi.org/10.1007/s11244-017-0735-y.
(94) Verendel, J. J.; Pàmies, O.; Diéguez, M.; Andersson, P. G. Asymmetric Hydrogenation of Olefins Using Chiral Crabtree-Type Catalysts: Scope and Limitations. *Chem. Rev.* **2014**, *114* (4), 2130–2169. https://doi.org/10.1021/cr400037u.
(95) Shende, V. S.; Singh, P.; Bhanage, B. M. Recent Trends in Organocatalyzed Asymmetric Reduction of Prochiral Ketones. *Catal. Sci. Technol.* **2018**, *8* (4), 955–969. https://doi.org/10.1039/C7CY02409F.
(96) Visco, M. D.; Attard, J.; Guan, Y.; Mattson, A. E. Anion-Binding Catalyst Designs for Enantioselective Synthesis. *Tetrahedron Lett.* **2017**, *58* (27), 2623–2628. https://doi.org/10.1016/j.tetlet.2017.05.045.
(97) Brook, M. A. *Silicon in Organic, Organometallic and Polymer Chemistry*; John Wiley & Sons, Inc., 2000.
(98) Shintani, R. Recent Advances in the Transition-Metal-Catalyzed Enantioselective Synthesis of Silicon-Stereogenic Organosilanes. *Asian J. Org. Chem.* **2015**, *4*, 510–514. https://doi.org/10.1002/ajoc.201500066.
(99) Shintani, R. Recent Progress in Catalytic Enantioselective Desymmetrization of Prochiral Organosilanes for the Synthesis of Silicon-Stereogenic Compounds. *Synlett* **2018**, *29* (4), 388–396. https://doi.org/10.1055/s-0036-1591839.
(100) Corriu, R. J. P.; Moreau, J. J. E. Asymmetric Synthesis at Silicon. *J. Organomet. Chem.* **1976**, *120* (3), 337–346. https://doi.org/http://dx.doi.org/10.1016/S0022-328X(00)98043-4.
(101) Corriu, R. J. P.; Guérin, C.; Moreau, J. J. E. Stereochemistry at Silicon. *Topics in Stereochemistry*. January 1, 1984, pp 43–198. https://doi.org/doi:10.1002/9780470147245.ch2.
(102) Koga, S.; Ueki, S.; Shimada, M.; Ishii, R.; Kurihara, Y.; Yamanoi, Y.; Yuasa, J.; Kawai, T.; Uchida, T. A.; Iwamura, M.; Nozaki, K.; Nishihara, H. Access to Chiral Silicon Centers for Application to Circularly Polarized Luminescence Materials. *J. Org. Chem.* **2017**, *82* (12), 6108–6117. https://doi.org/10.1021/acs.joc.7b00583.
(103) Schmidt, D. R.; O'Malle, S. J.; Leighton, J. L. Catalytic Asymmetric Silane Alcoholysis: Practical Access to Chiral Silanes. *J. Am. Chem. Soc.* **2003**, *125* (5), 1190–1191. https://doi.org/10.1021/ja0283201.
(104) Nakagawa, Y.; Chanthamath, S.; Fujisawa, I.; Shibatomi, K.; Iwasa, S. Ru(Ii)-Pheox-Catalyzed Si–H Insertion Reaction: Construction of Enantioenriched Carbon and Silicon Centers. *Chem. Commun.* **2017**, *53* (26), 3753–3756.

https://doi.org/10.1039/C7CC01070B.
(105) Yasutomi, Y.; Suematsu, H.; Katsuki, T. Iridium(III)-Catalyzed Enantioselective Si−H Bond Insertion and Formation of an Enantioenriched Silicon Center. *J. Am. Chem. Soc.* **2010**, *132* (13), 4510–4511. https://doi.org/10.1021/ja100833h.
(106) Cui, Y.-M.; Lin, Y.; Xu, L.-W. Catalytic Synthesis of Chiral Organoheteroatom Compounds of Silicon, Phosphorus, and Sulfur via Asymmetric Transition Metal-Catalyzed C–H Functionalization. *Coord. Chem. Rev.* **2017**, *330*, 37–52. https://doi.org/http://dx.doi.org/10.1016/j.ccr.2016.09.011.
(107) Keipour, H.; Carreras, V.; Ollevier, T. Recent Progress in the Catalytic Carbene Insertion Reactions into the Silicon-Hydrogen Bond. *Org Biomol Chem* **2017**, *15* (26), 5441–5456. https://doi.org/10.1039/c7ob00807d.
(108) Doyle, M. P.; Duffy, R.; Ratnikov, M.; Zhou, L. Catalytic Carbene Insertion into C-H Bonds. *Chem. Rev.* **2010**, *110* (2), 704–724. https://doi.org/10.1021/cr900239n.
(109) Qu, Z.; Shi, W.; Wang, J. A Kinetic Study on the Pairwise Competition Reaction of α-Diazo Esters with Rhodium(II) Catalysts: Implication for the Mechanism of Rh(II)-Carbene Transfer. *J. Org. Chem.* **2001**, *66* (24), 8139–8144. https://doi.org/10.1021/jo0107352.
(110) Landais, Y.; Planchenault, D. Asymmetric Metal Carbene Insertion into the Si□H Bond. *Tetrahedron Lett.* **1994**, *35* (26), 4565–4568. https://doi.org/https://doi.org/10.1016/S0040-4039(00)60729-3.
(111) Bagheri, V.; Doyle, M. P.; Taunton, J.; Claxton, E. E. A New and General Synthesis of .Alpha.-Silyl Carbonyl Compounds by Silicon-Hydrogen Insertion from Transition Metal-Catalyzed Reactions of Diazo Esters and Diazo Ketones. *J. Org. Chem.* **1988**, *53* (26), 6158–6160. https://doi.org/10.1021/jo00261a045.
(112) Tseberlidis, G.; Caselli, A.; Vicente, R. Carbene XH Bond Insertions Catalyzed by Copper(I) Macrocyclic Pyridine-Containing Ligand (PcL) Complexes. *J. Organomet. Chem.* **2017**, *835*, 1–5. https://doi.org/https://doi.org/10.1016/j.jorganchem.2017.02.027.
(113) Liu, Z.; Li, Q.; Yang, Y.; Bi, X. Silver(i)-Promoted Insertion into X–H (X = Si, Sn, and Ge) Bonds with N-Nosylhydrazones. *Chem. Commun.* **2017**, *53* (16), 2503–2506. https://doi.org/10.1039/C6CC09650F.
(114) Davies, H. M. L.; Hansen, T.; Churchill, M. R. Catalytic Asymmetric C−H Activation of Alkanes and Tetrahydrofuran. *J. Am. Chem. Soc.* **2000**, *122* (13), 3063–3070. https://doi.org/10.1021/ja994136c.
(115) Zhu, D.; Chen, L.; Fan, H.; Yao, Q.; Zhu, S. Recent Progress on Donor and Donor–Donor Carbenes. *Chem. Soc. Rev.* **2020**, *49* (3), 908–950. https://doi.org/10.1039/C9CS00542K.
(116) Davies, H. M. L.; Morton, D. Guiding Principles for Site Selective and Stereoselective Intermolecular C–H Functionalization by Donor/Acceptor Rhodium Carbenes. *Chem. Soc. Rev.* **2011**, *40* (4), 1857–1869. https://doi.org/10.1039/C0CS00217H.

# Chapter 1: $^{19}$F NMR Kinetic Analysis of Silsesquioxane H-bonding Catalysis [*]

## 1.1: Introduction

This chapter presents a rigorous kinetic study of incompletely condensed polyhedral oligomeric silsesquioxane (POSS) silanol H-bond-donor (HBD) catalysis using $^{19}$F NMR spectroscopy and modern kinetic analysis. The Franz lab has previously studied organosilanol-based catalysts for C–C bond forming reactions such as Friedel-Crafts alkylations,[1] [4+2] cycloadditions,[2] and anion-abstraction catalysis.[3] Former lab member Dr. Kayla Diemoz studied the catalytic activity of 1,3-disiloxanediols where their high catalytic activity was attributed to the siloxane backbone and vicinal silanols.[1] Because POSS-silanols contain an extended vicinal siloxanol arrangement, this prompted our studies of POSS silanols as a HBD catalyst. Dr. Kayla Diemoz first demonstrated the catalytic activity of POSS silanols and noted complex kinetics, which were further invesigated.[4] The results presented in this chapter were published in *Chemistry: A European Journal*.[5]

Silica gel is one of the most ubiquitous silanol-containing materials used today. Synthetic chemists interact with silanols daily using silica gel. Silanols are the functional group responsible in chromatography for the retention of compounds by H-bonding to acceptor sites.[6] Silica gel is also a solid-state support for heterogeneous catalysts as the silanols can coordinate metal ions.[7] Given the acidic nature of silica gel, it has been used as a catalyst in several C–C forming transformations.[8] Several silanol-containing motifs have been identified on silica gel, including isolated silanols, silanediols, and vicinal silanols (Figure 1.1).[9,10] However, the poor solubility of silica gel limits the use of spectroscopic techniques to learn more about the activity of discrete arrangements on the surface. In addition, silica surfaces often contain mixtures of these arrangements, so structure-activity relationships are challenging to construct.

[*] Reproduced in part with permission from: Jagannathan, J. R.; Diemoz, K. M.; Targos, K.; Fettinger, J. C.; Franz, A. K.. *Chem. – A Eur. J.* **2019**, *25* (65), 14953–14958. Copyright 2019 John Wiley and Sons.

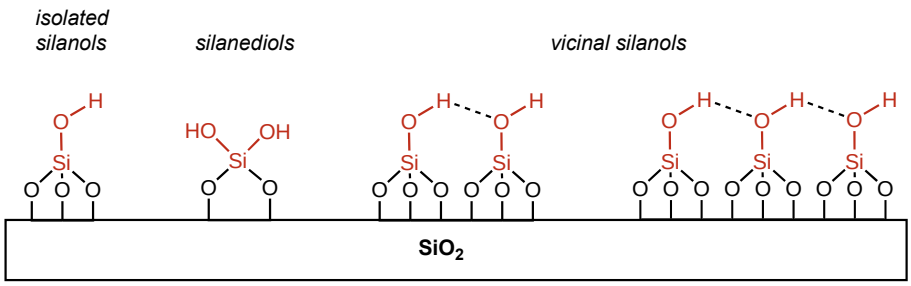


**Figure 1.1.** Silica surface with silanol arrangements known to be present on the surface.

Incompletely condensed polyhedral oligomeric silsesquioxane (POSS) silanols are compounds known for having structural similarities with β-cristobalite, a common polymorph of silica gel (Figure 1.2).[11] Specifically, POSS-triols are described as a "cube missing a corner" shape owing to their rich 3-D architecture. They consist of an inorganic siloxane core ending in silanols, surrounded by organic groups. Initially discovered by Feher, X-ray analysis highlighted similarities with mesoporous silica gel and dealuminated zeolites.[12] Specifically, the bond lengths, Si–Si distances, O–O distances, and silanol density (Figure 1.2) suggest POSS-triol **1.1a** H-bonds similar to vicinal silanols present on the surface of silica gel.[13] POSS-triol **1.1a** exhibits a p$K_a$ similar to silica gel (Figure 1.2).[13] POSS-triols are also soluble in solvents such as ether, $CHCl_3$, and $CCl_4$, allowing for spectroscopic study in solution with IR spectroscopy and NMR spectroscopy techniques. POSS-triols serve as a platform for synthesis of novel POSSs by altering the quantity and orientation of silanols. Overall, the properties of POSS-triols such as **1.1a** make them attractive targets for model studies.

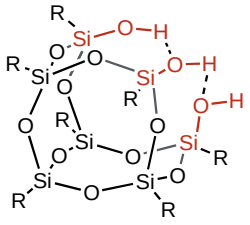

**1.1a**; R = $C_6H_{11}$


| | R = $C_5H_9$ | β-cristabolite |
|---|---|---|
| Si–Si distance (Å) | 3.12 | 3.08 |
| O–O distance (Å) | 2.63 | 2.52 |
| Si–OH's per 100 Å$^2$ | 4.81 | 4.55 |
| p$K_a$ | 7.6 | 6.8 |

**Figure 1.2.** Comparison of POSS-triols to β-cristobalite.

The synthetic routes to access POSS-triols are quite diverse depending on the organic substituent. Most routes start from trichlorosilanes or trialkoxy silanes **1.2**, which after hydrolysis, form silanetriol **1.3**, the key intermediate for siloxane synthesis.[14] Silane triols can partially condense onto each other (seven silicon units total) to furnish POSS-triols, controlled by pH, temperature, and concentration (Figure 1.3A).[11] Controlling the condensation-hydrolysis equilibrium is notably substrate-dependent and a current shortcoming of POSS methodology. Incompletely condensed POSS-triols can also be accessed through controlled hydrolysis of condensed POSS with a strong acid or base (Figure 1.3B).[15,16] Several POSS are commercially available, which are a platform for more complicated syntheses about the silanols.[17]

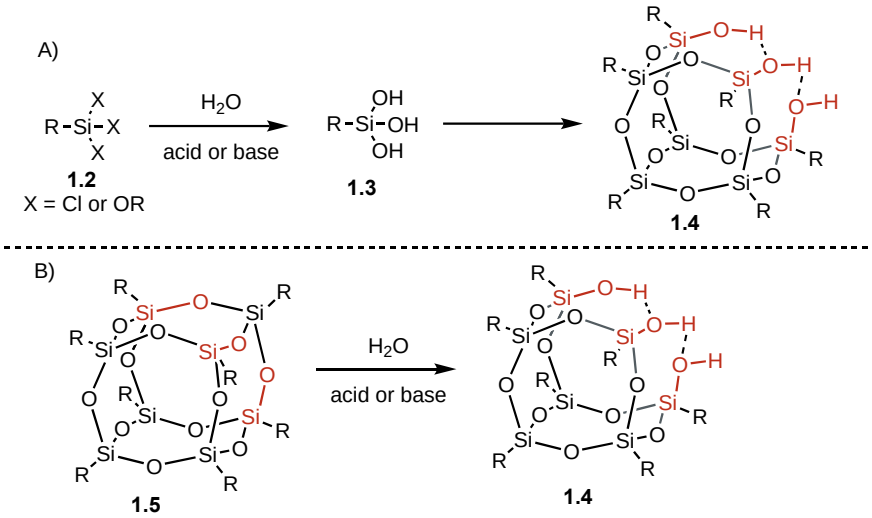


**Figure 1.3.** Synthetic routes to access POSS-triols.

The applications of POSS are quite diverse. Given the rich 3-D architecture of these molecules, they have been incorporated into composites,[18] polymers,[19] flame retardant materials,[20] and biomedical materials.[21,22] POSS-triols are used for applications in modeling silica surfaces, and several examples will be explained below. A model study with POSS included synthesis of novel silanols and subsequent spectroscopic investigation.[23] Yap and coworkers reported syntheses of POSS-silanols **1.6** and **1.7** from POSS-triol **1.1a** and chlorosilanes (Figure 1.5). The authors calculated p$K_a$'s of **1.1a**, **1.6** and **1.7** via ion-pairing acidity measurements using $Li^+$[9-(cyano)fluorenide]$^-$•2THF and $Li^+$[9-(methoxycarbonyl)fluorenide]$^-$•2THF. A two unit difference in p$K_a$ between triol **1.1a** and **1.6** was observed. The authors attributed this decrease in acidity to a shorter intramolecular H-bond network. A smaller p$K_a$ difference was observed between POSS **1.6** and **1.7**. Complementary studies using solid-state (nujol) and solution phase IR spectroscopy

in $CCl_4$ shows three distinct regions for silanols: isolated silanols (3700 $cm^{-1}$), silanediols (3700 $cm^{-1}$ and 3584 $cm^{-1}$), and POSS-triols (3225 $cm^{-1}$). Both POSSs **1.1a** and **1.6** participate in intermolecular H-bonding in solution and solid-state, evidenced by the broadening of the Si-OH stretch. POSS-triol **1.1a** produced identical IR spectra in solution and the solid-state, suggesting H-bonding is similar in both phases. The frequencies observed for isolated silanol **1.7** (3700 $cm^{-1}$) fit closely with silica gel containing isolated silanols. Overall, the authors concluded that the silanol configurations of POSS **1.1**, **1.6** and **1.7** H-bond similar to silanols found on a silica gel surface. Additionally, the most acidic sites on silica gel contain vicinal H-bonding arrangements, not silanediols.

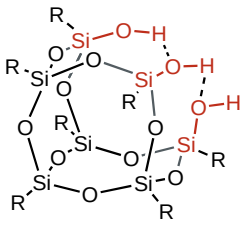

**1.1a**; R = $C_6H_{11}$

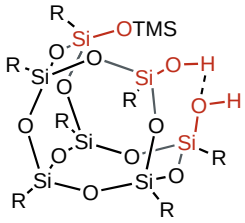

**1.6**; R = $C_6H_{11}$

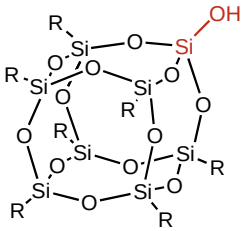

**1.7**; R = $C_6H_{11}$

| | **1.1a** | **1.6** | **1.7** |
|---|---|---|---|
| Si–OH stretch ($cm^{-1}$) | 3225 (br) | 3700 (s), 3582 (s) | 3700 (s) |
| p$K_a$ | 7.6 ± 0.2 | 9.5 ± 0.1 | 8.9 ± 0.4 |

**Figure 1.4.** Spectroscopic investigation of silanol arrangements in accordance to p$K_a$.

Feher reported another study using POSS-triols to model the silylation of silica gel.[24] Silylation of silica gel is a common reaction done to prepare functional silica surfaces,[25] functional materials,[26] and supported catalysts.[27] However, the selectivity of silylation between arrangements of silanols present on silica surfaces has not been clearly deduced due to the insolubility of silica gel. POSS **1.1a** was subjected to silylation using TMS–Cl and amine bases. In the presence of $Et_3N$, POSS **1.1a** exhibited >99:1 selectivity for monosilylated POSS **1.6** compared to disilylated **1.8** in several solvents including ether, THF, and $CHCl_3$ (Figure 1.6). Selectivity between **1.8** and **1.9** was approximately 10:1, correlating with p$K_a$ data.[23] The presence of base was crucial to provide reactivity and selectivity for the monosilylation product, suggesting acidity is an essential factor that imparts selectivity. The authors attribute this high selectivity to intramolecular H-bonding leading to lower acidity in triol **1.1a**. Overall, the authors concluded that vicinal silanol sites on silica surfaces are the fastest to be silylated, and acidity can be used to predict which sites will react first qualitatively.

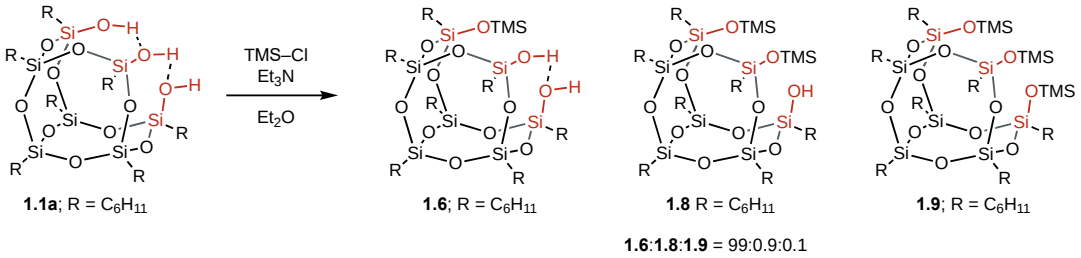


**Figure 1.5.** Modeling silylation of silica gel with POSS-triols.

Kondo and coworkers investigated POSS-triol H-bonding in solution with POSS-triol **1.1b**.[28] POSS-triol **1.1b** H-bonded in two possible conformations: intermolecular H-bonding with anionic Lewis bases (Figure 1.6A) and self-association into dimeric species (Figure 1.15b). The authors noted that binding studies needed to be conducted at a sufficiently low concentration (0.005 M) so that self-association would not interfere with H-bonding with Lewis bases. The strength of H-bonds to Lewis bases was comparable to previous work with 1,3-disloxanediols and silanediols, suggesting there are potential applications of POSS-triols as H-bonding catalysts.[29,30]

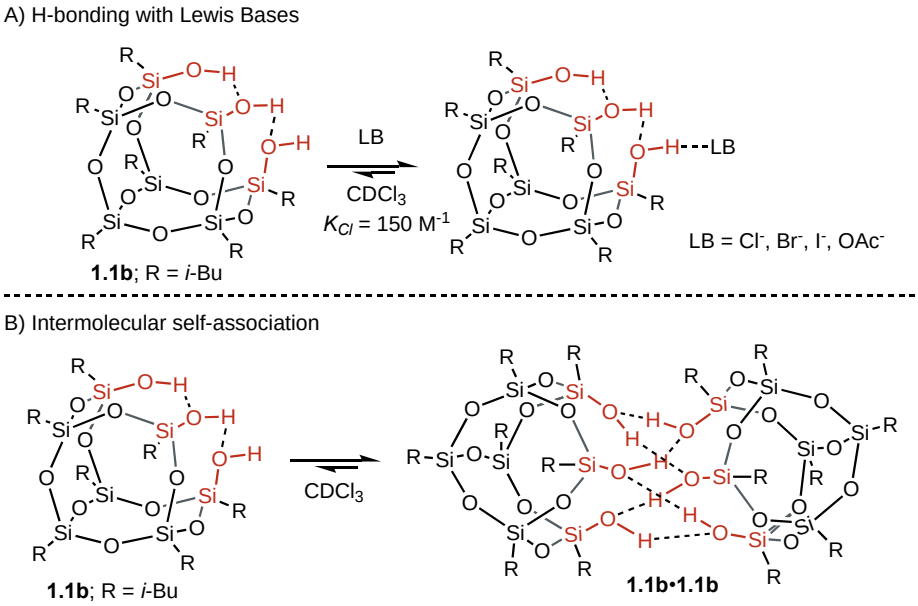


**Figure 1.6.** H-bonding of POSS-triols. A) H-bonding with Lewis bases; B) Intermolecular self-association.

The Franz group and others have recently highlighted the applications of silanols, such as **1.10**-**1.12** and related compounds, as small-molecule organocatalysts.[26–28] Silanols were active in several transformations, including conjugate addition reactions,[1] [4+2] cycloadditions,[2] and anion-abstraction catalysis.[3] Modes of catalysis are based on LUMO-lowering and anion abstraction to

accelerate rate. Binding studies using $^{1}$H NMR spectroscopy allow for the quantification of H-bonding ability which can then be related to catalyst activity. Additionally, concentration effects on H-bonding ability can be explored. In general, more acidic silanol arrangements tended to be more active catalysts. Given that POSS-triols such as **1.1a** are comparable in acidity to **1.11** (p$K_a$ = 6.8 vs. p$K_a$ = 5.9),[31,32] POSS-triols were predicted to be active H-bond-donor catalysts, but no studies had been completed prior to work in the Franz group. Given that silica gel is an active H-bond catalyst, studies of POSS-triol H-bond catalysis have potential to provide insight into the mechanism.

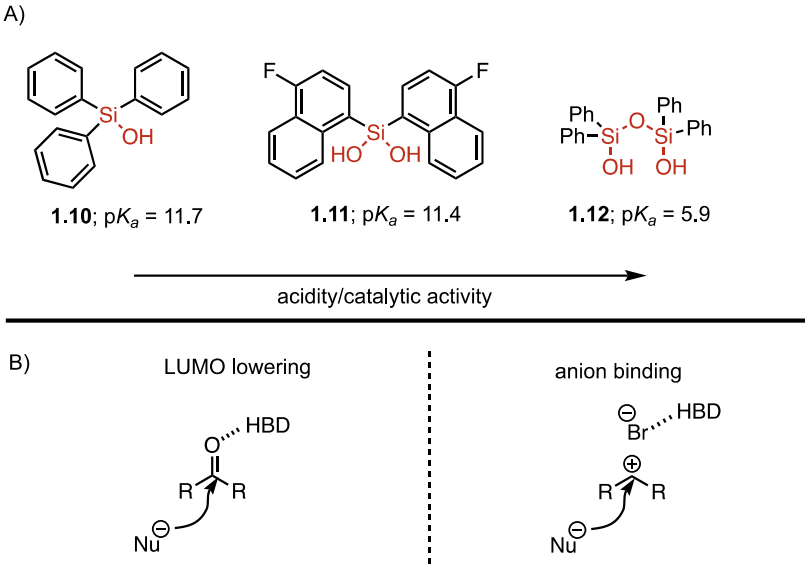


**Figure 1.7.** A) Previously studied organosilanol H-bonding catalysts from the Franz lab. B) Modes of activation for organosilanol HBD catalysis.

## 1.2: Addition of Indole to Nitrostyrene With Known HBD Catalysts and POSS-triols

POSS-triol HBD catalysis was examined using a reaction known to be catalyzed by H-bond donors. The reaction between nitrostyrene **1.13a** and indole **1.14a** has been studied previously with several compounds, including squaramides,[33] phosphoric acids,[34] and thioureas.[35] Silica gel is known to catalyze this transformation,[36] which allows for comparative studies with POSS **1.1b** and **1.1c**. Several control experiments in the absence of catalyst accounted for background rates in $CH_2Cl_2$, *o*-DCB, and neat (5%, 24% and 32% respectively, Table 1, entries 1-3). Solvent effects can also provide insight into possible cooperative or inhibitory H-bonding.[37] A

higher yield was observed with *o*-DCB given the higher dielectric constant. The addition of water did not affect the yield in $CH_2Cl_2$ (Table 1, entries 4-5).

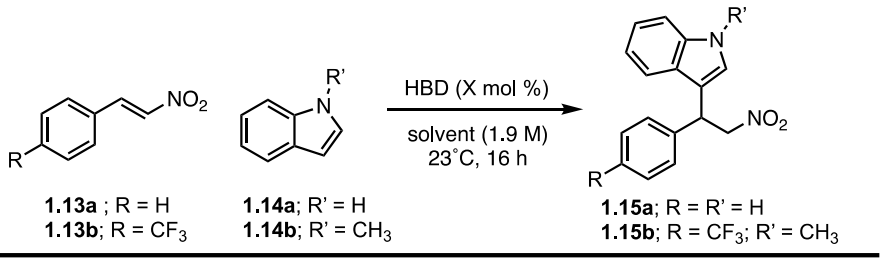


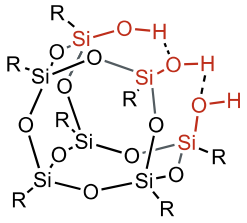


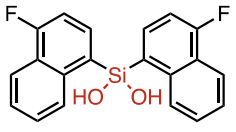


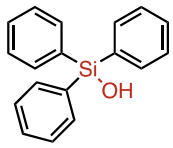


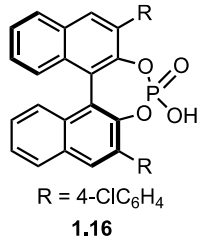


**Table 1.1.** NMR yields for the addition of **1.14a-b** to **1.13a-b** with H-bond-donor catalysts[a]

| Entry | HBD | Mol % | solvent | % Yield | %Yield - Background | $k_{rel}$[b] |
|---|---|---|---|---|---|---|
| 1 | none | - | $CH_2Cl_2$ | 5 | - | - |
| 2 | none | - | *o*-DCB | 24 | - | - |
| 3 | none | - | none | 32 | - | - |
| 4 | $H_2O$ (5 equiv) | - | $CH_2Cl_2$ | 5 | 0 | - |
| 5 | $H_2O$ (1 drop) | - | $CH_2Cl_2$ | 5 | 0 | - |
| 6 | **1.1b** | 20 | $CH_2Cl_2$ | 12 | 7 | ND |
| 7 | **1.1b** | 20 | none | 30 | 0 | - |
| 8 | **1.1c** | 20 | $CH_2Cl_2$ | 55 | 50 | 7.0 |
| 9 | **1.1c** | 20 | *o*-DCB | 49 | 25 | - |
| 10 | **1.1c** | 20 | none | 43 | 11 | - |
| 11 | **1.10** | 20 | *o*-DCB | 38 | 14 | 1 |
| 12 | **1.11** | 20 | $CH_2Cl_2$ | 49 | 44 | 3.6 |
| 13 | **1.12a** | 20 | $CH_2Cl_2$ | 78 | 73 | 4.1 |
| 14 | **1.12a** | 20 | *o*-DCB | 96 | 72 | - |
| 15 | **1.12b** | 10 | *o*-DCB | 99 | 75 | 5.8 |
| 16[c] | **1.16** | 10 | $CH_2Cl_2$ | 75 | - | - |

[a] 0.038 mmol **1.13a**, 1.5 equiv **1.14a**. Determined using $^1$H NMR spectroscopy with Ph-TMS as an internal standard. [b] [**1.13b**]$_o$ = 0.42 M [**1.14b**]$_o$ = 3.2 M, 10 mol% HBD, [fluorobenzene] = 0.1 M in $CD_2Cl_2$. [c] data from Ref. 34, 1.0 equiv **1.14a**, 0.3 M $CH_2Cl_2$, 48 h.

Several silanol-containing compounds **1.4a-d** previously studied in the Franz group[1,36] were compared to POSS **1.1b** and **1.1c**.[17] POSS **1.1b** provided no increased yield relative to background in $CH_2Cl_2$ and neat (Table 1.1, entries 6 and 7). POSS **1.1c** provided higher yields compared to **1.1b** (55% and 12% respectively) in $CH_2Cl_2$, which is attributed to inductive effects from phenyl substitution. With *o*-DCB as the solvent, the yield of product **1.15a** with POSS **1.1c** was reduced (25%, entries 9). In the absence of solvent, the yield of product **1.15a** with POSS **1.1c** was further reduced (11%, entry 10). Silanols **1.10** and **1.11** were active catalysts, providing similar yields to previous reports (Table 1, entries 11 and 12).[36,38] Silanol **1.12a**, which self-associates with minimal effects on catalytic activity,[3] yields similar amounts of product in $CH_2Cl_2$ (72%) and *o*-DCB (73%) (Table 1, entries 13 and 14). Phosphoric acid **1.16**, studied by Zhang, provided comparable yields to **1.12a** with reduced loading and longer reaction time (entry 16).[34] Overall, POSS **1.1c** was catalytically active in the addition of **1.13a** to **1.14a**, but previously studied silanols and phosphoric acids provide product **1.15a** in higher yield.

Relative rates were determined using a modified version of the reaction between **1.13b** and **1.14b**, shown in Figure 1.8. Fluorobenzene was used as an internal standard. The use of trifluoromethyl substitution for $^{19}F$ NMR enables facile processing by simplifying spectra. In a recent report, Dr. Kayla Diemoz showed that this reaction is useful for kinetic analysis of silanol H-bonding catalysis.[38] Relative rates under pseudo-first-order conditions showed that despite poor yields, POSS **1.1c** provided the highest rate enhancement in the addition of **1.14b** to **1.13b** ($k_{rel}$ = 7.0). The concentration of POSS **1.1c** varied between studies with NMR yields (0.38 M) and NMR rate (0.04 M), suggesting catalyst concentration affects activity. Additionally, nucleophile concentration may affect rate (2.9 M **1.14a** vs. 3.2 M **1.14b**). The rate of POSS **1.1c** surpassed disiloxanediol **1.4b**, one of the most active disiloxanediols synthesized to date ($k_{rel}$ = 5.8 for **1.4b** vs. $k_{rel}$ = 7.0 for **1.1c**). The results from this study inspired a more detailed kinetic analysis of POSS-triol **1.1c** H-bonding catalysis to determine the mechanism.

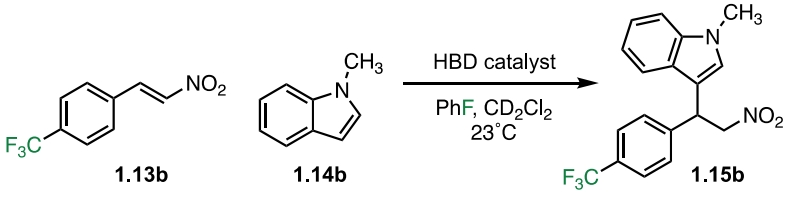


**Figure 1.8.** Indole addition to nitrostyrene for $^{19}F$ NMR reaction monitoring.

## 1.3: Reaction Progress Kinetic Analysis (RPKA) and Variable Time Normalization Analysis (VTNA) using $^{19}$F NMR Spectroscopy

For kinetic analysis, both variable time normalization analysis (VTNA) and reaction progress kinetic analysis (RPKA) were used. Both of these protocols allow for the analysis of chemical transformations at synthetically relevant concentrations. Discussions of these methods can be found on page 10-11 of the Introduction.

### 1.3.1: Catalyst Order Determination using VTNA

Determining catalyst order provides insight into how many catalyst molecules are present in the rate-determining step. VTNA is effective for determination of catalyst orders because there is no need to calculate rate prior to analysis. The effect of catalyst concentration on rate from 0.025 M to 0.15 M POSS **1.1c** was examined. Rate enhancement occurred as concentration increased from 0.025 M→0.075 M and diminished past 0.1 M. POSS **1.1c** was soluble at all concentrations studied.

**Table 1.2.** Concentrations of POSS **1.1c** for catalyst order determination.

| Trial | [**1.1c**] (M) | $k_{obs} \cdot 10^4$ |
|---|---|---|
| 1 | 0.025 | - |
| 2 | 0.05 | 6.1 |
| 3 | 0.075 | 9.0 |
| 4 | 0.10 | 9.9 |
| 5 | 0.125 | 10.6 |
| 6 | 0.150 | 11.7 |

Fluorobenzene = 0.1 M, [**1.13b**]$_o$ = 1.0 M, [**1.14b**]$_o$ = 2.0 M.

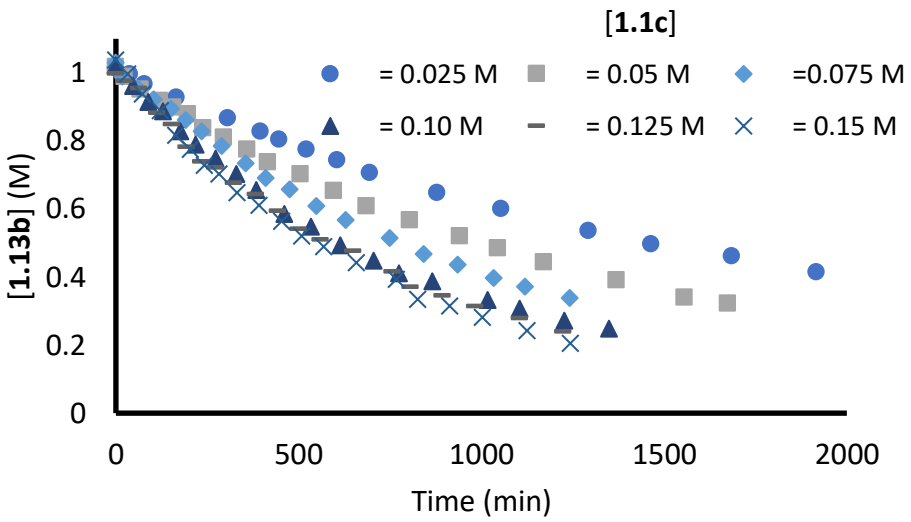


**Figure 1.9.** Concentration vs. time data for trials 1-6. For all trials, [fluorobenzene] = 0.1 M, [**1.13b**]$_o$ = 1.0 M, [**1.14b**]$_o$ = 2.0 M.

VTNA was completed from 0.025 M → 0.15 M according to Eq 1.1 where [A] = [**1.1c**].[39] From the trials, data can be manipulated as shown in Eq 1.1, where the effect of concentration is integrated out from the reaction profile to some value *a*, simplified using the trapezoid rule.[40] At the correct value of *a*, overlap of trials will be observed since all other concentrations are held constant. Assuming the catalyst concentration is constant, it simplifies to [**1.1c**]$^a$ • time vs. [**1.13b**]. The data split into two separate regimes from 0.025 M→0.075 M **1.1c** and 0.10 M to 0.15 M **1.1c**. From 0.025 M to 0.075 M, overlap of all trials occurred with *a* = 0.6 (Figure 1.10A) and from 0.100 M to 0.150 M **1.1c** overlap occurred with *a* = 0.3 (Figure 1.10B). The results indicate that the catalyst order of POSS **1.1c** decreased as total concentration increased. Non-integer catalyst orders could suggest a portion of the catalyst is inactive. For an order of 0.3, 30% of the total amount of catalyst present is active.[40]

$$\int_{t=0}^{t=n}[A]^a dt = \sum_{i=1}^{n}\left(\frac{[A]_i+[A]_{i-1}}{2}\right)^a (t_i - t_{i-1}) \qquad \text{(Eq 1.1)}$$

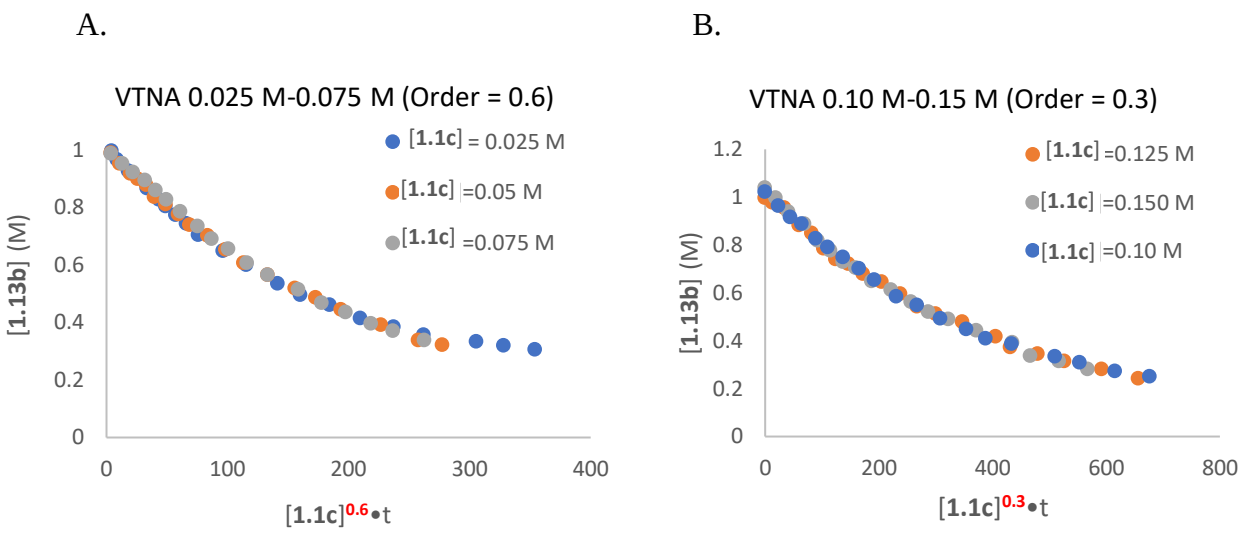


**Figure 1.10.** VTNA of catalyst order. A) From 0.025 M to 0.075 M **1.1c**, an order of 0.6 applied to these data was shown to cause overlap of trials; B) From 0.10 M to 0.15 M **1.1c**, an order of 0.3 applied to these data was shown to cause an overlap of trials. For all experiments, [fluorobenzene] = 0.1 M, [**1.13b**]$_o$ = 1.0 M, [**1.14b**]$_o$ = 2.0 M.

### 1.3.2 Apparent Turnover Frequency Calculations

Apparent turnover frequencies (TOF$_{app}$) were calculated to examine the activity of POSS **1.1c** as concentration changes. Apparent turnover frequency is distinct from turnover frequency (TOF) because it accounts for the effect of concentration on catalyst activity.[41] Previous reports detailing a catalyst concentration-dependent turnover frequency have hypothesized the formation of off-cycle species with varied activity.[42] If newly formed species are less active, TOF$_{app}$ will decrease as the total concentration of catalyst increases. With POSS **1.1c**, TOF$_{app}$ decreased for first-order profiles as the concentrations increased, which suggested the catalyst is less active at higher concentrations (Figure 1.11). The highest TOF$_{app}$ observed was at 0.025 M, the lowest concentration studied. Overall, the data supports reduced rate enhancement as concentration increases, suggesting an inhibitory process that lowers the activity of **1.1c** in solution.

$$TOF_{app}(hr^{-1}) = \frac{k_{obs}}{[cat]} \cdot \frac{60\ min}{1hr} \qquad \text{(Eq. 1.2)}$$

**Table 1.3.** Concentrations and used for apparent turnover frequency calculations.

| Trial | [**1.15a**] (M) | $k_{obs}$ • $10^4$ (M•min$^{-1}$) | TOF$_{app}$ (hr$^{-1}$) |
|---|---|---|---|
| 7 | 0.05 | 7.2 | 0.86 |
| 8 | 0.075 | 8.9 | 0.71 |
| 9 | 0.1 | 11.6 | 0.70 |
| 10 | 0.108 | 11.5 | 0.64 |
| 11 | 0.117 | 12.6 | 0.65 |
| 12 | 0.125 | 13.5 | 0.65 |

[**1.13b**]$_o$ = 0.5 M; [**1.14b**]$_o$ = 2.0 M; fluorobenzene = 0.1 M

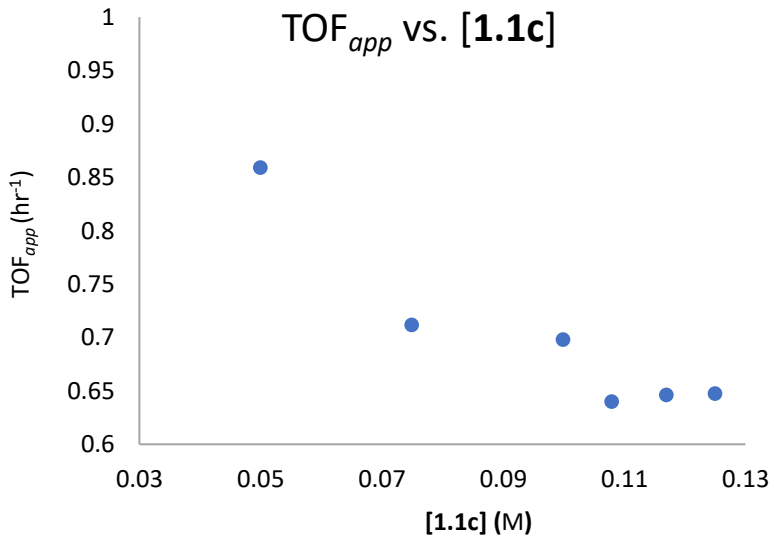


**Figure 1.11.** TOF$_{app}$ vs. [**1.1c**] for trials 7-12. For all experiments, [fluorobenzene] = 0.1 M, [**1.13b**]$_o$ = 0.5 M, [**1.14b**]$_o$ = 2.0 M.

### 1.3.3: "*Different Excess*" Experiments

The order in the reaction between **1.13b** and **1.14b** changes with concentration of POSS-triol **1.1c** (Figure 1.12). A change in the overall order of the reaction can indicate a change in catalyst resting state or even the rate-determining step.[43,44] Determining the orders in reagents for both profiles provided insight into how the mechanism changes.

A. [**1.1c**] = 0.025 M B. [**1.1c**] = 0.10 M

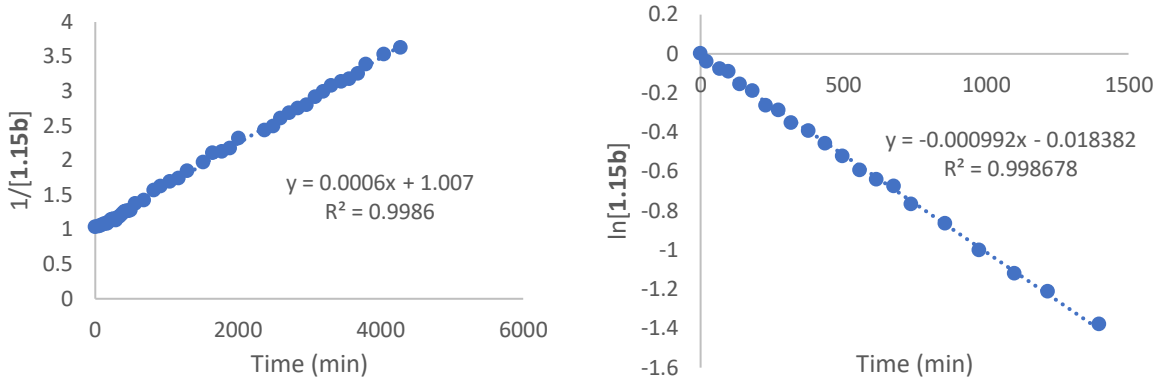


**Figure 1.12.** Variable reaction order observed at varied POSS-triol concentrations, A) Second-order kinetics are observed at 0.025 M **1.1c.** B) First-order kinetics are observed above 0.025 M **1.1c**. For both experiments, [fluorobenzene] = 0.1 M, [**1.13b**]$_o$ = 1.0 M, [**1.14b**]$_o$ = 2.0 M.

In order to investigate the change in mechanism between POSS concentrations, "*different excess*" experiments[45] combined with the VTNA protocol were conducted.[40] These experiments depend on the difference in concentration between two reagents (Eq 1.3) that is varied between trials to calculate the order in a reagent. Two concentrations of POSS **1.1c** were selected (0.1 M and 0.025 M) based on the two profiles observed during catalyst order determination.

$$[\mathbf{1.14b}] = [\mathbf{1.13}\boldsymbol{b}] + [xs] \qquad \text{(Eq. 1.3)}$$

From the "*different excess*" trials, data can be manipulated as shown in Eq 1.4, where the effect of concentration is integrated out from the reaction profile to some value *a*, simplified using the trapezoid rule.[40] At the correct value of *a*, overlap of trials is observed since all other concentrations are held constant.

$$\int_{t=0}^{t=n}[A]^a dt = \sum_{i=1}^{n}\left(\frac{[A]_i+[A]_{i-1}}{2}\right)^a (t_i - t_{i-1}) \qquad \text{(Eq 1.4)}$$

The first set of experiments aimed to determine the order in nitrostyrene **1.13b** at 0.025 M and 0.1 M POSS **1.1c**. A series of four trials were designed where the initial concentration of **1.13b** were varied, and the amount of **1.14b** and POSS **1.1c** were held constant (Table 1.4). The concentration of **1.13b** vs. time for all trials at 0.1 M POSS **1.1c** exhibited 1$^{st}$ order profiles. The concentration of **1.13b** vs. time for all trials at 0.025 M POSS exhibited 2$^{nd}$ order profiles.

**Table 1.4.** Amounts used with varied concentration of nitrostyrene **1.13b** at 0.1 M POSS **1.1c.**

| Trial | [**1.13b**]$_o$ (M) | [**1.14b**]$_o$ (M) | [**1.1c**] (M) |
|---|---|---|---|
| 13 | 1.5 | 2.0 | 0.025 |
| 14 | 1.25 | 2.0 | |
| 15 | 1.5 | 1.6 | 0.1 |
| 16 | 1.25 | 1.6 | |

[fluorobenzene] = 0.1 M

From the data obtained from "*different excess*" experiments, the order in **1.13b** was determined by overlaying trials of **1.15b** vs. Eq 1.4 where [A] = [**1.13b**]. At the correct value of *a*, the effect of [**1.13b**] on rate would integrate out, and overlap of trials would occur. At 0.025 M POSS-triol **1.1c**, rate enhancement occurred when the concentration of **1.13b** was increased, indicating positive order. Overlap of trials occurred when $a = 1$, indicating first order rate dependence with **1.13b** (Figure 1.13 A and B). At 0.025 M POSS **1.1c,** the second-order profile is first order in nitrostyrene **1.13b** and first order in indole **1.14b**, a bimolecular kinetic profile. In the "*different excess*" experiments using 0.1 M POSS **1.1c**, no rate enhancement occurs with increased concentration of nitrostyrene **1.13b.** Overlap of trials occurred at $a = 0$ (Figure 1.13C). The result indicated that the reaction is zeroth order in nitrostyrene **1.13b** and first order in indole **1.14b**, a saturation kinetic profile.

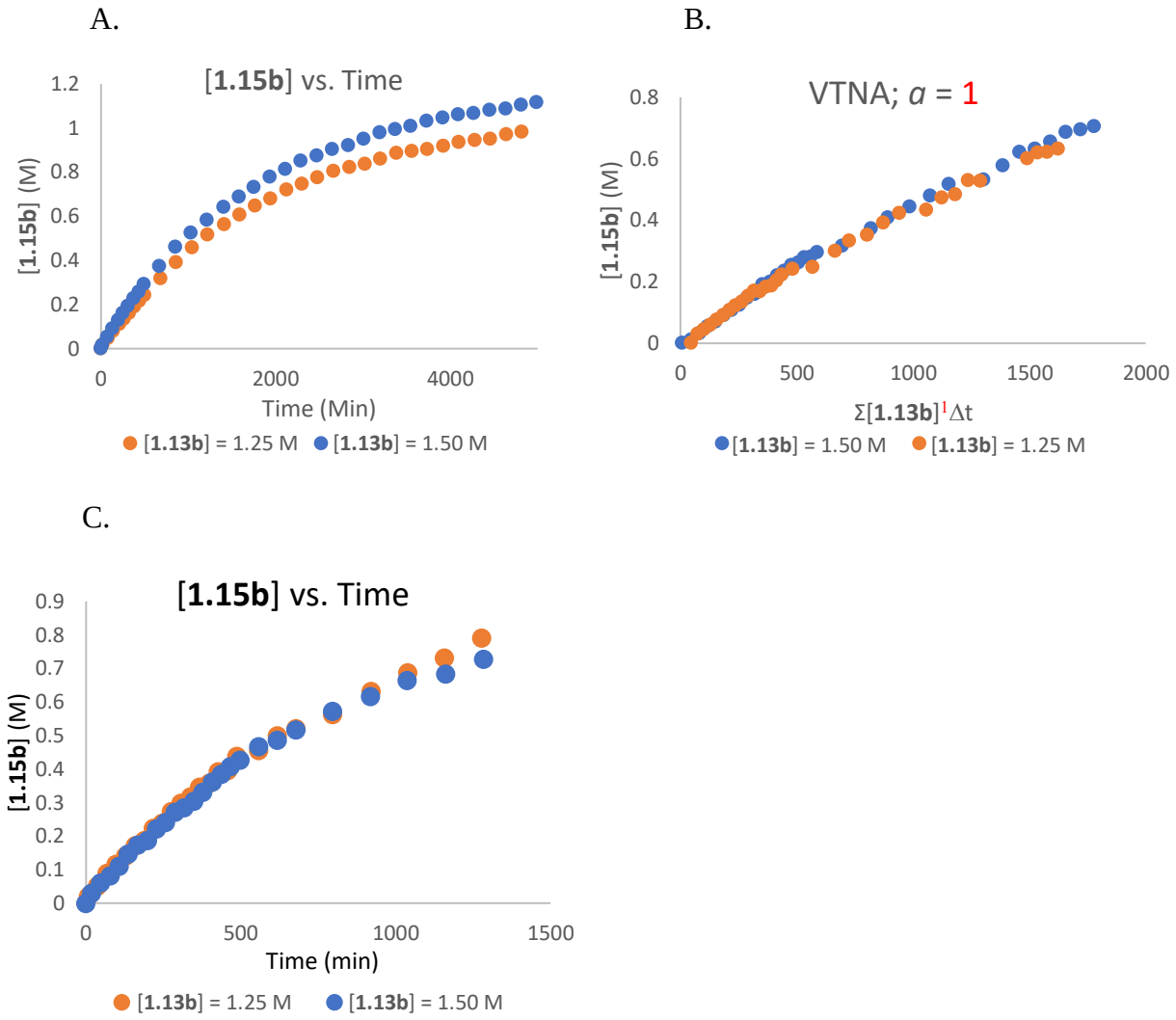


**Figure 1.13**. VTNA for varied nitrostyrene concentration. A) Concentration vs. time plot for varied concentration of **1.13b** with [**1.1c**] = 0.025 M and [**1.14b**]$_o$ = 2.0 M. B) VTNA of reagent order, 1$^{st}$ order was determined from this data when [**1.1c**] = 0.025 M. C) Concentration vs. time data for varied concentration of **1.13b** when [**1.1c**] = 0.1 M and [**1.14b**]$_o$ = 1.6 M; no rate dependence was observed, indicating zero order in nitrostyrene. For all experiments, [fluorobenzene] = 0.1 M.

To confirm both kinetic profiles from the first set of "*different excess*" experiments with **1.13b**, reciprocal "*different excess*" experiments with **1.14b** were conducted (Table 1.5 and Figure 1.14). The order in **1.13b** was determined by overlaying trials of **1.15b** vs. Eq 1.4 where [A] = [**1.14b**]. For both profiles, rate enhancement is observed. Overlap of trials occurred when $a$ = 1, indicating first order rate dependence with **1.14b** (Figure 1.13A and B). These results match those

determined from "*different excess*" experiments with **1.13b**, further supporting the change in order between profiles.

**Table 1.5.** Amounts used for experiments with varied concentration of N-methylindole **1.14b** at 0.1 M and 0.025 M POSS **1.1c.**

| Trial | [**1.13b**]$_o$ (M) | [**1.14b**]$_o$ (M) | [**1.1c**] (M) |
|---|---|---|---|
| 17 | 1.5 | 2.0 | 0.025 |
| 18 | 1.5 | 1.25 | |
| 19 | 1.5 | 2.0 | 0.1 |
| 20 | 1.5 | 1.75 | |

[fluorobenzene] = 0.1 M

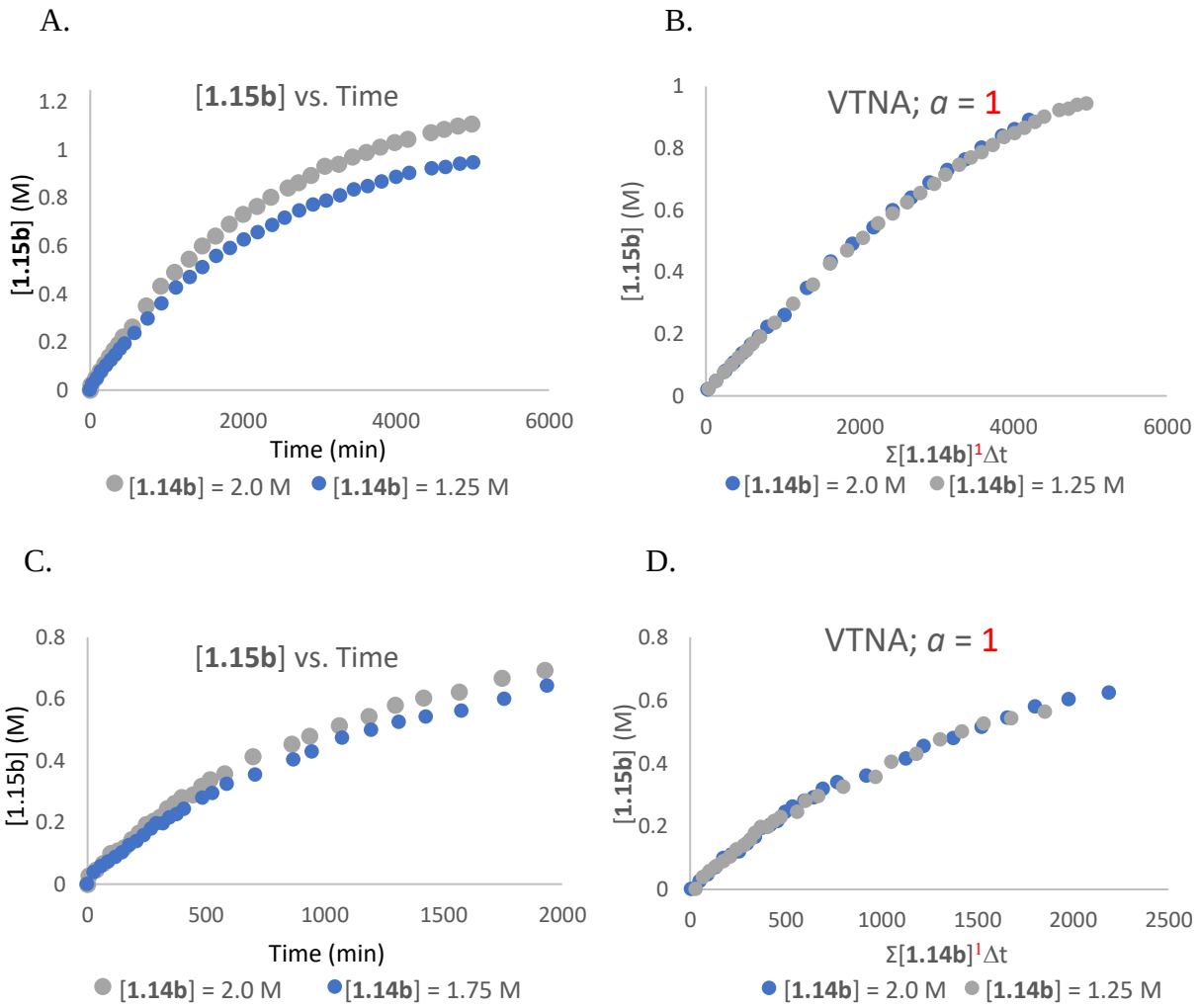


**Figure 1.14**. VTNA for varied indole concentration. A) Concentration vs. time plot for varied concentration of **1.14b** with [**1.1c**] = 0.025 M and [**1.13b**]$_o$ = 1.5 M. B) VTNA of reagent order, 1$^{st}$ order was determined from this data when [**1.1c**] = 0.025 M. C) Concentration vs. time plot for varied concentration of **1.14b** with [**1.1c**] = 0.10 M and [**1.13b**]$_o$ = 1.5 M. D) VTNA of reagent order, 1$^{st}$ order was determined from this data when [**1.1c**] = 0.10 M. For all experiments, [fluorobenzene] = 0.1 M.

### 1.3.4: "*Same Excess*" Experiments

The product contains a nitro group, which has the potential to H-bond with the catalyst. To probe the possibility of catalyst decomposition or product inhibition, "*same excess*" experiments from the RPKA protocol were performed.[45] Time-adjusted kinetic profiles can be constructed by overlaying the trials that started with a lower concentration (trial 22 and 24) of nitrostyrene **1.13b** onto trials with higher concentration of **1.13b** (21 and 23, respectively). A time adjustment should result in the overlap of the reaction profiles if the catalyst performs at the same rate throughout the whole reaction despite product present or fewer turnovers of the catalyst. If the reaction slows down, it can be attributed to product inhibition or catalyst decomposition. Two trials with the "*same excess*" conditions for POSS **1.1c** = 0.10 M and 0.025 M were investigated with nitrostyrene **1.13b** and indole **1.14b** (Figure 1.15). Excellent overlap is observed for time-adjusted trials, demonstrating that the catalyst works at the same efficiency throughout the whole reaction.

**Table 1.6:** Amounts used for experiments under "*same excess*" conditions with POSS **1.1c.**

| Trial | [**1.13b**]$_o$ (M) | [**1.14b**]$_o$ (M) | [**1.1c**] |
|---|---|---|---|
| 21 | 1.0 | 2.0 | 0.025 |
| 22 | 0.5 | 1.5 | |
| 23 | 1.5 | 2.0 | 0.10 |
| 24 | 1.0 | 1.5 | |

[Fluorobenzene] = 0.1 M

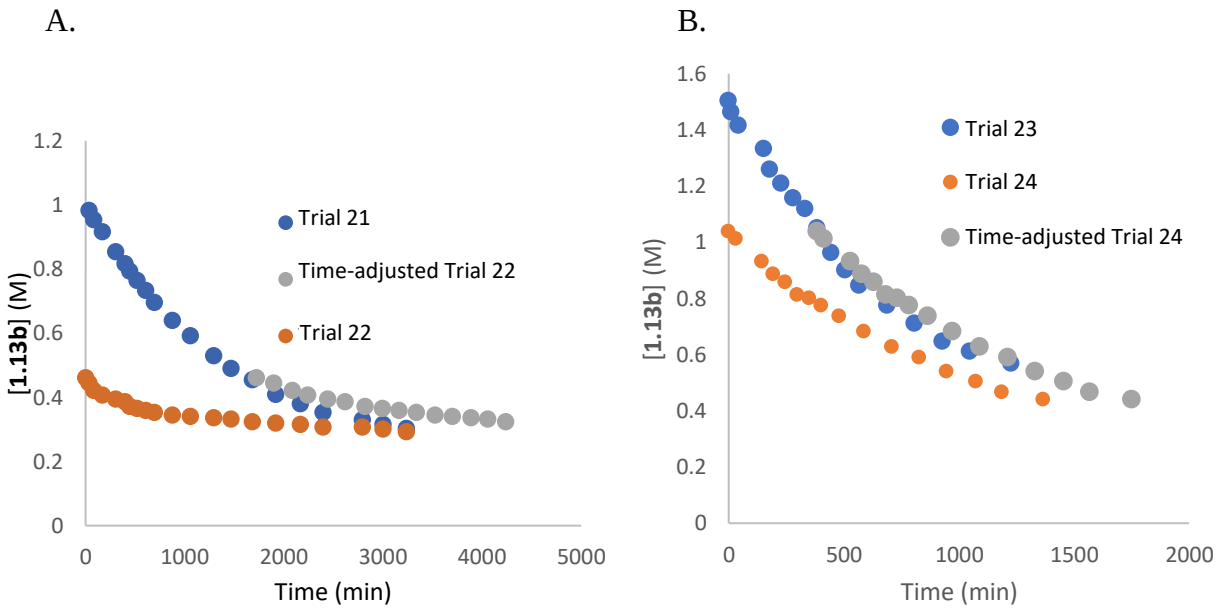


**Figure 1.15.** A) RPKA analysis of "same excess" experiment with [**1.1c**] = 0.10 M. No evidence of product inhibition or catalyst degradation is observed. B) RPKA analysis of "*same excess*" experiment

with [**1.1c**] = 0.025 M. No evidence of product inhibition or catalyst degradation is observed. For all experiments, [fluorobenzene] = 0.1 M.

## 1.3.5: Kinetic Isotope Effect Experiments

Kinetic isotope effect experiments provide complementary information to VTNA and RPKA by probing the rate-determining step in the transformation. Indole **1.14b**-*d* was synthesized because there would be three distinct KIEs based on the steps in the catalytic cycle. Typically, the rate-determining step in this transformation is C–C bond formation,[46] although binding of nitrostyrene **1.13b** has been found to be the rate-determining step with 1,3-disloxanediols.[1] Kinetic isotope effects were measured using **1.14b**-*d* that contained 90% incorporation of deuterium at the 3-position. Parallel experiments under identical concentrations of all components were monitored by $^{19}$F NMR until 75% conversion was observed. A calculated KIE of 1.1 supports C–C bond formation as the rate-determining step. Experiments at 0.025 M POSS **1.1c** were attempted but could not be reproduced.

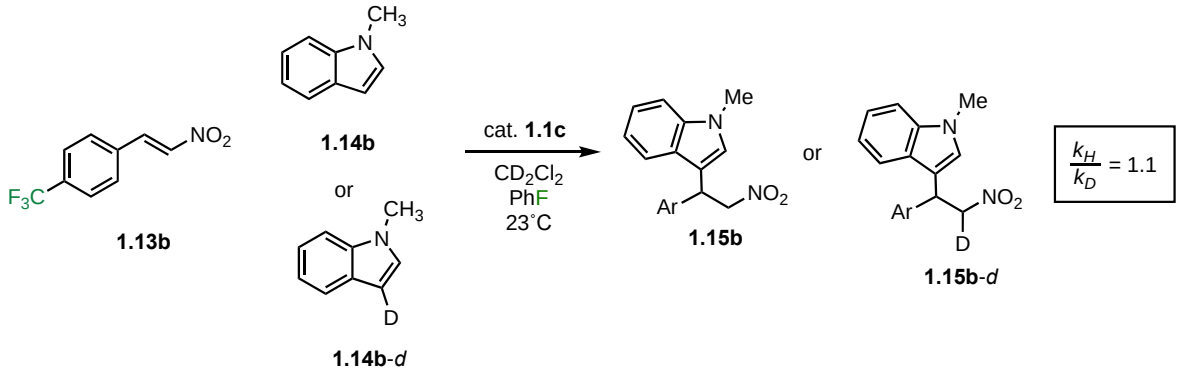


**Table 1.7**. Concentrations of Nitrostyrene **1.13b** and indole **1.14b** and POSS **1.1c**.

| Trial | [**1.13b**]$_o$ (M) | [**1.14b**]$_o$ or [**1.14b**-*d*]$_o$ (M) | [**1.1c**] (M) | $k_{obs}$•$10^4$ (min$^{-1}$) |
|---|---|---|---|---|
| 25 | 1.0 | 2.0, [**1.14b**] | 0.1 | 9.40 |
| 26 | 1.0 | 2.0, [**1.14b**-*d*] | 0.1 | 9.01 |
| 27 | 1.0 | 2.0, [**1.14b**] | 0.1 | 9.40 |
| 28 | 1.0 | 2.0, [**1.14b**-*d*] | 0.1 | 8.32 |

[Fluorobenzene] = 0.1 M

## 1.3.6: Nitrobenzene Additive Experiments

Monitoring reactions in the presence of an inert competitive H-bond acceptor can provide insight into the equilibrium between POSS and **1.13b** prior to C–C bond formation. Previous work

with 1,3-disiloxanediols has shown that the use of competitive H-bonding species can provide mechanistic evidence on the nature of binding to the nitro group.[1] If the equilibrium strongly favors the bound **1.1c•1.13b** species, the presence of an additive such as nitrobenzene would reduce rate compared to a control. If the equilibrium is dynamic between **1.1c** and **1.13b**, the rate should not change with equimolar quantities of **1.13b** and nitrobenzene.

Experiments at 0.075 M and 0.025 M **1.1c** were performed to test both profiles. Nitrobenzene was selected as the Lewis base because it is nitro-containing similar to **1.13b** and would not react with **1.14b**. When overlayed with trials without nitrobenzene, almost perfect overlap is observed. This result indicates that H-bonding to nitro groups is dynamic and reversible. Considering the first order profile fits with a saturation kinetic profile, this result shows it is not actually saturation kinetics. The formation of a **1.13b•1.1c** complex would compete with **1.1c•**nitrobenzene, leading to a reduction in rate.

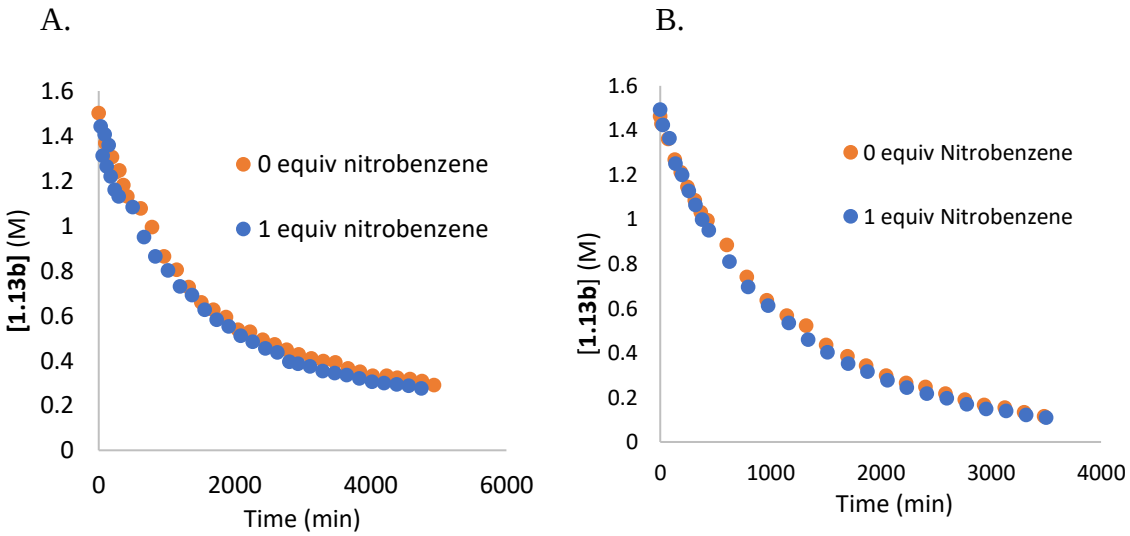


**Figure 1.16.** A) Graph of concentration of [**1.13b**] vs. time, overall first order behavior was observed. [**1.13b**]$_o$ = 1.50 M; [**1.14b**]$_o$ = 2.0 M; B) Graph of concentration of [**1.13b**] vs. time for trials, overall second order behavior was observed. [**1.13b**]$_o$ = 1.50 M; [**1.14b**] = 2.0 M. For all experiments, [fluorobenzene] = 0.1 M.

## 1.4: Diffusion Ordered Spectroscopy (DOSY) studies with POSS-triol 1.1c

$^1$H NMR Diffusion-Ordered Spectroscopy (DOSY) experiments were performed to provide supporting evidence for the formation of self-associated species. The $^1$H NMR DOSY

experiment relies on a pair of gradient pulses that establish a magnetic field gradient within the sample.[47] After a period of time, the sample is pulsed again to determine the change in the magnetic field gradient, and spectra at varied field strength are collected (Figure 1.17A). For samples containing larger molecular weights, the gradient will change less because of the lower diffusion constant. When paired with internal standards that do not coordinate, one can estimate molecular weights of species in solution by generating a standard curve.[48] For analysis, a stacked plot of spectra at varied magnetic field strength can be manipulated to a $^1$H NMR DOSY spectrum using Mestrenova (Figure 1.17B). A diffusion constant (D in $m^2$/sec) for a resonance can be estimated from the value in the F1 domain (Y-axis). $^1$H NMR DOSY has been used to estimate the molecular weights of polymers[49] and to characterize metal-ligand complexes[48] and organolithium compounds.[50] The Franz group has used $^1$H NMR DOSY to study silanediol H-bonding with bifunctional heterocycles[51] and 1,3-disiloxanediol self-association.[3]

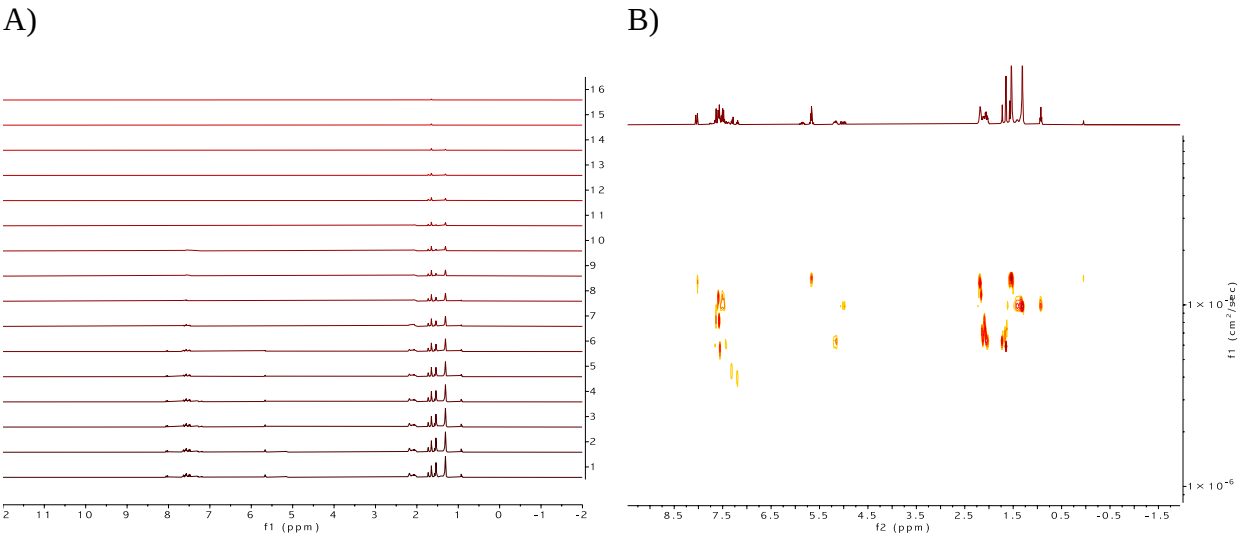


**Figure 1.17**. A) Stacked plot of $^1$H NMR spectrum collected at varied field strength. B) $^1$H NMR DOSY plot.

$^1$H NMR DOSY was used to study the intermolecular self-association of **1.1c** into **1.1c•1.1c** (Figure 1.17). Based on previous reports,[28] internal standards cyclooctene, squalene, and tetradecane were used. Concentrations between 0.05−0.3 M were studied. As concentration increased from 0.05 M to 0.2 M, the calculated molecular weights increased from 927 to 1149

g/mol for POSS **1.1c**. The measured molecular weight is slightly higher than the monomer (931.34 g/mol), indicating some formation of a higher-order species. When concentration increased to 0.3 M, measured molecular weight increased to 1637.8 g/mol, indicating a large portion of POSS **1.1c** in a self-associated species (**1.1c•1.1c**). Overall, $^{1}$H DOSY NMR data supports the formation of self-associated species in solution at higher concentrations.

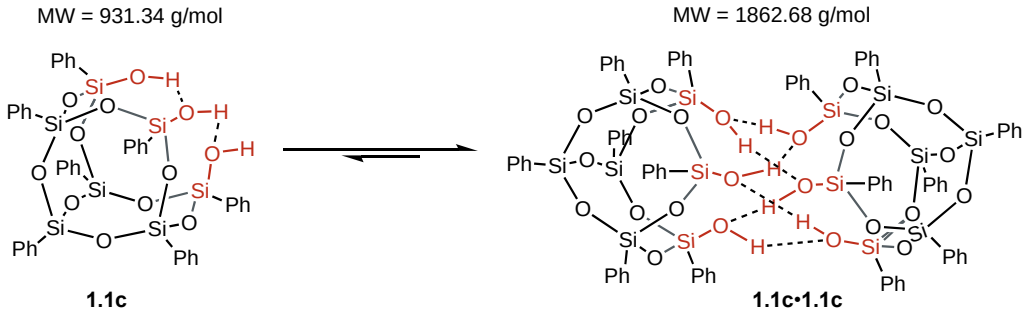


**Figure 1.18**. Self-association equilibrium of POSS-triols with calculated molecular weights.

**Table 1.8**. Diffusion coefficient and measured molecular weights of **1.1c** in $CDCl_3$.

| [**1.1c**] (M) | D ($m^2/s$) • $10^{-6}$ | Molecular Weight (g/mol) |
|---|---|---|
| 0.05 | 4.200 | 925.7 |
| 0.1 | 3.018 | 1041.1 |
| 0.2 | 3.060 | 1149.6 |
| 0.3 | 3.214 | 1637.8 |

## 1.5: Concentration and NMR Binding Studies with POSS-triols and Lewis Bases

### 1.5.1 Dilution Studies/self-association Constants

Studies using $^{1}$H NMR DOSY NMR spectroscopy support the formation of higher-order species with increased concentration. Binding studies using $^{1}$H NMR spectroscopy can provide insight into the strength of H-bonds formed by calculating association constants.[52] Additionally,

quantifying association constants at regular intervals of concentrations can provide insight into competitive or synergistic effects. Several organocatalysts are known to self-associate, including phosphoric acids,[53,54] thioureas,[43,44] and silanediols.[36] POSS-triol **1.1b** is known to self-associate in solution into dimeric species forming an extended H-bonding network between neighboring silanols (Figure 1.19).[28]

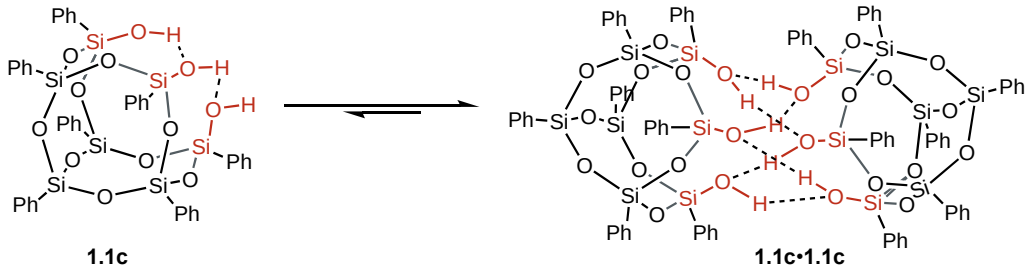


**Figure 1.19.** Self-association equilibrium of **1.1c.**[28]

Binding studies using $^{1}$H NMR spectroscopy were utilized to investigate the H-bonding of POSS-triol **1.1c**. For POSS **1.1c** in $CDCl_3$, a downfield silanol chemical shift change ($\Delta\delta$ = 0.51 ppm) from 0.013 M to 0.2 M was observed (Figure 1.20). A model equation was generated for the observed chemical shift of the SiOH resonance using $^{1}$H NMR spectroscopy based on self-association into dimeric species from an unbound state ($\delta_1$) to a bound state ($\delta_2$). From this data, a self-association constant ($K_{dim}$) was calculated to be 400 ± 80 $M^{-1}$.[28] This data, along with $^{1}$H DOSY NMR data, supports the formation of self-associated species in solution.

$$[U] = \frac{\sqrt{8K[U]_T+1}-1}{4K_{dim}} \qquad \text{(Eq. 1.5)}$$

$$\delta_{calc} = \frac{[U]\delta_1+2K_{dim}[U]^2\delta_2}{[U]_T} \qquad \text{(Eq. 1.6)}$$

A) B)

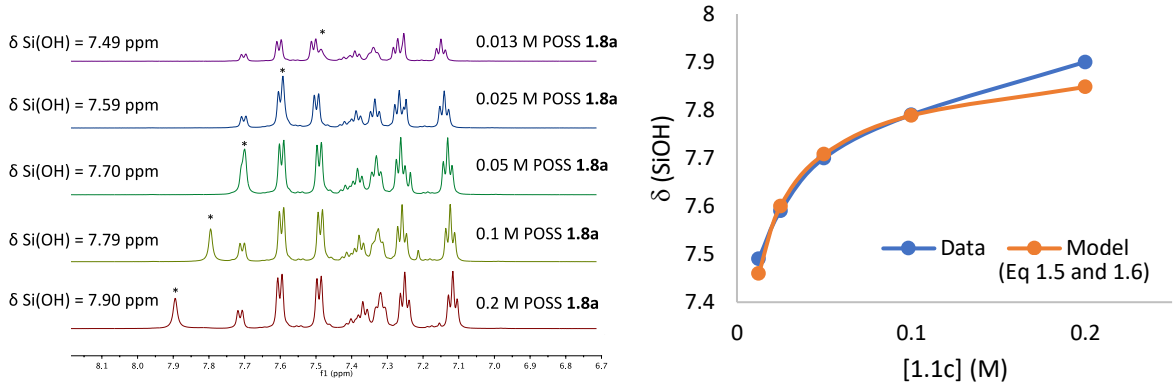


**Figure 1.20.** A) $^{1}$H NMR study of POSS-triol **1.1c** from 0.2 to 0.013 M in $CDCl_3$. Δδ (Si−OH) = 0.51 ppm. B) Self-association constant ($K_{dim}$) of 400 ± 80 $M^{-1}$ was calculated from $^{1}$H NMR data.

## 1.5.2 NMR Binding Studies with Nitrostyrene 1.13b and POSS 1.1c

Binding studies using $^{1}$H NMR spectroscopy with nitrostyrene **1.13b** were performed with POSS **1.1c** to investigate H-bonding in solution. At a POSS **1.1c** concentration of 0.05 M, when between zero to 10.0 equivalents of **1.13a** were titrated in, a downfield silanol chemical shift of 0.46 ppm was observed (Figure 1.21). Broadening of the Si–OH resonance indicates some exchange between **1.13a** and POSS **1.1c**, although a formally bound state was not observed. At a POSS **1.1c** concentration of 0.005 M, when between zero to 10.0 equivalents of **1.13a** were titrated in, no downfield silanol chemical shift was observed (Figure 1.21). A hypothesis for this result is H-bonding may be too weak to detect by $^{1}$H NMR spectroscopy. Binding studies with indole **1.14b** were not conducted based on previous silanol binding studies showing no interaction.[38]

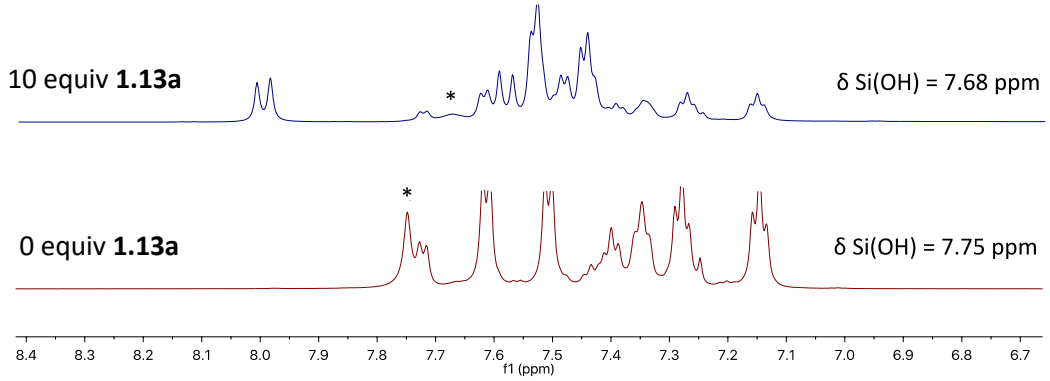


**Figure 1.21**. NMR binding study of POSS **1.1c** (0.05 M in $CDCl_3$) in the presence of nitrostyrene **1.13a**. Siloxanol Δδ = -0.07 ppm are observed in the presence of 10 equivalents of nitrostyrene **1.13a** and broadening of the silanol resonance is observed.

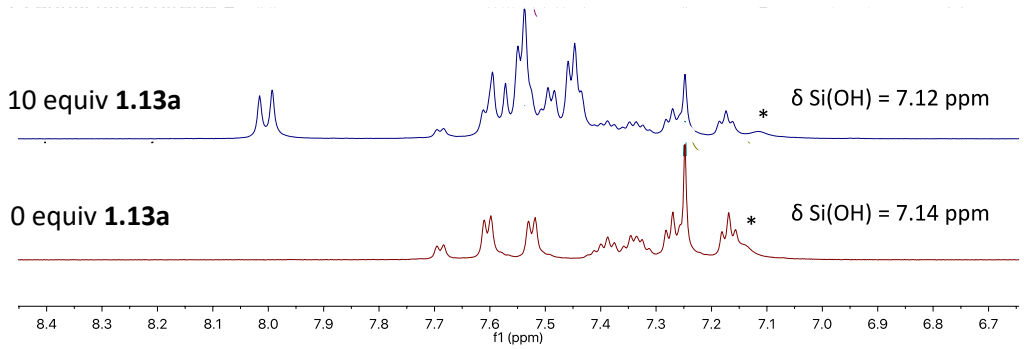


**Figure 1.22**. NMR binding study of POSS **1.1c** (0.005 M in $CDCl_3$) in the presence of nitrostyrene **1.13a**. Siloxanol Δδ = -0.02 ppm are observed in the presence of 10 equivalents of nitrostyrene **1.13a**.

## 1.5.3: NMR Binding Studies with POSS 1.1c and Lewis Bases

In previous work by Dr. Kayla Diemoz, the H-bonding ability of organosilanols can be investigated using binding studies with Lewis bases such as DMF and *n*Bu$_4$NCl.[3] Dr. Ngon Tran previously showed how concentration effects on H-bonding ability can be investigated with binding studies with $^1$H NMR spectroscopy.[36] The Lewis bases chosen (*n*Bu$_4$NCl and DMF) are notably more basic than nitrostyrene **1.13a**, which should perturb the equilibrium to detectable levels using binding studies with $^1$H NMR spectroscopy. POSS concentrations of 0.005 M and 0.05 M for binding studies were selected to examine the effect of self-association on H-bonding ability.

NMR Binding studies were conducted with POSS **1.1c** and *n*Bu$_4$NCl. At a concentration of 0.005 M in POSS **1.1c**, when between zero to 5.0 equivalents of *n*Bu4NCl were titrated in, a downfield silanol chemical shift of 0.46 ppm was observed (Figure 1.23A). From the $^1$H NMR data, a binding constant ($K_a$) of 750 ± 12 M$^{-1}$ was calculated for the SiOH binding affinity to the chloride anion (Figure 1.23B). The data shows POSS **1.1c** forms stronger H-bonds with *n*Bu$_4$NCl than 1,3-disloxanediols.[3]

$$\Delta\delta_i = \delta_{obs,i} - \delta_{free} = \frac{C}{R_0}\Delta\delta \qquad \text{(Eq. 1.7)}$$

$$C = \frac{(K_a R_0 + 1 + K_a S_i) \pm \sqrt{(K_a R_0 + 1 + K_a S_i)^2 - 4K_a^2 R_0 S_i}}{2K_a} \qquad \text{(Eq. 1.8)}$$

A.

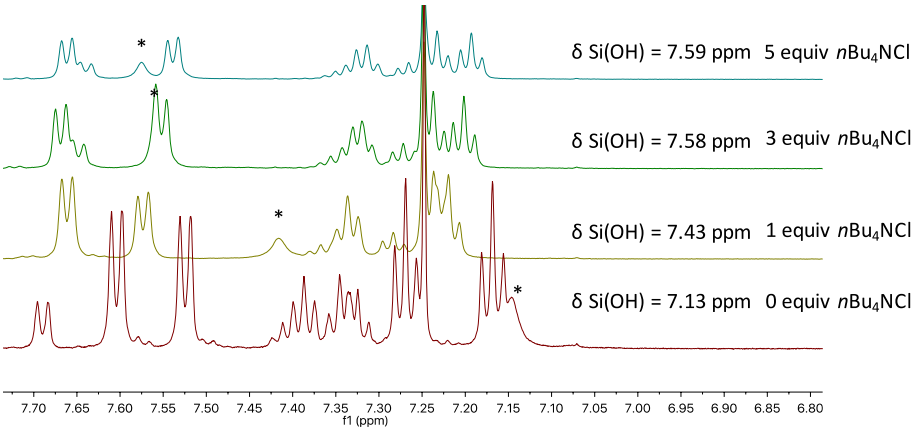


B.

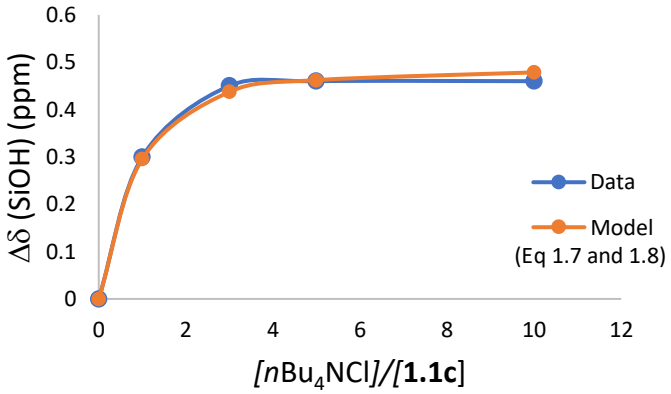


**Figure 1.23.** A) $^{1}$H NMR binding study of POSS **1.1c** (0.005 M in $CDCl_3$) in the presence of *n*$Bu_4Cl$. Siloxanol Δδ = 0.46 ppm are observed in the presence of 15 equivalents of *n*$Bu_4Cl$. B) Binding constants were calculated using $^{1}$H NMR titration data for the silanol peak; $K_a$ = 750 ± 12 $M^{-1}$.

At a concentration of 0.05 M in POSS **1.1c**, when between zero to 10.0 equivalents of *n*Bu4NCl were titrated in, an upfield silanol chemical shift of 0.25 ppm was observed (Figure 1.24). From 1–10 equivalents, the Si–OH resonance broadens then sharpens, indicating a transition from exchange to a bound state with *n*$Bu_4NCl$. Based on these results, **1.1c** binds *n*$Bu_4NCl$ from self-associated **1.1c•1.1c**. As seen with POSS **1.1b**, competitive self-association reduces the effective H-bonding ability of POSS, considering more equivalents were required to saturate.

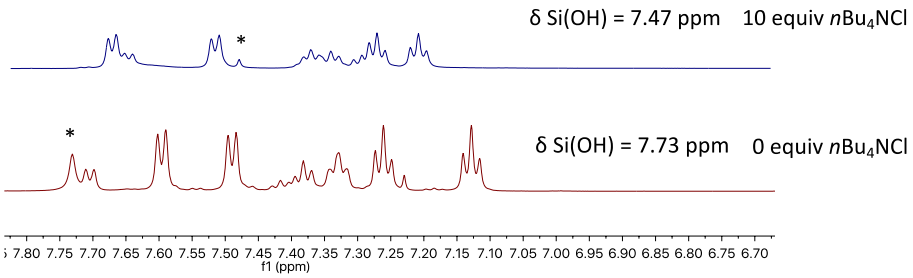


**Figure 1.24.** NMR binding study of POSS **1.1c** (0.05 M in $CDCl_3$) in the presence of $n$Bu$_4$NCl. Siloxanol $\Delta\delta$ = – 0.26 ppm are observed in the presence of 10 equivalents of $n$Bu$_4$NCl. An association constant could not be calculated, due to the direction of the Si–OH shift.

Binding studies with DMF using $^1$H NMR spectroscopy at 0.005 and 0.05 M POSS **1.1c** produced similar results (Figure 1.25 and Figure 1.26). Upfield chemical shifts of the silanols were observed with the addition of Lewis base of 0.20 ppm and 0.59 ppm, respectively. At 0.005 M POSS **1.1c**, saturation was observed by 10 equivalents of DMF, although an association constant could not be accurately calculated (error was higher than the magnitude of the measurement). In the 0.05 M study, saturation of POSS **1.1c** was not observed until 15 equivalents. Overall, the data supports that POSS **1.1c** forms H-bonds with DMF, but competitive self-association leads to reduced H-bonding ability at higher concentrations.

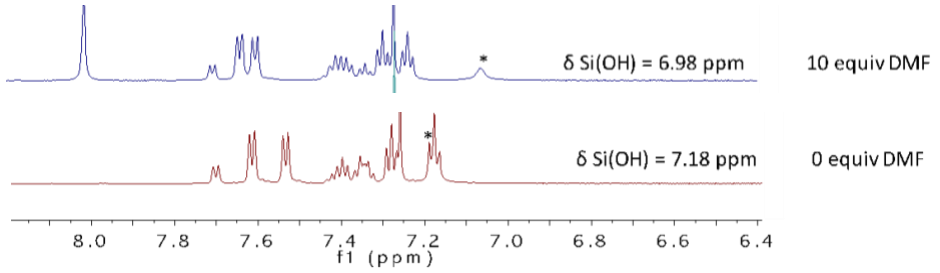


**Figure 1.25.** NMR binding study of POSS **1.1c** (0.005 M in $CDCl_3$) in the presence of DMF. Siloxanol $\Delta\delta$ = – 0.20 ppm are observed in the presence of 15 equivalents of DMF. An association constant could not be calculated, due to the direction of the SiOH shift.

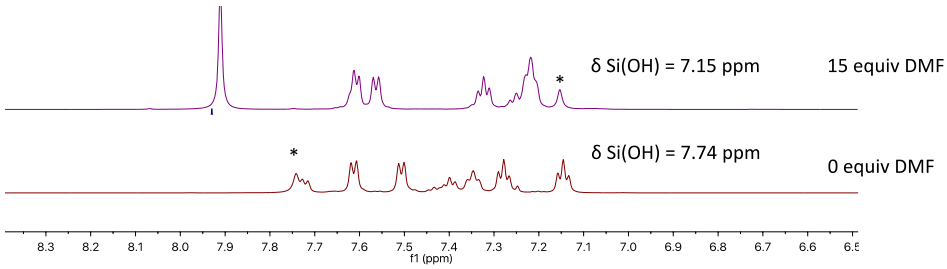

**Figure 1.26.** NMR binding study of POSS **1.1c** (0.05 M in $CDCl_3$) in the presence of DMF. Siloxanol $\Delta\delta$ = – 0.59 ppm are observed in the presence of 15 equivalents of DMF. An association constant could not be calculated, due to the direction of the SiOH shift.

The data supports that monomeric POSS **1.1c** is the active H-bond-donor catalyst in the addition of indole **1.14b** to nitrostyrene **1.13b**. Competitive self-association into an inactive dimeric species leads to reduced H-bonding ability as concentration increases (Figure 1.27). Self-association as the cause of decreased catalytic activity is supported by the lack of product inhibition or catalyst degradation since it is a reversible process. The change in the direction of Si–OH shifts demonstrate the concentration-dependent resting states of POSS-triols when making H-bonds to Lewis bases. Upfield shifts are observed at higher concentrations with the addition of Lewis bases because the H-bonding network of **1.1c•Cl**$^-$ is reduced (i.e. fewer H-bonds) compared to **1.1c•1.1c**. At higher concentrations (0.05M), POSS **1.1c** are mostly self-associated, so H-bonds to Lewis bases involve disruption of the self-associated species, and free monomeric POSS **1.1c** is low in concentration. Despite the presence of self-association, H-bonding to DMF and *n*Bu$_4$NCl is preferred. At lower concentrations (0.005 M) POSS **1.1c** is monomeric, so H-bonds to Lewis bases form directly with the silanols. Based on the kinetic data, 0.025 M is attributed as the approximate concentration at which POSS **1.1c** transitions from a resting state within the catalytic cycle to an off-cycle inactive species (Figure 1.27).

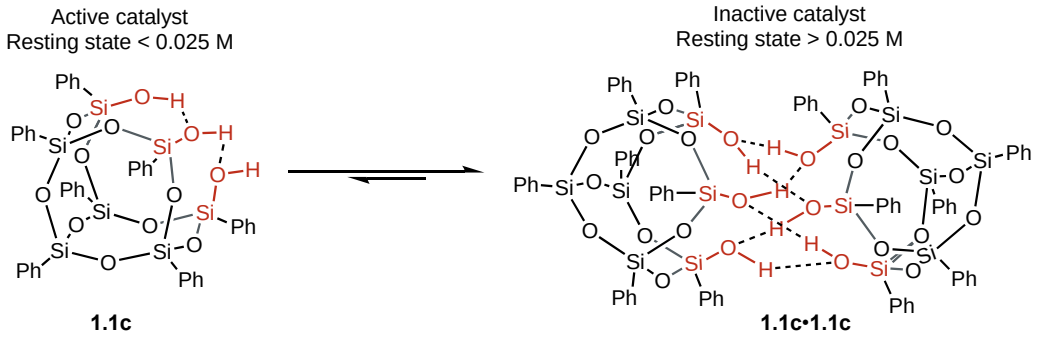


**Figure 1.27.** Proposed activities of POSS species in solution for HBD catalysis.

## 1.5.4: NMR Binding Studies with POSS 1.1b and Lewis Bases

Binding studies with *n*Bu$_4$NCl and DMF using $^1$H NMR spectroscopy were utilized to investigate the H-bonding of POSS-triol **1.1b.** At a concentration of 0.005 M in POSS **1.1b**, when between zero to 5.0 equivalents of *n*Bu4NCl were titrated in, a downfield silanol chemical shift of

0.61 ppm was observed (Figure 1.28A). From the $^{1}$H NMR data, a binding constant ($K_a$) of 62 ± 2 $M^{-1}$ was calculated for the SiOH binding affinity to the chloride anion, which is lower than what was reported previously (Figure 1.28B).[28]

A. B.

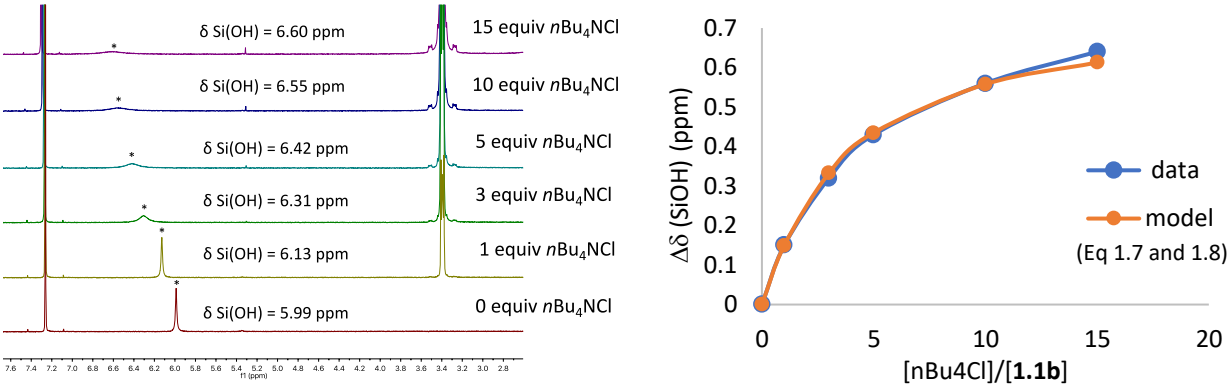


**Figure 1.28.** A) NMR binding study of POSS **1.1b** (0.005 M in $CDCl_3$) in the presence of $n$Bu$_4$Cl. Siloxanol Δδ = 0.61 ppm are observed in the presence of 15 equivalents of $n$Bu$_4$Cl, B) Binding constants were calculated using $^{1}$H NMR titration data for the siloxanol peak with $K_a$= 62 ± 2 $M^{-1}$.

Binding studies were performed with $n$Bu4NCl and POSS **1.1b** where self-association occurs in solution. At a concentration of 0.05 M in POSS **1.1b**, when between zero to 10.0 equivalents of $n$Bu$_4$NCl were titrated in, no silanol chemical shift was observed (Figure 1.29). At 10 equivalents, peak broadening of the Si–OH resonance indicates exchange of H-bonds in solution. Considering the magnitude of $n$Bu$_4$NCl binding affinity to self-association constant (150 $M^{-1}$ vs. 62 $M^{-1}$),[28] self-association is more favorable than binding to $n$Bu$_4$NCl. This result can explain why POSS **1.1b** is catalytically inactive, as self-associated species are more favorable than intermolecular H-bonding with another Lewis base. This data supports that self-associated POSS-triols are catalytically inactive in the addition of indole **1.14b** to nitrostyrene **1.13b**.

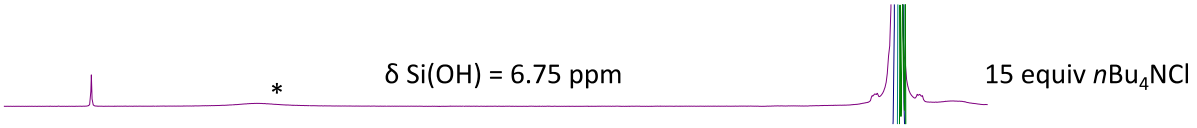

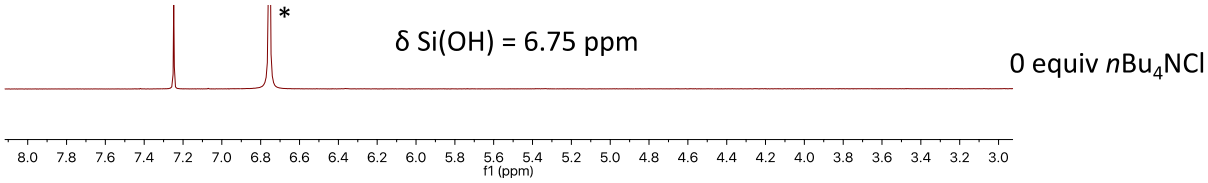


**Figure 1.29.** NMR binding study of POSS **1.1b** (0.05 M in $CDCl_3$) in the presence of *n*$Bu_4Cl$. Siloxanol $\Delta\delta$ = 0 ppm are observed in the presence of 15 equivalents of *n*$Bu_4Cl$, although significant peak broadening is observed. An association constant could not be calculated..

Binding studies were performed with DMF and POSS **1.1b** to study H-bonding with neutral Lewis bases. At a concentration of 0.005 M in POSS **1.1b**, when between zero to 15.0 equivalents of DMF were titrated in, no change chemical shift was observed (Figure 1.30). Based on previous reports, stronger Lewis bases, such as *n*Bu4NCl and acetate, are required to bind to POSS **1.1b**.[28] At a concentration of 0.05 M POSS **1.1b**, when between zero to 15.0 equivalents of DMF were titrated in, an upfield silanol chemical shift ($\Delta\delta$ = –0.32 ppm) was observed (Figure 1.31). The observed interaction between **1.1b** and DMF at 0.05 M suggests that self-association is affecting H-bonding ability in solution with POSS **1.1b**.

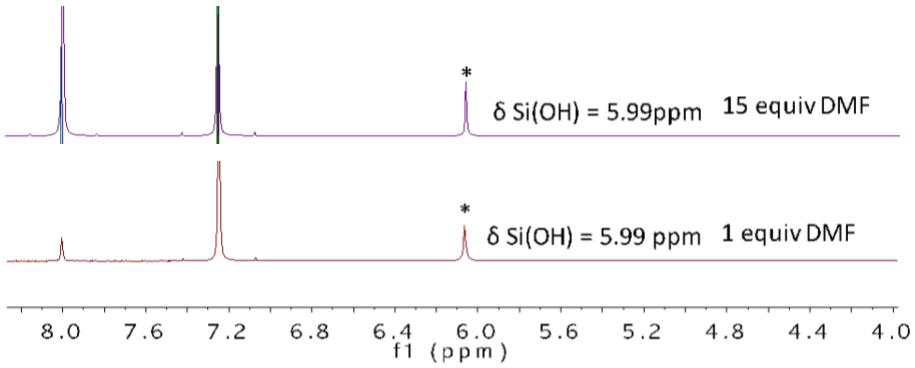


**Figure 1.30.** NMR binding study of POSS **1.1b** (0.005 M in $CDCl_3$) in the presence of DMF. Siloxanol $\Delta\delta$ = 0 ppm are observed in the presence of 15 equivalents of DMF. An association constant could not be calculated.

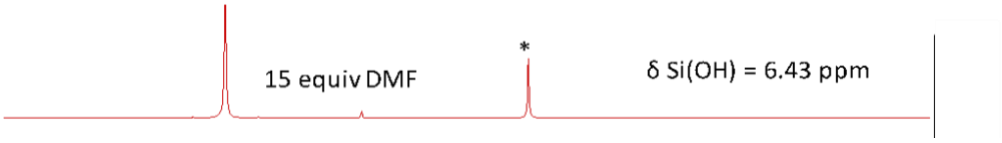

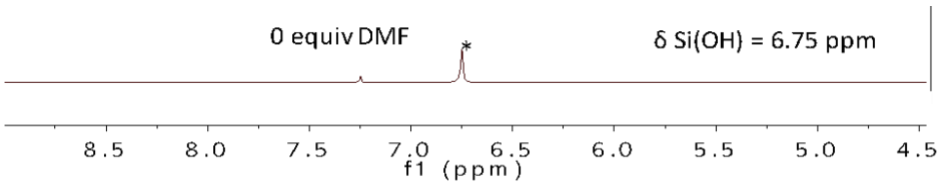


**Figure 1.31.** NMR binding study of POSS **1b** (50 mM in $CDCl_3$) in the presence of DMF. Siloxanol Δδ = – 0.32 ppm are observed in the presence of 15 equivalents of DMF.

In summary, for POSS **1.1b**, the presence of self-association leads to a competitive equilibrium with forming H-bonds to Lewis bases such as *n*Bu$_4$NCl and DMF. As this relates to the addition of **1.14b** to **1.13b**, POSS **1.1b** does not form H-bonds with nitrostyrene **1.13b** but preferentially self-associates, leading to no observable rate enhancement. The self-associated species **1.1b•1.1b** is proposed to be catalytically inactive. Considering *n*Bu$_4$NCl exchanges with **1.1b** at 0.05 M, nitrostyrene **1.13b** likely does not form H-bonds with POSS **1.1b** because it less Lewis basic. No interactions are assumed between POSS **1.1b** and indole **1.14b** based on previous reports.[1]

## 1.6: Synthesis of Silylated POSS 1.17 Investigation of H-bonding

POSS **1.17** was synthesized to examine the effects of reduced intramolecular H-bonding on rate. Replacing a proton of POSS **1.1c** with a trimethylsilyl group allows for only a single intramolecular H-bond to occur, which typically leads to reduced acidity.[23] POSS **1.17** was synthesized in 25% yield from POSS **1.1c** with TMSCl and *N*-methylimidazole (Figure 1.32).

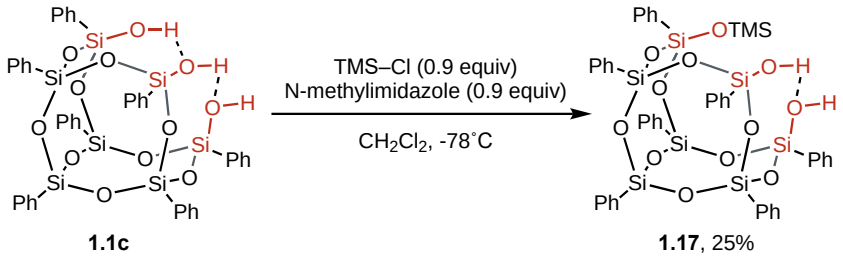


**Figure 1.32.** Synthesis of POSS **1.17** using POSS-triol **1.1c**.

In the addition of indole **1.14b** to **1.13b**, POSS-diol **1.17** provided no rate enhancement relative to the background. Comparing to POSS **1.1c**, this leads to more than an order of magnitude loss of rate (Figure 1.33). The data supports that intramolecular H-bonding in POSS-triols is required for catalytic activity.

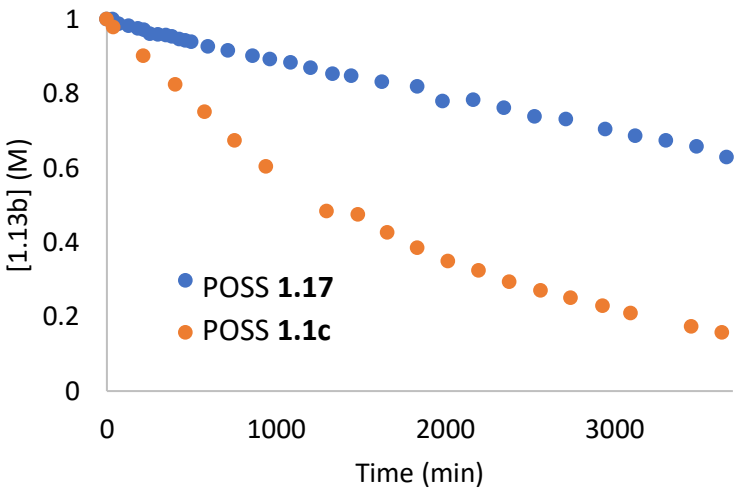


**Figure 1.33.** Comparison of catalytic activity between POSS-diol **1.17** and POSS **1.1c**.[**1.14b**]$_o$ = 2.0 M and [fluorobenzene] = 0.1 M.

Reduced H-bonding ability was observed with POSS-diol **1.17** using binding studies with *n*Bu$_4$NCl and DMF (Table 1.9). At 0.005 M, the binding constant to *n*Bu$_4$NCl was calculated to be 20 ± 1 M$^{-1}$, approximately 40 times weaker than POSS **1.1c**. A lower value of 7-11 M$^{-1}$ was calculated for DMF, which is at the limit of quantification for $^1$H NMR titration constants.[52] Similar values for binding constants for both *n*Bu$_4$NCl and DMF were measured using 0.05 M POSS-diol **1.17**, suggesting no self-association occurred. The Si-OH resonance in the $^1$H NMR spectrum showed a small shift (Δδ = 0.08 ppm) from 0.2 to 0.025 M with no Lewis base present, indicating no self-association with POSS-diol **1.17** (Figure 1.34). Overall, these studies indicate that the intramolecular H-bonding of the triol moiety is required to provide rate enhancement for catalysis. However, the triol moiety also leads to self-association, which reduces the effective H-bonding of POSS-triols at higher concentrations.

**Table 1.9**. Binding data with POSS **1.17** and Lewis bases at varied concentrations

| Lewis base | [**1.17**] (M) | Equivalents | Δδ (Si–OH) (ppm) | $K_a$ (M$^{-1}$) |
|---|---|---|---|---|
| *n*Bu$_4$NCl | 0.005 | 5 | 1.92 | 20 ± 1 |
| | 0.05 | 15 | 1.20 | 22 ± 1 |
| DMF | 0.005 | 15 | 1.87 | 7 ± 1 |
| | 0.05 | 15 | 0.92 | 11 ± 1 |

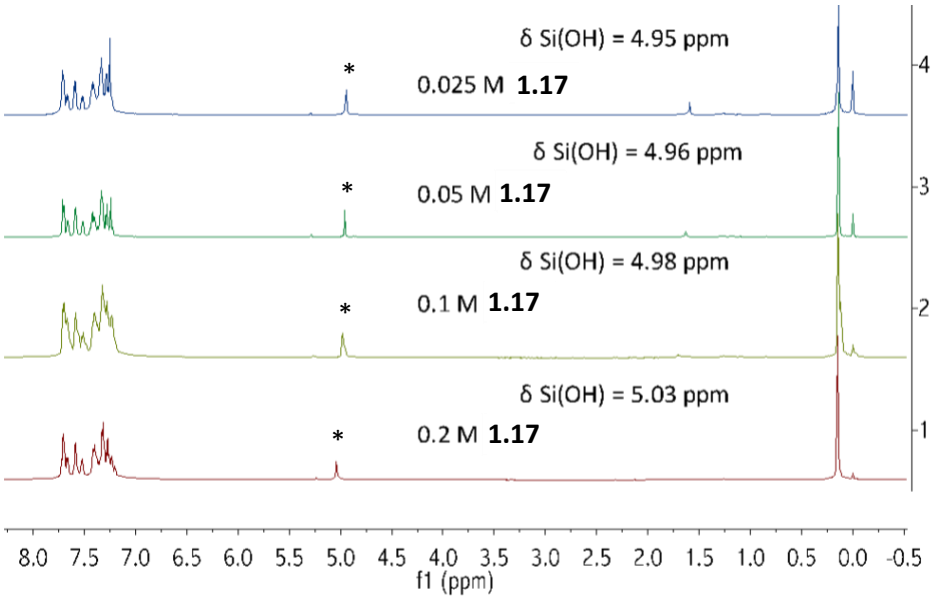


**Figure 1.34.** $^{1}$H NMR dilution study of POSS-diol **1.17** from 0.2 to 0.013 M in $CDCl_3$. Δδ (SiOH) = 0.11 ppm.

## 1.7: X-ray crystallography of POSS compounds

X-ray crystallography can provide insight into the H-bonding interactions between silanols within or between POSSs. Crystals of POSSs **1.1c** and **1.17** were grown using slow evaporation in $CH_2Cl_2$. X-ray data was collected and solved by Dr. Jim Fettinger. The crystal structure of triol-substituted POSS **1.1c** shows a cyclic H-bonding network that is formed with another POSS where all silanols act as H-bond donors and acceptors (Figure 1.35). No intramolecular H-bonding between silanols was observed, H-bonding occurs between silanols of the other POSS. H-bonding distances vary slightly between 1.977 to 2.162 Å. Unno has previously reported a crystal structure of **1.1b**, which crystallizes in the same manner, meaning that phenyl substitution does not significantly affect the overall structure.[28] Complex **1.1c•1.1c** is proposed to be the self-associated species in solution, as no silanols are available for H-bonding with nitrostyrene **1.13b**.

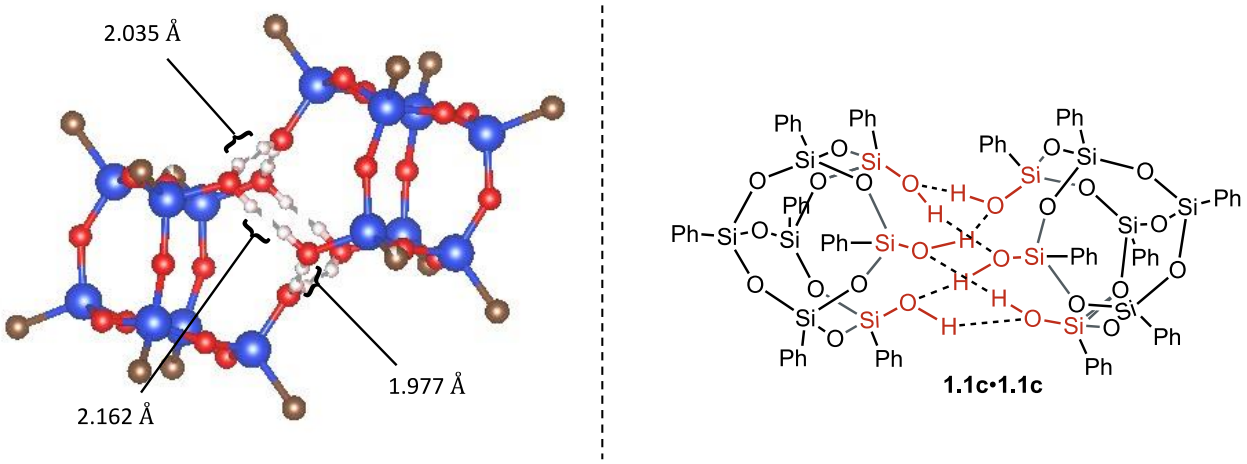


**Figure 1.35.** Ball and stick model of POSS **1.1c** in the solid-state, based on X-ray data. Phenyl groups have been removed for clarity.

Crystals of POSS-diol **1.17** were grown using slow evaporation in $CH_2Cl_2$. The crystal structure of POSS **1.17** crystallizes in a self-associated species where the TMS groups are positioned anti to each other (Figure 1.36). Previous reports of POSS-diol derivatives crystallize similarly.[23,32] Silanols are H-bonded in a network that contains both intramolecular and intermolecular H-bonds. The range of H-bond distances are smaller as well ( 1.919 Å and 1.952 Å, respectively).

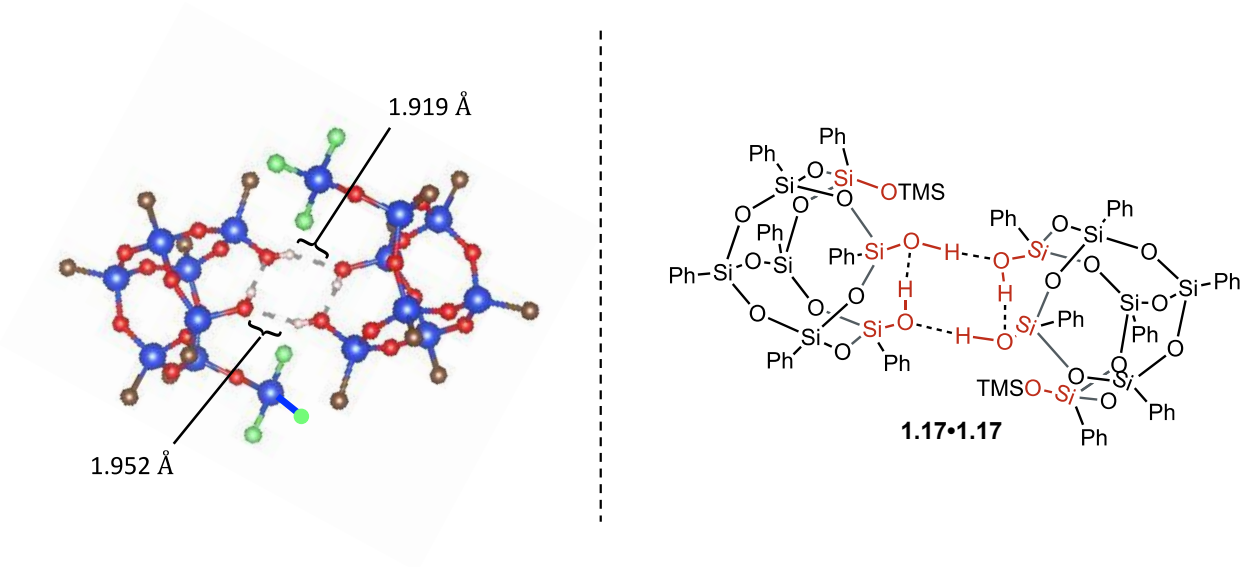


**Figure 1.36.** Ball and stick model of POSS **1.17** in the solid-state, based on X-ray data. Phenyl groups have been removed for clarity.

## 1.8: Derivation of Rate Law and Analysis of Variable Reagent Order

Catalyst orders measured directly from kinetic data are limited in that the measured order is an average between any two concentrations studied. This becomes difficult for transformations where the order changes as a function of concentration, and valuable information can be lost. If one wanted to know the exact effect of catalyst concentration at a *particular* concentration, the elasticity (not the order) needs to be measured.[55] Elasticity (ε) is a measurement typically used in economics,[56] but has found use in fields such as enzymology[57] and physics.[58] In kinetics, differentiation with respect to catalyst of a rate law can produce an elasticity function that is useful for reactions where the catalyst order continuously changes. Take, for example, a reaction of A and B catalyzed to make C shown in Eq. 1.9 with the power-law shown in Eq. 1.10. As shown with Eq. 1.11 and Eq. 1.12, taking the derivative with respect to [catalyst] produces a function that models the percent activity of a catalyst where the value of *c* (highlighted in *red*) would be the order in catalyst at a particular concentration. A plot of [catalyst] vs. Eq. 1.12 can be generated to compare with experimental results.

$$\mathrm{A} + \mathrm{B} \xrightarrow{\text{catalyst}} \mathrm{C} \qquad \text{(Eq. 1.9)}$$

$$\text{rate} = k[\mathrm{A}]^a[\mathrm{B}]^b[\text{catalyst}]^c \qquad \text{(Eq. 1.10)}$$

$$\frac{d(rate)}{d([catalyst])} = \frac{d}{d([catalyst])} k[\mathrm{A}]^a[\mathrm{B}]^b[\text{catalyst}]^c \qquad \text{(Eq 1.11)}$$

$$\frac{d(rate)}{d([catalyst])} = kc[\mathrm{A}]^a[\mathrm{B}]^b[\text{catalyst}]^{c-1} \qquad \text{(Eq 1.12)}$$

A rate expression was derived detailing the competitive self-association and C−C bond formation as the rate-determining step. Assumptions for the rate law are included in Figure 1.37. Given the presence of self-association in solution, an equilibrium is established that removes active catalyst from the system. Starting with the dimerization equilibrium and mass balance, the amount of active catalyst must be expressed in terms of total catalyst concentration ($[\mathbf{1.1c}]_T$) and the self-association constant ($K_{dim}$).

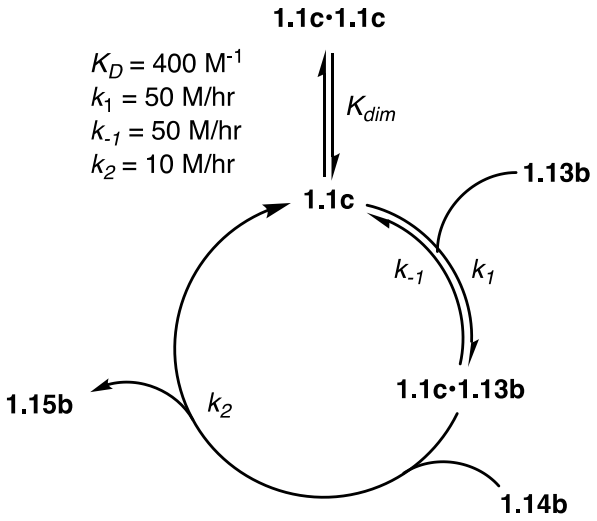


**Figure 1.37.** Catalytic cycle with proposed rates and equilibria. It is assumed that the formation of **1a•1.13b** is reversible and that the rate-determining step is C−C bond formation, based on kinetic studies of reagent order. The reverse step of C−C bond formation is considered so slow that it is assumed to be 0.

$$K_{dim} = \frac{[\mathbf{1.1c \bullet 1.1c}]}{[\mathbf{1.1c}]^2} \quad \text{(Eq. 1.13)}$$

$$[\mathbf{1.1c}]_T = [\mathbf{1.1c}] + 2[\mathbf{1.1c \bullet 1.1c}] \quad \text{(Eq. 1.14)}$$

$$[\mathbf{1.1c}] = \frac{2[\mathbf{1.1c}]_T}{1+\sqrt{1+8K_{dim}[\mathbf{1.1c}]_T}} \quad \text{(Eq. 1.15)}$$

Starting with a simplified rate law and applying the rapid equilibrium assumption:

$$rate = k_2[\mathbf{1.1c \bullet 1.13b}][\mathbf{1.14b}] \quad \text{(Eq. 1.16)}$$

$$rate = (k_2 + k_{-1})[\mathbf{1.1c \bullet 1.13b}] = k_1[\mathbf{1.1c}][\mathbf{1.13b}] \quad \text{(Eq. 1.17)}$$

The rate law becomes:

$$rate = \frac{k_2 k_1}{k_2 + k_{-1}}[\mathbf{1.1c}][\mathbf{1.13b}][\mathbf{1.14b}] \quad \text{(Eq. 1.18)}$$

Substituting $[\mathbf{1.1c}]$in terms of $[\mathbf{1.1c}]_T$ (Eq. 1.15), the rate law becomes

$$rate = \frac{k_2 k_1}{k_2 + k_{-1}} \frac{2[\mathbf{1.1c}]_T[\mathbf{1.13b}][\mathbf{1.14b}]}{1+\sqrt{1+8K_{dim}[\mathbf{1.1c}]_T}} \quad \text{(Eq. 1.19)}$$

For simplification, let $A = \frac{2k_2k_1}{k_2+k_{-1}}[\mathbf{1.13b}][\mathbf{1.14b}]$ and $B = 8K_{dim}$

Taking the derivative with respect to $[\mathbf{1.1c}]_T$, the following elasticity (ε) expression is generated:

$$\frac{d(rate]}{d[\mathbf{1.1c}]_T} = \varepsilon = \frac{A(1+\sqrt{1+B[\mathbf{1.1c}]_T}) - A[\mathbf{1.1c}]_T\left(\frac{B}{2\sqrt{B[\mathbf{1.1c}]_T}}\right)}{\left(1+\sqrt{1+B[\mathbf{1.1c}]_T}\right)^2} \quad \text{(Eq. 1.20)}$$

Plotting $[\mathbf{1.1c}]$ vs Eq. 1.20 (Figure 1.38), we observe non-integer catalyst orders in the region studied for catalysis. The data matches well with measured catalyst orders, suggesting the self-associated equilibrium with POSS **1.1c** accounts for observed changes in order.

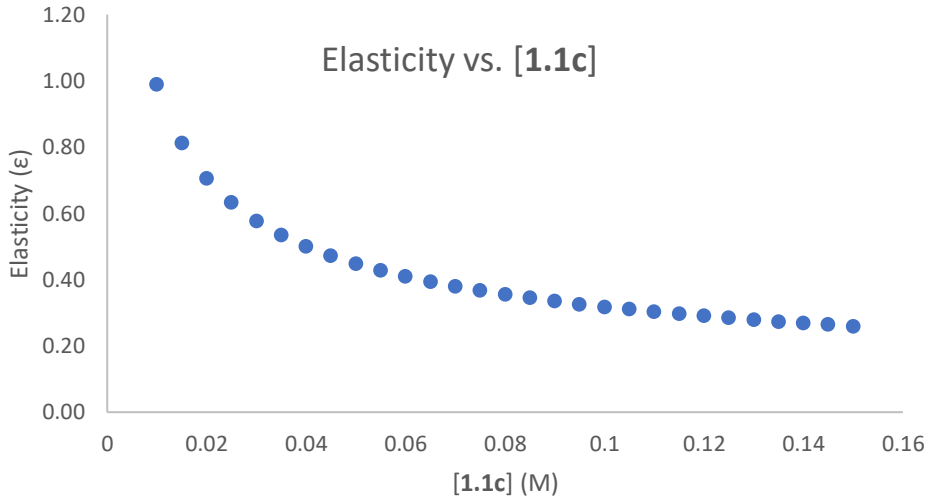


**Figure 1.38**. [**1.1c**] (M) vs. elasticity (ε). The average value from 0.025 M to 0.10 M is 0.5. The average value from 0.10 M to 0.15 M is 0.3.

## 1.9: Catalytic Cycle and Implications for Silica Surface Modeling

Based on the data collected from kinetic analysis, synthesis of POSS derivatives, and $^1$H NMR binding studies, the following catalytic cycle is proposed (Figure 1.39). Previous studies of 1,3-dilsoxanediol HBD catalysis determined binding to nitro groups as the rate-determining step.[1] At catalyst concentrations at or above 0.025 M, complex **1.1c•1.1c** is the proposed resting state, which must dissociate to the active monomer **1.1c**. POSS-triol **1.1c** activates nitrostyrene **1.13b** (i.e. complex **1.1c•1.13b**). The addition of indole **1.14b** to complex **1.1c•1.14b** is rate-determining, supported by the "*different excess*" experiments and KIE data. The dissociation of **1.1c•1.1c** is not the rate-determining step given that indole **1.14b** provides rate enhancement. A change in the overall reaction order is seen when the concentration of POSS-triol **1.1c** is less than 0.025 M. A catalyst order of 0.6 indicates that the equilibrium at lower concentration favors the monomeric active catalyst species **1.1c**. A first-order dependence was observed for both nitrostyrene **1.13b** and indole **1.14b**, suggesting the formation of **1.1c•1.13b** is not strongly favored, and a bimolecular reaction profile is observed with C–C formation as the rate-determining step.

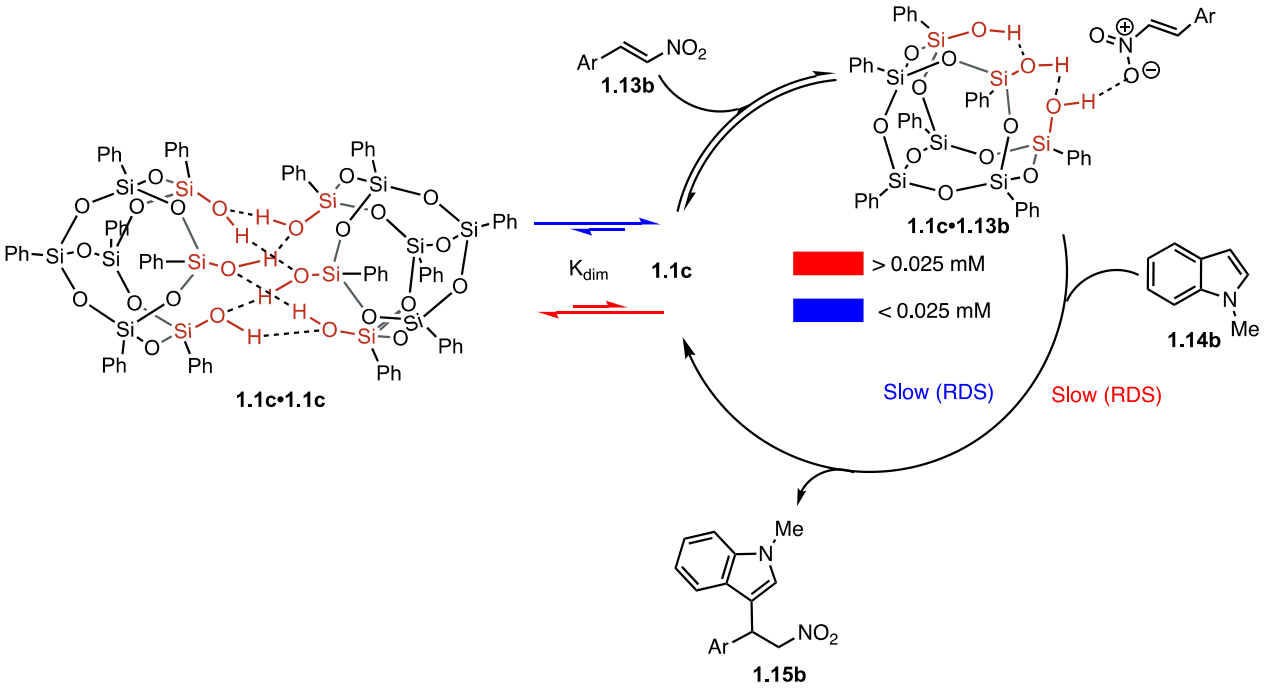


**Figure 1.39.** Proposed catalytic cycle with concentration-dependent resting states.

Comparing the mechanism of POSS **1.1c** HBD catalysis to a silica surface, the presence of self-association adds an equilibrium to the reaction not present in the bulk material that ultimately

alters observed kinetics (Figure 1.40). Future work in this area should make note of this, quantify the self-association, and design experiments such that it is no longer affecting catalysis. Silica gel remains a superior catalyst to POSS **1.1c** both in activity and recyclability.

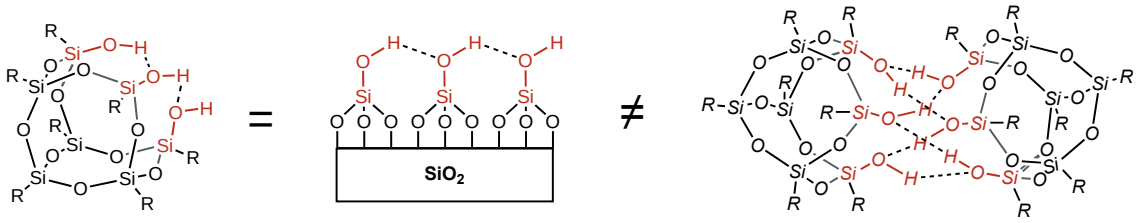


**Figure 1.40:** Comparison of POSS **1.1c** resting states to silica surfaces.

The difference in activity between POSS-triols **1.1c** and POSS-diol **1.17** supports that silanols within an extended H-bond network are more active due to more significant acidification (Figure 1.41). Therefore, surfaces containing a higher quantity of extended vicinal silanols should be more active than surfaces populated with isolated silanols.

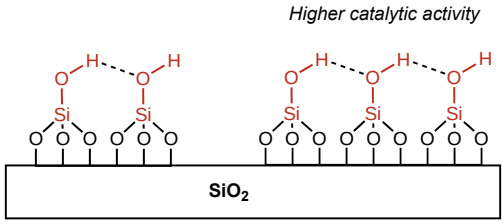


**Figure 1.41:** Proposal for more active H-bonding sites in silica surface catalysis.

## 1.10: Conclusions

In conclusion, a rigorous kinetic study of POSS-triol HBD catalysis using $^{19}F$ NMR spectroscopy and modern kinetic analysis packages (RPKA and VTNA) was performed. POSS-triol **1.1c** was found to be an active HBD catalyst in the addition of indole **1.14b** to nitrostyrene **1.13b**. However, silica gel remains a superior catalyst compared to POSS **1.1c** both in activity and ease of separation in the addition of indole **1.14b** to nitrostyrene **1.13b**. Data supports that the catalyst becomes less active per unit as concentration increases, although no product inhibition or catalyst degradation is present. Self-association into dimeric species is proposed to cause the kinetics observed by removing free monomeric POSS **1.1c** from solution and altering resting states. Titration and concentration studies using $^{1}H$ NMR spectroscopy support the formation of

self-associated species, which reduced the effective H-bonding ability to Lewis bases. The presence of self-association adds an equilibrium that is not present in the bulk material, so future work should note concentration effects present. Observed catalysis of POSS-triols does not mimic a silica surface for most concentrations studied.

## 1.11: Experimental Procedures and Data

### 1.11.1: General Information

All nuclear magnetic resonance (NMR) spectra were obtained on Bruker Nanobay AVIIIHD 400 (376 MHz for $^{19}F$), and/or Varian VNMRS 600 (600 MHz for $^{1}H$; 151 MHz for $^{13}C$; 119 MHz for $^{29}Si$) at room temperature unless noted otherwise. Chemicals shifts were reported in parts per million (δ scale), and referenced according the following standards: tetramethylsilane internal standard for $^{1}H$ signals in chloroform (δ 0.00 ppm), benzene residual solvent (δ 7.16 ppm) for $^{1}H$ signals in benzene, deuterated chloroform or benzene carbon resonances (middle peak is δ 77.1 or δ 128.1 ppm, respectively) for $^{13}C\{^{1}H\}$ signals, tetramethylsilane external standard in $CDCl_3$ for $^{29}Si\{^{1}H\}$ signals (δ 0.00), trifluoromethyl-benzene external standard in $CDCl_3$ for $^{19}F(^{1}H)$ signals. For all $^{29}Si$ NMR spectra, chromium(III) acetylacetonate was added at 0.01 M as a T1 relaxation agent, and relaxation delays were set to 5 seconds. Coupling constants were reported in Hertz (Hz) and multiplicities were reported as follows: singlet (s), doublet (d), triplet (t), quartet (q), and multiplet (m). Compounds were analyzed by HRMS on a Thermo Fisher Orbitrap XL (Davis, CA) using electrospray in the positive ion mode at >60,000 resolution and using 5 kV spray voltage, with a curtain plate temperature of 275 °C and sheath gas setting of 15. These settings result in mass accuracies <5 ppm. Samples were analyzed via flow injection analysis by injecting 5 μL samples into a stream of 50% acetonitrile and 50% aqueous solution of 0.1% formic acid, flowing at 200 μL/minute. X-ray crystallography was completed using a Bruker APEX-II CCD Diffractometer.

Commercially available reagents were purchased and used without further purification unless otherwise indicated. All deuterated solvents were dried using 4 Å molecular sieves, then transferred to a bottle of fresh mole sieves prior to binding and dilution studies. All silsesquioxanes were purchased from HybridPlastics.com, indoles **1.14a** and **1.14b** were purchased from TCI. Fluorobenzene was obtained from Sigma Aldrich. Tetrabutylammonium chloride was purchased from Acros, and dried with $Na_2SO_4$ prior to binding studies. Silanols **1.4a-d** were synthesized

using previously reported procedures.[1] Nitrostyrenes **1.13a** and **1.13b** was synthesized according to previous literature procedures. Indole **1.14b**-*d* was synthesized according to previously reported procedures. Reactions were analyzed by thin-layer chromatography (TLC) on EMD glass plates that were pre-coated with silica gel 60 F254, and the reactions were purified by column chromatography using Acros silica gel 60 Å (0.035−0.070 mm).

## 1.11.2: Synthetic Procedures

### Procedure A: Indole addition reaction

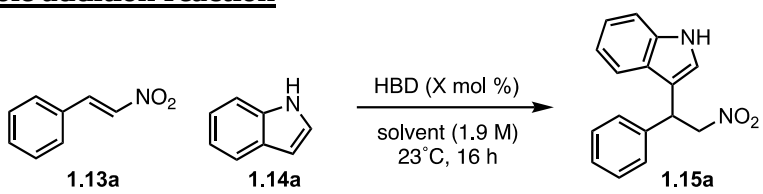


**1.13a** **1.14a** **1.15a**

Nitrostyrene **1.13a** (1.0 equiv, 56 mg, 0.38 mmol) was added to a flame-dried, Ar-charged vial, followed by solvent (0.2 mL). Next, a H-bond donor or deionized water was added, and the reaction stirred for 5 min. Indole **1.14a** (1.5 equiv, 67 mg, 0.57 mmol) was added, and the reaction stirred at 23 ˚C for 16 h. After 16 h, the reaction was diluted with $CH_2Cl_2$ (2 mL), and $MgSO_4$ was added in several portions over a 5 min period. The reaction was filtered and the solvent was removed under reduced pressure. Phenyltrimethylsilane (10 μL) was added as an internal standard, followed by $CDCl_3$ (0.6 mL), and the solution was transferred to an oven-dried NMR tube. A $^1H$ NMR with 4 scans with 25 second relaxation delay was taken to determine yield. The reaction was shown to have minimal rate enhancement from water under the given conditions.

### Procedure B: Synthesis of POSS 1.17

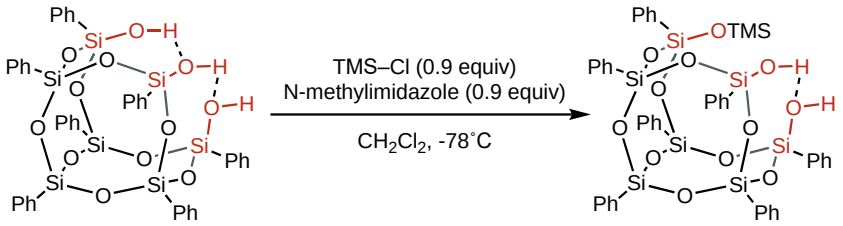


**1.1c** **1.17**, 25%

To a flame-dried, Ar-charged round-bottom flask, Phenyl POSS-triol **1.1c** (4.65 g, 5.00 mmol) followed by *N*-methylimidazole (0.255 g, 3.75 mmol) was added. Next, $CH_2Cl_2$ (50 mL) was added, and the flask was cooled to 0˚C and stirred for 10 min. Freshly distilled TMS-Cl (0.475 mL, 3.75 mmol) was slowly added at a rate of 0.05 mL/min. A white solid immediately started to

precipitate, and the reaction stirred for 3 h at 0 ˚C. After 3 h, the reaction mixture was filtered to remove precipitate, washed with saturated aq. $NaHCO_3$ (15 mL). The organic layer was separated and dried with $Na_2SO_4$ for 10 min and concentrated in vacuo. The crude product was purified via flash chromatography in $CH_2Cl_2$, followed by washes with pentanes (3 x 10 mL) to yield POSS diol **1.17** as a white solid (0.960 g, 25% yield based on TMSCl). $^1$H NMR (600 MHz, $CDCl_3$) δ 7.76 - 7.65 (m, 8H, ArH), 7.64 - 7.58 (d, *J* = 7.4 Hz, 4H, ArH), 7.53 (d, *J* = 7.4 Hz, 2H, ArH), 7.47 – 7.20 (m, ArH), 5.04 (s, 2H, SiOH), 0.16 (s, 9H, Si-CH). $^{13}$C NMR (151 MHz, $CDCl_3$) δ 134.3 134.2, 134.2, 134.1, 134.1, 130.8, 130.8, 130.7, 130.6, 130.6, 130.5, 127.9, 127.9, 127.8, 1.6. $^{29}$Si NMR (119 MHz, $CDCl_3$, $Cr(acac)_3$ = 0.01 M) δ 14.6, –68.5, –76.4, –77.3, –77.5, –78.4. Exact Mass calcd for $C_{45}H_{46}O_{12}Si_8$ $(M + H)^+$, 1003.1222. Found: 1003.1218.

### 1.11.3: Procedures for Reaction Monitoring and Kinetic Analysis

### Procedure A: General Procedure for Reaction Monitoring

The procedure for general reaction monitoring was adopted from a literature procedure.[1] A stock solution of 4-trifluoromethyl-*trans*-β-nitrostyrene **1.13b** and fluorobenzene in $CD_2Cl_2$ was prepared. The catalyst was weighed directly into an oven-dried and argon-purged NMR tube followed by the addition of a 4-trifluoromethyl-*trans*-β-nitrostyrene **1.13b** stock solution in $CD_2Cl_2$. An initial $^{19}$F NMR scan was taken before the addition of *N*-methylindole **1.14b** and then the reaction was monitored by taking a spectrum every 30–60 min. 4 scans with a 25 second relaxation delay were taken to assure complete relaxation for accurate integrations. Fluorobenzene was used as an internal standard (–113 ppm) and integrations compared to 4-trifluoromethyl-*trans*-β-nitrostyrene and product. Integration ranges for 4-trifluoromethyl-*trans*-β-nitrostyrene = – 62.9 to –63.0 ppm; product = –62.1 to –62.3 ppm; and internal standard: = –113.0 to –113.3 ppm.

Concentrations of starting materials and product were calculated based off the raw integrals and the excess [*xs*].

$$[\mathbf{1.13b}] = \frac{(\text{Integral of nitrostyrene}/3)*[\text{Fluorobenzene}]}{\text{Integral of fluorobenzene}} \qquad \text{(Eq. 1.21)}$$

$$[\mathbf{1.14b}] = [\mathbf{1.13}\boldsymbol{b}] + [xs] \qquad \text{(Eq. 1.1)}$$

$$[\mathbf{1.15b}] = \frac{(\text{Integral of product}/3)*[\text{Fluorobenzene}]}{\text{Integral of fluorobenzene}} \qquad \text{(Eq. 1.22)}$$

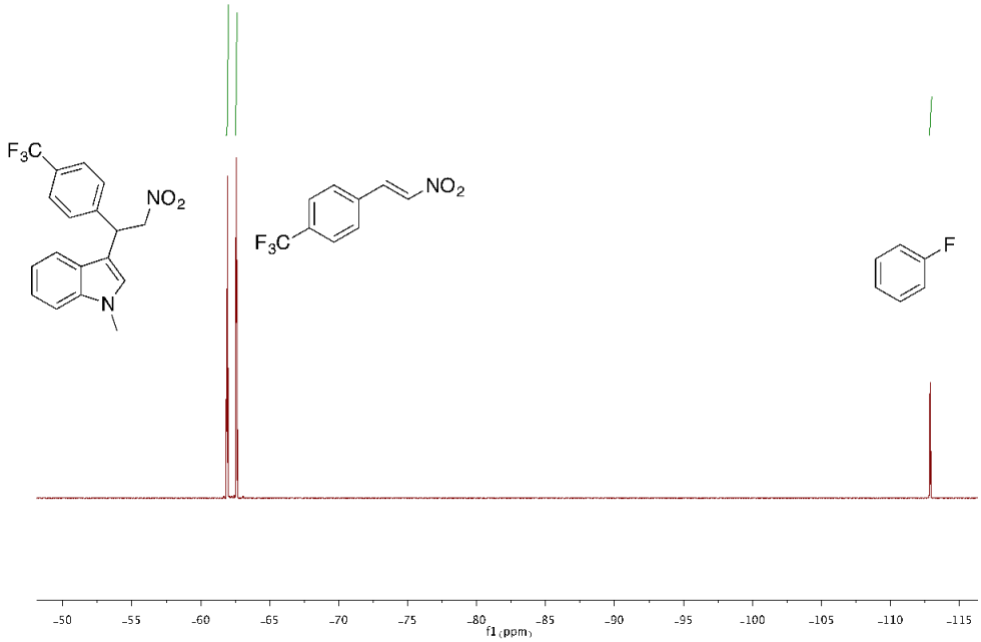


**Figure 1.42**. Example of $^{19}$F NMR spectrum collected for monitoring the consumption of 4-trifluoromethyl-*trans*-β-nitrostyrene **1.13b** and formation of product **1.15b**.

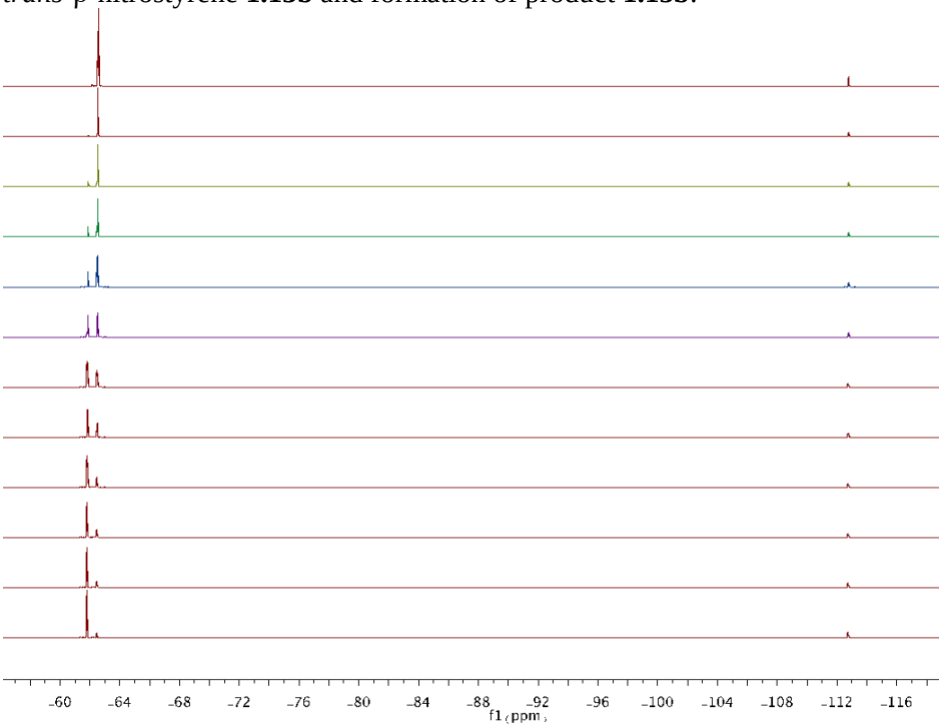


**Figure 1.43**. Example of $^{19}$F NMR spectra collected over the course of the reaction monitoring the consumption of 4-trifluoromethyl-*trans*-β-nitrostyrene **1.13b** and formation of product **1.15b**. Fluorobenzene was used as an internal standard (–113 ppm).

**Procedure B: Relative Rates**

The general procedure for reaction monitoring was followed for catalysts **1.10**-**1.12** and **1.1b**-**c**. Initial concentrations are: [**1.13b**] = 0.42 M, [**1.14b**] = 3.2 M, [HBD] = 0.04 M. Observed rate constants ($k_{obs}$) were calculated by taking the ln[**1.13b**] for individual trials. Lines were observed with high $R^2$ for all catalysts. $k_{cat}$ and $k_{rel}$ were calculated according to the following formulas:

$$k_{cat} = k_{obs} - k_{background} \quad \text{(Eq. 1.23)}$$

$$k_{rel} = k_{cat}/k_{background} \quad \text{(Eq. 1.24)}$$

**Procedure C: Catalyst Order**

The general procedure for reaction monitoring was followed for POSS **1.1c** at varied concentrations. A 1.33 M stock solution of **1.13b** in $CD_2Cl_2$ was prepared (0.450 mL for each trial). Indole **1.14b** (0.150 mL) was added after initial scans. Data was analyzed using catalyst order determination analysis using VTNA,[39] where a plot of multiple trials are graphed on time*[**1.1c**]$^x$ vs. [**1.13b**]. The variable $x$ was altered in 0.1 increments until overlap of trials is observed.

**Table 1.10.** Amounts used for experiments with varied concentration of **1a.**

| Trial | [**1.1c**] (M) | **1.13b** Stock (mL) | **1.14b** (mL) | Mass **1.1c** (mg) |
|---|---|---|---|---|
| 1 | 0.025 | 0.450 | 0.150 | 14.0 |
| 2 | 0.05 | 0.450 | 0.150 | 28.0 |
| 3 | 0.075 | 0.450 | 0.150 | 42.0 |
| 4 | 0.10 | 0.450 | 0.150 | 56.0 |
| 5 | 0.125 | 0.450 | 0.150 | 70.0 |
| 6 | 0.150 | 0.450 | 0.150 | 84.0 |

[**1.13b**]$_o$ = 1.0 M; [**1.14b**]$_o$ = 2.0 M; [fluorobenzene] = 0.1 M

**Procedure D: Apparent Turnover Frequency**

The general procedure for reaction monitoring was followed for POSS **1.1c** at varied concentrations. A 0.65 M stock solution of **1.13b** in $CD_2Cl_2$ was prepared (0.450 mL for each trial). Concentrations of **1.1c** used are in Table 1.11. Apparent turnover frequencies were calculated from observed rate constants using the following equation:

$$TOF_{app}(hr^{-1}) = \frac{k_{obs}}{[cat]} \cdot \frac{60\ min}{1hr} \quad \text{(Eq. 1.2)}$$

**Table 1.11.** Amounts used for experiments for determination of $TOF_{app}$

| Trial | [**1.1c**] (M) | Mass of **1a** (mg) | $k_{obs} \bullet 10^4$ (M•min$^{-1}$) | $TOF_{app}$ (hr$^{-1}$) |
|---|---|---|---|---|
| 7 | 0.05 | 27.9 | 7.2 | 0.86 |
| 8 | 0.075 | 41.9 | 8.9 | 0.71 |
| 9 | 0.1 | 55.9 | 11.6 | 0.70 |
| 10 | 0.108 | 60.3 | 11.5 | 0.64 |
| 11 | 0.117 | 65.4 | 12.6 | 0.65 |
| 12 | 0.125 | 69.8 | 13.5 | 0.65 |
| 13 | 0.15 | 83.8 | 14.8 | 0.59 |
| 14 | 0.175 | 97.8 | 15.6 | 0.53 |

[**1.13b**]$_o$ = 0.5 M; [**1.14b**]$_o$ = 2.0 M; [fluorobenzene] = 0.1 M

## Procedure E: "Different Excess" Experiments

The general procedure was followed for reaction monitoring for "*different excess*" experiments. A 1.95 M stock solution of **1.13b** in $CD_2Cl_2$ was prepared and amounts used are included in Table 1.12 and 1.13. Indole **1.14b** was added after initial scans. Reactions displayed high $R^2$.

**Table 1.12.** Amounts used for experiments with varied concentration of Nitrostyrene **1.13b** with POSS **1.1c.**

| Trial | [**1.13b**]$_o$ (M) | [**1.14b**]$_o$ (M) | [**1.1c**] (M) | **1.13b** Stock (mL) | **1.14b** (mL) | Mass **1.1c** (mg) | $CD_2Cl_2$ (mL) |
|---|---|---|---|---|---|---|---|
| 15 | 1.5 | 1.6 | 0.1 | 0.450 | 0.130 | 55.0 | 0.020 |
| 16 | 1.25 | 1.6 | 0.1 | 0.375 | 0.130 | 55.0 | 0.075 |
| 17 | 1.5 | 2.0 | 0.025 | 0.450 | 0.150 | 14.0 | 0 |
| 18 | 1.25 | 2.0 | 0.025 | 0.375 | 0.150 | 14.0 | 0.075 |

[fluorobenzene] = 0.1 M

**Table 1.13.** Amounts used for experiments with varied concentration of N-methylindole **1.14b** at 0.1 M and 0.025 M POSS **1.1c.**

| Trial | [**1.13b**]$_o$ (M) | [**1.14b**]$_o$ (M) | [**1.1c**] (M) | **1.13b** Stock (mL) | **1.14b** (mL) | Mass **1.1c** (mg) | $CD_2Cl_2$ (mL) |
|---|---|---|---|---|---|---|---|
| 19 | 1.5 | 2.0 | 0.1 | 0.450 | 0.150 | 55.9 | 0 |
| 20 | 1.5 | 1.75 | 0.1 | 0.450 | 0.130 | 55.9 | 0.020 |
| 21 | 1.5 | 1.75 | 0.025 | 0.450 | 0.130 | 14.0 | 0.020 |
| 22 | 1.5 | 1.25 | 0.025 | 0.450 | 0.110 | 14.0 | 0.040 |

[fluorobenzene] = 0.1 M

**Procedure F: "Same Excess" Experiments**

The general procedure was followed for reaction monitoring for "*different excess*" experiments. A 1.95 M stock solution of **1.13b** in $CD_2Cl_2$ was prepared and amounts used are included in Table 1.12 and 1.13. Indole **1.14b** was added after initial scans. Reactions displayed high $R^2$.

**Table 1.14.** Amounts used for experiments under "*same excess*" conditions at 0.1 and 0.025 M POSS **1.1c.**

| Trial | [**1.13b**]$_o$ (M) | [**1.14b**]$_o$ (M) | [**1.1c**] (M) | [**1.13b**] Stock (mL) | **1.14b** (mL) | Mass **1.1c** (mg) | $CD_2Cl_2$ (mL) |
|---|---|---|---|---|---|---|---|
| 23 | 1.5 | 2.0 | 0.1 | 0.450 | 0.130 | 84.0 | 0.020 |
| 24 | 1.25 | 1.6 | 0.1 | 0.360 | 0.110 | 84.0 | 0.040 |
| 25 | 1.0 | 2.0 | 0.025 | 0.450 | 0.150 | 14.0 | - |
| 26 | 0.5 | 1.5 | 0.025 | 0.450 | 0.112 | 14.0 | 0.038 |

[fluorobenzene] = 0.1 M

**Procedure G: Kinetic Isotope Effect Experiments**

Kinetic isotope effects were measured following the general procedure for $^{19}F$ NMR reaction monitoring, and were determined by dividing 1$^{st}$ order rate constants from reactions run in parallel. A 1.33 M stock solution of **1.13b** was made (0.450 mL for each trial). Indole was added (0.150 mL) after initial scans. Concentrations are included in Table 1.15.

**Table 1.15**. Concentrations of nitrostyrene **1.13b** and indole **1.14b** and POSS **1.1c.**

| Trial | [**1.13b**] (M) | [**1.14b**] or [**1.14b**-*d*] (M) | [**1a**] (M) | Mass **1a** (mg) | $k_{obs}$•$10^4$ ($min^{-1}$) |
|---|---|---|---|---|---|
| 27 | 1.0 | 2.0, [**1.14b**] | 0.1 | 55.9 | 9.4 |
| 28 | 1.0 | 2.0, [**1.14b**-*d*] | 0.1 | 55.9 | 9.01 |
| 29 | 1.0 | 2.0, [**1.14b**] | 0.1 | 55.9 | 9.4 |
| 30 | 1.0 | 2.0, [**1.14b**-*d*] | 0.1 | 55.9 | 8.3 |

[fluorobenzene] = 0.1 M

Corrected $k_{obs}$ for **1.14b**-*d*, assuming 90% incorporation, is 8.96 $min^{-1}$ for trial 2, and trial 4 is 8.18 $m^{-1}$, with an average of 8.57 $min^{-1}$

Trial 1 in parallel with average; KIE = 1.10

Trial 3 in parallel with average; KIE = 1.09

Avg = 1.10

Our data is consistent with a secondary kinetic isotope effect, which supports our conclusion that C-C bond formation is the rate determining step when [**1.1c**] = 0.1 M.

**Procedure H: Nitrobenzene competition experiments**

The general procedure for reaction monitoring was followed for POSS **1.1c** in the presence of nitrobenzene. A 1.95 M stock solution of **1.13b** in $CD_2Cl_2$ (0.31 mL per trial) was prepared and amounts used are included in Table 1.16. Additional $CD_2Cl_2$ was used for trials without nitrobenzene to account for total volume. Trials were overlayed to observe rate effects. All reactions displayed high $R^2$.

**Table 1.16**. Amounts used for experiments with nitrobenzene additive.

| Trial | [**1.1c**] (M) | Mass **1.1c** (mg) | [**1.13b**]$_o$ (M) | [**1.14b**]$_o$ (M) | Nitrobenzene (mL) | $CD_2Cl_2$ (mL) |
|---|---|---|---|---|---|---|
| 31 | 0.075 | 41.9 | 1.5 | 2.0 | 0 | 0.140 |
| 32 | 0.075 | 41.9 | 1.5 | 2.0 | 0.11 | 0.070 |
| 33 | 0.025 | 14.0 | 1.5 | 2.0 | 0 | 0.140 |
| 34 | 0.025 | 14.0 | 1.5 | 2.0 | 0.11 | 0.070 |

[fluorobenzene] = 0.1 M

**1.11.4: Procedures for DOSY, Binding, and Dilution studies**

**Procedure A: Procedure for $^1$H NMR DOSY Spectroscopy of POSS 1.1c**

Samples for $^1$H NMR Diffusion Oriented Spectroscopy (DOSY) were made by making solutions of the appropriate POSS concentration in $CDCl_3$ (0.6 mL), followed by the addition of squalene, cyclooctene, and tetradecane (10 μL each). The sample was placed in an NMR tube. Spectra were acquired on a Varian 600 with 2D one-shot DOSY parameters. Experimental parameters transmitter offset (o1p), sweep width (sw), and receiver gain (rg) were obtained from $^1$H NMR spectra prior to acquisition. A linear gradient from 5% to 95% strength with 15 or 20 data points (8 scans each) was used. Diffusion constants from the resulting spectra were processed using the $T_1/T_2$ relaxation function within the DOSY toolbox software after phase correction. Estimated molecular weights of NMR-observed species were calculated by plotting log(MW) vs. log(diffusion constant) of the internal standards and fitting to a straight line of these data points. The diffusion coefficient from the Si–OH of POSS **1.1c** was used to estimate molecular weight.

**Table 1.17**. Diffusion coefficient and calculated molecular weights at 0.025 M **1.1c**

| Molecule | D ($m^2/s$) | Molecular Weight (g/mol) | Log MW |
|---|---|---|---|
| COE | $1.34 \cdot 10^{-5}$ | 110.20 | 2.042 |
| TDE | $9.90 \cdot 10^{-6}$ | 196.37 | 2.293 |
| Squalene | $6.00 \cdot 10^{-6}$ | 410.72 | 2.613 |
| **1.1c** (0.05 M) | $4.20 \cdot 10^{-6}$ | 925.70 | 2.966 |

**Table 1.18**. Diffusion coefficient and calculated molecular weights at 0.1 M **1.1c**

| Molecule | D($m^2/s$) | Molecular Weight (g/mol) | Log MW |
|---|---|---|---|
| COE | $1.34 \cdot 10^{-5}$ | 110.20 | 2.042 |
| TDE | $9.90 \cdot 10^{-6}$ | 196.37 | 2.293 |
| Squalene | $6.00 \cdot 10^{-6}$ | 410.72 | 2.613 |
| **1.1c** (0.1 M) | $3.44 \cdot 10^{-6}$ | 1041.11 | 3.018 |

**Table 1.19**. Diffusion coefficient and calculated molecular weights at 0.2 M **1.1c**

| Molecule | D($m^2/s$) | Molecular Weight (g/mol) | Log MW |
|---|---|---|---|
| COE | $1.18 \cdot 10^{-5}$ | 110.20 | 2.042 |
| TDE | $8.47 \cdot 10^{-6}$ | 196.37 | 2.293 |
| Squalene | $5.00 \cdot 10^{-6}$ | 410.72 | 2.613 |
| **1.1c** (0.2 M) | $2.58 \cdot 10^{-6}$ | 1149.58 | 3.060 |

**Table 1.20**. Diffusion coefficient and calculated molecular weights at 0.3 M **1.1c**

| Molecule | D($m^2/s$) | Molecular Weight (g/mol) | Log MW |
|---|---|---|---|
| COE | $9.87 \cdot 10^{-6}$ | 110.20 | 2.042 |
| TDE | $7.34 \cdot 10^{-6}$ | 196.37 | 2.293 |
| Squalene | $4.51 \cdot 10^{-6}$ | 410.72 | 2.613 |
| **1.1c** (0.3 M) | $9.87 \cdot 10^{-6}$ | 1637.8 | 3.214 |

**Procedure B: Dilution Studies and Calculation of Self-association Constants**

A solution of 0.2 M POSS-siloxanol was made in $CDCl_3$ (1.2 mL). A 1:1 serial dilution of transfers (0.6 mL) was done to dilute solutions to lower concentrations. Adequate mixing was done prior to and after transfers. A $^1H$ NMR spectrum was collected at room temperature with 8 scans. Association constants were calculated using Microsoft Excel Solver to fit with the model equation below. K was optimized and no constraints were used. Error was calculated as 95% confidence intervals based on the fit of the NMR data to the model. The values for $\delta_1$ and $\delta_2$ were set to 7.00 ppm and 8.00 ppm, respectively.

$$[U] = \frac{\sqrt{8K[U]_T+1}-1}{4K_{dim}} \qquad \text{(Eq. 1.5)}$$

$$\delta_{calc} = \frac{[U]\delta_1+2K_{dim}[U]^2\delta_2}{[U]_T} \qquad \text{(Eq. 1.6)}$$

$\delta_1$ = chemical shift for the unbound, $\delta_2$ = chemical shift for the self-associated, $[U]_T$ = total concentration in solution, [U] = concentration of unbound, $K_{dim}$ = self-association constant in $M^{-1}$

**Procedure C: $^1$H NMR Binding Studies with Lewis Bases and Determination of Association Constants**

Two stock solutions were each made by dissolving a POSS-siloxanol (116.4 mg **1.1c** or 98.9 mg **1.1b**, 0.125 mmol) in $CDCl_3$ (2.5 mL). The Lewis base, either *n*$Bu_4NCl$ or DMF, was added to only one of the stock solutions, up to 5 (0.048 mL DMF, or 173.7 mg *n*$Bu_4NCl$) or 15 (0.144 mL DMF, or 521.1 mg *n*$Bu_4NCl$) equivalents. It should be noted for DMF, the volume of the reagent was taken into account to provide a total solution volume of 2.5 mL. Different volumes of each stock solution were mixed to make a solution (0.6 mL) with the desired equivalents of Lewis Base. A $^1$H NMR spectrum of each solution was recorded after 8 scans at room temperature.

Association constants were calculated using Microsoft Excel Solver to fit with the model equation below. K, $\delta_1$, $\delta_2$ were optimized and no constraints were used. Error was calculated as 95% confidence intervals based on the fit of the NMR data to the model. $\Delta\delta = \delta_{complex} - \delta_{free}$; $\delta_{complex}$ = chemical shift (ppm) of the SiOH proton in the bound Lewis base complex, estimated from extrapolation of where the binding curve levels off, $\delta_{free}$ = chemical shift (ppm) of the SiOH proton when no Lewis base is present; $\delta_{obs,i}$ = chemical shift of SiOH proton at *i* equivalents of Lewis base. $R_0$ = initial concentration of POSS-triols and $S_i$ = concentration of Lewis base at *i* equivalents in M, $K_a$ = binding constant in $M^{-1}$. Data was verified with repeated experiments.

$$\Delta\delta_i = \delta_{obs,i} - \delta_{free} = \frac{C}{R_0}\Delta\delta \qquad \text{(Eq. 1.7)}$$

$$C = \frac{(K_aR_0+1+K_aS_i)\pm\sqrt{(K_aR_0+1+K_aS_i)^2-4K_a^2R_0S_i}}{2K_a} \qquad \text{(Eq. 1.8)}$$

## 1.11.5: Kinetic Data

### Relative Rate

**Table 1.21**. Data from monitoring the uncatalyzed reaction using $^{19}F$ NMR spectroscopy.

| Time (min) | [**1.13b**] (M) | [**1.15b**] (M) | ln[**1.13b**] |
|---|---|---|---|
| 0 | 0.405 | 0.000 | -0.903 |
| 30 | 0.403 | 0.003 | -0.910 |
| 98 | 0.398 | 0.006 | -0.921 |
| 205 | 0.392 | 0.013 | -0.936 |
| 377 | 0.383 | 0.027 | -0.959 |
| 688 | 0.365 | 0.042 | -1.007 |
| 928 | 0.351 | 0.055 | -1.046 |
| 1170 | 0.340 | 0.067 | -1.079 |
| 1528 | 0.331 | 0.078 | -1.105 |
| 1878 | 0.315 | 0.096 | -1.154 |
| 2322 | 0.299 | 0.109 | -1.206 |
| 2668 | 0.283 | 0.124 | -1.261 |
| 3035 | 0.269 | 0.140 | -1.314 |
| 3395 | 0.253 | 0.153 | -1.373 |
| 3759 | 0.239 | 0.167 | -1.433 |
| 4230 | 0.223 | 0.187 | -1.499 |
| 4709 | 0.205 | 0.201 | -1.586 |

**Table 1.22**. $^{19}F$ NMR data from monitoring the reaction catalyzed using **1.4a**.

| Time (min) | [**1.13b**] (M) | [**1.15b**] (M) | ln[**1.13b**] |
|---|---|---|---|
| 0 | 0.437 | 0.000 | -0.829 |
| 30 | 0.437 | 0.001 | -0.827 |
| 87 | 0.438 | 0.008 | -0.826 |
| 206 | 0.437 | 0.013 | -0.829 |
| 326 | 0.416 | 0.027 | -0.877 |
| 506 | 0.412 | 0.035 | -0.887 |
| 687 | 0.402 | 0.045 | -0.911 |
| 866 | 0.393 | 0.054 | -0.935 |
| 1046 | 0.381 | 0.063 | -0.966 |
| 1226 | 0.376 | 0.073 | -0.978 |
| 1406 | 0.363 | 0.085 | -1.014 |
| 1646 | 0.353 | 0.097 | -1.042 |

| | | | |
|---|---|---|---|
| 1886 | 0.341 | 0.107 | -1.075 |
| 2126 | 0.328 | 0.119 | -1.115 |
| 2426 | 0.315 | 0.135 | -1.154 |
| 2726 | 0.301 | 0.147 | -1.202 |
| 2966 | 0.290 | 0.158 | -1.238 |
| 3436 | 0.269 | 0.177 | -1.314 |
| 3910 | 0.249 | 0.197 | -1.392 |

**Table 1.23**. $^{19}$F NMR data from monitoring the reaction catalyzed using **1.4b**.

| Time (min) | [**1.13b**] (M) | [**1.15b**] (M) | ln[**1.13b**] |
|---|---|---|---|
| 0 | 0.433 | 0.000 | -0.838 |
| 30 | 0.415 | 0.012 | -0.880 |
| 121 | 0.386 | 0.040 | -0.952 |
| 219 | 0.361 | 0.065 | -1.020 |
| 278 | 0.349 | 0.079 | -1.054 |
| 400 | 0.323 | 0.107 | -1.131 |
| 519 | 0.298 | 0.131 | -1.211 |
| 699 | 0.264 | 0.165 | -1.332 |
| 939 | 0.227 | 0.205 | -1.481 |
| 1066 | 0.208 | 0.222 | -1.570 |
| 1238 | 0.189 | 0.245 | -1.668 |
| 1425 | 0.165 | 0.262 | -1.800 |
| 1600 | 0.149 | 0.281 | -1.902 |
| 1959 | 0.118 | 0.314 | -2.137 |
| 2139 | 0.105 | 0.329 | -2.257 |
| 2319 | 0.093 | 0.342 | -2.379 |
| 2591 | 0.078 | 0.359 | -2.551 |
| 2930 | 0.063 | 0.373 | -2.770 |

**Table 1.24**. $^{19}$F NMR data from monitoring the reaction catalyzed using **1.4c**.

| Time (min) | [**7**] (M) | [**9**] (M) | ln[**7**] |
|---|---|---|---|
| 0 | 0.431 | 0.000 | -0.842 |
| 15 | 0.416 | 0.005 | -0.877 |
| 82 | 0.395 | 0.034 | -0.928 |
| 142 | 0.385 | 0.057 | -0.954 |
| 203 | 0.362 | 0.078 | -1.016 |
| 322 | 0.317 | 0.112 | -1.150 |
| 442 | 0.289 | 0.149 | -1.242 |
| 569 | 0.253 | 0.185 | -1.376 |
| 681 | 0.226 | 0.211 | -1.487 |
| 801 | 0.195 | 0.237 | -1.636 |

| | | | |
|---|---|---|---|
| 1041 | 0.159 | 0.285 | -1.837 |
| 1289 | 0.124 | 0.305 | -2.087 |
| 1521 | 0.102 | 0.337 | -2.283 |
| 1762 | 0.083 | 0.359 | -2.485 |
| 2009 | 0.064 | 0.373 | -2.749 |
| 2481 | 0.040 | 0.387 | -3.219 |

**Table 1.25**. $^{19}$F NMR data from monitoring the reaction catalyzed using **1.1c**.

| Time (min) | [**1.13b**] (M) | [**1.15b**] (M) | ln[**1.13b**] |
|---|---|---|---|
| 0 | 0.416 | 0.000 | -0.877 |
| 21 | 0.397 | 0.025 | -0.923 |
| 62 | 0.374 | 0.048 | -0.983 |
| 94 | 0.360 | 0.064 | -1.022 |
| 121 | 0.349 | 0.077 | -1.054 |
| 151 | 0.334 | 0.089 | -1.097 |
| 188 | 0.321 | 0.104 | -1.135 |
| 241 | 0.299 | 0.123 | -1.206 |
| 278 | 0.287 | 0.137 | -1.247 |
| 322 | 0.275 | 0.153 | -1.292 |
| 383 | 0.255 | 0.166 | -1.368 |
| 457 | 0.236 | 0.191 | -1.444 |
| 543 | 0.213 | 0.206 | -1.548 |
| 606 | 0.199 | 0.218 | -1.613 |
| 671 | 0.185 | 0.231 | -1.689 |
| 721 | 0.174 | 0.247 | -1.749 |
| 909 | 0.143 | 0.275 | -1.947 |
| 1013 | 0.126 | 0.288 | -2.071 |
| 1133 | 0.111 | 0.313 | -2.201 |
| 1254 | 0.095 | 0.325 | -2.350 |

**Catalyst Order**

**Table 1.26.** $^{19}$F NMR data from monitoring trial 1.

| Time (min) | [**1.13b**] (M) | [**1.15b**] (M) |
|---|---|---|
| 0 | 0.97 | 0.00 |
| 48 | 0.95 | 0.03 |
| 78 | 0.95 | 0.04 |
| 108 | 0.93 | 0.06 |
| 138 | 0.92 | 0.08 |

| | | |
|---|---|---|
| 169 | 0.92 | 0.09 |
| 199 | 0.90 | 0.11 |
| 228 | 0.88 | 0.12 |
| 257 | 0.87 | 0.13 |
| 290 | 0.89 | 0.15 |
| 320 | 0.85 | 0.17 |
| 350 | 0.84 | 0.17 |
| 380 | 0.81 | 0.18 |
| 412 | 0.79 | 0.19 |
| 443 | 0.79 | 0.20 |
| 470 | 0.79 | 0.22 |
| 498 | 0.78 | 0.24 |
| 561 | 0.73 | 0.25 |
| 681 | 0.70 | 0.30 |
| 826 | 0.64 | 0.33 |
| 921 | 0.62 | 0.35 |
| 1169 | 0.57 | 0.42 |
| 1291 | 0.54 | 0.43 |
| 1515 | 0.51 | 0.47 |
| 1649 | 0.47 | 0.48 |
| 1772 | 0.47 | 0.53 |
| 1891 | 0.46 | 0.53 |
| 2011 | 0.43 | 0.53 |
| 2372 | 0.41 | 0.60 |
| 2493 | 0.40 | 0.62 |
| 2603 | 0.38 | 0.62 |
| 2719 | 0.37 | 0.63 |
| 2844 | 0.36 | 0.64 |
| 2960 | 0.36 | 0.66 |
| 3081 | 0.34 | 0.66 |
| 3201 | 0.33 | 0.67 |
| 3310 | 0.33 | 0.68 |
| 3449 | 0.32 | 0.68 |
| 3560 | 0.31 | 0.69 |
| 3680 | 0.31 | 0.69 |
| 3800 | 0.30 | 0.66 |
| 4052 | 0.28 | 0.69 |
| 4278 | 0.28 | 0.72 |

**Table 1.27.** $^{19}$F NMR data from monitoring trial 2.

| Time (min) | [**1.13b**] (M) | [**1.15b**] (M) | ln[**1.13b**] |
|---|---|---|---|
| 0 | 1.00 | 0.00 | 0.00 |
| 15 | 0.99 | 0.02 | -0.01 |
| 54 | 0.96 | 0.05 | -0.05 |
| 121 | 0.91 | 0.10 | -0.09 |
| 161 | 0.89 | 0.12 | -0.12 |
| 206 | 0.87 | 0.14 | -0.14 |
| 254 | 0.84 | 0.17 | -0.17 |
| 297 | 0.82 | 0.19 | -0.19 |
| 401 | 0.77 | 0.25 | -0.26 |
| 521 | 0.71 | 0.31 | -0.34 |
| 581 | 0.68 | 0.33 | -0.38 |
| 641 | 0.66 | 0.36 | -0.41 |
| 702 | 0.64 | 0.38 | -0.45 |
| 761 | 0.62 | 0.41 | -0.48 |
| 881 | 0.57 | 0.44 | -0.56 |
| 1055 | 0.51 | 0.50 | -0.67 |
| 1243 | 0.46 | 0.56 | -0.77 |
| 1454 | 0.39 | 0.61 | -0.94 |
| 1843 | 0.32 | 0.70 | -1.14 |
| 2015 | 0.28 | 0.72 | -1.26 |
| 2255 | 0.25 | 0.77 | -1.38 |
| 2505 | 0.22 | 0.81 | -1.53 |

**Table 1.28.** $^{19}$F NMR data from monitoring trial 3.

| Time (min) | [**1.13b**] (M) | [**1.15b**] (M) | ln[**1.13b**] |
|---|---|---|---|
| 0 | 1.03 | 0.00 | 0.03 |
| 18 | 0.98 | 0.04 | -0.012 |
| 62 | 0.95 | 0.07 | -0.048 |
| 104 | 0.92 | 0.10 | -0.080 |
| 151 | 0.89 | 0.13 | -0.111 |
| 191 | 0.86 | 0.16 | -0.150 |
| 234 | 0.82 | 0.20 | -0.188 |
| 289 | 0.78 | 0.24 | -0.242 |
| 355 | 0.73 | 0.29 | -0.309 |
| 410 | 0.69 | 0.33 | -0.369 |
| 476 | 0.65 | 0.37 | -0.420 |
| 548 | 0.60 | 0.42 | -0.496 |
| 629 | 0.56 | 0.46 | -0.568 |
| 749 | 0.51 | 0.51 | -0.666 |

| | | | |
|---|---|---|---|
| 842 | 0.46 | 0.56 | -0.758 |
| 935 | 0.43 | 0.59 | -0.829 |
| 1033 | 0.39 | 0.63 | -0.923 |
| 1120 | 0.37 | 0.65 | -0.991 |
| 1241 | 0.33 | 0.69 | -1.085 |

**Table 1.29.** $^{19}$F NMR data from monitoring trial 4.

| Time (min) | [**1.13b**] (M) | [**1.15b**] (M) | ln[**1.13b**] |
|---|---|---|---|
| 0 | 1.00 | 0.00 | 0.00 |
| 22 | 0.96 | 0.03 | -0.04 |
| 67 | 0.93 | 0.08 | -0.08 |
| 98 | 0.91 | 0.10 | -0.09 |
| 137 | 0.86 | 0.15 | -0.15 |
| 182 | 0.83 | 0.19 | -0.19 |
| 230 | 0.77 | 0.23 | -0.26 |
| 273 | 0.75 | 0.26 | -0.29 |
| 317 | 0.70 | 0.29 | -0.35 |
| 378 | 0.67 | 0.34 | -0.39 |
| 437 | 0.63 | 0.38 | -0.46 |
| 498 | 0.59 | 0.42 | -0.52 |
| 558 | 0.55 | 0.45 | -0.59 |
| 617 | 0.53 | 0.49 | -0.64 |
| 679 | 0.51 | 0.53 | -0.67 |
| 738 | 0.46 | 0.54 | -0.77 |
| 858 | 0.42 | 0.59 | -0.86 |
| 978 | 0.37 | 0.63 | -1.00 |
| 1100 | 0.33 | 0.67 | -1.12 |
| 1218 | 0.30 | 0.72 | -1.21 |

**Table 1.30.** $^{19}$F NMR data from monitoring trial 5.

| Time (min) | [**1.13b**] (M) | [**1.15b**] (M) | ln[**1.13b**] |
|---|---|---|---|
| 0 | 0.998 | 0.000 | -0.002 |
| 23 | 0.977 | 0.021 | -0.024 |
| 63 | 0.955 | 0.043 | -0.046 |
| 112 | 0.883 | 0.115 | -0.124 |
| 153 | 0.850 | 0.148 | -0.163 |
| 193 | 0.784 | 0.214 | -0.243 |
| 232 | 0.741 | 0.257 | -0.300 |
| 272 | 0.722 | 0.276 | -0.326 |
| 322 | 0.678 | 0.320 | -0.389 |

| | | | |
|---|---|---|---|
| 382 | 0.645 | 0.353 | -0.439 |
| 443 | 0.596 | 0.402 | -0.518 |
| 499 | 0.543 | 0.455 | -0.611 |
| 559 | 0.511 | 0.487 | -0.671 |
| 648 | 0.477 | 0.521 | -0.740 |
| 756 | 0.417 | 0.581 | -0.874 |
| 805 | 0.373 | 0.625 | -0.987 |
| 894 | 0.345 | 0.653 | -1.063 |
| 983 | 0.314 | 0.684 | -1.158 |
| 1104 | 0.280 | 0.718 | -1.273 |
| 1224 | 0.241 | 0.757 | -1.422 |

**Table 1.31.** $^{19}$F NMR data from monitoring trial 6.

| Time (min) | [**1.13b**] (M) | [**1.15b**] (M) | ln[**1.13b**] |
|---|---|---|---|
| 0 | 1.00 | 0.00 | 0.00 |
| 22 | 0.96 | 0.04 | -0.04 |
| 56 | 0.92 | 0.09 | -0.08 |
| 95 | 0.88 | 0.13 | -0.13 |
| 126 | 0.85 | 0.16 | -0.16 |
| 155 | 0.83 | 0.19 | -0.19 |
| 184 | 0.79 | 0.22 | -0.23 |
| 224 | 0.77 | 0.26 | -0.26 |
| 264 | 0.73 | 0.29 | -0.31 |
| 310 | 0.71 | 0.33 | -0.34 |
| 359 | 0.67 | 0.36 | -0.41 |
| 399 | 0.64 | 0.39 | -0.44 |
| 445 | 0.59 | 0.42 | -0.53 |
| 490 | 0.59 | 0.45 | -0.53 |
| 534 | 0.54 | 0.48 | -0.61 |
| 595 | 0.51 | 0.50 | -0.68 |
| 656 | 0.48 | 0.54 | -0.74 |
| 715 | 0.45 | 0.57 | -0.79 |
| 775 | 0.43 | 0.60 | -0.84 |
| 887 | 0.38 | 0.63 | -0.96 |

**Apparent Turnover Frequency**

**Table 1.32.** $^{19}$F NMR data from monitoring trial 7.

| Time (min) | [**1.13b**] (M) | [**1.15b**] (M) | ln[**1.13b**] |
|---|---|---|---|
| 0 | 0.53 | 0.00 | -0.64 |
| 27 | 0.51 | 0.01 | -0.68 |
| 67 | 0.49 | 0.03 | -0.72 |

| | | | |
|---|---|---|---|
| 107 | 0.47 | 0.04 | -0.75 |
| 155 | 0.45 | 0.05 | -0.79 |
| 194 | 0.44 | 0.06 | -0.83 |
| 232 | 0.43 | 0.08 | -0.85 |
| 287 | 0.41 | 0.09 | -0.88 |
| 327 | 0.40 | 0.10 | -0.91 |
| 367 | 0.39 | 0.12 | -0.93 |
| 407 | 0.38 | 0.13 | -0.96 |
| 447 | 0.37 | 0.14 | -1.00 |
| 487 | 0.36 | 0.15 | -1.03 |
| 587 | 0.33 | 0.18 | -1.10 |
| 702 | 0.30 | 0.20 | -1.22 |
| 807 | 0.28 | 0.23 | -1.28 |
| 927 | 0.26 | 0.25 | -1.37 |
| 1054 | 0.24 | 0.28 | -1.44 |
| 1174 | 0.22 | 0.30 | -1.52 |
| 1407 | 0.19 | 0.33 | -1.67 |
| 1587 | 0.17 | 0.36 | -1.79 |
| 1767 | 0.14 | 0.37 | -1.93 |
| 1948 | 0.12 | 0.39 | -2.09 |
| 2127 | 0.11 | 0.41 | -2.20 |
| 2315 | 0.10 | 0.42 | -2.35 |
| 2492 | 0.09 | 0.43 | -2.42 |
| 2675 | 0.07 | 0.44 | -2.60 |
| 2849 | 0.07 | 0.45 | -2.72 |

**Table 1.33.** $^{19}$F NMR data from monitoring trial 8.

| Time (min) | [**1.13b**] (M) | [**1.15b**] (M) | ln[**1.13b**] |
|---|---|---|---|
| 0 | 0.54 | 0.00 | -0.62 |
| 18 | 0.51 | 0.02 | -0.67 |
| 57 | 0.49 | 0.03 | -0.71 |
| 97 | 0.47 | 0.05 | -0.75 |
| 148 | 0.45 | 0.08 | -0.79 |
| 186 | 0.44 | 0.09 | -0.82 |
| 224 | 0.41 | 0.10 | -0.88 |
| 257 | 0.41 | 0.12 | -0.89 |
| 298 | 0.39 | 0.14 | -0.94 |
| 337 | 0.38 | 0.15 | -0.98 |
| 377 | 0.36 | 0.16 | -1.02 |
| 417 | 0.34 | 0.18 | -1.07 |

| | | | |
|---|---|---|---|
| 457 | 0.34 | 0.19 | -1.08 |
| 557 | 0.31 | 0.23 | -1.19 |
| 679 | 0.28 | 0.26 | -1.29 |
| 798 | 0.25 | 0.29 | -1.40 |
| 917 | 0.22 | 0.31 | -1.50 |
| 1047 | 0.19 | 0.33 | -1.64 |
| 1160 | 0.18 | 0.35 | -1.73 |
| 1277 | 0.16 | 0.37 | -1.83 |
| 1397 | 0.14 | 0.39 | -1.93 |
| 1577 | 0.13 | 0.41 | -2.06 |
| 1757 | 0.10 | 0.43 | -2.25 |
| 1937 | 0.09 | 0.45 | -2.39 |
| 2117 | 0.07 | 0.46 | -2.60 |
| 2301 | 0.07 | 0.47 | -2.70 |
| 2484 | 0.06 | 0.48 | -2.86 |
| 2666 | 0.05 | 0.49 | -3.02 |

**Table 1.34.** $^{19}$F NMR data from monitoring trial 9..

| Time (min) | [**1.13b**] (M) | [**1.15b**] (M) | ln[**1.13b**] |
|---|---|---|---|
| 0 | 0.51 | 0.00 | -0.67 |
| 13 | 0.50 | 0.02 | -0.70 |
| 52 | 0.48 | 0.04 | -0.73 |
| 91 | 0.46 | 0.06 | -0.78 |
| 130 | 0.44 | 0.08 | -0.82 |
| 168 | 0.42 | 0.10 | -0.87 |
| 210 | 0.40 | 0.11 | -0.92 |
| 249 | 0.38 | 0.13 | -0.96 |
| 287 | 0.36 | 0.15 | -1.01 |
| 327 | 0.35 | 0.17 | -1.05 |
| 367 | 0.33 | 0.19 | -1.11 |
| 408 | 0.32 | 0.21 | -1.15 |
| 447 | 0.30 | 0.22 | -1.21 |
| 607 | 0.24 | 0.27 | -1.41 |
| 788 | 0.20 | 0.32 | -1.61 |
| 968 | 0.16 | 0.33 | -1.83 |
| 1152 | 0.14 | 0.38 | -1.98 |
| 1329 | 0.11 | 0.37 | -2.21 |

**Table 1.35.** $^{19}$F NMR data from monitoring trial 10.

| Time (min) | [**1.13b**] (M) | [**1.15b**] (M) | ln[**1.13b**] |
|---|---|---|---|
| 0 | 0.54 | 0.00 | -0.61 |
| 23 | 0.51 | 0.02 | -0.67 |
| 62 | 0.49 | 0.05 | -0.72 |
| 102 | 0.47 | 0.07 | -0.75 |
| 140 | 0.45 | 0.09 | -0.80 |
| 180 | 0.43 | 0.11 | -0.85 |
| 220 | 0.40 | 0.13 | -0.91 |
| 258 | 0.39 | 0.15 | -0.93 |
| 300 | 0.37 | 0.17 | -0.98 |
| 340 | 0.36 | 0.19 | -1.03 |
| 381 | 0.34 | 0.20 | -1.09 |
| 419 | 0.32 | 0.22 | -1.13 |
| 459 | 0.30 | 0.23 | -1.20 |
| 619 | 0.25 | 0.29 | -1.39 |
| 799 | 0.20 | 0.33 | -1.59 |
| 979 | 0.17 | 0.37 | -1.79 |
| 1162 | 0.14 | 0.40 | -1.97 |
| 1339 | 0.12 | 0.43 | -2.15 |

**Table 1.36**. $^{19}$F NMR data from monitoring trial 11.

| Time (min) | [**1.13b**] (M) | [**1.15b**] (M) | ln[**1.13b**] |
|---|---|---|---|
| 0 | 0.50 | 0.00 | -0.70 |
| 33 | 0.48 | 0.03 | -0.73 |
| 73 | 0.48 | 0.06 | -0.74 |
| 112 | 0.45 | 0.08 | -0.80 |
| 149 | 0.43 | 0.10 | -0.84 |
| 189 | 0.41 | 0.12 | -0.90 |
| 229 | 0.38 | 0.14 | -0.96 |
| 270 | 0.37 | 0.16 | -1.00 |
| 309 | 0.35 | 0.19 | -1.05 |
| 349 | 0.33 | 0.20 | -1.11 |
| 390 | 0.32 | 0.22 | -1.15 |
| 428 | 0.30 | 0.24 | -1.20 |
| 468 | 0.28 | 0.26 | -1.26 |
| 628 | 0.22 | 0.31 | -1.51 |
| 808 | 0.18 | 0.36 | -1.69 |
| 989 | 0.15 | 0.39 | -1.91 |

| | | | |
|---|---|---|---|
| 1172 | 0.12 | 0.40 | -2.16 |
| 1357 | 0.09 | 0.43 | -2.36 |

**Table 1.37.** $^{19}$F NMR data from monitoring trial 12.

| Time (min) | [**1.13b**] (M) | [**1.15b**] (M) | ln[**1.13b**] |
|---|---|---|---|
| 0 | 0.52 | 0.00 | -0.65 |
| 42 | 0.48 | 0.04 | -0.74 |
| 82 | 0.45 | 0.06 | -0.79 |
| 121 | 0.44 | 0.09 | -0.82 |
| 159 | 0.41 | 0.10 | -0.89 |
| 200 | 0.39 | 0.12 | -0.94 |
| 239 | 0.37 | 0.15 | -0.98 |
| 279 | 0.35 | 0.16 | -1.05 |
| 319 | 0.33 | 0.20 | -1.11 |
| 359 | 0.31 | 0.21 | -1.17 |
| 399 | 0.29 | 0.23 | -1.25 |
| 438 | 0.27 | 0.25 | -1.32 |
| 478 | 0.25 | 0.25 | -1.38 |
| 638 | 0.21 | 0.32 | -1.54 |
| 818 | 0.16 | 0.36 | -1.80 |
| 999 | 0.12 | 0.37 | -2.08 |
| 1191 | 0.10 | 0.40 | -2.30 |
| 1367 | 0.09 | 0.42 | -2.44 |

**Table 1.38**. $^{19}$F NMR data from monitoring trial 13.

| Time (min) | [**1.13b**] (M) | [**1.15b**] (M) | ln[**1.13b**] |
|---|---|---|---|
| 0 | 0.52 | 0.00 | -0.66 |
| 18 | 0.50 | 0.03 | -0.69 |
| 58 | 0.48 | 0.06 | -0.74 |
| 98 | 0.43 | 0.09 | -0.83 |
| 138 | 0.42 | 0.11 | -0.88 |
| 178 | 0.38 | 0.13 | -0.96 |
| 218 | 0.37 | 0.16 | -0.99 |
| 258 | 0.34 | 0.18 | -1.07 |
| 298 | 0.32 | 0.20 | -1.16 |
| 338 | 0.31 | 0.23 | -1.18 |
| 378 | 0.29 | 0.24 | -1.24 |
| 418 | 0.27 | 0.26 | -1.32 |
| 458 | 0.25 | 0.27 | -1.39 |
| 553 | 0.21 | 0.31 | -1.54 |

| | | | |
|---|---|---|---|
| 617 | 0.20 | 0.34 | -1.60 |
| 797 | 0.17 | 0.39 | -1.78 |

**Table 1.39.** $^{19}$F NMR data from monitoring trial 14.

| Time (min) | [**1.13b**] (M) | [**1.15b**] (M) | ln[**1.13b**] |
|---|---|---|---|
| 0 | 0.52 | 0.00 | -0.66 |
| 28 | 0.49 | 0.03 | -0.72 |
| 68 | 0.45 | 0.06 | -0.79 |
| 108 | 0.43 | 0.09 | -0.85 |
| 148 | 0.41 | 0.12 | -0.89 |
| 188 | 0.37 | 0.13 | -0.99 |
| 228 | 0.35 | 0.16 | -1.05 |
| 268 | 0.33 | 0.18 | -1.10 |
| 308 | 0.31 | 0.20 | -1.18 |
| 348 | 0.30 | 0.23 | -1.22 |
| 388 | 0.27 | 0.24 | -1.32 |
| 428 | 0.25 | 0.26 | -1.39 |
| 468 | 0.24 | 0.27 | -1.43 |
| 561 | 0.21 | 0.30 | -1.54 |
| 628 | 0.18 | 0.33 | -1.69 |

**"Different excess" experiments with nitrostyrene 1.13b**

**Table 1.40.** $^{19}$F NMR data from monitoring trial 15.

| Time (min) | [**1.13b**] (M) | [**1.15b**] (M) | ln[**1.13b**] |
|---|---|---|---|
| 7 | 1.438 | 1.583 | 0.363 |
| 37 | 1.388 | 1.551 | 0.328 |
| 67 | 1.361 | 1.513 | 0.308 |
| 97 | 1.316 | 1.486 | 0.274 |
| 127 | 1.291 | 1.460 | 0.255 |
| 158 | 1.273 | 1.431 | 0.241 |
| 187 | 1.234 | 1.414 | 0.210 |
| 217 | 1.222 | 1.380 | 0.200 |
| 246 | 1.189 | 1.362 | 0.173 |
| 276 | 1.176 | 1.328 | 0.162 |
| 307 | 1.149 | 1.304 | 0.138 |
| 337 | 1.132 | 1.286 | 0.124 |

| | | | |
|---|---|---|---|
| 367 | 1.103 | 1.257 | 0.098 |
| 397 | 1.070 | 1.244 | 0.068 |
| 427 | 1.062 | 1.210 | 0.060 |
| 457 | 1.027 | 1.207 | 0.026 |
| 487 | 1.010 | 1.164 | 0.010 |
| 557 | 0.966 | 1.146 | -0.034 |
| 617 | 0.938 | 1.102 | -0.064 |
| 677 | 0.894 | 1.081 | -0.112 |
| 797 | 0.827 | 1.039 | -0.191 |
| 921 | 0.780 | 0.971 | -0.248 |
| 1038 | 0.741 | 0.915 | -0.299 |
| 1158 | 0.701 | 0.870 | -0.355 |
| 1278 | 0.664 | 0.812 | -0.410 |

**Table 1.41.** $^{19}$F NMR data from monitoring trial 16

| Time (min) | [**1.13b**] (M) | [**1.15b**] (M) | ln[**1.13b**] |
|---|---|---|---|
| . 0 | 1.244 | 1.603 | 0.218 |
| 17 | 1.190 | 1.572 | 0.174 |
| 47 | 1.158 | 1.542 | 0.147 |
| 77 | 1.140 | 1.521 | 0.131 |
| 107 | 1.134 | 1.492 | 0.126 |
| 137 | 1.094 | 1.455 | 0.090 |
| 167 | 1.075 | 1.429 | 0.072 |
| 198 | 1.044 | 1.416 | 0.043 |
| 228 | 1.016 | 1.381 | 0.016 |
| 257 | 1.006 | 1.361 | 0.006 |
| 287 | 0.980 | 1.331 | -0.020 |
| 317 | 0.962 | 1.317 | -0.038 |
| 347 | 0.944 | 1.298 | -0.057 |
| 377 | 0.920 | 1.272 | -0.083 |
| 407 | 0.907 | 1.241 | -0.097 |
| 437 | 0.882 | 1.218 | -0.126 |
| 467 | 0.869 | 1.195 | -0.140 |
| 497 | 0.845 | 1.176 | -0.169 |
| 557 | 0.813 | 1.136 | -0.208 |

| | | | |
|---|---|---|---|
| 617 | 0.787 | 1.117 | -0.240 |
| 677 | 0.744 | 1.086 | -0.296 |
| 797 | 0.691 | 1.030 | -0.369 |
| 918 | 0.636 | 0.986 | -0.453 |
| 1037 | 0.591 | 0.937 | -0.526 |
| 1162 | 0.531 | 0.918 | -0.634 |
| 1284 | 0.490 | 0.875 | -0.713 |

**Table 1.42.** $^{19}$F NMR data from monitoring trial 17

| Time (min) | [**1.13b**] (M) | [**1.15b**] (M) | 1/[**1.13b**] |
|---|---|---|---|
| . 0 | 1.419 | 2.000 | 0.705 |
| 10 | 1.424 | 1.983 | 0.702 |
| 70 | 1.389 | 1.946 | 0.720 |
| 131 | 1.364 | 1.908 | 0.733 |
| 197 | 1.315 | 1.869 | 0.761 |
| 250 | 1.290 | 1.839 | 0.775 |
| 309 | 1.263 | 1.807 | 0.792 |
| 370 | 1.237 | 1.772 | 0.809 |
| 429 | 1.201 | 1.743 | 0.833 |
| 490 | 1.174 | 1.708 | 0.852 |
| 668 | 1.090 | 1.625 | 0.918 |
| 851 | 1.026 | 1.539 | 0.975 |
| 1031 | 0.941 | 1.474 | 1.063 |
| 1209 | 0.868 | 1.416 | 1.152 |
| 1401 | 0.796 | 1.358 | 1.256 |
| 1578 | 0.741 | 1.310 | 1.349 |
| 1750 | 0.689 | 1.268 | 1.452 |
| 1931 | 0.655 | 1.220 | 1.527 |
| 2111 | 0.615 | 1.187 | 1.627 |
| 2289 | 0.582 | 1.148 | 1.719 |
| 2470 | 0.551 | 1.125 | 1.815 |
| 2649 | 0.525 | 1.095 | 1.904 |
| 2832 | 0.497 | 1.078 | 2.012 |

| | | | |
|---|---|---|---|
| 3008 | 0.478 | 1.049 | 2.094 |
| 3190 | 0.459 | 1.021 | 2.179 |
| 3371 | 0.440 | 1.006 | 2.270 |
| 3548 | 0.423 | 0.990 | 2.366 |
| 3731 | 0.407 | 0.968 | 2.455 |
| 3910 | 0.392 | 0.953 | 2.551 |
| 4088 | 0.378 | 0.939 | 2.643 |
| 4269 | 0.365 | 0.932 | 2.743 |
| 4448 | 0.352 | 0.918 | 2.843 |
| 4632 | 0.340 | 0.912 | 2.945 |
| 4810 | 0.334 | 0.895 | 2.994 |
| 4990 | 0.320 | 0.883 | 3.123 |

**Table 1.43.** $^{19}$F NMR data from monitoring trial 18

| Time (min) | [**1.13b**] (M) | [**1.15b**] (M) | 1/[**1.13b**] |
|---|---|---|---|
| . 0 | 1.217 | 2.000 | 0.822 |
| 21 | 1.241 | 1.980 | 0.806 |
| 79 | 1.224 | 1.951 | 0.817 |
| 141 | 1.205 | 1.919 | 0.830 |
| 208 | 1.161 | 1.888 | 0.862 |
| 261 | 1.141 | 1.864 | 0.876 |
| 320 | 1.118 | 1.838 | 0.894 |
| 379 | 1.088 | 1.810 | 0.919 |
| 439 | 1.074 | 1.783 | 0.931 |
| 500 | 1.046 | 1.757 | 0.956 |
| 679 | 0.976 | 1.682 | 1.025 |
| 860 | 0.920 | 1.608 | 1.086 |
| 1041 | 0.871 | 1.540 | 1.148 |
| 1220 | 0.799 | 1.482 | 1.252 |
| 1411 | 0.720 | 1.438 | 1.388 |
| 1587 | 0.665 | 1.392 | 1.503 |
| 1762 | 0.620 | 1.351 | 1.612 |
| 1940 | 0.573 | 1.320 | 1.746 |
| 2122 | 0.547 | 1.280 | 1.828 |
| 2301 | 0.511 | 1.254 | 1.956 |
| 2481 | 0.489 | 1.222 | 2.047 |
| 2661 | 0.466 | 1.194 | 2.147 |
| 2843 | 0.441 | 1.178 | 2.268 |
| 3020 | 0.423 | 1.163 | 2.364 |

| | | | |
|---|---|---|---|
| 3203 | 0.406 | 1.139 | 2.465 |
| 3381 | 0.387 | 1.114 | 2.583 |
| 3560 | 0.372 | 1.105 | 2.689 |
| 3739 | 0.353 | 1.095 | 2.831 |
| 3922 | 0.344 | 1.081 | 2.910 |
| 4100 | 0.334 | 1.064 | 2.994 |
| 4280 | 0.317 | 1.055 | 3.151 |
| 4460 | 0.306 | 1.048 | 3.272 |
| 4642 | 0.299 | 1.028 | 3.339 |
| 4822 | 0.289 | 1.017 | 3.459 |
| 5002 | 0.279 | 1.009 | 3.587 |

**Varied Concentration of Indole 1.14b**

**Table 1.44** $^{19}$F NMR data from monitoring trial 19

| Time (min) | [**1.13b**] (M) | [**1.15b**] (M) | ln[**1.15b**] |
|---|---|---|---|
| 0 | 1.548 | 2 | 0.437 |
| 10 | 1.475 | 1.952 | 0.389 |
| 47 | 1.405 | 1.892 | 0.340 |
| 76 | 1.356 | 1.846 | 0.304 |
| 107 | 1.331 | 1.798 | 0.286 |
| 137 | 1.275 | 1.757 | 0.243 |
| 165 | 1.233 | 1.720 | 0.209 |
| 191 | 1.207 | 1.686 | 0.188 |
| 220 | 1.182 | 1.651 | 0.167 |
| 248 | 1.129 | 1.614 | 0.121 |
| 279 | 1.095 | 1.577 | 0.091 |
| 310 | 1.057 | 1.549 | 0.055 |
| 340 | 1.028 | 1.511 | 0.027 |
| 371 | 0.993 | 1.477 | -0.006 |
| 398 | 0.975 | 1.444 | -0.024 |
| 428 | 0.942 | 1.422 | -0.059 |
| 460 | 0.912 | 1.389 | -0.091 |
| 550 | 0.828 | 1.321 | -0.188 |
| 669 | 0.753 | 1.233 | -0.282 |
| 790 | 0.672 | 1.170 | -0.396 |
| 910 | 0.619 | 1.091 | -0.479 |
| 1030 | 0.568 | 1.030 | -0.565 |
| 1149 | 0.506 | 1.005 | -0.680 |
| 1270 | 0.467 | | -0.760 |

| | | | |
|---|---|---|---|
| 1390 | 0.424 | 0.946 | -0.857 |
| 1508 | 0.398 | 0.919 | -0.919 |
| 1628 | 0.372 | 0.868 | -0.987 |
| 1750 | 0.330 | 0.813 | -1.107 |
| 1870 | 0.315 | 0.827 | -1.154 |
| 1989 | 0.292 | 0.785 | -1.230 |
| 2110 | 0.267 | 0.748 | -1.317 |
| 2228 | 0.249 | 0.726 | -1.388 |
| 2349 | 0.233 | 0.719 | -1.453 |
| 2469 | 0.216 | 0.694 | -1.529 |
| 2590 | 0.197 | 0.690 | -1.624 |
| 2710 | 0.187 | 0.661 | -1.672 |
| 2834 | 0.175 | 0.656 | -1.737 |

**Table 1.45**. $^{19}$F NMR data from monitoring trial 20

| Time (min) | [**1.13b**] (M) | [**1.15b**] (M) | ln[**1.13b**] |
|---|---|---|---|
| 0 | 1.579 | 1.5 | 0.457 |
| 21 | 1.520 | 1.435 | 0.419 |
| 56 | 1.478 | 1.402 | 0.390 |
| 89 | 1.431 | 1.368 | 0.358 |
| 118 | 1.388 | 1.335 | 0.328 |
| 147 | 1.357 | 1.306 | 0.305 |
| 176 | 1.336 | 1.278 | 0.290 |
| 204 | 1.300 | 1.253 | 0.263 |
| 231 | 1.275 | 1.226 | 0.243 |
| 263 | 1.247 | 1.199 | 0.221 |
| 290 | 1.220 | 1.176 | 0.198 |
| 322 | 1.183 | 1.148 | 0.168 |
| 353 | 1.140 | 1.121 | 0.131 |
| 382 | 1.128 | 1.098 | 0.120 |
| 411 | 1.109 | 1.073 | 0.104 |
| 438 | 1.083 | 1.053 | 0.080 |
| 470 | 1.055 | 1.031 | 0.053 |
| 560 | 0.981 | 0.977 | -0.018 |
| 679 | 0.903 | 0.908 | -0.101 |
| 810 | 0.840 | 0.838 | -0.173 |
| 928 | 0.783 | 0.787 | -0.244 |
| 1045 | 0.724 | 0.728 | -0.321 |
| 1164 | 0.675 | 0.708 | -0.392 |

| | | | |
|---|---|---|---|
| 1286 | 0.627 | 0.650 | -0.466 |
| 1406 | 0.599 | 0.615 | -0.511 |
| 1526 | 0.558 | 0.589 | -0.581 |
| 1645 | 0.535 | 0.553 | -0.623 |
| 1766 | 0.499 | 0.528 | -0.695 |
| 1886 | 0.467 | 0.509 | -0.760 |
| 2006 | 0.446 | 0.480 | -0.806 |
| 2127 | 0.422 | 0.434 | -0.862 |
| 2246 | 0.399 | 0.408 | -0.916 |
| 2365 | 0.376 | 0.390 | -0.975 |
| 2484 | 0.356 | 0.368 | -1.031 |
| 2605 | 0.336 | 0.341 | -1.088 |
| 2724 | 0.323 | 0.334 | -1.129 |
| 2849 | 0.302 | 0.314 | -1.197 |

**Table 1.46.** $^{19}$F NMR data from monitoring trial 21

| Time (min) | [**1.13b**] (M) | [**1.15b**] (M) | 1/[**1.13b**] |
|---|---|---|---|
| 0 | 1.512 | 1.500 | 0.662 |
| 23 | 1.489 | 1.475 | 0.672 |
| 81 | 1.459 | 1.442 | 0.686 |
| 142 | 1.429 | 1.410 | 0.700 |
| 202 | 1.392 | 1.379 | 0.718 |
| 260 | 1.371 | 1.349 | 0.729 |
| 321 | 1.345 | 1.317 | 0.744 |
| 380 | 1.321 | 1.288 | 0.757 |
| 442 | 1.291 | 1.260 | 0.775 |
| 566 | 1.235 | 1.204 | 0.810 |
| 740 | 1.170 | 1.128 | 0.855 |
| 927 | 1.110 | 1.051 | 0.901 |
| 1102 | 1.023 | 0.992 | 0.977 |
| 1292 | 0.949 | 0.935 | 1.054 |
| 1463 | 0.889 | 0.886 | 1.125 |
| 1641 | 0.825 | 0.844 | 1.211 |
| 1821 | 0.773 | 0.800 | 1.294 |
| 2001 | 0.734 | 0.756 | 1.362 |
| 2180 | 0.694 | 0.719 | 1.441 |
| 2362 | 0.657 | 0.685 | 1.521 |
| 2526 | 0.617 | 0.646 | 1.621 |
| 2729 | 0.600 | 0.618 | 1.668 |
| 2912 | 0.572 | 0.583 | 1.748 |

| | | | |
|---|---|---|---|
| 3080 | 0.548 | 0.561 | 1.825 |
| 3260 | 0.525 | 0.550 | 1.906 |
| 3440 | 0.502 | 0.522 | 1.993 |
| 3625 | 0.482 | 0.495 | 2.073 |
| 3805 | 0.470 | 0.478 | 2.129 |
| 3993 | 0.450 | 0.459 | 2.221 |
| 4163 | 0.435 | 0.439 | 2.300 |
| 4460 | 0.413 | 0.401 | 2.423 |
| 4640 | 0.403 | 0.397 | 2.483 |
| 4819 | 0.385 | 0.399 | 2.596 |
| 5003 | 0.377 | 0.374 | 2.656 |

**Table 1.47.** $^{19}$F NMR data from monitoring trial 22.

| Time (min) | [**1.13b**] (M) | [**1.15b**] (M) | 1/[**1.13b**] |
|---|---|---|---|
| 0 | 1.432 | 1.250 | 0.698 |
| 33 | 1.472 | 1.226 | 0.679 |
| 92 | 1.447 | 1.201 | 0.691 |
| 144 | 1.427 | 1.174 | 0.701 |
| 213 | 1.389 | 1.150 | 0.720 |
| 271 | 1.372 | 1.127 | 0.729 |
| 330 | 1.347 | 1.104 | 0.743 |
| 391 | 1.320 | 1.080 | 0.758 |
| 451 | 1.304 | 1.058 | 0.767 |
| 578 | 1.260 | 1.013 | 0.794 |
| 751 | 1.207 | 0.953 | 0.829 |
| 938 | 1.158 | 0.890 | 0.864 |
| 1123 | 1.130 | 0.823 | 0.885 |
| 1303 | 1.057 | 0.780 | 0.946 |
| 1471 | 1.005 | 0.739 | 0.995 |
| 1652 | 0.956 | 0.693 | 1.046 |
| 1831 | 0.915 | 0.660 | 1.093 |
| 2012 | 0.870 | 0.624 | 1.150 |
| 2191 | 0.839 | 0.594 | 1.192 |
| 2382 | 0.801 | 0.565 | 1.248 |
| 2551 | 0.782 | 0.534 | 1.279 |
| 2739 | 0.751 | 0.503 | 1.331 |
| 2922 | 0.726 | 0.480 | 1.378 |
| 3091 | 0.701 | 0.461 | 1.427 |
| 3272 | 0.679 | 0.439 | 1.473 |
| 3451 | 0.664 | 0.415 | 1.506 |

| | | | |
|---|---|---|---|
| 3636 | 0.643 | 0.402 | 1.556 |
| 3814 | 0.630 | 0.384 | 1.586 |
| 4005 | 0.603 | 0.364 | 1.658 |
| 4173 | 0.596 | 0.348 | 1.679 |
| 4471 | 0.571 | 0.327 | 1.752 |
| 4651 | 0.554 | 0.321 | 1.805 |
| 4837 | 0.539 | 0.310 | 1.854 |

**"Same Excess" Experiments**

**Table 1.48.** $^{19}$F NMR data from monitoring trial 23.

| Time (min) | [**1.13b**] (M) | [**1.14b**] (M) | ln[**1.13b**] |
|---|---|---|---|
| 0 | 1.502 | 2.000 | 0.407 |
| 10 | 1.462 | 1.971 | 0.380 |
| 42 | 1.415 | 1.923 | 0.347 |
| 153 | 1.331 | 1.814 | 0.286 |
| 179 | 1.258 | 1.750 | 0.230 |
| 229 | 1.209 | 1.692 | 0.190 |
| 280 | 1.155 | 1.639 | 0.144 |
| 332 | 1.119 | 1.607 | 0.113 |
| 384 | 1.049 | 1.540 | 0.048 |
| 447 | 0.961 | 1.447 | -0.040 |
| 508 | 0.899 | 1.382 | -0.106 |
| 568 | 0.845 | 1.329 | -0.168 |
| 688 | 0.773 | 1.261 | -0.257 |
| 809 | 0.710 | 1.206 | -0.342 |
| 929 | 0.646 | 1.138 | -0.436 |
| 1049 | 0.610 | 1.102 | -0.494 |
| 1229 | 0.568 | 1.050 | -0.566 |

**Table 1.49.** $^{19}$F NMR data from monitoring trial 24.

| Time (min) | [**1.13b**] (M) | [**1.14b**] (M) | ln[**1.13b**] |
|---|---|---|---|
| 0 | 1.204 | 1.700 | 0.186 |
| 22 | 1.179 | 1.667 | 0.165 |
| 52 | 1.125 | 1.631 | 0.118 |
| 187 | 1.005 | 1.502 | 0.005 |
| 237 | 0.966 | 1.458 | -0.035 |
| 288 | 0.929 | 1.415 | -0.074 |
| 341 | 0.876 | 1.377 | -0.132 |
| 393 | 0.846 | 1.336 | -0.168 |
| 473 | 0.795 | 1.303 | -0.230 |

| | | | |
|---|---|---|---|
| 578 | 0.724 | 1.235 | -0.323 |
| 697 | 0.659 | 1.174 | -0.417 |
| 818 | 0.625 | 1.118 | -0.469 |
| 938 | 0.565 | 1.073 | -0.570 |
| 1064 | 0.530 | 1.020 | -0.634 |
| 1178 | 0.504 | 0.977 | -0.684 |

**Table 1.50.** $^{19}$F NMR data from monitoring trial 25

| Time (min) | [**1.13b**] (M) | [**1.15b**] (M) |
|---|---|---|
| 0 | 0.97 | 0.00 |
| 48 | 0.95 | 0.03 |
| 78 | 0.95 | 0.04 |
| 108 | 0.93 | 0.06 |
| 138 | 0.92 | 0.08 |
| 169 | 0.92 | 0.09 |
| 199 | 0.90 | 0.11 |
| 228 | 0.88 | 0.12 |
| 257 | 0.87 | 0.13 |
| 290 | 0.89 | 0.15 |
| 320 | 0.85 | 0.17 |
| 350 | 0.84 | 0.17 |
| 380 | 0.81 | 0.18 |
| 412 | 0.79 | 0.19 |
| 443 | 0.79 | 0.20 |
| 470 | 0.79 | 0.22 |
| 498 | 0.78 | 0.24 |
| 561 | 0.73 | 0.25 |
| 681 | 0.70 | 0.30 |
| 826 | 0.64 | 0.33 |
| 921 | 0.62 | 0.35 |
| 1169 | 0.57 | 0.42 |
| 1291 | 0.54 | 0.43 |
| 1515 | 0.51 | 0.47 |
| 1649 | 0.47 | 0.48 |
| 1772 | 0.47 | 0.53 |
| 1891 | 0.46 | 0.53 |
| 2011 | 0.43 | 0.53 |
| 2372 | 0.41 | 0.60 |

| | | |
|---|---|---|
| 2493 | 0.40 | 0.62 |
| 2603 | 0.38 | 0.62 |
| 2719 | 0.37 | 0.63 |
| 2844 | 0.36 | 0.64 |
| 2960 | 0.36 | 0.66 |
| 3081 | 0.34 | 0.66 |
| 3201 | 0.33 | 0.67 |
| 3310 | 0.33 | 0.68 |
| 3449 | 0.32 | 0.68 |
| 3560 | 0.31 | 0.69 |
| 3680 | 0.31 | 0.69 |
| 3800 | 0.30 | 0.66 |
| 4052 | 0.28 | 0.69 |
| 4278 | 0.28 | 0.72 |

**Table 1.51.** $^{19}$F NMR data from monitoring trial 26.

| Time (min) | [**1.13b**] (M) | [**1.15b**] (M) | 1/[**1.13b**] |
|---|---|---|---|
| 670 | 0.479 | 1.408 | 2.087 |
| 848 | 0.518 | 1.389 | 2.162 |
| 1035 | 0.512 | 1.374 | 2.277 |
| 1188 | 0.518 | 1.359 | 2.367 |
| 1390 | 0.519 | 1.348 | 2.434 |
| 1570 | 0.533 | 1.337 | 2.495 |
| 1770 | 0.528 | 1.327 | 2.586 |
| 1945 | 0.525 | 1.320 | 2.632 |
| 2110 | 0.514 | 1.313 | 2.685 |
| 2290 | 0.479 | 1.308 | 2.727 |
| 2473 | 0.463 | 1.300 | 2.791 |
| 2650 | 0.439 | 1.295 | 2.824 |
| 2841 | 0.423 | 1.291 | 2.864 |
| 3010 | 0.411 | 1.287 | 2.906 |
| 3189 | 0.401 | 1.279 | 2.963 |
| 3369 | 0.387 | 1.275 | 3.015 |
| 3550 | 0.380 | 1.271 | 3.046 |
| 3730 | 0.373 | 1.267 | 3.125 |
| 3910 | 0.367 | 1.267 | 3.141 |
| 4090 | 0.358 | 1.262 | 3.200 |
| 4269 | 0.354 | 1.253 | 3.288 |
| 4450 | 0.349 | 1.250 | 3.333 |
| 4630 | 0.344 | 1.242 | 3.429 |

**Nitrobenzene binding experiments**

**Table 1.52.** $^{19}$F NMR data from monitoring trial 27.

| Time (min) | [**1.13b**](M) | [**1.15b**] (M) | ln[**1.13b**] |
|---|---|---|---|
| 0 | 1.460 | 2.000 | 0.379 |
| 13 | 1.427 | 1.958 | 0.356 |
| 71 | 1.358 | 1.883 | 0.306 |
| 133 | 1.266 | 1.815 | 0.236 |
| 191 | 1.211 | 1.752 | 0.191 |
| 251 | 1.144 | 1.686 | 0.134 |
| 313 | 1.085 | 1.626 | 0.081 |
| 372 | 1.031 | 1.574 | 0.031 |
| 428 | 0.995 | 1.524 | -0.005 |
| 608 | 0.885 | 1.374 | -0.122 |
| 790 | 0.739 | 1.270 | -0.302 |
| 969 | 0.634 | 1.189 | -0.455 |
| 1151 | 0.566 | 1.100 | -0.568 |
| 1328 | 0.520 | 1.047 | -0.654 |
| 1510 | 0.435 | 0.966 | -0.832 |
| 1698 | 0.383 | 0.912 | -0.960 |
| 1870 | 0.341 | 0.874 | -1.076 |
| 2051 | 0.296 | 0.843 | -1.216 |
| 2233 | 0.262 | 0.818 | -1.339 |
| 2410 | 0.245 | 0.764 | -1.407 |
| 2587 | 0.215 | 0.724 | -1.538 |
| 2765 | 0.188 | 0.723 | -1.669 |
| 2943 | 0.164 | 0.659 | -1.805 |
| 3127 | 0.152 | 0.642 | -1.881 |
| 3304 | 0.132 | 0.655 | -2.025 |
| 3486 | 0.115 | 0.636 | -2.161 |

**Table 1.53.** $^{19}$F NMR data from monitoring trial 28.

| Time (min) | [**1.13b**] (M) | [**1.15b**] (M) | ln[**1.13b**] |
|---|---|---|---|
| 0 | 1.490 | 2.000 | 0.399 |
| 23 | 1.422 | 1.944 | 0.352 |
| 85 | 1.361 | 1.857 | 0.309 |
| 142 | 1.249 | 1.795 | 0.222 |
| 200 | 1.199 | 1.722 | 0.182 |
| 261 | 1.126 | 1.648 | 0.119 |

| | | | |
|---|---|---|---|
| 323 | 1.063 | 1.584 | 0.061 |
| 383 | 0.998 | 1.533 | -0.002 |
| 440 | 0.950 | 1.485 | -0.051 |
| 629 | 0.809 | 1.339 | -0.211 |
| 800 | 0.694 | 1.239 | -0.365 |
| 979 | 0.611 | 1.134 | -0.493 |
| 1166 | 0.534 | 1.058 | -0.627 |
| 1342 | 0.460 | 0.993 | -0.777 |
| 1521 | 0.403 | 0.933 | -0.910 |
| 1707 | 0.349 | 0.895 | -1.052 |
| 1884 | 0.316 | 0.830 | -1.153 |
| 2061 | 0.276 | 0.808 | -1.287 |
| 2242 | 0.241 | 0.771 | -1.422 |
| 2420 | 0.215 | 0.744 | -1.538 |
| 2604 | 0.193 | 0.717 | -1.644 |
| 2783 | 0.169 | 0.697 | -1.777 |
| 2960 | 0.148 | 0.668 | -1.909 |
| 3143 | 0.137 | 0.654 | -1.989 |
| 3320 | 0.120 | 0.642 | -2.120 |
| 3504 | 0.107 | 0.626 | -2.237 |

**Table 1.54.** $^{19}$F NMR data from monitoring trial 29.

| Time (min) | [**1.13b**] (M) | [**1.15b**] (M) | 1/[**1.13b**] |
|---|---|---|---|
| 0 | 1.500 | 2.000 | 0.667 |
| 102 | 1.367 | 1.941 | 0.732 |
| 129 | 1.358 | 1.899 | 0.736 |
| 200 | 1.305 | 1.846 | 0.766 |
| 250 | 1.237 | 1.817 | 0.809 |
| 308 | 1.246 | 1.762 | 0.803 |
| 369 | 1.180 | 1.735 | 0.848 |
| 427 | 1.130 | 1.719 | 0.885 |
| 620 | 1.075 | 1.615 | 0.931 |
| 791 | 0.993 | 1.489 | 1.007 |
| 970 | 0.862 | 1.453 | 1.161 |
| 1150 | 0.803 | 1.359 | 1.246 |
| 1327 | 0.725 | 1.321 | 1.379 |
| 1512 | 0.659 | 1.291 | 1.518 |
| 1692 | 0.623 | 1.220 | 1.604 |
| 1873 | 0.592 | 1.174 | 1.690 |

| | | | |
|---|---|---|---|
| 2051 | 0.535 | 1.170 | 1.868 |
| 2231 | 0.528 | 1.103 | 1.894 |
| 2414 | 0.492 | 1.076 | 2.033 |
| 2594 | 0.469 | 1.057 | 2.131 |
| 2773 | 0.448 | 1.047 | 2.234 |
| 2950 | 0.425 | 1.024 | 2.354 |
| 3133 | 0.409 | 1.000 | 2.444 |
| 3309 | 0.395 | 0.972 | 2.529 |
| 3491 | 0.390 | 0.946 | 2.564 |
| 3670 | 0.364 | 0.954 | 2.746 |
| 3851 | 0.347 | 0.940 | 2.879 |
| 4035 | 0.331 | 0.940 | 3.019 |
| 4402 | 0.323 | 0.888 | 3.092 |
| 4581 | 0.317 | 0.867 | 3.151 |
| 4762 | 0.306 | 0.863 | 3.268 |
| 4942 | 0.288 | 0.849 | 3.472 |

**Table 1.55.** $^{19}$F NMR data from monitoring trial 30.

| Time (min) | [**1.13b**] (M) | [**1.15b**] (M) | 1/[**1.13b**] |
|---|---|---|---|
| 0 | 1.498 | 2.000 | 0.668 |
| 31 | 1.442 | 1.960 | 0.693 |
| 94 | 1.407 | 1.909 | 0.711 |
| 150 | 1.358 | 1.881 | 0.736 |
| 59 | 1.310 | 1.823 | 0.763 |
| 121 | 1.262 | 1.782 | 0.793 |
| 183 | 1.220 | 1.745 | 0.820 |
| 243 | 1.160 | 1.704 | 0.862 |
| 301 | 1.130 | 1.669 | 0.885 |
| 507 | 1.083 | 1.525 | 0.923 |
| 667 | 0.949 | 1.483 | 1.054 |
| 838 | 0.862 | 1.399 | 1.160 |
| 1027 | 0.800 | 1.311 | 1.250 |
| 1205 | 0.730 | 1.251 | 1.371 |
| 1374 | 0.691 | 1.226 | 1.448 |
| 1563 | 0.626 | 1.159 | 1.598 |
| 1740 | 0.579 | 1.122 | 1.727 |
| 1917 | 0.550 | 1.072 | 1.818 |
| 2098 | 0.508 | 1.050 | 1.970 |
| 2274 | 0.482 | 1.011 | 2.073 |
| 2457 | 0.453 | 0.987 | 2.208 |

| | | | |
|---|---|---|---|
| 2637 | 0.434 | 0.958 | 2.302 |
| 2813 | 0.394 | 0.958 | 2.537 |
| 2940 | 0.386 | 0.943 | 2.592 |
| 3114 | 0.373 | 0.894 | 2.680 |
| 3301 | 0.352 | 0.910 | 2.844 |
| 3473 | 0.342 | 0.868 | 2.924 |
| 3653 | 0.333 | 0.849 | 3.003 |
| 3837 | 0.319 | 0.840 | 3.139 |
| 4026 | 0.304 | 0.844 | 3.294 |
| 4208 | 0.299 | 0.821 | 3.340 |
| 4386 | 0.291 | 0.822 | 3.436 |
| 4568 | 0.286 | 0.804 | 3.494 |

**Kinetic isotope effect**

**Table 1.56.** $^{19}$F NMR data from monitoring trial 31.

| Time (min) | [**1.13b**] (M) | [**1.15b**] (M) | ln[**1.13b**] |
|---|---|---|---|
| 0 | 0.973 | 0.0 | -0.027 |
| 8 | 0.940 | 0.022 | -0.062 |
| 37 | 0.914 | 0.051 | -0.090 |
| 68 | 0.886 | 0.080 | -0.122 |
| 98 | 0.862 | 0.107 | -0.149 |
| 128 | 0.825 | 0.132 | -0.192 |
| 158 | 0.806 | 0.160 | -0.215 |
| 188 | 0.779 | 0.183 | -0.250 |
| 218 | 0.760 | 0.207 | -0.274 |
| 248 | 0.739 | 0.232 | -0.303 |
| 278 | 0.716 | 0.253 | -0.334 |
| 308 | 0.696 | 0.277 | -0.363 |
| 338 | 0.676 | 0.298 | -0.392 |
| 368 | 0.659 | 0.321 | -0.417 |
| 488 | 0.590 | 0.396 | -0.527 |
| 608 | 0.531 | 0.466 | -0.632 |
| 728 | 0.479 | 0.530 | -0.736 |

**Table 1.57.** $^{19}$F NMR data from monitoring trial 32.

| Time (min) | [**1.13b**] (M) | [**1.15b**] (M) | ln[**1.13b**] |
|---|---|---|---|
| 0 | 0.960 | 0.000 | -0.040 |
| 18 | 0.937 | 0.029 | -0.065 |
| 48 | 0.916 | 0.057 | -0.088 |

| | | | |
|---|---|---|---|
| 78 | 0.890 | 0.084 | -0.116 |
| 109 | 0.860 | 0.109 | -0.150 |
| 137 | 0.839 | 0.132 | -0.176 |
| 168 | 0.811 | 0.156 | -0.209 |
| 197 | 0.792 | 0.179 | -0.234 |
| 228 | 0.770 | 0.201 | -0.261 |
| 258 | 0.750 | 0.222 | -0.288 |
| 289 | 0.727 | 0.245 | -0.319 |
| 318 | 0.706 | 0.259 | -0.349 |
| 347 | 0.690 | 0.280 | -0.371 |
| 378 | 0.671 | 0.296 | -0.400 |
| 498 | 0.606 | 0.363 | -0.502 |
| 618 | 0.551 | 0.420 | -0.596 |
| 738 | 0.501 | 0.472 | -0.691 |

**Table 1.58.**. $^{19}$F NMR data from monitoring trial 33.

| Time (min) | [**1.13b**] (M) | [**1.15b**] (M) | ln[**1.13b**] |
|---|---|---|---|
| 0 | 1.00 | 0.00 | 0.00 |
| 22 | 0.96 | 0.03 | -0.04 |
| 67 | 0.93 | 0.08 | -0.08 |
| 98 | 0.91 | 0.10 | -0.09 |
| 137 | 0.86 | 0.15 | -0.15 |
| 182 | 0.83 | 0.19 | -0.19 |
| 230 | 0.77 | 0.23 | -0.26 |
| 273 | 0.75 | 0.26 | -0.29 |
| 317 | 0.70 | 0.29 | -0.35 |
| 378 | 0.67 | 0.34 | -0.39 |
| 437 | 0.63 | 0.38 | -0.46 |
| 498 | 0.59 | 0.42 | -0.52 |
| 558 | 0.55 | 0.45 | -0.59 |
| 617 | 0.53 | 0.49 | -0.64 |
| 679 | 0.51 | 0.53 | -0.67 |
| 738 | 0.46 | 0.54 | -0.77 |
| 858 | 0.42 | 0.59 | -0.86 |
| 978 | 0.37 | 0.63 | -1.00 |
| 1100 | 0.33 | 0.67 | -1.12 |
| 1218 | 0.30 | 0.72 | -1.21 |

**Table 1.59**. $^{19}$F NMR data from monitoring trial 34.

| Time (min) | [**1.13b**] (M) | [**1.15b**] (M) | ln[**1.13 b**] |
|---|---|---|---|
| 0 | 1.04 | 0.00 | 0.04 |
| 9 | 0.99 | 0.03 | -0.01 |
| 46 | 0.96 | 0.07 | -0.04 |
| 69 | 0.94 | 0.09 | -0.07 |
| 98 | 0.90 | 0.12 | -0.11 |
| 129 | 0.88 | 0.15 | -0.13 |
| 260 | 0.86 | 0.18 | -0.15 |
| 289 | 0.82 | 0.20 | -0.20 |
| 319 | 0.80 | 0.23 | -0.22 |
| 348 | 0.76 | 0.25 | -0.27 |
| 380 | 0.74 | 0.27 | -0.30 |
| 408 | 0.72 | 0.29 | -0.33 |
| 438 | 0.72 | 0.32 | -0.34 |
| 470 | 0.68 | 0.33 | -0.38 |
| 501 | 0.66 | 0.36 | -0.41 |
| 528 | 0.65 | 0.40 | -0.44 |
| 708 | 0.56 | 0.47 | -0.58 |
| 890 | 0.48 | 0.56 | -0.74 |

## 1.11.6: X-ray data

**Table 1.60.** Crystal Data for **1.1c.**

| | | |
|---|---|---|
| Identification code | JF2728FFMI | |
| Empirical formula | $C_{42}\ H_{38}\ O_{12}\ Si_7$ | |
| Formula weight | 931.35 | |
| Temperature | 100(2) K | |
| Wavelength | 0.71073 Å | |
| Crystal system | Triclinic | |
| Space group | P-1 | |
| Unit cell dimensions | a = 14.4652(11) Å | α = 84.9923(19)°. |
| | b = 14.7780(12) Å | β = 83.150(2)°. |
| | c = 22.8037(18) Å | γ = 68.288(2)°. |
| Volume | 4491.6(6) $Å^3$ | |
| Z | 4 | |
| Density (calculated) | 1.377 $Mg/m^3$ | |
| Absorption coefficient | 0.273 $mm^{-1}$ | |
| F(000) | 1936 | |
| Crystal size | 0.422 x 0.226 x 0.162 $mm^3$ | |

| | |
|---|---|
| Crystal color and habit | Colorless Block |
| Diffractometer | Bruker Photon100 CMOS |
| Theta range for data collection | 2.246 to 27.500°. |
| Index ranges | -18<=h<=18, -19<=k<=19, -29<=l<=29 |
| Reflections collected | 41211 |
| Independent reflections | 20619 [R(int) = 0.0104] |
| Observed reflections (I > 2sigma(I)) | 18247 |
| Completeness to theta = 25.242° | 99.9 % |
| Absorption correction | Semi-empirical from equivalents |
| Max. and min. transmission | 0.9470 and 0.8736 |
| Solution method | SHELXT (Sheldrick, 2014) |
| Refinement method | SHELXL-2018/3 (Sheldrick, 2018) Full-matrix least-squares on $F^2$ |
| Data / restraints / parameters | 20619 / 59 / 1256 |
| Goodness-of-fit on $F^2$ | 1.045 |
| Final R indices [I>2sigma(I)] | R1 = 0.0345, wR2 = 0.0866 |
| R indices (all data) | R1 = 0.0403, wR2 = 0.0906 |
| Extinction coefficient | 0.00324(17) |
| Largest diff. peak and hole | 0.541 and -0.422 e.$Å^{-3}$ |

**Table 1.61**. Crystal data for POSS **1.16**.

| | | |
|---|---|---|
| Identification code | JF2708FMI | |
| Empirical formula | C45 H46 O12 Si8 | |
| Formula weight | 1003.54 | |
| Temperature | 90(2) K | |
| Wavelength | 0.71073 Å | |
| Crystal system | Triclinic | |
| Space group | P-1 | |
| Unit cell dimensions | a = 11.0506(3) Å | ⟨= 96.5374(15)°. |
| | b = 14.9694(4) Å | ®= 103.0616(14)°. |
| | c = 15.8952(5) Å | © = 104.7571(15)°. |
| Volume | 2435.52(12) $Å^3$ | |
| Z | 2 | |
| Density (calculated) | 1.368 $Mg/m^3$ | |
| Absorption coefficient | 0.281 $mm^{-1}$ | |
| F(000) | 1048 | |
| Crystal size | 0.710 x 0.354 x 0.098 $mm^3$ | |
| Crystal color and habit | Colorless Plate | |
| Diffractometer | Bruker APEX-II CCD | |
| Theta range for data collection | 1.977 to 30.616°. | |
| Index ranges | -15<=h<=14, -21<=k<=21, -21<=l<=22 | |

| | |
|---|---|
| Reflections collected | 21904 |
| Independent reflections | 14894 [R(int) = 0.0139] |
| Observed reflections (I > 2sigma(I)) | 13401 |
| Completeness to theta = 25.242° | 99.7 % |
| Absorption correction | Semi-empirical from equivalents |
| Max. and min. transmission | 0.9226 and 0.8113 |
| Solution method | SHELXT (Sheldrick, 2014) |
| Refinement method | SHELXL-2017/1 (Sheldrick, 2017) Full-matrix least-squares on $F^2$ |
| Data / restraints / parameters | 14894 / 2 / 770 |
| Goodness-of-fit on $F^2$ | 1.027 |
| Final R indices [I>2sigma(I)] | R1 = 0.0301, wR2 = 0.0824 |
| R indices (all data) | R1 = 0.0341, wR2 = 0.0854 |
| Largest diff. peak and hole | 0.521 and -0.338 e.Å$^{-3}$ |

## 1.12. References


(1) Diemoz, K. M.; Hein, J. E.; Wilson, S. O.; Fettinger, J. C.; Franz, A. K. Reaction Progress Kinetics Analysis of 1,3-Disiloxanediols as Hydrogen-Bonding Catalysts. *J. Org. Chem.* **2017**, *82* (13), 6738–6747. https://doi.org/10.1021/acs.joc.7b00875.

(2) Tran, N. T.; Min, T.; Franz, A. K. Silanediol Hydrogen Bonding Activation of Carbonyl Compounds. *Chemistry (Easton).* **2011**, *17* (36), 9897–9900. https://doi.org/10.1002/chem.201101492.

(3) Diemoz, K. M.; Wilson, S. O.; Franz, A. K. Synthesis of Structurally Varied 1,3-Disiloxanediols and Their Activity as Anion-Binding Catalysts. *Chemistry (Easton).* **2016**, *22* (51), 18349–18353. https://doi.org/10.1002/chem.201604103.

(4) Diemoz, K. M. Design, Synthesis, and Investigation of Siloxanol Hydrogen-Bonding Catalysts and Chiral Silanol Ligands, University of California, Davis, 2018.

(5) Jagannathan, J. R.; Diemoz, K. M.; Targos, K.; Fettinger, J. C.; Franz, A. K. Kinetic and Binding Studies Reveal Cooperativity and Off-Cycle Competition for H-Bonding Catalysis with Silsesquioxane Silanols. *Chem. – A Eur. J.* **2019**, *25* (65), 14953–14958. https://doi.org/10.1002/chem.201903693.

(6) Nawrocki, J. The Silanol Group and Its Role in Liquid Chromatography. *J. Chromatogr. A* **1997**, *779* (1–2), 29–71. https://doi.org/10.1016/s0021-9673(97)00479-2.

(7) Shinde, P. S.; Suryawanshi, P. S.; Patil, K. K.; Belekar, V. M.; Sankpal, S. A.; Delekar, S. D.; Jadhav, S. A. A Brief Overview of Recent Progress in Porous Silica as Catalyst Supports. *J. Compos. Sci.* **2021**, *5* (3), 1–17. https://doi.org/10.3390/jcs5030075.

(8) Onitsuka, S.; Jin, Y. Z.; Shaikh, A. C.; Furuno, H.; Inanaga, J. Silica Gel-Mediated Organic Reactions under Organic Solvent-Free Conditions. *Molecules* **2012**, *17* (10), 11469–11483. https://doi.org/10.3390/molecules171011469.

(9) Roder, A.; Kob, W.; Binder, K. Structure and Dynamics of Amorphous Silica Surfaces. *J. Chem. Phys.* **2001**, *114* (17), 7602–7614. https://doi.org/10.1063/1.1360257.

(10) Chuang, I. S.; Maciel, G. E. A Detailed Model of Local Structure and Silanol Hydrogen Bonding of Silica Gel Surfaces. *J. Phys. Chem. B* **1997**, *101* (16), 3052–3064. https://doi.org/10.1021/jp9629046.

(11) Pescarmona, P. P.; Aprile, C.; Swaminathan, S. Silsesquioxanes and Their Use as Precursors for Catalysts and as Model Compounds. In *New and Future Developments in Catalysis*; 2013; pp 385–422. https://doi.org/10.1016/b978-0-444-53876-5.00018-0.

(12) Hanssen, R. W. J. M.; van Santen, R. A.; Abbenhuis, H. C. L. The Dynamic Status Quo of

Polyhedral Silsesquioxane Coordination Chemistry. *Eur. J. Inorg. Chem.* **2004**, *2004* (4), 675–683. https://doi.org/10.1002/ejic.200300412.
(13) Feher, F. J.; Newman, D. A.; Walzer, J. F. Silsesquioxanes as Models for Silica Surfaces. *J. Am. Chem. Soc.* **1989**, *111* (5), 1741–1748. https://doi.org/10.1021/ja00187a028.
(14) Duchateau, R. Incompletely Condensed Silsesquioxanes: Versatile Tools in Developing Silica-Supported Olefin Polymerization Catalysts. *Chem. Rev.* **2002**, *102* (10), 3525–3542. https://doi.org/10.1021/cr010386b.
(15) J. Feher, F.; Soulivong, D.; Nguyen, F. Practical Methods for Synthesizing Four Incompletely Condensed Silsesquioxanes from a Single R8Si8O12 Framework. *Chem. Commun.* **1998**, No. 12, 1279–1280. https://doi.org/10.1039/A802670J.
(16) J. Feher, F.; Terroba, R.; W. Ziller, J. A New Route to Incompletely-Condensed Silsesquioxanes: Base-Mediated Cleavage of Polyhedral Oligosilsesquioxanes. *Chem. Commun.* **1999**, No. 22, 2309–2310. https://doi.org/10.1039/A906242D.
(17) Hybrid Plastics.Com. Several POSS including XX and XX are available for.
(18) Li, Z.; Zhang, H.; Xiong, G.; Zhang, J.; Guo, R.; Li, L.; Zhou, H.; Chen, G.; Zhou, Z.; Li, Q. A Low-Shrinkage Dental Composite with Epoxy-Polyhedral Oligomeric Silsesquioxane. *J. Mech. Behav. Biomed. Mater.* **2020**, *103*, 103515. https://doi.org/https://doi.org/10.1016/j.jmbbm.2019.103515.
(19) Zhou, H.; Ye, Q.; Xu, J. Polyhedral Oligomeric Silsesquioxane-Based Hybrid Materials and Their Applications. *Mater. Chem. Front.* **2017**, *1* (2), 212–230. https://doi.org/10.1039/C6QM00062B.
(20) Turgut, G.; Dogan, M.; Tayfun, U.; Ozkoc, G. The Effects of POSS Particles on the Flame Retardancy of Intumescent Polypropylene Composites and the Structure-Property Relationship. *Polym. Degrad. Stab.* **2018**, *149*, 96–111. https://doi.org/https://doi.org/10.1016/j.polymdegradstab.2018.01.025.
(21) Blanco, I. Polyhedral Oligomeric Silsesquioxanes (POSS)s in Medicine. *J. Nanomedicine* **2018**, *1* (1), 1–3. https://doi.org/10.33582/2578-8760/1002.
(22) Feghhi, M.; Rezaie, J.; Akbari, A.; Jabbari, N.; Jafari, H.; Seidi, F.; Szafert, S. Effect of Multi-Functional Polyhydroxylated Polyhedral Oligomeric Silsesquioxane (POSS) Nanoparticles on the Angiogenesis and Exosome Biogenesis in Human Umbilical Vein Endothelial Cells (HUVECs). *Mater. Des.* **2021**, *197*, 109227. https://doi.org/https://doi.org/10.1016/j.matdes.2020.109227.
(23) Dijkstra, T. W.; Duchateau, R.; Van Santen, R. A.; Meetsma, A.; Yap, G. P. Silsesquioxane Models for Geminal Silica Surface Silanol Sites. A Spectroscopic Investigation of Different Types of Silanols. *J. Am. Chem. Soc.* **2002**, *124* (33), 9856–9864. https://doi.org/10.1021/ja0122243.
(24) Feher, F. J.; Newman, D. A. Enhanced Silylation Reactivity of a Model for Silica Surfaces. *J. Am. Chem. Soc.* **1990**, *112* (5), 1931–1936. https://doi.org/10.1021/ja00161a044.
(25) Der Voort, P. Van; Vansant, E. F. Silylation of the Silica Surface A Review. *J. Liq. Chromatogr. Relat. Technol.* **1996**, *19* (17–18), 2723–2752. https://doi.org/10.1080/10826079608015107.
(26) Park, J.-W.; Park, Y. J.; Jun, C.-H. Post-Grafting of Silica Surfaces with Pre-Functionalized Organosilanes: New Synthetic Equivalents of Conventional Trialkoxysilanes. *Chem. Commun.* **2011**, *47* (17), 4860–4871. https://doi.org/10.1039/C1CC00038A.
(27) El-Nahhal, I. M.; El-Ashgar, N. M. A Review on Polysiloxane-Immobilized Ligand Systems: Synthesis, Characterization and Applications. *J. Organomet. Chem.* **2007**, *692* (14), 2861–2886. https://doi.org/https://doi.org/10.1016/j.jorganchem.2007.03.009.
(28) Liu, H.; Kondo, S.; Tanaka, R.; Oku, H.; Unno, M. A Spectroscopic Investigation of Incompletely Condensed Polyhedral Oligomeric Silsesquioxanes (POSS-Mono-Ol, POSS-Diol and POSS-Triol): Hydrogen-Bonded Interaction and Host–Guest Complex. *J. Organomet. Chem.* **2008**, *693* (7), 1301–1308. https://doi.org/10.1016/j.jorganchem.2008.01.027.
(29) Kondo, S. ichi; Okada, N.; Tanaka, R.; Yamamura, M.; Unno, M. Anion Recognition by 1,3-Disiloxane-1,1,3,3-Tetraols in Organic Solvents. *Tetrahedron Lett.* **2009**, *50* (23), 2754–2757. https://doi.org/10.1016/j.tetlet.2009.03.134.
(30) Kondo, S.; Fukuda, A.; Yamamura, T.; Tanaka, R.; Unno, M. Anion Recognition by a Disiloxane-

1,3-Diol in Organic Solvents. *Tetrahedron Lett.* **2007**, *48* (45), 7946–7949. https://doi.org/10.1016/j.tetlet.2007.09.067.
(31) Liu, M.; Tran, N. T.; Franz, A. K.; Lee, J. K. Gas-Phase Acidity Studies of Dual Hydrogen-Bonding Organic Silanols and Organocatalysts. *J. Org. Chem.* **2011**, *76* (17), 7186–7194. https://doi.org/10.1021/jo201214x.
(32) Duchateau, R.; Dijkstra, T. W.; van Santen, R. A.; Yap, G. P. Silsesquioxane Models for Silica Surface Silanol Sites with Adjacent Siloxide Functionalites and Olefin Polymerization Catalysts Thereof. *Chemistry (Easton).* **2004**, *10* (16), 3979–3990. https://doi.org/10.1002/chem.200400206.
(33) Dündar, E.; Tanyeli, C. Enantioselective Friedel-Crafts Alkylation of Indole with Nitroalkenes in the Presence of Bifunctional Squaramide Organocatalysts. *Tetrahedron Lett.* **2021**, *73*, 16–19. https://doi.org/10.1016/j.tetlet.2021.153153.
(34) Tang, H.-Y.; Zhang, Z.-B. Chiral Phosphoric Acid Catalyzed Asymmetric Friedel–Crafts Alkylation of Indoles with Nitroolefins. *Phosphorus. Sulfur. Silicon Relat. Elem.* **2011**, *186* (10), 2038–2046. https://doi.org/10.1080/10426507.2010.536189.
(35) Herrera, R. P.; Sgarzani, V.; Bernardi, L.; Ricci, A. Catalytic Enantioselective Friedel-Crafts Alkylation of Indoles with Nitroalkenes by Using a Simple Thiourea Organocatalyst. *Angew. Chemie - Int. Ed.* **2005**, *44* (40), 6576–6579. https://doi.org/10.1002/anie.200500227.
(36) Tran, N. T.; Wilson, S. O.; Franz, A. K. Cooperative Hydrogen-Bonding Effects in Silanediol Catalysis. *Org. Lett.* **2012**, *14* (1), 186–189. https://doi.org/10.1021/ol202971m.
(37) Dyson, P. J.; Jessop, P. G. Solvent Effects in Catalysis: Rational Improvements of Catalysts via Manipulation of Solvent Interactions. *Catal. Sci. Technol.* **2016**, *6* (10), 3302–3316. https://doi.org/10.1039/C5CY02197A.
(38) Diemoz, K. M.; Hein, J. E.; Wilson, S. O.; Fettinger, J. C.; Franz, A. K. Reaction Progress Kinetics Analysis of 1,3-Disiloxanediols as Hydrogen-Bonding Catalysts. *J. Org. Chem.* **2017**, *82* (13), 6738–6747. https://doi.org/10.1021/acs.joc.7b00875.
(39) Bures, J. A Simple Graphical Method to Determine the Order in Catalyst. *Angew. Chemie, Int. Ed. English* **2016**, *55* (6), 2028–2031. https://doi.org/10.1002/anie.201508983.
(40) Bures, J. Variable Time Normalization Analysis: General Graphical Elucidation of Reaction Orders from Concentration Profiles. *Angew. Chemie, Int. Ed. English* **2016**, *55* (52), 16084–16087. https://doi.org/10.1002/anie.201609757.
(41) Kozuch, S.; Martin, J. M. L. "Turning Over" Definitions in Catalytic Cycles. *ACS Catal.* **2012**, *2* (12), 2787–2794. https://doi.org/10.1021/cs3005264.
(42) Crooks, A. B.; Yih, K.-H.; Li, L.; Yang, J. C.; Özkar, S.; Finke, R. G. Unintuitive Inverse Dependence of the Apparent Turnover Frequency on Precatalyst Concentration: A Quantitative Explanation in the Case of Ziegler-Type Nanoparticle Catalysts Made from [(1,5-COD)Ir(μ-O2C8H15)]2 and AlEt3. *ACS Catal.* **2015**, *5* (6), 3342–3353. https://doi.org/10.1021/acscatal.5b00347.
(43) Kennedy, C. R.; Lehnherr, D.; Rajapaksa, N. S.; Ford, D. D.; Park, Y.; Jacobsen, E. N. Mechanism-Guided Development of a Highly Active Bis-Thiourea Catalyst for Anion-Abstraction Catalysis. *J. Am. Chem. Soc.* **2016**. https://doi.org/10.1021/jacs.6b09205.
(44) Ford, D. D.; Lehnherr, D.; Kennedy, C. R.; Jacobsen, E. N. On- and Off-Cycle Catalyst Cooperativity in Anion-Binding Catalysis. *J. Am. Chem. Soc.* **2016**, *138* (25), 7860–7863. https://doi.org/10.1021/jacs.6b04686.
(45) Blackmond, D. G. Kinetic Profiling of Catalytic Organic Reactions as a Mechanistic Tool. *J. Am. Chem. Soc.* **2015**, *137* (34), 10852–10866. https://doi.org/10.1021/jacs.5b05841.
(46) Shubina, T. E.; Freund, M.; Schenker, S.; Clark, T.; Tsogoeva, S. B. Synthesis and Evaluation of New Guanidine-Thiourea Organocatalyst for the Nitro-Michael Reaction: Theoretical Studies on Mechanism and Enantioselectivity. *Beilstein J. Org. Chem.* **2012**, *8*, 1485–1498. https://doi.org/10.3762/bjoc.8.168.
(47) Groves, P. Diffusion Ordered Spectroscopy (DOSY) as Applied to Polymers. *Polym. Chem.* **2017**, *8* (44), 6700–6708. https://doi.org/10.1039/C7PY01577A.

(48) Crockett, M. P.; Zhang, H.; Thomas, C. M.; Byers, J. A. Adding Diffusion Ordered NMR Spectroscopy (DOSY) to the Arsenal for Characterizing Paramagnetic Complexes. *Chem. Commun.* **2019**, *55* (96), 14426–14429. https://doi.org/10.1039/C9CC08229H.
(49) Li, W.; Chung, H.; Daeffler, C.; Johnson, J. A.; Grubbs, R. H. Application of 1H DOSY for Facile Measurement of Polymer Molecular Weights. *Macromolecules* **2012**, *45* (24), 9595–9603. https://doi.org/10.1021/ma301666x.
(50) Keresztes, I.; Williard, P. G. Diffusion-Ordered NMR Spectroscopy (DOSY) of THF Solvated n-Butyllithium Aggregates. *J. Am. Chem. Soc.* **2000**, *122* (41), 10228–10229. https://doi.org/10.1021/ja002278x.
(51) Tran, N. T.; Wilson, S. O.; Franz, A. K. Supramolecular Hydrogen-Bonding Assembly of Silanediols with Bifunctional Heterocycles. *Chem. Commun.* **2014**, *50* (28), 3738–3740. https://doi.org/10.1039/c4cc00672k.
(52) Thordarson, P. Determining Association Constants from Titration Experiments in Supramolecular Chemistry. *Chem. Soc. Rev.* **2011**, *40* (3), 1305–1323. https://doi.org/10.1039/C0CS00062K.
(53) Octa-Smolin, F.; Mitra, R.; Thiele, M.; Daniliuc, C. G.; Stegemann, L.; Strassert, C.; Niemeyer, J. Rigidly Tethered Bis-Phosphoric Acids: Generation of Tunable Chiral Fluorescent Frameworks and Unexpected Selectivity for the Detection of Ferric Ions. *Chem. – A Eur. J.* **2017**, *23* (42), 10058–10067. https://doi.org/https://doi.org/10.1002/chem.201700954.
(54) DeFord, J.; Chu, F.; Anslyn, E. V. Dimerization Constants for Phosphoric Acid Diesters. *Tetrahedron Lett.* **1996**, *37* (12), 1925–1928. https://doi.org/https://doi.org/10.1016/0040-4039(96)00184-0.
(55) Burés, J. What Is the Order of a Reaction? *Top. Catal.* **2017**, *60* (8), 631–633. https://doi.org/10.1007/s11244-017-0735-y.
(56) López, L. F. G. The Concept of Elasticity and Strategies for Teaching It in Introductory Courses of Economics. *Semest. Económico* **2019**, *22* (51 SE-Artículos de investigación). https://doi.org/10.22395/seec.v22n51a7.
(57) Heinrich, R.; Rapoport, T. A. A Linear Steady-State Treatment of Enzymatic Chains. *Eur. J. Biochem.* **1974**, *42* (1), 89–95. https://doi.org/https://doi.org/10.1111/j.1432-1033.1974.tb03318.x.
(58) Sydsaeter, K.; Hammond, P.; Seierstad, A. Further Mathematics for Economic Analysis. 2008, p 616.

# Chapter 2: Studies of Diarylcarbene Insertion into Si–H Bonds for the Synthesis of Silicon-Stereogenic Silanes[*]

## 2.1: Introduction

This chapter represents the development of enantioselective diarylcarbene insertion methodology to desymmetrize prochiral silanes to produce silicon-stereogenic silanes. The Franz Lab is interested in developing methods to generate silicon-stereogenic silanes capable of further functionalization for applications in ligand development, drug design, and silicon-based materials. Several previous lab members have contributed to studies of enantioselective methodology to produce silicon-stereogenic silanes including Dr. Kayla Diemoz[1] and Dr. Austin Kelly. In particular, Dr. Austin Kelly developed a Rh(I)-catalyzed enantioselective alcoholysis of prochiral silanes which highlighted the utility of using Si–H bonds as reactive sites.[2] After desymmetrization, the remaining Si–H bond is a valuable functional handle capable of further transformations. The work described in this chapter has been published in *Journal of the American Chemical Society* in collaboration with Professor Jared Shaw at UC Davis.[3]

Strategies to synthesize silicon-stereogenic silanes vary from methods to produce stereogenic carbon compounds due to the instability of $sp^2$ silicon centers. Instead, the approach towards silicon-stereogenic silanes is to desymmetrize prochiral $sp^3$ silicon centers with two identical reactive groups (Figure 2.1A).[4] The remaining reactive group could be used for further functionalization to produce more complex molecules. Carbene insertion into Si–H bonds is an ideal transformation for the formation of silicon-centered chirality due to the well-developed methodology for analogous enantioselective C–H insertion of prochiral $sp^3$ carbon centers (Figure 2.1B).[5] As such, there are a plethora of catalysts commercially available and efforts can be focused on expanding the scope of prochiral silanes. The mechanism of C–H insertion is proposed to occur through an asynchronous concerted mechanism where hydride transfer precedes C–C bond formation (Figure 2.1C).[6] The reaction can form two contiguous stereocenters with a prochiral diazo compound. Given the increased hydridic character of Si–H bonds,[7] substrates deemed

[*] Reproduced in part with permission from Jagannathan, J. R.; Fettinger, J. C.; Shaw, J. T.; Franz, A. K. *J. Am. Chem. Soc.* **2020**, *142* (27), 11674–11679. Copyright 2020 American Chemical Society.

unreactive to C–H insertion could be examined. Prior to this work there were three known examples of carbene insertion to produce a silicon-stereogenic molecule.

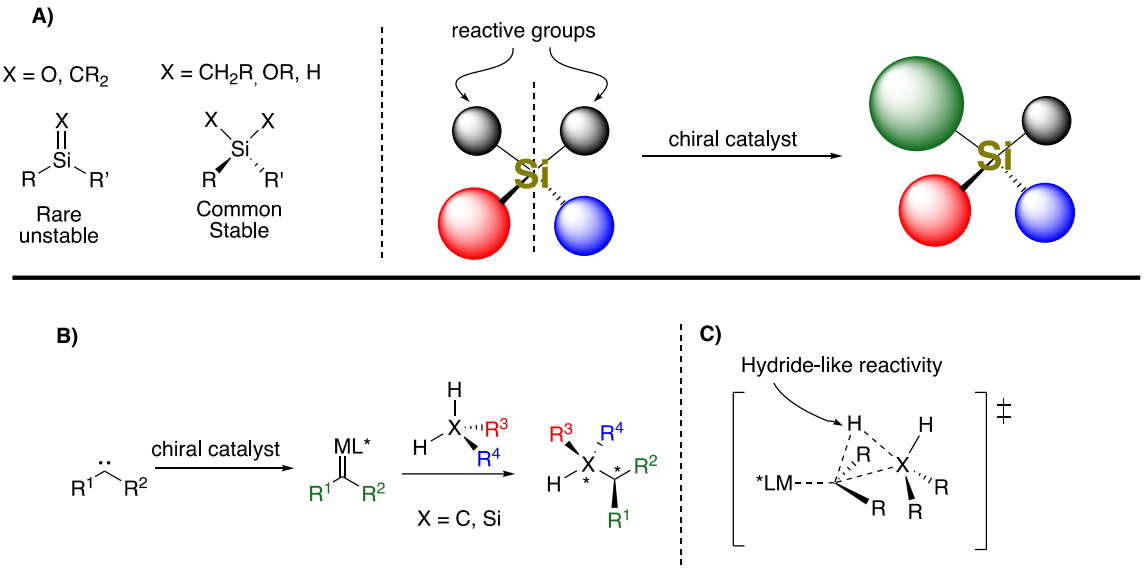


**Figure 2.1**. A) Strategies towards synthesis of silicon-stereogenic silanes. B) Carbene Insertion as a *sp*$^3$ desymmetrization strategy. B) Transition-state structure of concerted X–H insertion step (X = C or Si).

In 2010, Katsuki reported an enantioselective carbene insertion into silanes with prochiral Si–H bonds (**2.1a-d**) using alkyl diazoacetates (**2.2a)** (Figure 2.2).[8] The most active and selective catalyst synthesized and tested was Ir(II)-salen **2.3**, noted for its bowl-like structure. This report was noted as the first example of desymmetrization of prochiral silanes using chiral metal complexes undergoing an Si–H insertion pathway. The authors demonstrated the method with four prochiral silanes containing sterically demanding substituents such as, 1-naphthyl (**2.4a**), 2,6-xylyl (**2.4b**), isopropyl (**2.4c**), and cyclohexyl (**2.4d**) groups with yields between 73-86% and up to 99.5:05 dr and er. Interestingly, the stereochemistry set at carbon was identical whether silicon-centered chirality was formed in the reaction or not. Kinetic isotope effect studies using prochiral silanes match that of symmetrical silanes (KIE = 1.6), suggesting that both processes proceed through concerted mechanisms where the Si–H insertion step is rate-determining.

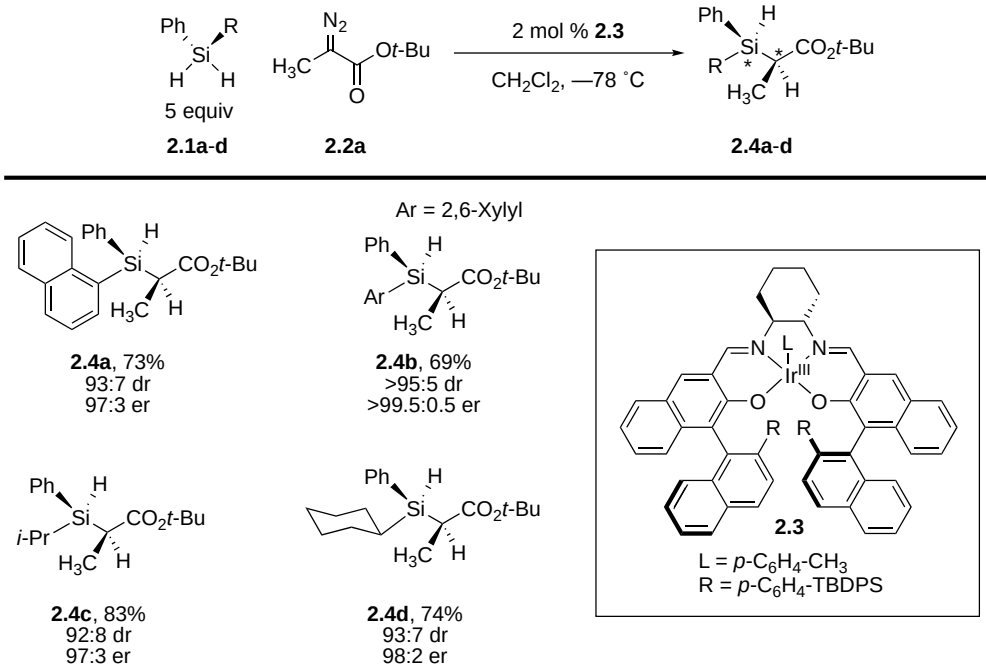


**Figure 2.2**. Katsuki's Ir(III)-salen complex and application for carbene insertion into Si–H bonds to produce silicon-stereogenic silanes.

In 2012, Iwasa reported an enantioselective carbene insertion into silanes with prochiral Si–H bonds (**2.1b**-**2.1e**) using alkyl diazoacetate (**2.2b)** (Figure 2.3).[9] The catalyst chosen was Ru(II)-Pheox **2.5**, noted for its activity in enantioselective cyclopropanations.[10] Although diastereoselectivity ranged from 58:42 to 79:21 dr, the enantioselectivities of both diastereomers ranged from 92:8 to 99.5:0.5 er for silanes **2.6a**-**2.6d**. The authors noted that enantioselectivity was dependent on the steric demand of the ester group of **2.2b**, requiring a bis-1-naphthyl containing group to achieve high enantioselectivity.

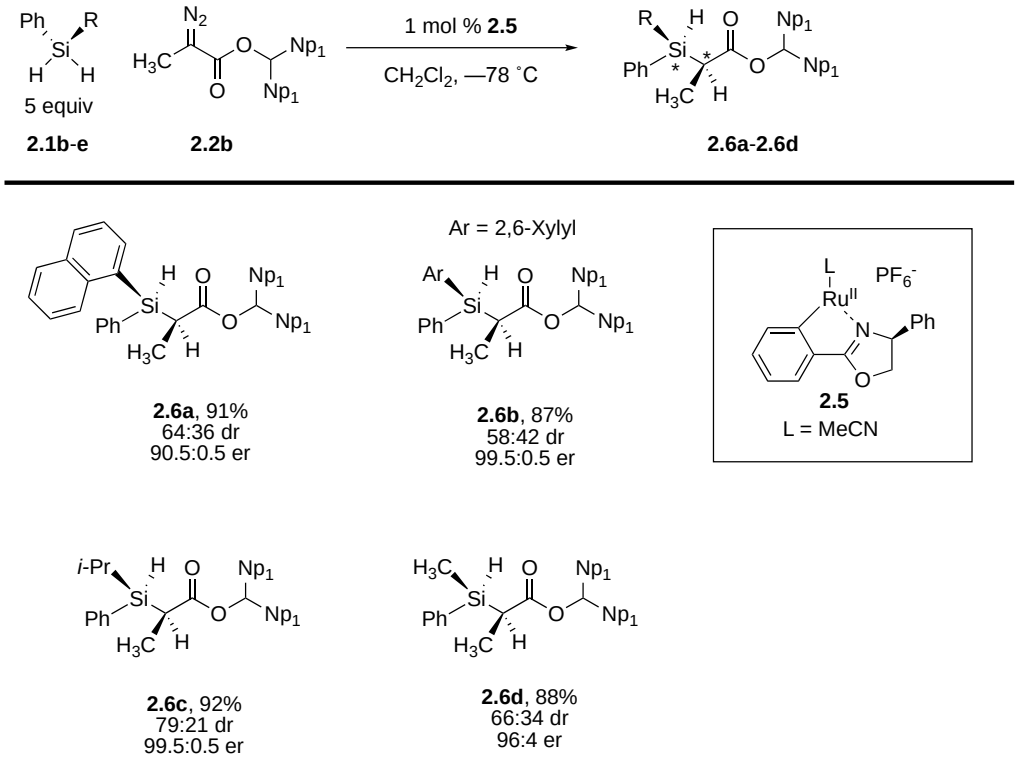


**Figure 2.3**. Iwasa's Ru(II)-Pheox catalyst and examples for carbene insertion into Si–H bonds to produce silicon-stereogenic silanes.

Most carbenes studied have been alkyl(ester) or aryl(ester) based on increased reactivity and diazo compound stability.[11] The use of diarylcarbenes represents a current challenge in carbene chemistry due to the presence of two aryl rings to stabilize the electron-poor carbon center, leading to reduced reactivity (Figure 2.4A).[12] Additionally, diaryldiazo compounds are less stable to because of the presence of two electron-donating groups that increase basicity.[5] However, stabilizing the carbene could lead to a more selective insertion reaction and generalized scope. To date, there are three known examples of diarylcarbene insertion into Si–H bonds, with one setting carbon-centered chirality.

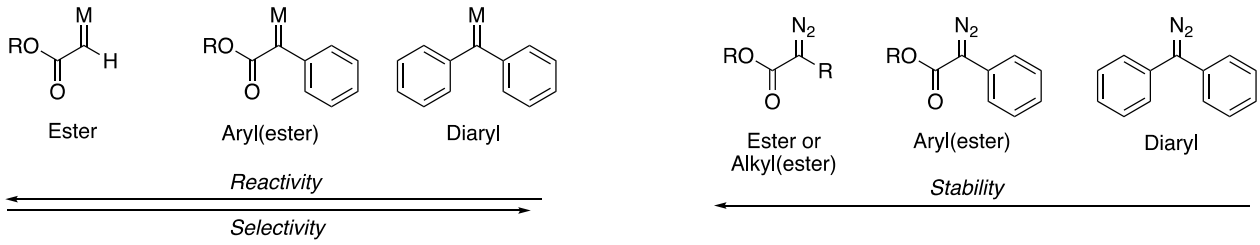


**Figure 2.4** A) Stability of metal carbenoids based on substituents. B) Stability of diazo compounds.

In 2012 Vincente and coworkers expanded the scope of carbenes capable of inserting into Si–H bonds with their report of Zn(II)-catalyzed insertion into Si–H bonds (Figure 2.5).[13] Carbenes were generated *in situ* from functionalized alkynes where the alkyne reacts with the carbonyl to form a furanyl(aryl) carbene intermediate which can undergo Si–H insertion.[14] The synthesis of diaryl-containing **2.9a** was optimized up to 90% yield and could be performed on gram-scale. The reaction was tolerant to substitution about the alkyne, ketone and silane, with yields ranging from 59-97%. Alternative donor groups such as an alkyl or vinyl group provided products in good to excellent yields (**2.9b** and **2.9c**, 85% and 68% respectively). Silanes with two Si–H bonds provided excellent reactivity (**2.9d**, 97%) as well as siloxanes (**2.9e**, 90%). Based on DFT calculations, the reaction proceeds through a concerted mechanism where the Si–H insertion step is rate-limiting.

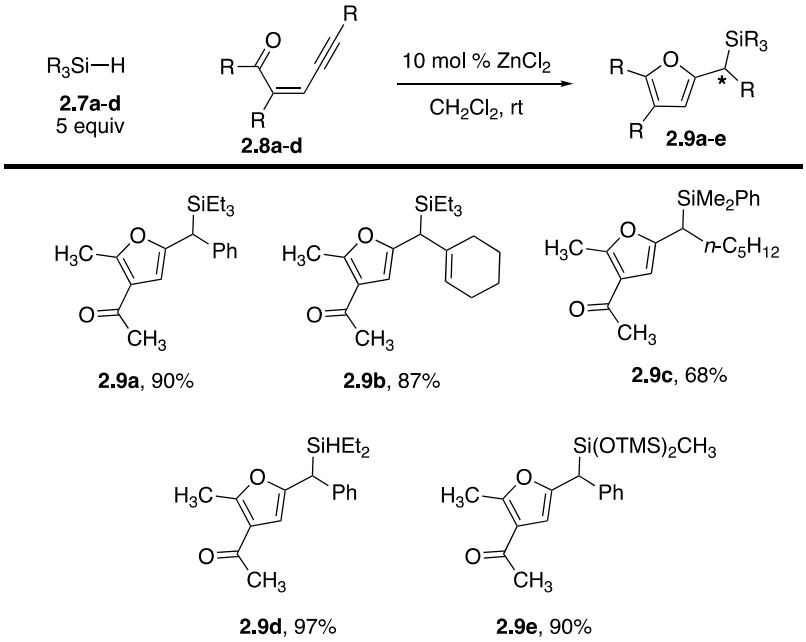


**Figure 2.5** Vincente's Zn(II)-catalyzed carbene insertion using alkynes as carbene precursors.

In 2017, Liu and coworkers expanded the scope of carbene precursors to diazo-derived carbenes with their report on Ag(I)-catalyzed carbene insertion into Si–H bonds(Figure 2.6). Diazo compounds were formed *in situ* from tosylhydrazones in the presence of NaH which could then react with Ag(I). Aryl and aryl-alkyl carbenes were tolerated (**2.11a**-**2.11e**), including heterocyclic compounds (**2.11c)**. Benzhydryl-containing **2.11f** was synthesized in 45% yield. Silanes containing two or more Si–H bonds were not tested with this method.

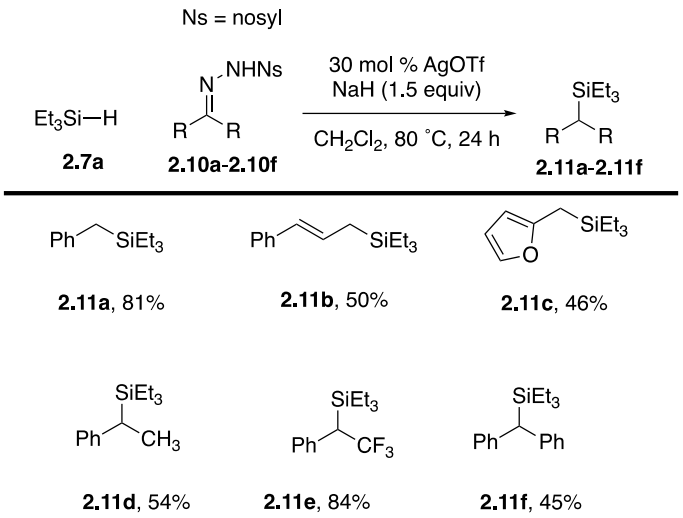


**Figure 2.6** Liu's Ag(I)-catalyzed carbene insertion with aryl and diaryl hydrazones.

In 2018 Wang reported a Pd(0)-catalyzed carbene insertion into tosyl hydrazones as diazo compound precursors (Figure 2.7). The use of electron-rich phosphines led to higher yields compared to ligand-free conditions, suggesting an electron-rich metal promotes catalytic activity.[15] Other catalysts such as Rh(II) or Cu(I) complexes provided no reactivity under these conditions. Substitution at the 2-, 3- and 4-position is tolerated for diaryl substrates and generated synthetically useful quantities of benzhydryl products (**2.11f, 2.14a-d**). Using silanes with two Si–H bonds, the authors performed two separate carbene insertions to rapidly functionalize (**2.14e**) or form a ring (**2.14f**) in excellent yields. Based on previous work with disilanes,[15,16] the authors propose a Pd(0)/Pd(II) cycle where the rate-determining step is migratory insertion of hydride to a palladium carbenoid.

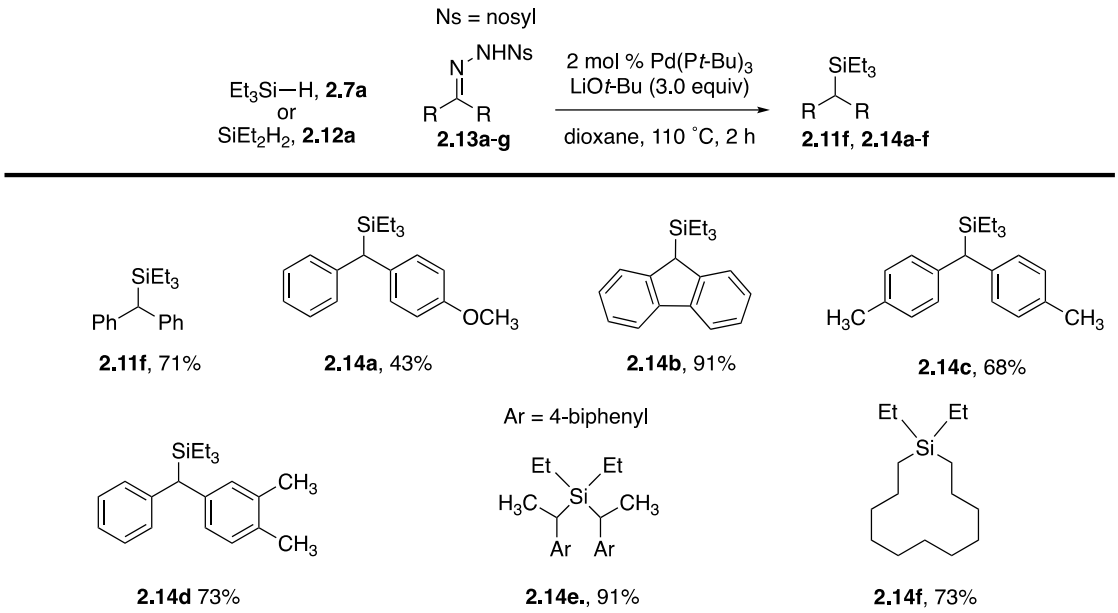


**Figure 2.7** Wang's Pd(0)-catalyzed carbene insertion with nosylhydrazones.

In 2019, Zhu reported a Rh(II)-catalyzed insertion into Si–H bonds using enyne-derived ketones as carbene precursors (Figure 2.8). The catalyst $Rh_2$(*R*-BTPCP)$_4$ has been noted as an exceptionally active carbene insertion catalyst for C–H insertion and cyclopropanation.[17] The reaction was tolerant to substitution about the ketone and alkyne, allowing for sulfonyl, furanyl, and naphthyl groups while maintaining above 88:12 er at the carbon center (**2.18a**-**e**). Silanes with two Si–H bonds were tested (**2.18f**) but formed in low yield and enantioselectivity (78:22 er). Competition and parallel KIE experiments support a concerted, rate-determining insertion step similar to studies using diazo compounds.

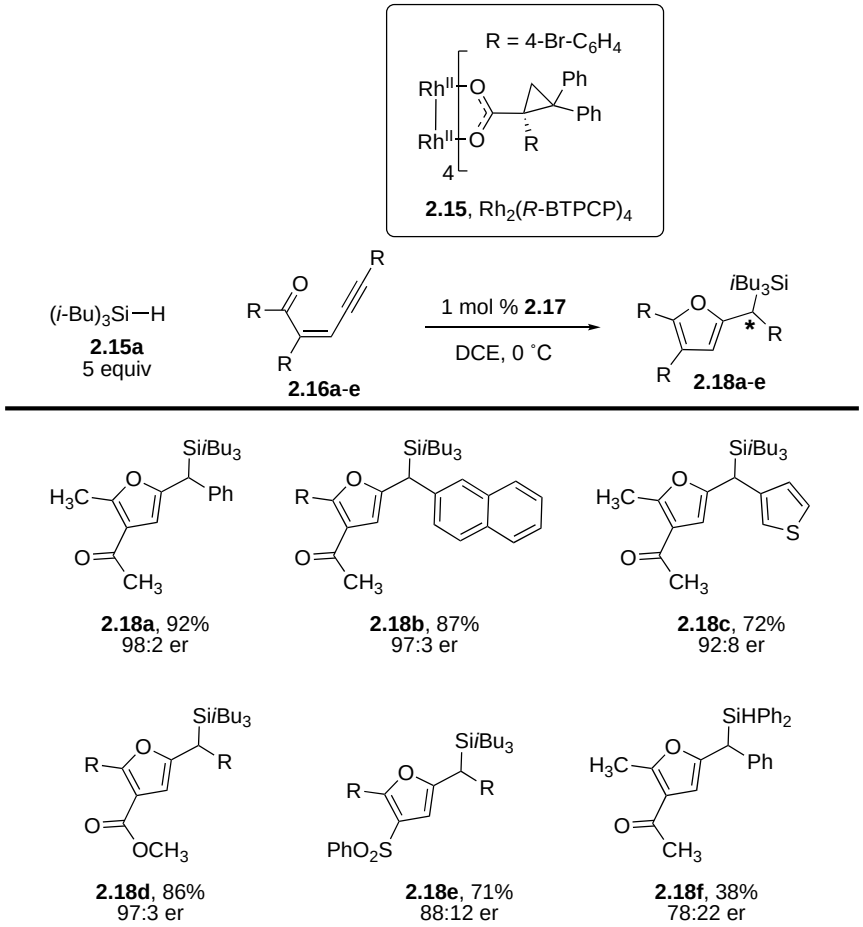


**Figure 2.8** Zhu's Rh(II)-catalyzed enantioselective carbene insertion into Si–H bonds using functionalized alkynes.

Prior to our work, there were no reported examples of diarylcarbene insertion into Si–H bonds to produce silicon-stereogenic silanes. We envisioned a strategy where prochiral silanes reacted with diaryldiazo compounds as carbene precursors to access benzhydryl silanes with the potential for contiguous stereocenters (Figure 2.9). In this strategy, chiral metal catalysts were screened with prochiral silanes and diazo compounds to identify steric and electronic effects on enantioselectivity. Furthermore, prochiral diazo compounds can also be investigated to examine effects from setting two chiral centers. Finally, we envisioned that further transformations would be explored in order to demonstrate the utility of the insertion products. To accomplish this research, we collaborated with Dr. Jared Shaw at UC Davis given his lab's previous work in diarylcarbene insertion.[18–21]

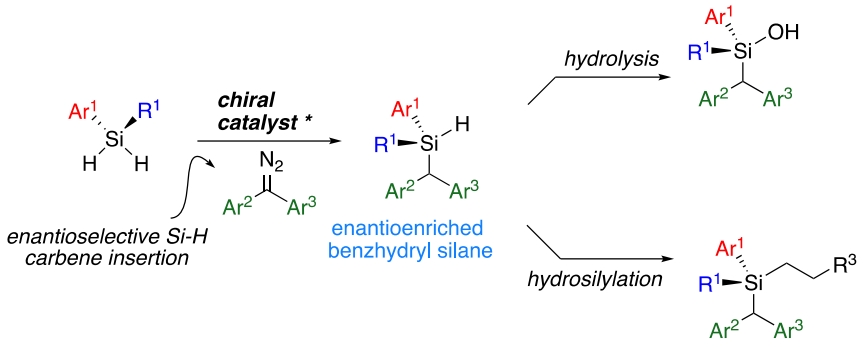


**Figure 2.9** Project overview.

## 2.2: Synthesis of Prochiral Silanes and Diazo Compounds

Silanes investigated were synthesized in 1-3 steps from commercially available materials and one silane studied with this method was commercially available (**2.1e**, methylphenylsilane). A method developed by Dr. Kayla Diemoz and Dr. Austin Kelly, originally to synthesize silanediols and 1,3-disiloxanediols, was applied to the synthesis of prochiral silanes.[22,23] Starting from Grignard reagents or organolithium reagents, addition to an alkyldichlorosilane followed by reduction with $LiALH_4$ produced silanes (**2.19a-2.19l**) in 21-87% yield (Figure 2.10, Route A). Silanes were synthesized on up to 40 mmol scale with facile purification using Kugelrohr distillation or flash chromatography. With this methodology, organolithium reagents tended to afford faster, cleaner single additions to dichlorosilanes. This is especially true when using electron-poor aryl bromides (**2.19j**). Prochiral silanes **2.19k** and **2.19l** were synthesized from alkyl Grignard reagents added to chlorophenylsilane to control a single addition to the silicon center (Figure 2.7, route B). Reduced yields of silanes are attributed to three reasons: 1) difficulty with isolation of volatile liquids (**2.19f**, 2.**19a**), 2) formation of double-addition silane byproducts (**2.19d**, **2.19j**), and 3) difficulty with formation of Grignard reagent (**2.19k**). Siloxane **2.19m** was synthesized using a previously reported procedure.[24]

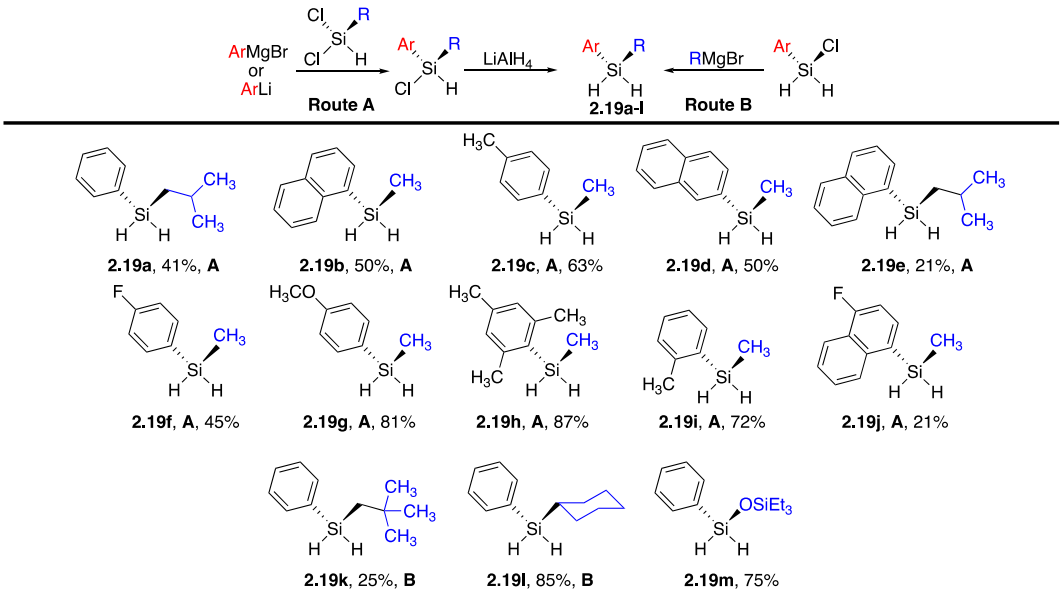


**Figure 2.10** Synthesis of prochiral silanes using silyl electrophiles.

Symmetrical diazo compounds **2.20a-c** were synthesized following a previously reported procedure using hydrazine hydrate and diarylketones followed by oxidation with $MnO_2$ (Figure 2.11).[25] Diazo compounds **2.20a-c** were synthesized to study electronic effects on yield and enantioselectivity.

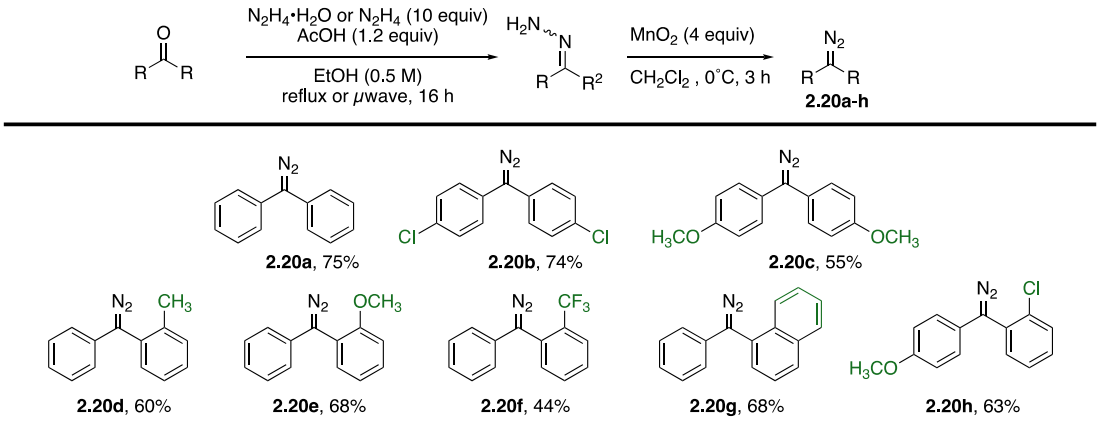


**Figure 2.11** Synthesis of symmetrical and prochiral diazo compounds.

Prochiral diazo compounds were synthesized using a previously reported procedure developed within the Shaw laboratory (Figure 2.11).[20,26] Diarylketones were subjected to hydrazine and acetic acid in refluxing or microwave conditions to synthesize hydrazones.

Hydrazones were isolated as a mixture of isomers and oxidized with $MnO_2$ to furnish diazo compounds. All purifications of diaryldiazo compounds were on basic alumina, as they readily decompose on silica ($pk_a$ = 9.7). In general, prochiral diazo compounds were more stable than symmetrical diazo compounds.

## 2.3: Screening of Metal Catalysts for Diaryl Carbene Insertion Into Si–H Bonds

Several metals were screened in the reaction between **2.1e** and **2.20a** that catalyze carbene insertion into Si–H bonds. Metal complexes include Fe(II), Cu(I), Ir(I), Ru(I), and Rh(I) routinely provided poor conversion of the diazo compound (Table 1 entries 1-6). $Rh_2(OAc)_4$ provided conversion of diazo compound **2.20a** (Table 1, entry 7). $^1$H NMR analysis revealed that insertion product **2.21a** was synthesized in 12% yield.

**Table 1.** Optimization of carbene insertion of **2.20a** into **2.1e** using metal catalysts.

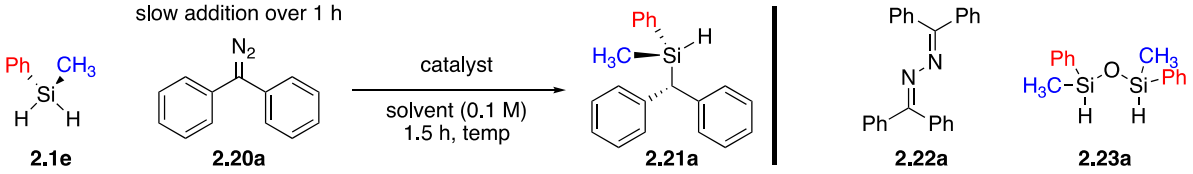


| Entry | Catalyst | Loading (%) | Additive | % Yield[a] |
|---|---|---|---|---|
| 1 | $Cu(OTf)_2$ | 10 | - | <5 |
| 2 | $Cu[MeCN]_4PF_6$ | 10 | - | <5 |
| 3 | $(Ir[COD]Cl)_2$ | 5 | - | <5 |
| 4 | $[IrCpCl]_2$ | 5 | - | <5 |
| 5 | $[Ru(p\text{-cymeme})Cl]_2$ | 5 | - | <5 |
| 6 | $Fe(OTf)_2$ | 20 | - | <5 |
| 7 | $Rh_2(OAc)_4$ | 1 | - | 12 |
| 8[b] | $Rh_2OAc_4$ | 1 | - | 35 |
| 9[b] | $Rh_2OAc_4$ | 1 | 4Å MS[c] | 42 |

[a] NMR yield using Ph-TMS as an internal standard. [b] **2.20a** added over 1 hour using a syringe pump. [c] 100 mg/ 0.1 mmol **2.20a.**

The major side product of the transformation was azine **2.22a**.[18] Inverse addition of the diazo compound over 1 hour using a syringe pump was conducted to limit the diazo compound's concentration in the flask to promote carbene insertion into **2.1e**.[27] Silane **2.21a** was synthesized

in 35% yield as determined by $^1$H NMR analysis. Formation of **2.23a** was observed using $^1$H NMR spectroscopy. Rh(II) carboxylates are known to hydrolyze Si–H bonds in the presence of hydroxyl-containing compounds, including water.[28] The addition of 4Å MS increased the yield of **2.21a** (42%) and **2.23a** was not observed under these conditions.

## 2.4: Screening of Chiral Rhodium(II)-Carboxylates for Enantioselective Variant

The enantioselectivity of the reaction between **2.1e** and **2.20a** was evaluated with structurally varied Rh(II) catalysts (**2.24a-j**) using conditions developed from Table 1 (Figure 2.12). The enantiomers of product **2.21a** were not polar enough to separate on CSP-HPLC, so Pd/C catalyzed hydrolysis to the silanol (**2.25a**)[29] was implemented to allow separation and determine enantioselectivity. Results show that catalyst **2.24h**, also known as tetrakis[*N*-tetrachlorophthaloyl-(*S*)-*tert*-leucinato]dirhodium ($Rh_2$(S-TCPTTL)$_4$), provided the highest enantioselectivity (76:24 er) and increased yield (76%). This catalyst is also commercially available.

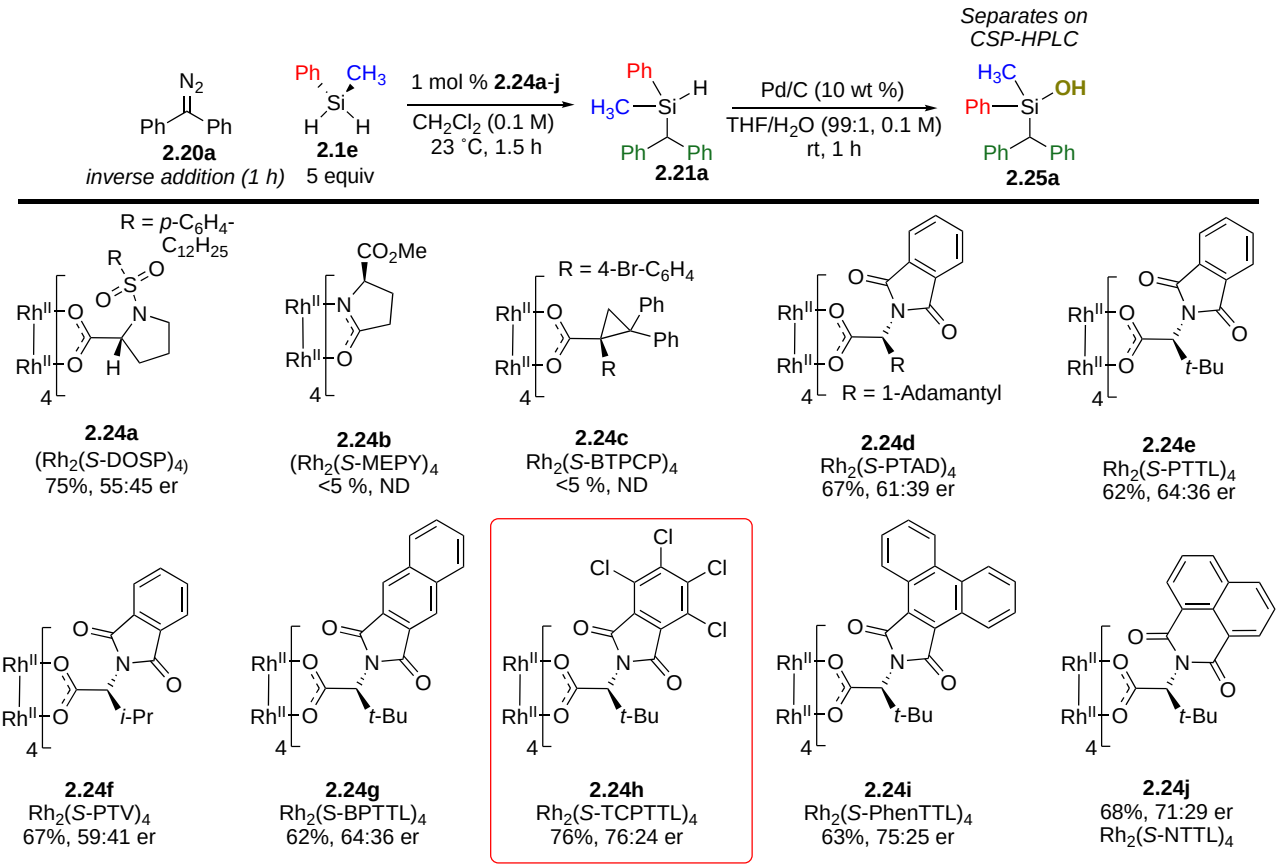

**Figure 2.12** Ligand screen for enantioselective carbene insertion into Si–H bonds.

Further optimization of solvent and reaction temperature was accomplished. Literature precedent suggested that Lewis basic solvents would significantly reduce reactivity and were not examined.[30] Non-polar solvents such as heptane, benzene, and toluene were observed to increase enantioselectivity (Table 2, entries 1-4). Several reactions at reduced temperatures were screened and no insertion occurred below –30 ˚C (Table 2, entries 6 and 7). Several reactions at temperatures above –30 ˚C were attempted using heptane but were often difficult to replicate because of having to setup the entire reaction (syringe pump + vial) in the refrigerator. Toluene was selected over other solvents because it provided identical enantioselectivity and is less expensive. Lastly, a slightly more dilute reaction with toluene provided an increased yield for **2.21a** (Table 2, entry 8). From these results, optimized conditions for symmetrical diazo compounds were 1 mol % $Rh_2$(S-TCPTTL)$_4$ in toluene (0.05 M) with the addition of 4Å MS.

**Table 2.** Optimization of solvent in Rh(II)-catalyzed insertion of **2.20a** into **2.1e** using **2.24h**.

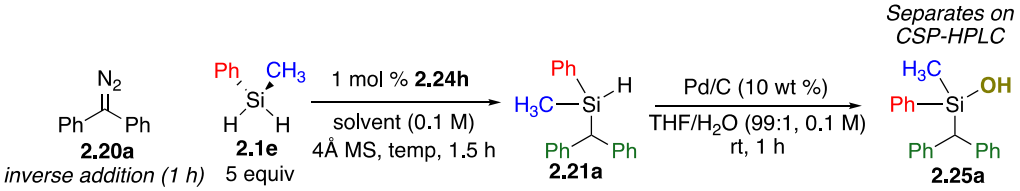


| Entry | Solvent | Temp | % Yield [a] | er [b] |
|---|---|---|---|---|
| 1 | $CH_2Cl_2$ | rt | 76 | 76:24 |
| 2 | heptane | rt | 78 | 82:18 |
| 3 | benzene | rt | 74 | 82:18 |
| 4 | cyclohexane | rt | 74 | 82:18 |
| 5 | PhMe | rt | 68 | 82:18 |
| 6 | heptane | -78 ˚C | <5 | - |
| 7 | heptane | -30 ˚C | <5 | - |
| 8 | PhMe (0.05 M) | rt | 78 | 82:18 |

[a] 0.1 mmol **2.20a**, NMR yield using Ph-TMS as an internal standard. [b] Determined using CSP-HPLC.

## 2.5: Studies of Si–H Insertion With Symmetrical Diazo Compounds

Silanes were tested with diazo **2.20a** with optimized conditions to determine substituent effects (Figure 2.13). Using optimized conditions, diphenyldiazomethane **2.20a** and phenylmethylsilane **2.1e** form benzhydryl silane **2.21a** in 78% yield and 82:18 er up to mmol scale. Using methoxy-substituted **2.20b** led to a reduced yield of silane **2.21b** (45%) and maintained enantioselectivity (81:19 er). Despite the stabilized carbene intermediate resulting from the donating groups, only a deleterious effect on yield is observed. Using dichloro-substituted **2.20c** provided **2.21c** in excellent yield (91%), although enantioselectivity is reduced (76:24 er). Symmetrical electronic substitution at the 4-position of diaryl diazo compounds allowed for carbene insertion, albeit at reduced yield or enantioselectivity.

Electronic effects were investigated on the aryl ring of the silane using diazo compound **2.20a** (Figure 2.13, **2.21d**-**g**). Electron-donating effects were deleterious to enantioselectivity, exemplified in silane **2.21d** (70%, 50:50 er), with yields of products comparable to silane **2.21a**. Electron-withdrawing groups such as 4-fluoro (**2.21f**) or a 2-naphthyl (**2.21g**) maintained enantioselectivity (80:20 er and 82:18 er) although yields were slightly lower (66 and 69%). Overall these results show that electron-donating effects on the silane are deleterious to enantioselectivity, while electron-withdrawing effects are tolerated at a slight impact to yield.

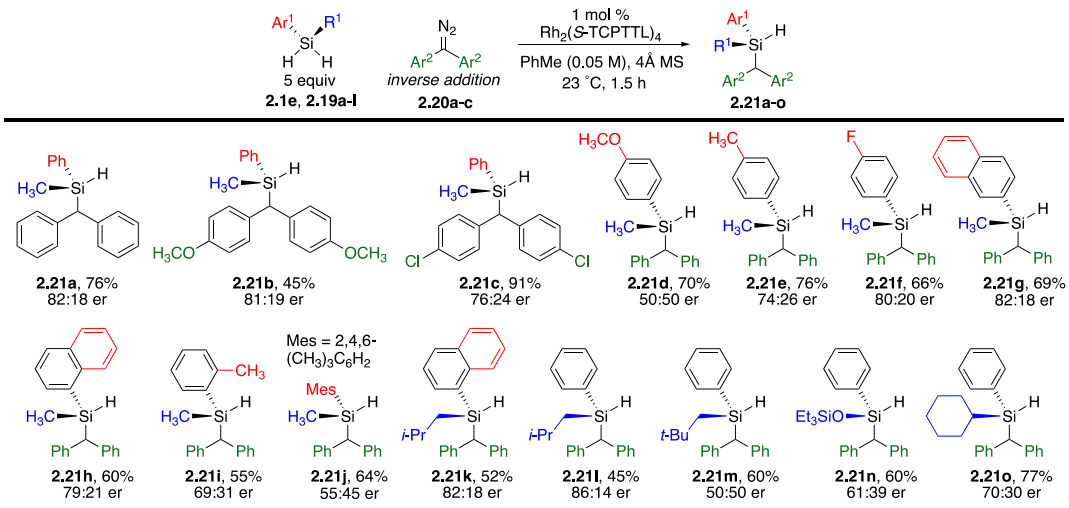


**Figure 2.13** Scope of silicon-stereogenic silanes synthesized using symmetrical diazo compounds.

The effect of steric interactions on both the aryl ring and alkyl portions of the silane were investigated (Figure 2.13, **2.21h-o**). Increasing steric bulk on the aryl ring proved deleterious to enantioselectivity. Both 1-naphthyl (**2.21h**) and o-tolyl (**2.21i**) groups provided reduced enantioselectivity (79:21 and 69:31 er, respectively) and yields are reduced (60% and 55%, respectively) compared to **2.21a**. In the case of mesityl-substituted **2.21j**, almost no enantioselectivity (55:45 er) was observed, and yields are lower (64% vs 78% yield for **2.21a**). Steric bulk on the alkyl portion of the silane appeared to have no observable trend but led to products in fair to good yields. Isobutyl-containing **2.21l** led to the highest observable selectivity with symmetrical diazo compounds (86:14 er) and was performed on mmol scale (45%). Isobutyl substitution partially recovered enantioselectivity as seen with 1-naphthyl containing **2.21k** (82:18 er). However, with an additional methyl group, neopentyl-containing **2.21m** afforded no enantioselectivity (50:50 er) and switching to a siloxane with similar substitution (**2.21n**) led to a slight recovery in enantioselectivity (61:39 er). Lastly, cyclohexyl substituted **2.21o** formed in 77% yield with 70:30 er, indicating bulk closer to the silicon center is deleterious to enantioselectivity.

## 2.6: Studies of Si–H Insertion with Prochiral Diazo Compounds

The effect of using a prochiral diazo compound on enantioselectivity was examined. Using diazo compound **2.20d** in lieu of **2.20a**, several chiral dirhodium(II) compounds were tested and

$Rh_2$(*S*-TCPTTL)$_4$ formed silane **2.26a** in *91% yield, 93:7 dr and 93:7 er*. A trial with $Rh_2$(*R*-TCPTTL)$_4$ confirmed the identities of stereoisomers using CSP-HPLC to have confidence in the measurement of 93:7 er. Reducing the temperature did not improve yield or enantioselectivity, with no product observed below –30 ˚C (Table 3, entries 6-8).

**Table 3.** Optimization of metal-catalyzed insertion of **2.20d** into **2.1e** using Rh(II) catalysts.

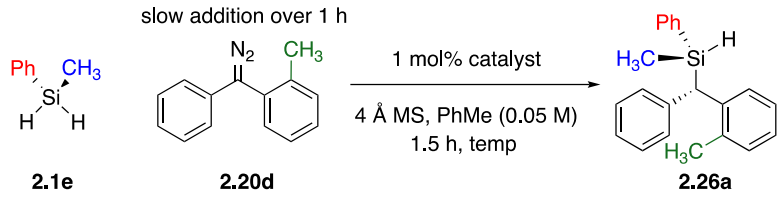


| Entry | Catalyst | Temp | % Yield[a] | dr[b] | er[c] |
|---|---|---|---|---|---|
| 1 | *R*-**2.24d** | rt | 75 | 63:37 | ND |
| 2 | **2.24a** | rt | 70 | 61:39 | ND |
| 3 | **2.24c** | rt | <5 | - | ND |
| 4 | **2.24h** | rt | 91 | 93:7 | 93:7 |
| 5 | *R*-**2.24h** | rt | 91 | 93:7 | 7:93 |
| 6 | **2.24h** | 0 ˚C | 78 | 93:7 | 93:7 |
| 7 | **2.24h** | -30 ˚C | <5 | - | ND |
| 8 | **2.24h** | -78 ˚C | <5 | - | ND |

[a] 0.1 mmol scale, NMR yield using Ph-TMS as an internal standard. [b] Determined using $^1$H NMR. [c] Determined using CSP-HPLC after Pd/C hydrolysis to the silanol.

Prochiral silanes were tested with diazo **2.20d**, and all demonstrated better than 90:10 er for the major diastereomer (Figure 2.14, **2.26a-f**). Additionally, the reaction performed with 1 gram of **2.20d** using 0.05 mol % **2.24h** affords **2.26a** good yield, diastereoselectivity, and enantioselectivity (89%, 93:7 dr, 93:7 er). Overall, the data shows that diastereoselectivity is substrate controlled, while enantioselectivity is controlled by the rhodium catalyst **2.24h**. Notably, using a diastereoselective reaction with silane **2.19g** promotes enantioselectivity with **2.26c** (94:6 er) compared to **2.21d** (50:50 er).

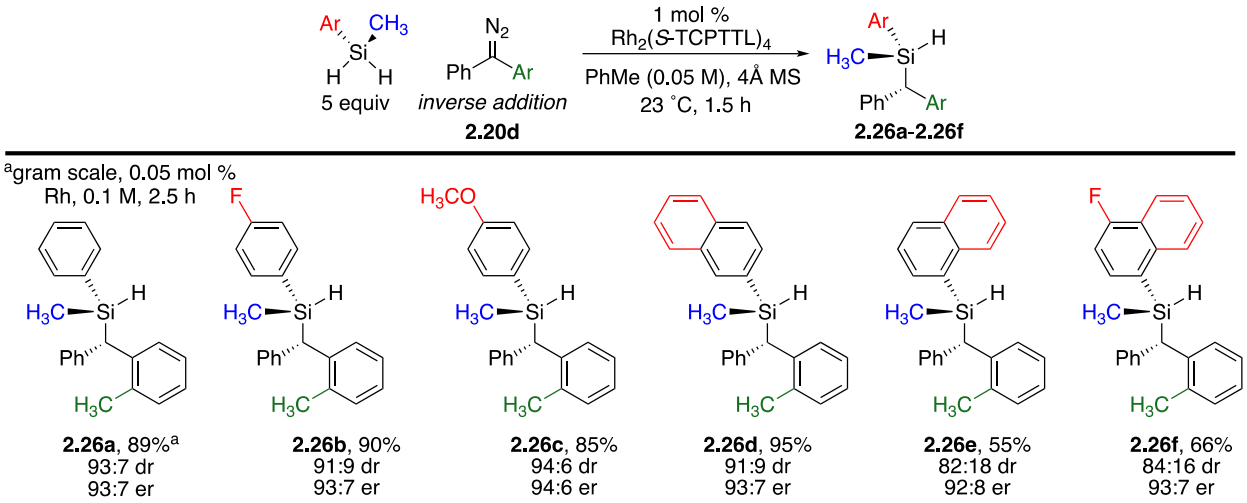


**Figure 2.14** Scope of silicon-stereogenic silanes synthesized using **2.20d**.

Substitution on the ortho position of diaryl diazo compounds was explored to investigate effects on enantioselectivity (Figure 2.15). With an electron-withdrawing group (**2.26g**), excellent yield and enantioselectivity are observed (93%, 93:7 er), and diastereoselectivity increased (98:2 vs 93:7 dr). Recent work has noted potential synergistic effects of electronics and ortho substitution on enantioselectivity in diarylcarbene chemistry.[31] Electron-donating substituents lower diastereoselectivity (**2.26h**, 90:10 dr vs 93:7 dr), but slightly improve enantioselectivity (95:5 vs 93:7 er). Substitution on both phenyl rings achieved excellent yield and good selectivity in **2.26i** (98% yield, 90:10 dr. 89:11 er), although slightly lower compared to other substitution patterns. These substrates demonstrate that the presence of ortho-substitution iso-steric to a methyl may increase enantioselectivity. Replacing a phenyl group with a 1-naphthyl group led to decreased diastereoselectivity (**2.26j**, 85:15 dr) and low enantioselectivity (61:39 er), suggesting that the location of steric bulk is essential. When steric bulk on the silane is used, high er is still observed but dr is lower, suggesting that er and dr are set independently.

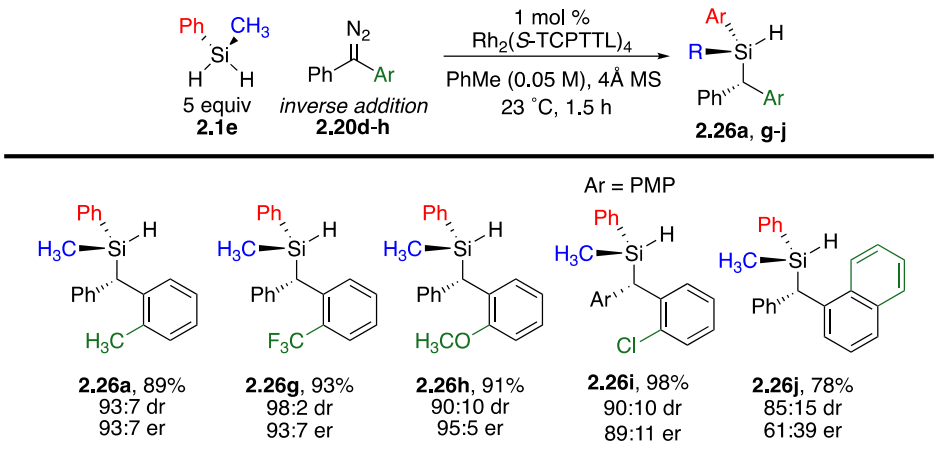


**Figure 2.15** Scope of silicon-stereogenic silanes synthesized using **2.20d-h**.

## 2.7: Mechanistic Studies

Yields with diazo compound **2.20a-c** were lower than with prochiral diazo compounds **2.20d-2.20h**. Based on results from optimization, the formation of azine **2.22a** is the most significant contributor to loss of yield, and rates of formation may vary based on ortho substitution. It was confirmed that azines **2.22a** and **2.27a** are the primary products formed with $Rh_2$(*S*-TCPTTL)$_4$ in the absence of silane (Figure 2.16A). There were no differences in overall reaction order, suggesting that the decompositions of both diazo compounds occur through similar mechanisms. Using ReactIR, rates of azine formation with diazo **2.20a** and **2.20d** were compared in the presence of $Rh_2$(*S*-TCPTTL)$_4$ at 2041 $cm^{-1}$. Both reactions had first-order profiles suggesting saturation of the rhodium-catalyst as previously observed in diarylcarbene insertion.[32] A dramatic rate difference between **2.20a** and **2.20d** was observed ($k_{rel}$>120), indicating that ortho substitution lowers the rate of azine formation. By limiting azine formation, insertion into a prochiral silane's Si–H bond becomes more favorable and leads to higher yields of silane **2.26a** (compared to **2.20a**, 89% vs. 76% respectively).

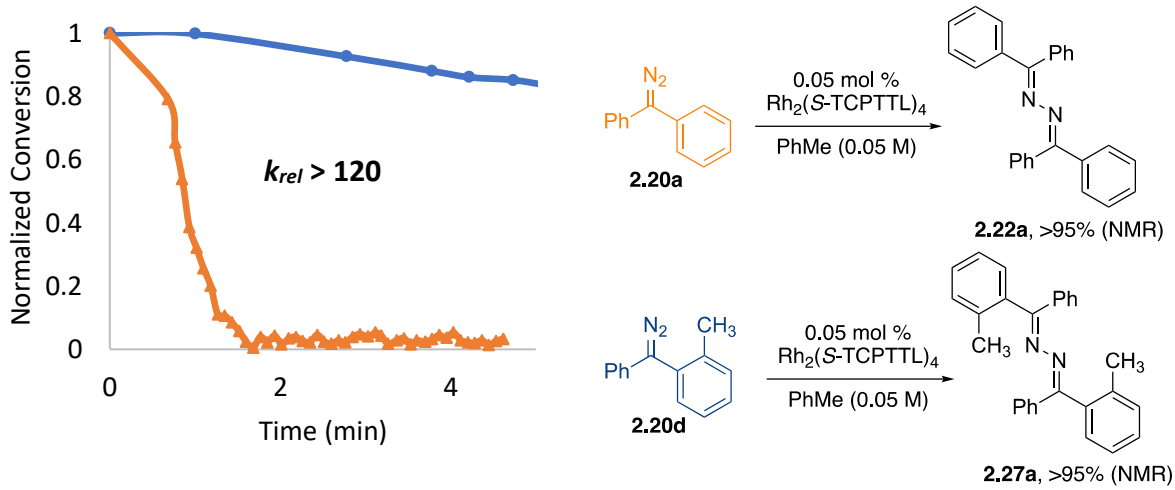


**Figure 2.16** ReactIR analysis of diazo decomposition for **2.20a** and **2.20d** using **2.24h**. The peak at 2041 $cm^{-1}$ was monitored for both reactions.

Competition kinetic isotope effect experiments were performed to probe the rate-limiting step in the transformation (Figure 2.17). Silane **1.6e**-$d^2$ was synthesized and tested in a 1:1 ratio with silane **1.6e**. A KIE of 1.6 was calculated, suggesting a rate-determining Si–H insertion step. Given the magnitude of the isotope effect, the Si–C and C–H bonds are proposed to form in a concerted fashion, with a small amount of positive charge building up on the silicon center.[33] This results fits with previous reports with both aryl(ester)carbenes[34] and diarylcarbenes,[32] suggesting identical reactivity for both carbene classes despite different substituents.

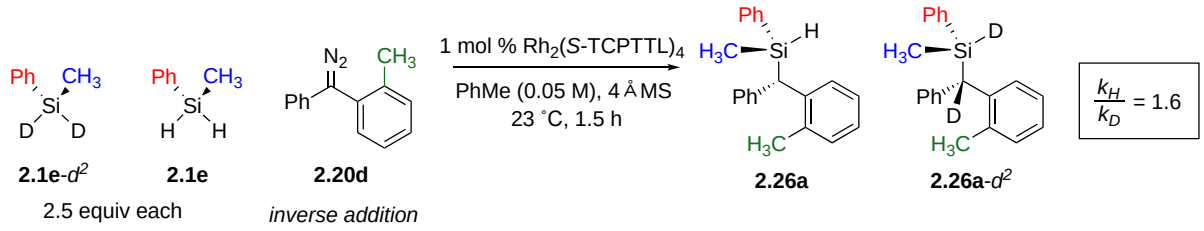


**Figure 2.17** Competition KIE experiment using **2.1e**-$d^2$.

From results examining the mechanism of the transformation, the following catalytic cycle is proposed (Figure 2.18): The rhodium catalyst (**2.24h**) reacts with the diazo compound (**2.20a** or **2.20d**) to form complex **2.28a**, which is approached by prochiral silane **2.1e** to produce the silicon-stereogenic silane **2.26a** (or **2.21a**) and regenerate the catalyst. Off-cycle formation of azine (**2.22a** or **2.27a**) can occur when metal carbene **2.28a** reacts with another diazo compound. The addition of 4Å mol sieves reduces off-cycle formation of siloxane **2.23a**.

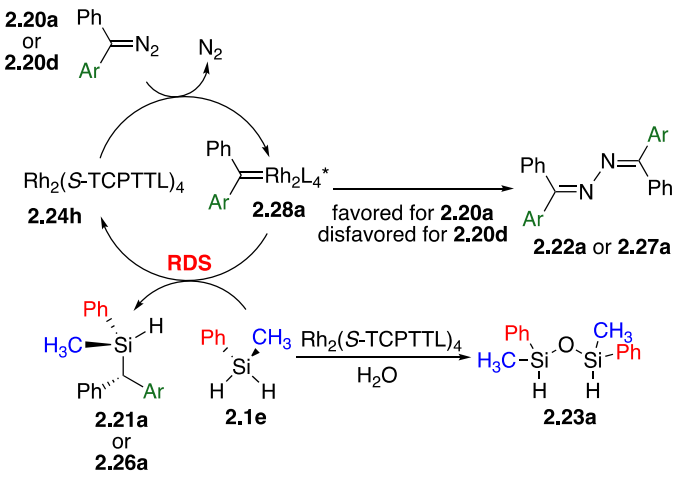


**Figure 2.18** Proposed catalytic cycle.

A hypothesis for increased selectivity for prochiral diazo compounds compared to symmetrical diazo compounds is attributed to the out-of-plane twist of the ortho-substituted aryl ring in rhodium carbene **2.28a** that blocks one face of the carbene from an approaching Si–H bond (Figure 2.19). Additionally, the combination of ligand steric effects and the ortho-substituent is proposed to limit isomerization of the aryl rings that would allow access to both faces of the carbene. As seen with ortho-substituted diazo compounds **2.20d**-**2.20g**, increasing electron-withdrawing effects leads to higher observed diastereoselectivity. The out-of-plane twist would limit conjugation of the electron-withdrawing group and lead to a more stable carbene intermediate. Recent work from Houk[35] and Davies[31] supports the out-of-plane twist with dirhodium carbenes. The authors observed similar effects from diazo compound sterics and electronics, supported by DFT calculations.

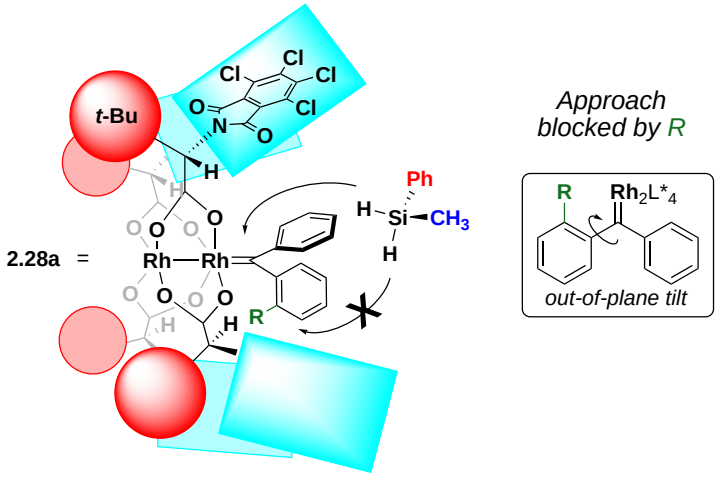


**Figure 2.19** Rationale for increased selectivity with prochiral diazo compounds.

## 2.8: Functionalization of Si–H insertion products

Transformations to demonstrate the further utility of insertion products were explored. Access to enriched silanol **2.29a** was accomplished using Pd/C catalyzed hydrolysis in THF/$H_2O$ in 90% yield, 90:10 dr and 93:7 er (Figure 2.20). Based on previous reports, this is known to occur with inversion of configuration at the silicon center.[36] Si–H hydrolyses were performed for all silanes in order to report enantioselectivities using CSP-HPLC.

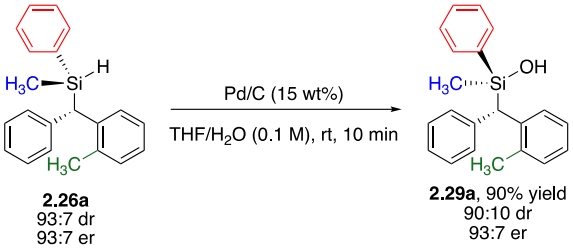


**Figure 2.20** Hydrolysis of **2.26a** to **2.29a** using Pd/C.

Conditions were screened for a hydrosilylation product with the remaining Si–H bond. Several metals known to insert into Si–H bonds with retention of configuration, including Pt, Ir, and Rh, were explored.[29] Initial experiments were performed with Pt-based catalysts. NHC-based Pt catalyst provided poor conversion and starting material was recovered (Table 4 entry 1). With platinum(0)-1,3-divinyl-1,1,3,3-tetramethyldisloxane (Pt(dvs)) and $PtO_2$, complete conversion of the Si–H bond was observed and small amounts of hydrosilylation product **2.30b** formed (Table 4, entries 2 and 3). Screening several solvents did not affect the reaction outcome (Table 4, entries

4-6). With Rh-based catalysts, unexpected formation of vinylsilane **2.30a** was observed in addition to **2.30b** (Table 4, entry 7). Switching to Wilkinson's catalyst, as well as switching from $CH_2Cl_2$ to DCE, provided lower selectivity for **2.30a** (Table 4, entries 8 and 9). When the reaction was scaled up a 1:1 ratio of the vinyl silane and hydrosilylation product was observed (Table 4, entry 10). At reduced scale, the equivalents of styrene could have been more than as written since the relative error is higher. A previous report supports that increased equivalents of alkene promote vinylsilane formation.[37] Here, an 85:15 selectivity was observed using three equivalents of 4-fluorostyrene at 82% mass recovery (Table 4, entry 11). The vinylsilane formed in 93:7 dr, indicating high fidelity of the stereochemical information. The enantiomers of vinylsilane **2.30a** did not separate on CSP-HPLC, so an er could not be determined.

**Table 4**: Optimization of dehydrocoupling to form vinylsilane **2.30a**

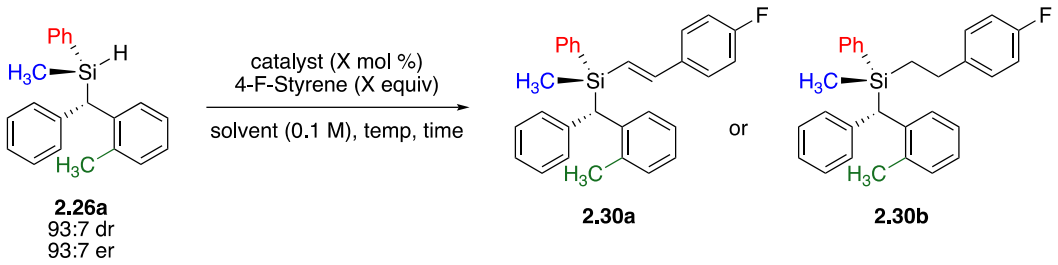


**2.26a**
93:7 dr
93:7 er

**2.30a** **2.30b**

| Entry | **2.26a** (mg) | Catalyst (mol %) | Solvent | Temp (˚C) | Conversion (%)[d] | **2.30a: 2.30b**[d] | % Mass Recovery |
|---|---|---|---|---|---|---|---|
| 1[a] | 31[b] | Pt•NHC[c] (10) | DCE | rt | 10 | - | ND |
| 2[a] | 32[b] | $PtO_2$ [c](10) | DCE | rt | > 95 | - | ND |
| 3[e] | 30[b] | Pt(dvs) (2.5) | pentane | rt | > 95 | - | ND |
| 4[e] | 102[b] | Pt(dvs) (5) | $CH_2Cl_2$ | rt | > 95 | - | ND |
| 5[e] | 104[b] | Pt(dvs) (5) | DCE | 80 | > 95 | - | ND |
| 6[a] | 32[b] | Pt(dvs) (5) | DCE | 80 | > 95 | - | ND |
| 7[e] | 16[b] | $[Rh(COD)Cl]_2$ (2.5) | $CH_2Cl_2$ | 40 | > 95 | 85:15 | ND |
| 8[e] | 33[f] | $[Rh(PPh_3)Cl]_2$ (2.5) | $CH_2Cl_2$ | 40 | > 95 | 75:25 | ND |
| 9[e] | 31[f] | $[Rh(COD)Cl]_2$ (2.5) | $CH_2Cl_2$ | 80 | > 95 | 75:25 | 80 |
| 10[e] | 102[b] | $[Rh(COD)Cl]_2$ (2.5) | $CH_2Cl_2$ | 40 | > 95 | 50:50 | 75 |
| 11[e] | 103[f] | $[Rh(COD)Cl]_2$ (2.5) | $CH_2Cl_2$ | 40 | > 95 | 85:15 | 82 |

[a] Stirred for 12 h.[b] 1.2 equiv styrene used [c] 10 weight %. [d] Determined using $^1$H NMR Spectroscopy.
[e] Stirred for 16 h. [f] 3.0 equiv styrene used.

Given the presence of benzylic C–H bonds from the ortho-methyl group of **2.26a**, an intramolecular C–H silylation could be accomplished with a chiral silane, leading to an enantioenriched silaindane. Previous reports from the Hartwig group have led to the development of a robust Ir(I)-catalyzed C–H silylation reaction for a variety of structures.[38] Several ligands were screened with **2.26a** (93:7 dr and 93:7 er) with an Ir-(I) source (Table 2.5 entries 1-3). Substituted 1,10-phenanthroline ligands provided Si–H conversion determined using TLC and the reaction was monitored (Table 5, entry 3). After 96 h, silane **2.31a** formed in 85 % yield and 90:10 dr. The product was isolated in excellent yield and good diastereoselectivity on larger scale (Table 5, entry

4). $^{1}$H NOE experiments confirmed a cis-relationship between the C–H and methyl groups (vide infra).

**Table 5**: Optimization of C–H silylation of **2.26a**

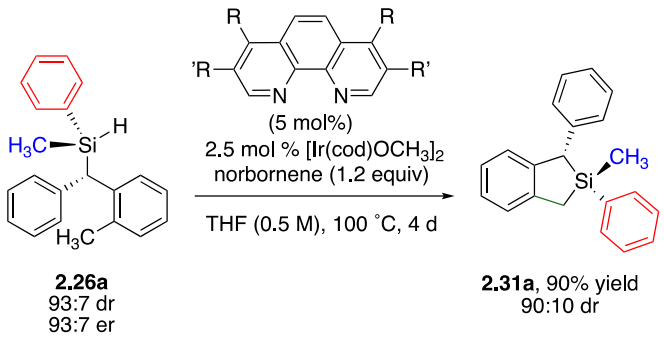


**2.26a**
93:7 dr
93:7 er

**2.31a**, 90% yield
90:10 dr

| Entry | R | R' | Time (h) | % yield[a] | dr[b] |
|---|---|---|---|---|---|
| 1 | H | H | 24 | 0 | ND |
| 2 | H | $CH_3$ | 24 | 0 | ND |
| 3 | $CH_3$ | $CH_3$ | 96 | 85 | 90:10 |
| 4 | $CH_3$ | $CH_3$ | 96 | 90[c] | 90:10 |

[a] Determined using $^{1}$H NMR analysis using PhTMS as an internal standard, 0.1 mmol silane **2.26a**. [b] Determined using $^{1}$H NMR spectroscopy [c] 0.33 mmol **2.26a**; isolated yield.

## 2.9: Determination of Absolute Configuration

The absolute configuration of the silicon and carbon centers were determined from two separate experiments. Tamao-Fleming oxidation of **2.26c** formed benzhydrol **2.32a** in 92:8 er (Figure 2.21A). Based on CSP-HPLC analysis and previous reports,[39] the *S* configuration is the enriched enantiomer and was applied to all other prochiral diazo compounds based on analogy. Separately, $^{1}$H NOE experiments confirmed a cis-relationship between the C–H and methyl groups in **2.31a** (Figure 2.21B). Assuming retention of configuration during the C–H silylation,[29] an *S* configuration was determined for the silicon center and applied to all other silanes by analogy.

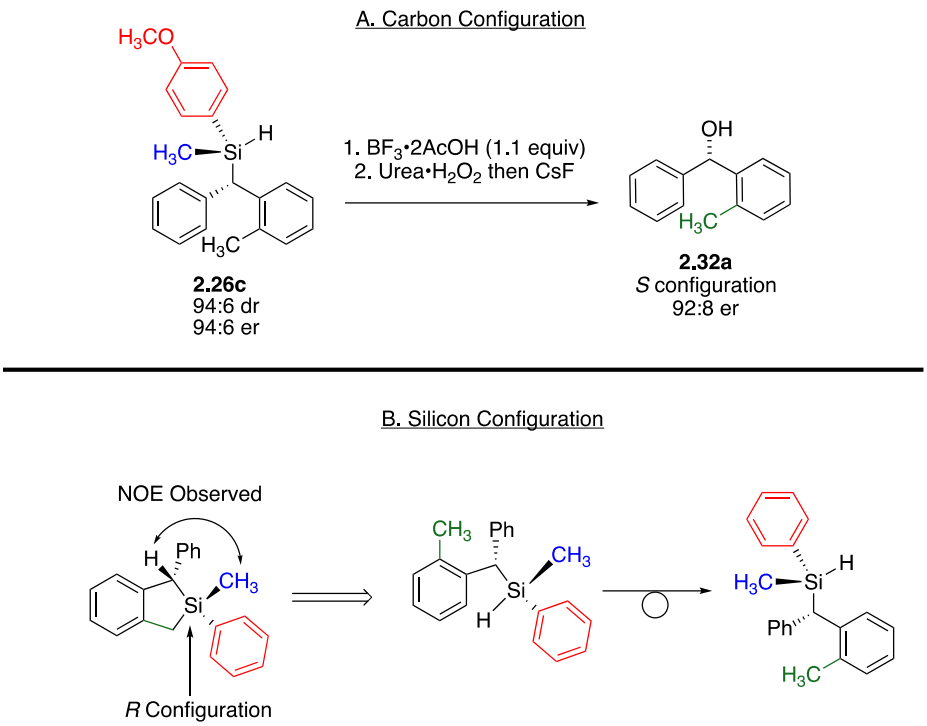


**Figure 2.21**: A) Tamao-Fleming oxidation of **2.26c** for carbon configuration; B) $^{1}$H NOE experiments of **2.31a** for Si configuration.

## 2.10: Conclusions

In conclusion, an enantioselective, intermolecular diarylcarbene insertion into Si−H bonds to synthesize silicon-stereogenic silanes was developed. Dirhodium(II) carboxylates were established as potent catalysts for the transformation, providing reactivity for symmetrical and prochiral diazo compounds with a small library of prochiral silanes. The serendipitous discovery that prochiral diaryldiazo compounds increased selectivity proved crucial to developing highly enantioselective carbene insertion methodology. The unique reactivity of prochiral diazo compounds increased yield of silane products by reducing the rate of off-cycle azine formation, supported by kinetic studies. Transformations of an enantioenriched silane derived from this method showcase the potential applications.

The prochiral silanes developed serve as a source of prochiral silanes for current efforts in the Franz Lab. Lab members Jacob Dalton and Adilene Bernal Sánchez are currently using prochiral silanes to access prochiral silanediols to investigate desymmetrization with enzymes and chiral organocatalysts. Additionally, lab member Yun-Pu Chang is studying silanes derived from this method as silanol-based ligands.

## 2.11: Experimental Procedures and Characterization

***CAUTION*** Diazo compounds are high energy compounds and require careful treatment. We observed no problems throughout our work, but care should always be taken when handling large quantities of diazo compounds. See Bull *et. al.*[40] for risk analysis for related diazo compounds.

### 2.11.1: General Information

General information on NMR spectroscopy can be found on page 64.

### 2.11.2: Materials

For chapter 2, cyclohexylphenylsilane,[41] triethylsiloxyphenylsilane,[24] 2-methoxybenzophenone,[18] naphthylphenylketone,[42] 2-triflouoromethyl benzophenone,[43] diphenyldiazomethane,[6] 4,4'-(diazomethylene)bis(chlorobenzene),[44] 4,4'-(diazomethylene) bis(methoxybenzene)[44] were made from previously published procedures. ($Rh_2$(S-TCPTTL)$_4$ was purchased from TCI; $Rh_2(OAc)_4$, $Rh_2$(R-PTAD)$_4$ and $Rh_2$(S-BTPCP)$_4$ purchased from Strem Chemicals Inc. $Rh_2$(*S*-PTV)$_4$, $Rh_2$(*S*-PTTL)$_4$, ($Rh_2$(*S*-BPTTL)$_4$ were donated by the Shaw Lab at UC Davis. Dry $CH_2Cl_2$, THF, $Et_2O$ and PhMe were dispensed from a solvent purification system that passes solvent through two columns of dry neutral alumina prior to use. NOTE: it is necessary that the $MnO_2$ used for the oxidation of hydrazones be ~85% pure with an average particle size of 2 microns, appearing as a fine black powder (e.g. Oakwood Chemical, CAS #: 1313-13-9, cat. #: 094454, lot #: 094454K03K or Sigma Aldrich, cat: 217646-100G, Lot # MKCJ7777).

### 2.11.3: Synthesis, Purification and Analysis

All microwave experiments were run in a Biotage Initiator EXP EU 400W microwave synthesizer 2.0 (serial number 11031). MALDI data was obtained at the Mass Spectrometry Facilities of University of California, Davis. Products were also analyzed by mass spectrometry on a Bruker UltraFlextreme MALDI mass spectrometer (Bruker Corp, Billeraca, MA) in reflectron mode. Samples were first mixed in a 1:1 ratio with a saturated solution of alpha-hydroxycinnamic acid (Sigma Chemical Co) in high-purity water:MeCN (35%:65%) and 1mg of NaI to promote cationization was added before being spotted on the plate and allowed to air dry. Samples were analyzed using the minimum laser fluence to obtain adequate signal (s/n > 20), generally requiring

1000 shots per sample. Data was analyzed in FlexAnalysis. Compounds were analyzed using low-resolution mass spectrometry with an Advion© ASAP-APCI-MS was achieved and the corresponding data is reported for those samples. Kinetic Analysis was performed using a Mettler Toldedo ReactIR 700 (serial number B929971514) with a liquid $N_2$ MCT detector fitted with a DiComp probe (serial number B939349478). The system was filled with liquid $N_2$ and allowed to cool for 1 h before kinetic experiments begun. Initial trends were found using iC IR 7.1 and further analyzed using Microsoft Excel. High performance liquid chromatography (HPLC) data were obtained on Shimadzu LC-20AB system with CHIRALPAK® AD-H column (4.6 x 250 mm, 5 μm), CHIRALPAK® OD-H column (4.6 x 250 mm, 5 μm) or CHIRALPAK® AS column (4.6 x 250 mm, 5 μm) and Shimadzu SPD-M20A photodiode array detector. Each HPLC sample was eluted at a constant flow rate with isocratic (90:10 hexanes/isopropanol)/hexanes or (90:10 heptane/isopropanol)/heptane system and 40 °C column oven temperature.

## 2.11.4: General Synthetic Procedures

### Method A: Synthesis of Donor/donor diazo Compounds 2.20a-e, h

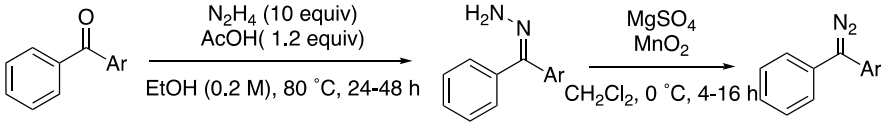


A 50-mL two-neck round-bottomed flask with a stir bar and condenser was charged with ketone and anhydrous EtOH (0.2 M). Hydrazine (10 equiv), followed by AcOH (1.2 equiv) were added, and the solution was heated to reflux. The reaction was monitored by TLC (7:3 hexanes/EtOAc) until the ketone was fully consumed. The reaction was allowed to cool to room temperature, and the solvent was removed via rotary evaporator. The resulting slurry was dissolved in $Et_2O$ (20 mL), washed with $H_2O$ (10 mL), brine (10 mL), and dried with $Na_2SO_4$. The solution was filtered, and the solvent was removed via rotary evaporator. The resulting hydrazone was verified to be present by TLC (7:3 hexanes/EtOAc) and $^1H$ NMR spectroscopy, then carried on without further purification.

The crude hydrazone mixture was transferred into a flame dried round-bottomed flask purged with argon and charged with a stir bar. $CH_2Cl_2$ (15 mL) was added, followed by $MgSO_4$ (100 mg/mmol). The solution was cooled down to 0˚C, and $MnO_2$ (8.0 equiv) was added in one portion. The solution was monitored by TLC (7:3 hexanes/EtOAc) until all hydrazone was consumed. The

solution was then filtered through celite, washed with $CH_2Cl_2$ (3 x 10 mL), and the solvent was removed via rotary evaporator. Diazo products were purified by flash chromatography using (99:1 hexanes: $Et_3N$) on basic alumina.

Diazo compound **2.20a-c** were found to readily decompose within 24 h at room temperature, so compounds was stored at -23 ˚C under argon, which increased stability to 2 weeks. Diazo compounds **2.20a-h** were found to be stable for > 48h at room temperature when stored under argon.

**Method B: Synthesis of 2.20f**

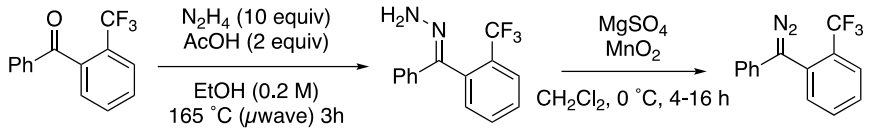


A 20-mL microwave vial with a stir bar was flamed dried, allowed to cool, then sealed. With an Ar-balloon to equilibrate pressure, the vial was charged with 2-trifluoromethylbenzophenone in (1.00 g, 4.00 mmol) in EtOH (10 mL). Hydrazine (1.28 mL, 40.0 mmol), followed by AcOH (5.00 mmol, 0.290 mL) were added, and the solution was sparged with Ar for 5 min. The microwave vial was heated in a microwave reactor to 165 ˚C for 3 h, with 15 sec of pre-stirring. The reaction was allowed to cool to room temperature and was diluted in $Et_2O$ (20 mL), washed with $H_2O$ (10 mL), brine (10 mL), and dried with $Na_2SO_4$. The solution was filtered, and the solvent was removed via rotary evaporator. The crude hydrazone mixture was transferred into a flame dried round-bottomed flask purged with argon and charged with a stir bar. $CH_2Cl_2$ (10 mL) was added, followed by $MgSO_4$ (100 mg/mmol). The solution was cooled down to 0 ˚C, and $MnO_2$ (32 mmol, 2.78 g) was added in one portion. The solution was monitored using TLC (7:3 hexanes/EtOAc) until all hydrazone was consumed. The solution was then filtered through celite, washed with $CH_2Cl_2$ (3 x 10 mL), and the solvent was removed via rotary evaporator. The product was purified by flash chromatography (99:1 hexanes/$Et_3N$) on basic alumina to furnish diazo **2.20f** as a red liquid in 44% yield (462 mg, 1.76 mmol) over 2 steps.

**Method C: Synthesis of Aryl-alkyl Silanes 2.19a-j Using Grignard Reagents**

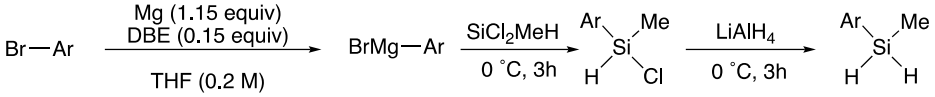


Magnesium turnings (1.15 equiv) were added to THF in a flamed dried, argon-purged 2-neck flask followed by the addition of DBE (0.15 equiv). The solution stirred for 1 h and turned black. The aryl bromide (1.0 equiv) was slowly added dropwise over a 20-min period, and the solution was brought to reflux for up to 16 h, or until magnesium was no longer observed in the flask. The reaction was allowed to cool to room temperature and stirred an additional 15 min. The reaction was cooled to 0 ˚C with vigorous stirring, and an alkyldichlorosilane was added quickly in one portion, and stirred for an additional 2-3 h with no further cooling. The reaction was cooled to 0 ˚C again, and $LiAlH_4$ (4.0 M solution in $Et_2O$, 1.0 equiv) was added dropwise over a 5-min period and stirred for an additional 2 h. The reaction was slowly quenched with the addition of saturated aq. Rochelle's salt, and filtered over celite. The organic layer was separated and the aqueous layer was washed with $Et_2O$, then the organic layers were combined and washed with brine, dried with $MgSO_4$, filtered, and then concentrated *in vacuo*. The products were purified either by bulb-to-bulb distillation via Kugelrohr, sublimation, or column chromatography in hexanes.

**Method D: Synthesis of Aryl-alkyl Silanes 2.19a-j Using Organolithium Reagents**

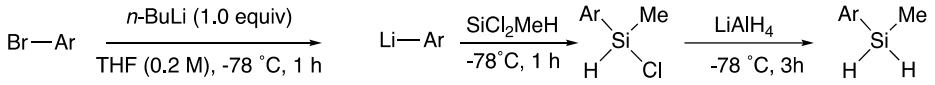


A flamed dried round-bottomed flask with a stir bar was charged with an aryl bromide (1.0 equiv), and THF (25 mL). The reaction was cooled to -78 ˚C with vigorous stirring, and *n*-BuLi (2.5 M solution in hexanes, 1.0 equiv) was added dropwise, and the reaction stirred for 1 h. The alkyldichlorosilane (1.0 equiv) was added quickly in one portion and the reaction stirred for 1 h at -78 ˚C. $LiAlH_4$ (4.0 M solution in $Et_2O$, 1.0 equiv) was added dropwise over a 5 min period and the reaction stirred for 2 h. The reaction was slowly quenched with the addition of saturated aq. Rochelle's salt, and filtered over celite. The organic layer was separated and the aqueous layer was washed with $Et_2O$, then the organic layers were combined and washed with brine, dried with $MgSO_4$, filtered, and then concentrated *in vacuo*. The products were purified either via Kugelrohr, sublimation, or flash chromatography (hexanes) to furnish pure silanes.

**Method E: Synthesis of 2.19k**

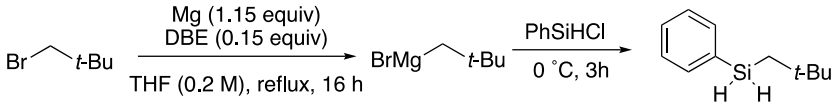


Magnesium turnings (1.15 equiv, 5.75 mmol, 140 mg) were added to a flamed dried argon-purged, 25-mL 2-neck flask. THF (10 mL), followed by DBE (0.15 equiv) were added to the flask. The solution stirred for 1 h at room temperature and turned black. Neopentyl bromide (1.0 equiv, 5.0 mmol, 630 mL) was added dropwise, and the solution was brought to reflux for up to 16 h. The reaction was allowed to cool to room temperature and stirred an additional 15 min. The reaction was cooled to 0 ˚C with vigorous stirring, and chlorophenylsilane (1.0 equiv, 5.0 mmol, 0.66 mL) was added quickly in one portion and stirred for an additional 2-3 h with no further cooling. The reaction was slowly quenched with the addition of saturated aqueous $NH_4Cl$ (10 mL) and filtered over celite. The organic layer was separated and the aqueous layer was washed with $Et_2O$, then the organic layers were combined and washed with brine, dried with $MgSO_4$, filtered, and then concentrated *in vacuo*. The crude mixture was purified by column chromatography (100 % hexanes) to furnish silane **2.19k** as an oil in 25% yield (231 mg, 1.30 mmol).

**Method F: Synthesis of Racemic Standard for CSP-HPLC analysis**

A 4-mL reaction vial equipped with a stir bar and 50 mg 4Å molecular sieves was heated under flame and dried under high vacuum (<1 torr). After the vial cooled to room temperature, it was purged with argon, followed by the addition of $Rh_2(OAc)_4$ (0.4 mg, 0.002 mmol), then silane (0.5 mmol). The vial was re-purged with argon, and $CH_2Cl_2$ (1 mL) was added. A diazo compound (0.1 mmol) was weighed into a separate flame-dried vial, and $CH_2Cl_2$ (1 mL) was added. The solution of diazo compound in $CH_2Cl_2$ was drawn into a syringe. Using a long needle, the syringe was placed on a syringe pump with the needle *in* the stirring solution. The syringe pump was programmed to add the solution over a period of 1 h at room temperature. After 1 h, the solution was diluted with hexane (5 mL), filtered through celite, and concentrated *in vacuo*. The presence of insertion product was verified by $^1H$ NMR analysis, and CSP-HPLC analysis was then conducted (Method I).

**Method G: General Procedure for Enantioselective Dirhodium(II)-catalyzed Carbene Insertion with Donor/donor Carbenes (Prochiral and Symmetrical)**

A 8-mL reaction vial equipped with a stir bar and 4Å molecular sieves (100 mg) was heated under flame and dried under high vacuum (<1 torr). After the vial cooled to room temperature, it was purged with argon, followed by addition of $Rh_2$(*S*-TCPTTL)$_4$ (0.0020 mmol, 3.6 mg) and silane (1.0 mmol). The vial was re-purged with argon, and PhMe (2 mL) was added. Diazo compound (0.2 mmol) was weighed into a separate flame-dried vial, and PhMe (2 mL) was added, then the solution was drawn into a syringe. Using a long needle, the syringe was placed on a syringe pump with the needle *in* the stirring solution of rhodium catalyst and silane. The syringe pump was programed to add the solution of diazo compound over a period of 1 h at room temperature.

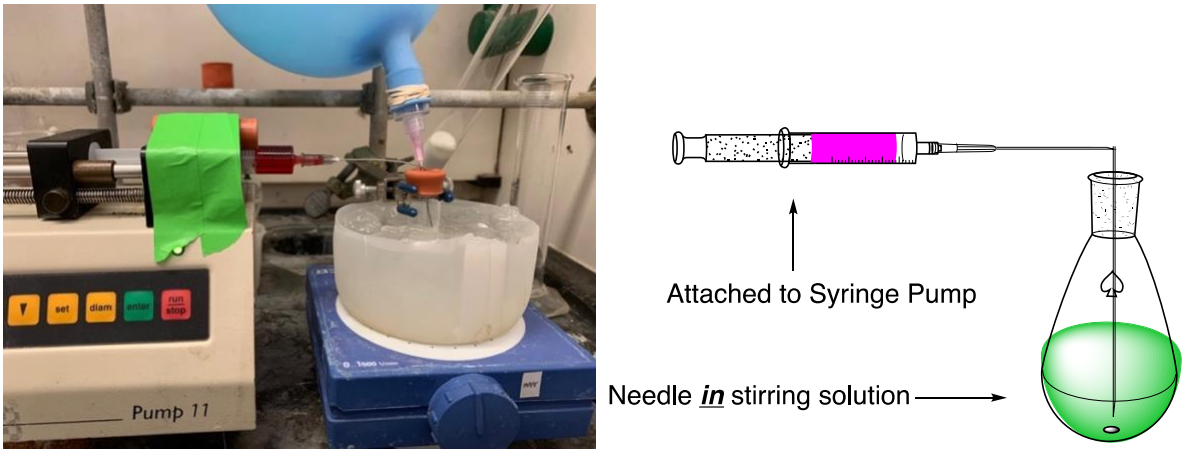


**Figure 2.22**. Example insertion with diagram

30 min after the addition of diazo compound, the solution was diluted with hexane (5 mL), filtered through celite, and concentrated *in vacuo*. The crude mixture was diluted in hexanes and ran through a short silica plug (4-cm in a Pasteur pipette) to remove catalyst and concentrated *in vacuo*. The crude mixture was analyzed by $^1$H NMR spectroscopy to determine diastereoselectivity, via the methyl resonance off the benzene ring. The product was then purified using flash chromatography (dry loaded sample in silica, 98:2 hexanes/$CH_2Cl_2$) to furnish silanes as pure compounds.

**Method H: Procedure for gram-scale enantioselective dirhodium(II)-catalyzed insertion of diazo 3a and methylphenylsilane 2.1e**

A 100-mL round-bottomed flask with 4Å molecular sieves (2.50 g) and equipped with a stir bar was heated in the oven for 24 h and dried under high vacuum (<1 torr). After the flask cooled to room temperature, $Rh_2$(*S*-TCPTTL)$_4$ (0.0025 mmol, 5.1 mg) and methylphenylsilane **2.1e** (25.5 mmol, 3.50 mL) were added. The flask was purged with argon, followed by addition of PhMe (25 mL). Diazo compound **2.26a** (5.1 mmol, 1.00 g) was weighed into a separate flame-dried vial, PhMe (25 mL) was added, then drawn into a 30-mL syringe. Using a long needle, the syringe was placed on a syringe pump with the needle *in* the stirring solution. The syringe pump was programed to add the solution of diazo compound over a period of 2.5 h at room temperature.


**Figure 2.23**. Gram-scale insertion.

After 2.5 h, the solution was filtered, and concentrated *in vacuo*. The crude mixture was analyzed by $^1$H NMR spectroscopy to determine diastereoselectivity via the methyl resonance off the benzene ring. The product was then purified using flash chromatography (dry loaded sample in silica, 98:2 hexanes/$CH_2Cl_2$) to furnish silane **2.26a** as an oil in 89% yield (93:7 dr, 93:7 er, 1.34 g, 4.50 mmol). Silane **2.26a** was found to be stable to air and atmospheric moisture for >3 weeks with minimal decomposition and no loss diastereoselectivity or enantioselectivity.

**Method I: General procedure for hydrolysis for CSP-HPLC Analysis**

Silane was added to a 4-mL reaction vial (10 mg) followed by THF/$H_2O$ (99:1 v/v, 0.5 mL), then Pd/C (10 mg) (preactivated with $PhSiH_3$). The reaction was monitored by TLC until full consumption of the silane was observed. The reaction was filtered through celite and concentrated *in vacuo*. $CH_2Cl_2$ (0.1 mL) was added, and the sample was spotted onto a TLC plate (5 x 5 cm). The plate was placed in a TLC chamber to develop (in 95:5 hexanes/EtOAc), and the silanol was etched off the plate with a razor blade. The loose silica was washed with 70:30 hexanes/IPA (1 mL) and filtered through celite to furnish CSP-HPLC samples.

**Method J: Tamao-Fleming Oxidation**[45]

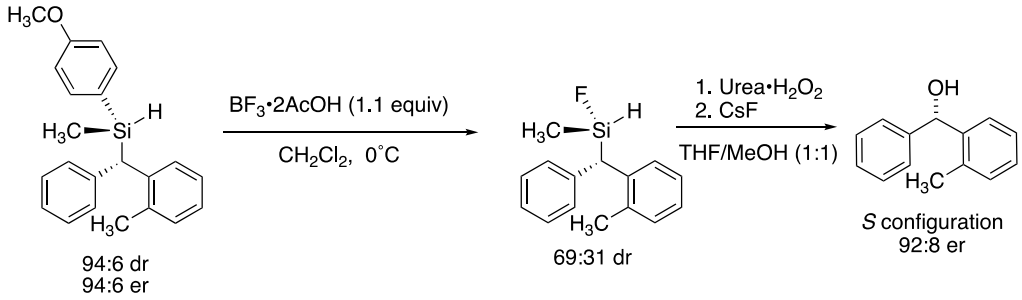


To a flame-dried, Ar-purged 8-mL reaction vial charged with a stir bar, silane **2.26c** (258 mg, 0.770 mmol), and $CH_2Cl_2$ (3 mL) was added. The vial was cooled to 0˚C, and $BF_3$•2AcOH (120 ul, 0.850 mmol) was added to the vial while stirring. The conversion of the arylsilane to the silyl-fluoride was monitored using TLC (9:1 hexanes/EtOAc). After 3 h, the reaction was diluted with $CH_2Cl_2$ (10 mL). Saturated aqueous $NaHCO_3$ solution (8 mL) was added and the reaction stirred until the evolution of gas ceased completely. The organic layer was separated, collected, and the aqueous layer was extracted with $CH_2Cl_2$ (2 x 15 mL). The organic layer was dried over $Na_2SO_4$ and concentrated *in vacuo* to afford a silyl-fluoride intermediate that could be isolated as a clear viscous oil and was identified using $^1H$ NMR and $^{19}F$ NMR spectroscopy. The silyl-fluoride was carried forward directly into the next step. The crude mixture was dissolved in 1:1 MeOH/THF (5 mL), and transferred to a flame-dried flask charged with a stir bar. Next, urea hydrogen peroxide was added (80.0 mg, 0.850 mmol), and the reaction was monitored by TLC until full consumption of the silyl-fluoride was observed. After 16 h, CsF (128 mg, 0.850 mmol) was added, and the reaction was monitored by TLC until benzhydrol was observed (based on TLC). After 1 h,tThe reaction mixture was filtered through celite, washed with $H_2O$ (5 mL), and dried over $Na_2SO_4$. The

solution was filtered and concentrated *in vacuo* to furnish crude benzhydrol **2.32a**. A CSP-HPLC sample of the reaction mixture was prepared and analyzed (92:8 er). When compared to literature values, they matched with previously reported data with the *S*-configuration.

**Method K: C–H Silylation**[46]

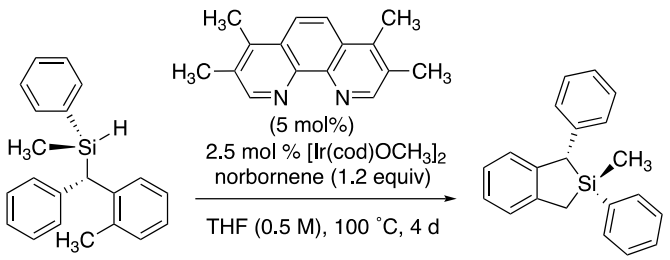


**2.26a**
93:7 dr
93:7 er

**2.31a**, 90% yield
90:10 dr

To a flame-dried, 4-mL reaction vial charged with stir bar, silane **2.26a** (100 mg, 0.330 mmol), norbornene (36 mg, 0.39 mmol), 3,4,7,8-tetramethyl-1,10-phenthroline (2.0 mg, 0.0084 mmol), and [Ir(cod)OMe]$_2$, (5.5 mg, 0.084 mmol), THF (0.7 mL) was added. A vial was purged with argon and a cap was tightly screwed on. The vial was heated to 100 ˚C and stirred for 4 d. The reaction was allowed to cool to room temperature, then diluted with hexanes (10 mL), and filtered through a pad of celite. The organic solution was concentrated *in vacuo*, and the product was purified using flash chromatography (98:2 hexanes/$CH_2Cl_2$) to furnish silane **2.31a** as an oil in 90 % yield (89.2 mg, 90:10 dr).

**Method L: General Procedure for Pd/C Hydrolysis**

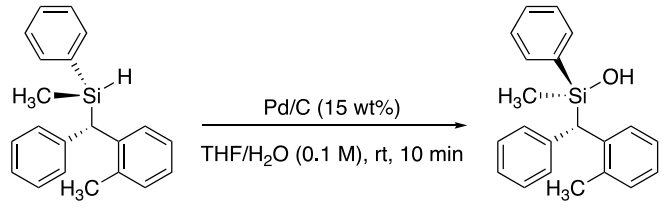


**2.26a**
93:7 dr
93:7 er

**2.29a**, 90% yield
90:10 dr
93:7 er

To a flame-dried 4-mL reaction vial charged with stir bar, silane **2.26a** (100 mg, 0.33 mmol, 93:7 dr; 93:7 er), Pd/C (15.0 mg, 15 wt%), and THF ( 3.30 mL, containing ~1% v/v $H_2O$) was added. The consumption of starting material was monitored by TLC. After 10 min, $CH_2Cl_2$ (5 mL) was added, and the reaction was filtered through a thin pad of celite. The solution was dried with

$Na_2SO_4$, filtered, and concentrated *in vacuo*. The product was purified using flash chromatography (95:5 hexanes/EtOAc) to furnish silanol **2.29a** as an oil in 90% yield (94.6 mg, 90:10 dr, 93:7 er).

**Method K: Dehydro-coupling reaction**

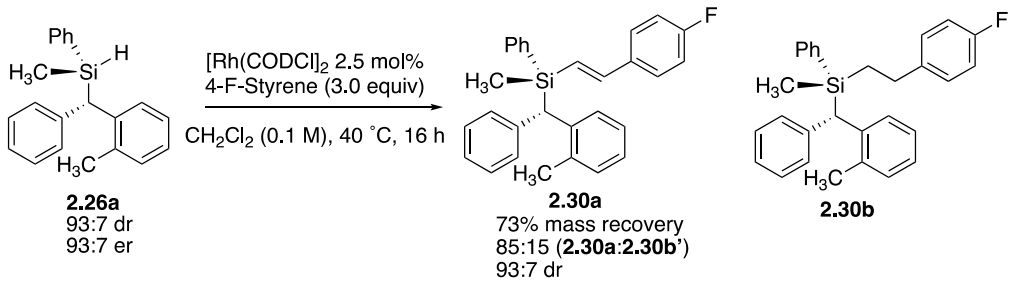


**2.26a**
93:7 dr
93:7 er

**2.30a**
73% mass recovery
85:15 (**2.30a**:**2.30b**')
93:7 dr

**2.30b**

To a flame-dried, argon purged 8-mL reaction vial charged with a stir bar, silane **2.26a** (104 mg, 0.34 mmol, 93:7 dr; 93:7 er), 4-fluorostyrene (19 μL, 1.0 mmol, 3.0 equiv), and $CH_2Cl_2$ (3.5 mL) was added. After 5 min, $[Rh(COD)Cl]_2$ (5.2 mg, 0.010 mmol, 0.025 equiv) was added, and the solution turned yellow, and was heated to 40˚C and stirred for 16 h. The reaction was diluted with hexanes and filtered through a thin silica pad to remove catalyst. The solvent was removed via rotary evaporator, and the product was purified using flash chromatography (98:2→90:10 hexanes/$CH_2Cl_2$) to furnish silane **2.30a** as an oil in 62% yield (73% mass recovery (104.1 mg); 85:15 mixture with hydrosilylation product **2.30b**, 93:7 dr by $^{19}F$ NMR). The determination of 85:15 was confirmed using $^1H$ NMR spectroscopy by comparing the relative integrals of the peaks at 4.10 and 3.97 ppm.

**2.11.5: Procedure for *in situ* ReactIR Analysis**

A 5-mL microwave reaction vial charged with a stir bar and 4 Å MS (100 mg) was flame-dried and cooled under vacuum (<1 torr). After cooling, the vial was sealed, and PhMe (3 mL) was added. A hole was punctured using a spatula on top of the vial, then quickly fitted to the ReactIR probe for background scans. The diazo compound was added as a solution (44.0 mg in 1.50 mL PhMe), and more background scans were taken to identify the diazo compound on the IR spectrum (2000-2100 $cm^{-1}$). $Rh_2$(*S*-TCPTTL)$_4$ was added as a solution in PhMe (0.5 mL of 0.3 mg/mL solution), and the disappearance of diazo **2.20a** or **2.20d** was monitored to determine a 1$^{st}$ order rate constant (*k*).

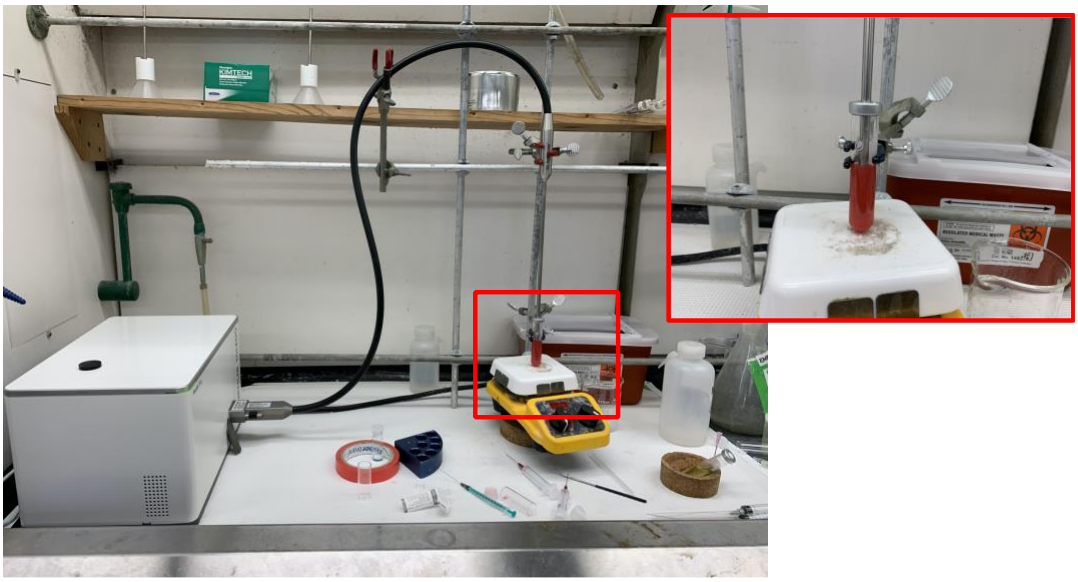

**Figure 2.24.** Example of ReactIR setup used for kinetic analysis.

The disappearance of diazo compounds **2.20a** and **2.20d** was monitored at 2041 $cm^{-1}$and data was transferred to Microsoft Excel for analysis. The values on the x-axis were manipulated to reflect the total number of minutes after addition of diazo for determination of rate constants. Y-axis values were normalized and data was presented in % conversion. The initial point used for 1$^{st}$ order rate constant determination was set to when $Rh_2$(*S*-TCPTTL)$_4$ was added to the reaction vial. For the determination of reaction order, and $R^2$ value, the final point was identified when the concentration plateaued. The reactions were then filtered through a celite plug, and azines **2.22a** and **2.27a** were analyzed using $^1$H NMR spectroscopy to determine yield. NMR yields using Ph-TMS as an internal standard were >90% for all trials.

Trial 1

A B

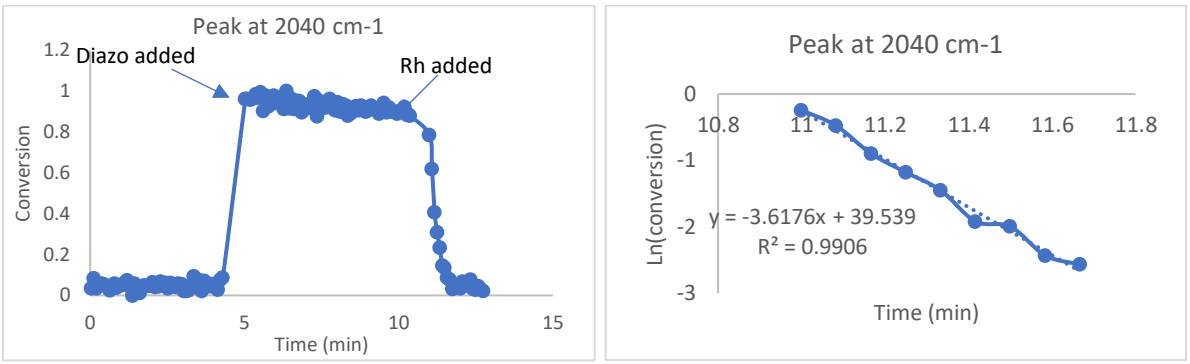


**Figure 2.25**. A: Data graphed for reaction with **2.20a** catalyzed by $Rh_2$(*S*-TCPTTL)$_4$: A) Graph of conversion vs. time. B) Graph of ln[conv] vs. time once catalyst was added.

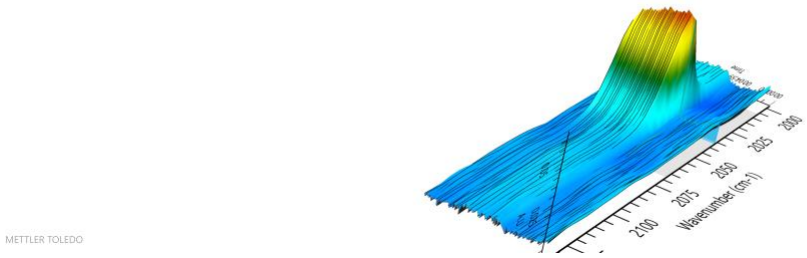


**Figure 2.26**. ReactIR surface plot for trial 1

Trial 2

A B

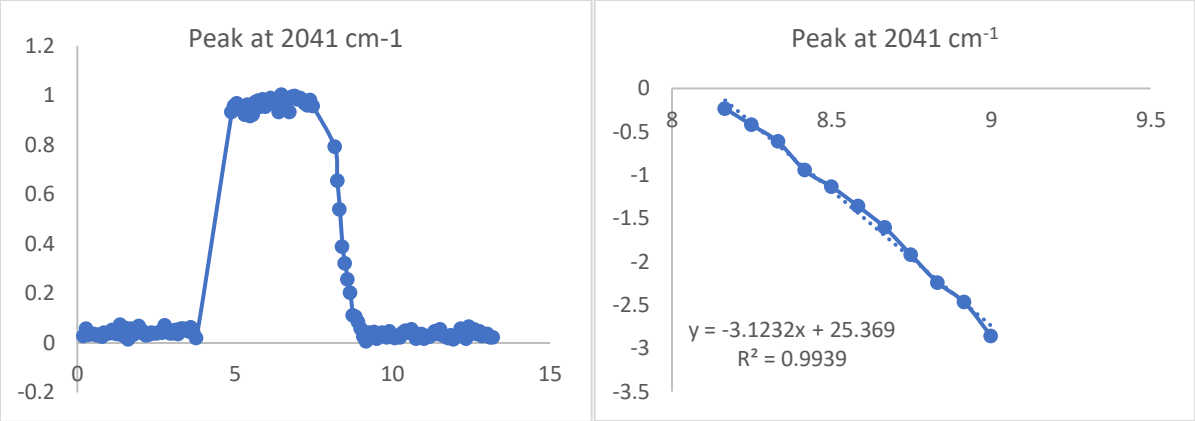


**Figure 2.27**. A: Data graphed for reaction with diazo compound **2.20a** catalyzed by $Rh_2$(*S*-TCPTTL)$_4$: A) Graph of conversion vs. time. B) Graph of ln[conv] vs. time once catalyst was added.

Trial 1

A B

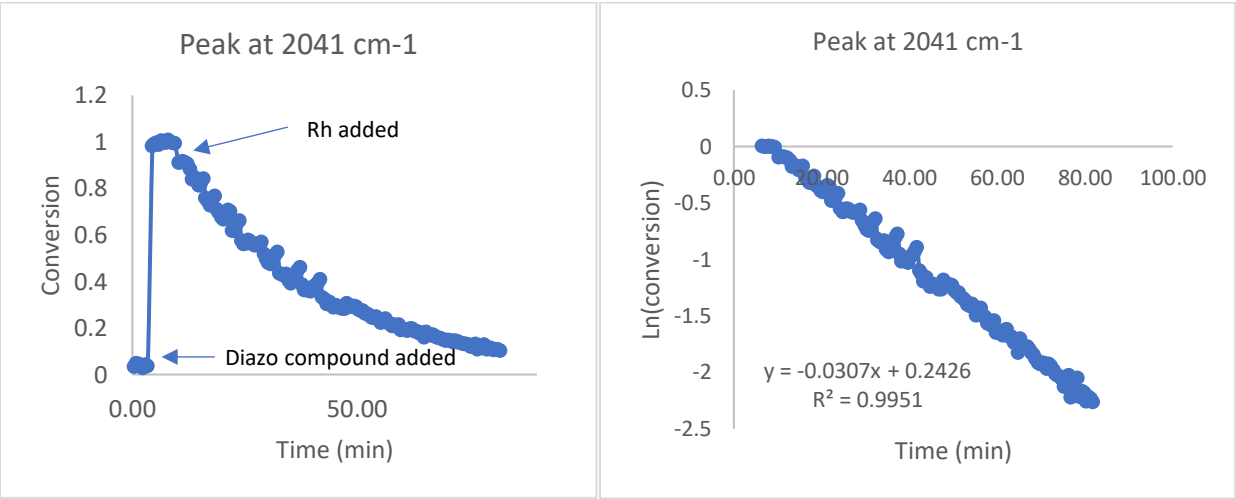


**Figure 2.28**. A: Data graphed for reaction with diazo compound **2.20d** catalyzed by $Rh_2$(*S*-TCPTTL)$_4$: A) Graph of conversion vs. time. B) Graph of ln[conv] vs. time once catalyst was added.

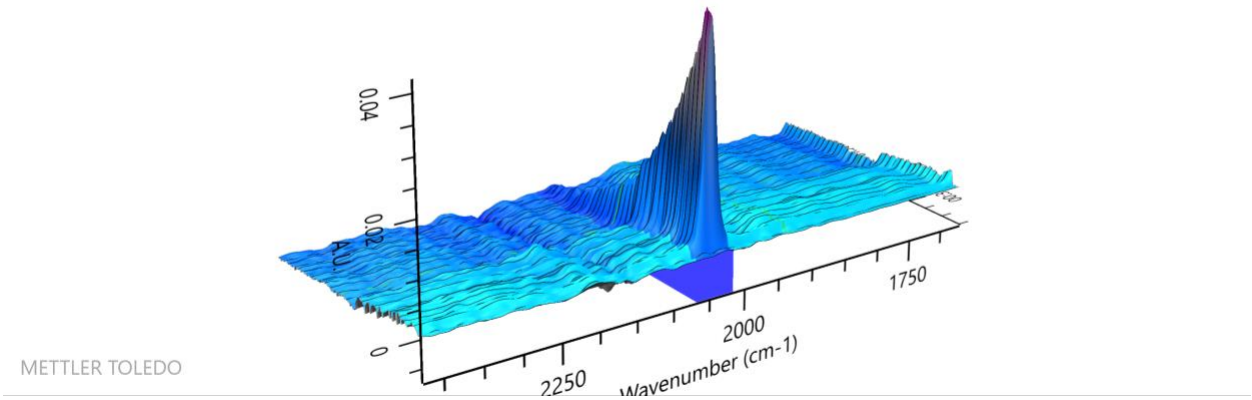


**Figure 2.29.** ReactIR surface plot for trial.

Trial 2

A B

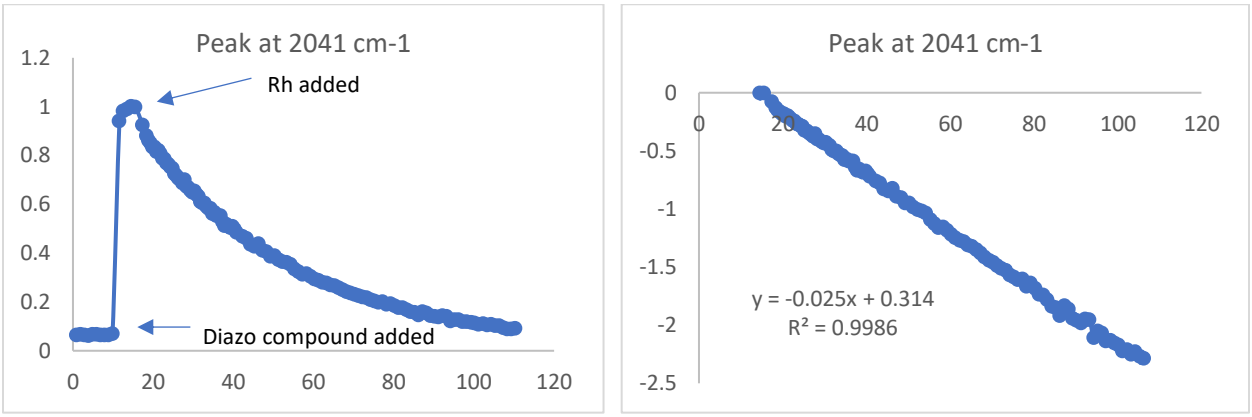


**Figure 2.30**. A: Data graphed for reaction with diazo compound **2.20d** catalyzed by $Rh_2$(*S*-TCPTTL)$_4$: A) Graph of conversion vs. time. B) Graph of ln[conv] vs. time once catalyst was added.

Based on the data observed, $k_{rel} = k_{2a}/k_{3a} = 117.8$ for trial 1 and 127.2 for trial 2.

## 2.11.6: Procedure for Kinetic Isotope Effect

An 8-mL reaction vial equipped with a stir bar and 4Å molecular sieves (100 mg) was heated under flame and dried under high vacuum (<1 torr). After the vial cooled to room temperature, it was purged with argon, followed by addition of $Rh_2$(*S*-TCPTTL)$_4$ (3.6 mg, 0.0020 mmol) and silane **2.1e** (61 mg, 0.50 mmol) and silane **2.1e**-$d_2$ (62 mg, 0.50 mmol). The vial was

re-purged with argon, and PhMe (2 mL) was added. Diazo compound **2.20d** (39 mg, 0.20 mmol) was weighed into a separate flame-dried vial, and PhMe (2 mL) was added, then the solution was drawn into a syringe. Using a long needle, the syringe was placed on a syringe pump with the needle *in* the stirring solution. The syringe pump was programed to add the solution over a period of 1 h at room temperature.

30 min after diazo compound addition, the solution was diluted with hexanes (5 mL), and filtered through celite, and concentrated *in vacuo*. The crude mixture was diluted in hexanes and ran through a short silica plug (4 cm in a Pasteur pipette) to remove catalyst and concentrated *in vacuo*. The product was then purified using column chromatography (dry loaded sample in silica, 98:2 hexanes/$CH_2Cl_2$) to furnish a mixture of silane **2.26a** and **2.26a**-$d_2$ as an oil. The kinetic isotope effect was determined using an integration ratio of the benzhydryl resonance for the major diastereomer present at 3.78. ppm and both benzyl resonances observed at 2.25 ppm (major diastereomer) using Equation 1:

$$KIE = \frac{I_A}{\frac{I_B}{3} - I_A} \qquad \text{(Eq. 1)}$$

Where $I_A$ is the integral of the benzhydryl resonance, and $I_B$ is the integral of both benzyl resonances. This equation takes into account both stoichiometry and the combined integration of both **2.26a** and **2.26a**-$d_2$ at 2.25 ppm.

Trial 1
$I_A$ = 1.00
$I_B$ =4.91
KIE = 1.57

Trial 2
$I_A$ = 1.0
$I_B$ = 4.90
KIE = 1.58

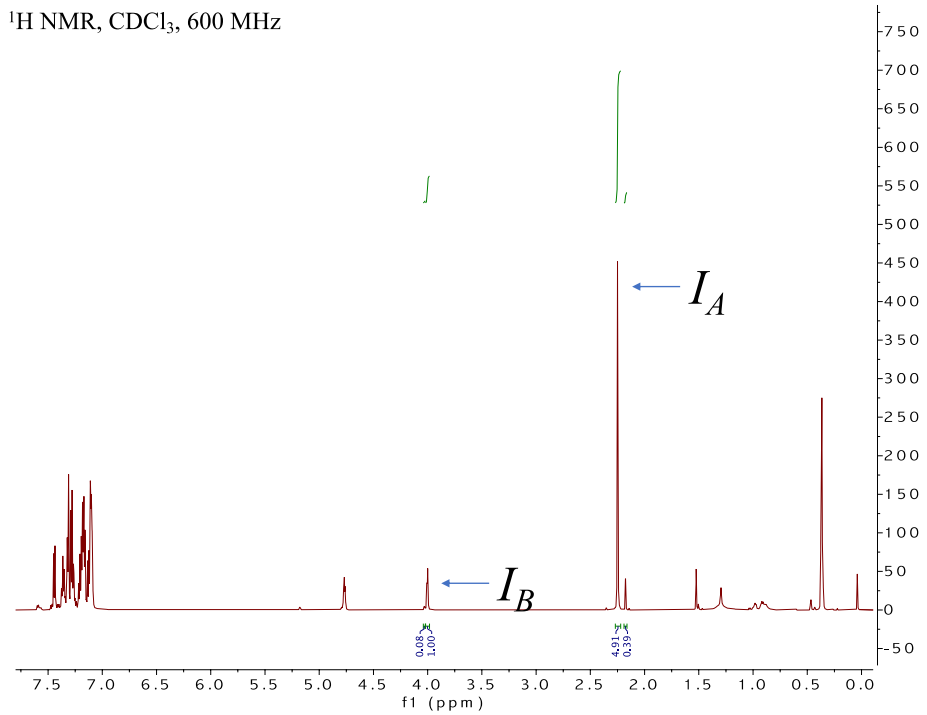


**Figure 2.31**. $^1$H NMR spectrum of **2.26a** and **2.26a-*d*$_2$** mixture, with $I_A$ and $I_B$ shown.

## 2.11.7: Characterization Data

### Silanes

**Methyl(phenyl)silane-*d*$_2$ (2.6e-*d*$_2$)**

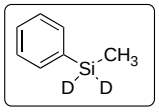

Made using previously reported procedures.[47] Spectrum matches with previous report.[47]

$^1$H NMR (600 MHz, CDCl$_3$) δ 7.59 (m, 2H), 7.45 – 7.35 (m, 3H), 0.43 (s, 3H).

**Isobutyl(phenyl)silane (2.19a)**

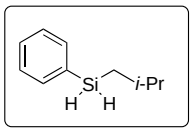

Synthesized according to method C for silane formation using bromobenzene (1.58 mL, 15.0 mmol) and dichlorosiobutylsilane (2.28 mL, 15.0 mmol) and purified via Kugelrohr (150 ˚C, 100 torr) to give a clear liquid in 41% yield (1.01 g, 6.15 mmol) over 2 steps from addition of the chlorosilane.

$^1$H NMR (600 MHz, CDCl$_3$) δ 7.57 (m, 2H), 7.36 (m, 3H), 4.31 (t, *J* = 3.9 Hz, 2H), 1.85 (dh, *J* = 13.4, 6.7 Hz, 1H), 0.99 (d, *J* = 6.6 Hz, 6H), 0.95 (dt, *J* = 7.5, 3.9 Hz, 2H). $^{13}$C NMR (151 MHz, CDCl$_3$) δ 135.35, 133.10, 129.58, 128.09, 25.75, 25.62, 20.61. $^{29}$Si NMR (119 MHz, CDCl$_3$) δ -33.8.

**Methyl(naphthalen-1-yl)silane (2.19b)**

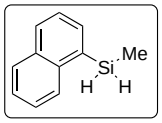

Synthesized according to the general procedure B for silane formation using 1-bromonaphthalene (2.10 mL, 15.0 mmol), *n*-BuLi (15.0 mmol, 6.00 mL of 2.50 M solution in hexanes) and dichloromethylsilane (1.09 mL, 15.0 mmol) and purified via Kugelrohr (150˚C, 20 torr) followed by sublimation (70 ˚C, 760 torr) to give a clear liquid that can be isolated in 50% yield (1.29 g, 7.5 mmol) over 2 steps from addition of the chlorosilane.

$^{1}$H NMR (600 MHz, $CDCl_3$) δ 8.04 (d, *J* = 8.2 Hz, 1H), 7.64 – 7.54 (m, 3H), 7.29 – 7.23 (m, 1H), 7.24 – 7.19 (m, 1H), 7.19 – 7.14 (m, 1H), 4.75 (q, *J* = 4.2 Hz, 2H), 0.24 (t, *J* = 4.2 Hz, 3H). $^{13}$C NMR (151 MHz, $CDCl_3$) δ 137.2, 135.3, 133.2, 132.2, 130.6, 129.0, 127.7, 126.3, 125.9, 125.4, -7.2. $^{29}$Si NMR (119 MHz, $CDCl_3$) δ –38.6.

**Methyl(*p*-tolyl)silane (2.19c)**

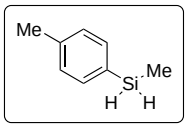

Synthesized according to the general procedure A for silane formation using 1-bromo-4-methylbenzene (1.85 mL, 15.0 mmol) and dichloromethylsilane (1.09 mL, 15.0 mmol) and purified via Kugelrohr to give a clear liquid that can be isolated in 63% yield (1.29 g, 9,48 mmol) over 2 steps from the addition of the chlorosilane.

$^{1}$H NMR (600 MHz, $C_6D_6$) δ 7.42 (d, *J* = 7.5 Hz, 2H), 7.01 (d, *J* = 7.5 Hz, 2H), 4.53 (q, *J* = 4.1 Hz, 2H), 2.09 (s, 3H), 0.22 (t, *J* = 4.1 Hz, 3H). $^{13}$C NMR (101 MHz, $CDCl_3$) δ 139.6, 135.0, 129.8, 129.0, 21.6, -7.4. $^{29}$Si NMR (119 MHz, $CDCl_3$) δ -36.1.

**Methyl(naphthalen-2-yl)silane (2.19d)**

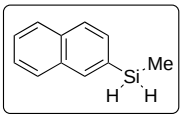

Synthesized according to the general procedure A for silane formation using 2-bromonaphthalene (3.26 g, 15.0 mmol) in THF (5 mL) and dichloromethylsilane (1.09 mL, 15.0 mmol) and purified via Kugelrohr (150 ˚C, 20 torr) followed by sublimation (70˚C, 760 torr) to give a clear liquid that can be isolated in 50% yield (1.29 g, 7.50 mmol, based on Si) over 2 steps from the addition of chlorosilane.

$^{1}$H NMR (600 MHz, $C_6D_6$) δ 7.99 (s, 1H), 7.61 (t, *J* = 7.2 Hz, 3H), 7.49 (d, *J* = 8.1 Hz, 2H), 7.30 – 7.22 (m, 2H), 4.60 (q, *J* = 4.3 Hz, 0H), 0.25 (t, *J* = 4.2 Hz, 1H).$^{13}$C NMR (101 MHz, $CDCl_3$) δ 136.0, 134.0, 133.1, 131.0, 130.9, 128.1, 127.9, 127.4, 126.7, 126.2, -7.4. $^{29}$Si NMR (119 MHz, $CDCl_3$) δ -35.4.

**Isobutyl(naphthalen-1-yl)silane (2.19e)**

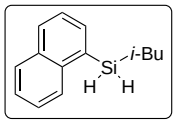

Synthesized according to Method C for silane formation using 1-bromonaphthalene (2.10 mL, 15.0 mmol), *n*-BuLi (15.0 mmol, 6.00 mL of 2.50 M solution in hexanes), and dichlorosiobutylsilane (2.28 mL, 15.0 mmol) and purified via Kugelrohr (150 ˚C, 20 torr) followed by sublimation (70˚C, 760 torr) to produce a clear liquid in 21% yield (675 mg, 3.20 mmol, based of Si) over 2 steps from addition of the chlorosilane.

$^{1}$H NMR (600 MHz, $C_6D_6$) δ 8.14 (m, 1H), 7.74 (m, 1H), 7.65 (m, 2H), 7.33 (m, 1H), 7.27 (m, 1H), 7.23 (m, 1H), 4.83 (t, *J* = 3.8 Hz, 2H), 1.76 (h, *J* = 6.7 Hz, 1H), 0.94 (dd, *J* = 7.1, 3.7 Hz, 2H), 0.91 (d, *J* = 6.6 Hz, 6H).$^{13}$C NMR (151 MHz, $CDCl_3$) δ 137.37, 135.85, 133.23, 131.87, 130.53, 129.04, 127.92, 126.31, 125.86, 125.39, 26.09, 25.62, 20.80. $^{29}$Si NMR (79 MHz, $CDCl_3$) δ -36.0.

**(4-fluorophenyl)(methyl)silane (2.19f)**

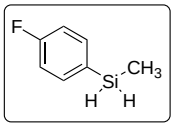

Synthesized according to the general procedure B for silane formation using 1-bromo-4-fluorobenzene (1.88 mL, 15.0 mmol), *n*-BuLi (15.0 mmol, 6.00 mL of 2.50 M solution in hexanes) and dichloromethylsilane (1.09 mL, 15.0 mmol) and purified via Kugelrohr to give a clear liquid that can be isolated in 45% yield (1.15 g, 6.75 mmol) over 2 steps from addition of the chlorosilane.

$^{1}$H NMR (600 MHz, $C_6D_6$) δ 7.19 – 7.16 (m, 1H), 6.79 (t, *J* = 8.7 Hz, 1H), 4.37 (q, *J* = 4.3 Hz, 1H), 0.10 (t, *J* = 4.3 Hz, 1H).$^{13}$C NMR (101 MHz, $CDCl_3$) δ 164.2 (d, *J* = 248.7 Hz), 137.0 (d, *J* = 7.6 Hz), 128.9 (d, *J* = 3.8 Hz), 115.4 (d, *J* = 19.9 Hz), -7.3. $^{19}$F NMR (376 MHz, $CDCl_3$) δ -111.16. $^{29}$Si NMR (119 MHz, $CDCl_3$) δ -35.8

**(4-methoxyphenyl)(methyl)silane (2.19g)**

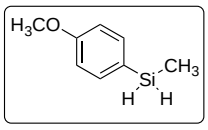

Synthesized according to the general procedure for silane formation using 4-bromoanisole (1.88 mL, 15.0 mmol) and dichloromethylsilane (1.09 mL, 15.0 mmol) and purified using flash chromatography (hexanes) to give a clear liquid that can be isolated in 81% yield (1.85 g, 12.2 mmol) over 2 steps from addition of the chlorosilane.

$^{1}$H NMR (600 MHz, $C_6D_6$) δ 7.41 (d, *J* = 8.1 Hz, 2H), 6.80 (d, *J* = 8.0 Hz, 2H), 4.55 (q, *J* = 4.0 Hz, 2H), 3.27 (s, 3H), 0.23 (t, *J* = 4.1 Hz, 3H). $^{13}$C NMR (100 MHz, $CDCl_3$) δ 161.0, 136.5, 124.2, 114.0, 55.2, -7.2. $^{29}$Si NMR (119 MHz, $CDCl_3$) δ -36.4.

**Mesityl(methyl)silane (2.19h)**

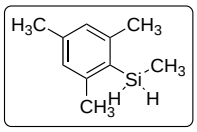

Synthesized according to the general procedure for silane formation using 2-bromomesitylene (2.30 mL, 15.0 mmol) and dichloromethylsilane (1.09 mL, 15.0 mmol) and purified using flash chromatography (hexanes) to give a clear liquid that can be isolated in 87% yield (2.14 g, 13.0 mmol) over 2 steps from addition of the chlorosilane. Spectral data matches previously reported values.[48]

$^{1}$H NMR (400 MHz, $CDCl_3$) δ 6.88 (s, 2H), 4.45 (q, *J* = 4.2 Hz, 2H), 2.47 (s, 6H), 2.30 (s, 3H), 0.36 (t, *J* = 4.2 Hz, 3H).

**Methyl(*o*-tolyl)silane (2.19i)**

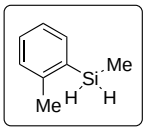

Synthesized according to the general procedure for silane formation using 2-bromotoluene (1.80 mL, 15.0 mmol) and dichloromethylsilane (1.09 mL, 15.0 mmol) and purified using flash chromatography (hexanes) to give a clear liquid that can be isolated in 72% yield (1.47g, 10.8 mmol) over 2 steps from the addition of the chlorosilane. Matches with previously reported spectra.[48]

$^{1}$H NMR (600 MHz, $CDCl_3$) δ 7.52 (d, *J* = 7.3 Hz, 1H), 7.32 (t, *J* = 7.5 Hz, 1H), 7.21 – 7.16 (m, 2H), 4.37 (q, *J* = 4.2 Hz, 2H), 2.46 (s, 3H), 0.43 (t, *J* = 4.2 Hz, 3H).

**(4-fluoronaphthalen-1-yl)(methyl)silane (2.19j)**

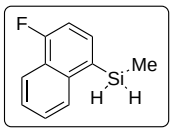


Synthesized according to the general procedure for silane formation using 4-fluoro-1-bromonaphthalene (3.38 g, 15.0 mmol in 5 mL THF) and dichloromethylsilane (1.09 mL, 15.0 mmol)) and purified via Kugelrohr (150 ˚C, 50 torr for 30 min then 105 ˚C, 10 torr) to give a clear liquid that can be isolated in 21% yield (597.0 mg, 3.1 mmol, based off Si) over 2 steps from addition of the chlorosilane.

$^{1}$H NMR (600 MHz, $CDCl_3$) δ 8.18 (d, *J* = 8.0 Hz, 1H), 8.05 (d, *J* = 8.0 Hz, 1H), 7.72 (t, *J* = 6.7 Hz, 1H), 7.60 (dt, *J* = 16.1, 7.0 Hz, 2H), 7.18 – 7.12 (m, 1H), 4.65 (q, *J* = 4.2, 3.7 Hz, 2H), 0.54 (t, *J* = 3.9 Hz, 3H). $^{13}$C NMR (150MHz, $CDCl_3$ δ 160.78 (d, $J_{CF}$ = 255.0 Hz), 138.82 (d, $J_{CCCF}$= 4.4 Hz), 135.28 (d, $J_{CCF}$= 8.3 Hz), 127.80 (d, $J_{CCCF}$= 4.8 Hz), 127.57 (d, *J* = 3.1 Hz), 127.32, 126.21 (d, $J_{CCCCF}$ = 1.7 Hz), 121.40 (d, $J_{CCCF}$ = 6.1 Hz), 109.17 (d, $J_{CCF}$ = 18.6 Hz), -7.19. $^{19}$F NMR (376 MHz, $CDCl_3$) δ -120.24. $^{29}$Si NMR (119 MHz, $CDCl_3$) δ -35.8

**Neopentyl(phenyl)silane (2.19k)**

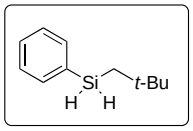


Synthesized using method H. Isolated as a clear liquid in 25 % yield (231 mg, 1.30 mmol).

$^{1}$H NMR (600 MHz, $CDCl_3$) δ 7.57 (d, *J* = 6.4 Hz, 1H), 7.36 (hept, *J* = 6.7, 6.2 Hz, 2H), 4.34 (t, *J* = 4.2 Hz, 2H), 1.08 (t, *J* = 4.2 Hz, 2H), 1.04 (s, 9H). $^{13}$C NMR (151 MHz, $CDCl_3$) δ 135.35, 133.53, 129.51, 128.08, 33.07, 32.31, 27.09. $^{29}$Si NMR (79 MHz, $CDCl_3$) δ -37.8.

**Cyclohexylphenylsilane (2.19l)**

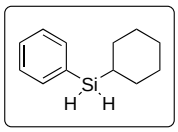


Made using previously reported procedures.[8] Spectra matches with previous report.

$^{1}$H NMR (600 MHz, $CDCl_3$) δ 7.55 (dt, *J* = 6.5, 1.5 Hz, 2H), 7.41 – 7.37 (m, 1H), 7.37 – 7.33 (m, 2H), 4.16 (d, *J* = 3.0 Hz, 2H), 1.83 – 1.58 (m, 7H), 1.22 – 0.91 (m, 4H).

**1,1,1-Triethyl-3-phenyldisiloxane (2.19m)**

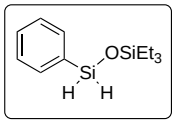


Made using previously reported procedure.[24] Spectra matches with previous report.

$^{1}$H NMR (400 MHz, $CDCl_3$) δ 7.69 – 7.60 (m, 2H), 7.52 – 7.35 (m, 3H), 5.14 (s, 1H), 0.96 (t, *J* = 8.0 Hz, 9H), 0.60 (q, *J* = 8.0 Hz, 6H).

**Diazo compounds**

**Diphenyldiazomethane (2.20a)**

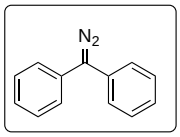

Synthesized using previously reported procedures. Spectrum matches previous report.[44]

$^1$H NMR (600 MHz, $CDCl_3$) δ 7.39 (t, *J* = 7.7 Hz, 3H), 7.30 (d, *J* = 8.4 Hz, 2H), 7.19 (t, *J* = 7.4 Hz, 1H).

**4,4'-(diazomethylene)bis(chlorobenzene) (2.20b)**

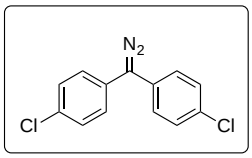

Made using previously published procedures. Spectrum matches previous report.[44]

$^1$H NMR (400 MHz, $CDCl_3$) δ 7.36 (d, *J* = 8.8 Hz, 4H), 7.18 (d, *J* = 8.7 Hz, 4H).

**4,4'-(diazomethylene)bis(methoxybenzene)** (**2.20c)**

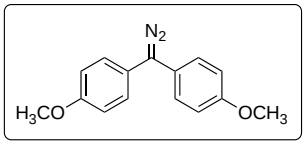

Made using previously published procedures. Spectrum matches previous report.[44]

$^1$H NMR (600 MHz, $CDCl_3$) δ 7.18 (d, *J* = 8.8 Hz, 4H), 6.94 (d, *J* = 8.8 Hz, 4H), 3.82 (s, 3H).

**Phenyl(*o*-tolyl)diazomethane (2.20d)**

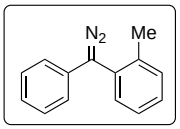

Synthesized using procedure A using 2-methylbenzophenone (0.36 mL, 2.0 mmol), hydrazine (20 mmol, 0.62 mL), acetic acid (0.14 mL, 2.4 mmol) in EtOH (10 mL). The hydrazone was isolated without purification, dissolved in $CH_2Cl_2$ (15 mL) and oxidized with $MnO_2$ (1.39 g, 16.0 mmol) to give a purple liquid that can be isolated in 60% yield (243.0 mg, 1.20 mmol) over 2 steps.

$^1$H NMR (400 MHz, $CDCl_3$δ 7.43 (d, *J* = 7.1 Hz, 1H), 7.31 (m, 5H), 7.07 (t, *J* = 7.3 Hz, 2H), 6.97 (d, *J* = 7.9 Hz, 1H), 2.28 (s, 3H). $^{13}$C NMR (151 MHz, $CDCl_3$) δ 138.5, 131.5, 131.25, 131.0, 129.1, 128.7, 127.2, 126.7, 124.1, 122.6, 20.6. APCI *m/z* calc for $C_{14}H_{12}N_2$ [M + H – $N_2$]

**Phenyl(*o*-methoxyphenyl)diazomethane (2.20e)**

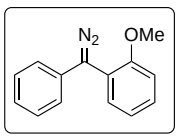

Synthesized using procedure A using 2-methoxybenzphenone (457 mg, 2.20 mmol), hydrazine (24 mmol, 0.68 mL), acetic acid (0.15 mL, 2.6 mmol) in EtOH (11 mL). The hydrazone was isolated without purification, dissolved in $CH_2Cl_2$

(15 mL) and oxidized with $MnO_2$ (1.53 g, 17.6 mmol) to give a purple oil that can be isolated in 68% yield (761.9 mg) over 2 steps.

$^1$H NMR (600 MHz, $CDCl_3$) δ 7.37 (d, *J* = 7.6 Hz, 1H), 7.31 (q, *J* = 6.9 Hz, 3H), 7.08 (m, 3H), 7.04 – 6.96 (m, 2H), 3.86 (s, 3H). $^{13}$C NMR (101 MHz, $CDCl_3$) δ 157.0, 131.6, 130.1, 129.0, 124.2, 123.2, 121.2, 117.2, 111.7, 55.7. APCI *m/z* calc for $C_{15}H_{15}N_2O$ $[M + H - N_2]^+$ . 197.1. Found 196.5.

**Phenyl(*o*-trifluoromethylphenyl)diazomethane (2.20f)**

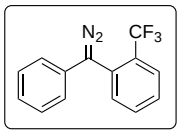


Synthesized using method B to give a red liquid that can be isolated in 44% yield (461.5 mg, 1.76 mmol) over 2 steps.

$^1$H NMR (400 MHz, $CDCl_3$) δ 7.83 (d, *J* = 7.9 Hz, 1H), 7.59 (ddt, *J* = 23.5, 15.2, 7.6 Hz, 3H), 7.31 (t, *J* = 7.7 Hz, 2H), 7.08 (t, *J* = 7.4 Hz, 1H), 6.86 (d, *J* = 7.9 Hz, 2H). $^{13}$C NMR (101 MHz, $CDCl_3$) δ 134.3, 132.6, 131.1 (q, $J_{CCF}$ = 30 Hz), 131.6, 129.2, 129.1 127.4 (q, $J_{CCCF}$ = 5.4 Hz), 127.0, 124.3, 124.0 (q, $J_{CF}$ = 275 Hz) 122.5.$^{19}$F NMR (376 MHz, $CDCl_3$) δ -61.93. APCI *m/z* calc for $C_{15}H_9F_3N_2$ $[M + H - N_2]^+$. 235.1. Found 234.4.

**Phenyl(1-naphthyl)diazomethane (2.20g)**

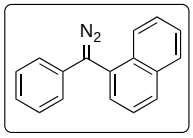


Synthesized according to procedure A for diazo compound formation using 1-naphthylphenylketone (1.34 g, 5.70 mmol), hydrazine (57 mmol, 0.88 mL), acetic acid (0.39 mL, 6.8 mmol) in EtOH (10 mL). The hydrazone was isolated without purification, dissolved in $CH_2Cl_2$ (15 mL) and oxidized with $MnO_2$ (3.96 g, 45.6 mmol) to give a purple solid that can be isolated in 68% yield (829 mg, 3.90 mmol) over 2 steps.

$^1$H NMR (600 MHz, $CDCl_3$) δ 7.97 – 7.90 (m, 2H), 7.88 (d, *J* = 8.2 Hz, 1H), 7.69 (d, *J* = 6.7 Hz, 1H), 7.56 (dt, *J* = 21.5, 7.3 Hz, 2H), 7.49 (t, *J* = 7.4 Hz, 1H), 7.31 (t, *J* = 7.1 Hz, 2H), 7.08 (t, *J* = 7.1 Hz, 1H), 6.97 (d, *J* = 7.5 Hz, 2H). $^{13}$C NMR (151 MHz, $CDCl_3$) δ 134.5, 132.2, 131.9, 129.5, 129.3, 129.1, 128.9, 126.8, 126.5, 126.0, 125.6, 125.44, 124.2, 122.7. APCI *m/z* calc for $C_{17}H_{12}N_2$ $[M + H - N_2]^+$ . 217.1. Found 216.5.

**1-chloro-2-(diazo(4-methoxyphenyl)methyl)benzene (2.20h)**

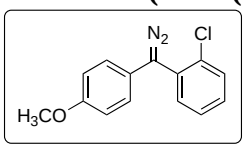


Synthesized according to previous procedures and isolated as a red oil.[31] Spectrum matches previous report. [31]

$^1$H NMR (600 MHz, $CDCl_3$) δ 7.48 (d, *J* = 7.8 Hz, 1H), 7.42 (d, *J* = 5.9 Hz, 1H), 7.30 (d, *J* = 7.5 Hz, 1H), 7.27 (m, *J* 2H), 6.96 (d, *J* = 7.0 Hz, 2H), 6.91 (d, *J* = 9.0 Hz, 3H), 3.80 (s, 1H).

## Insertion Products:

### (*S*)-benzhydryl(methyl)(phenyl)silane (2.21a)

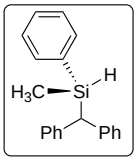


Synthesized using method F with diazo compound **2.20a** (1.000 mmol, 181.0 mg), silane **2.1e** (610 mg, 5.00 mmol) in PhMe (20 mL total) to give a white solid in 78% yield (225 mg, 0.780 mmol). Enantiomeric ratio was determined by HLPC after hydrolysis with a Daicel CHIRALPAK ® OD-H column (2% IPA/ hexanes), 1.0 mL/min. $t_R$ (**2.21aa**) = 11.3 min, $t_R$ (**2.21ab**) = 12.9 min, 82:18 er (Si-OH product). Absolute configuration was assigned to be (*S)* based on analogy to **2.26c.**

$^1$H NMR (400 MHz, $CDCl_3$) δ 7.32 (m, 2H), 7.28 – 7.21 (m, 7H), 7.18 (m, 4H), 7.12 (m, 2H), 4.84 – 4.59 (m, 1H), 3.81 (d, *J* = 3.7 Hz, 1H), 0.30 (d, *J* = 3.5 Hz, 3H). $^{13}$C NMR (101 MHz, $CDCl_3$) δ 142.3, 142.1, 135.0, 134.8, 129.6, 129.1, 129.0, 128.6, 128.5, 127.8, 125.6, 125.6, 43.3, -5.9. $^{29}$Si NMR (79 MHz, $CDCl_3$) δ -11.1. MALDI *m/z* calc for $C_{20}H_{20}Si$ $[M + H]^+$ . 289.141. Found 289.153.

Racemic Standard for **2.21a**:

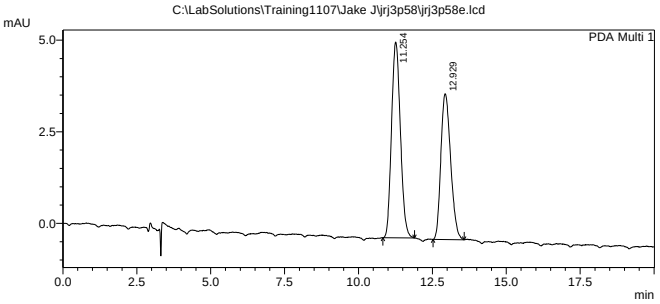


**< Peak Table >**

PeakTable C:\LabSolutions\Training1107\Jake J\jrj3p58\jrj3p58e.lcd

PDA Ch1 320nm 4nm

| Peak# | Ret. Time | Area | Height | Area % | Height % |
|---|---|---|---|---|---|
| 1 | 11.254 | 111525 | 5344 | 54.926 | 57.328 |
| 2 | 12.929 | 91520 | 3978 | 45.074 | 42.672 |
| Total | | 203045 | 9322 | 100.000 | 100.000 |

Enantiomerically enriched (*S*) **2.21a** using *S*-TCPTTL:

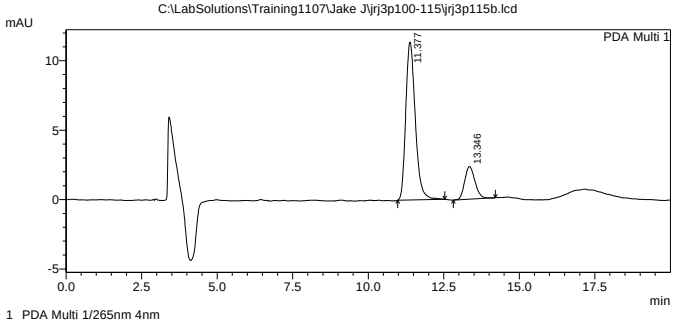


**< Peak Table >**

PeakTable C:\LabSolutions\Training1107\Jake J\jrj3p100-115\jrj3p115b.lcd

PDA Ch1 265nm 4nm

| Peak# | Ret. Time | Area | Height | Area % | Height % |
|---|---|---|---|---|---|
| 1 | 11.377 | 249390 | 11382 | 81.855 | 82.869 |
| 2 | 13.346 | 55284 | 2353 | 18.145 | 17.131 |
| Total | | 304673 | 13735 | 100.000 | 100.000 |

**(*S*)-(bis(4-methoxyphenyl)methyl)(methyl)(phenyl)silane (2.21b)**

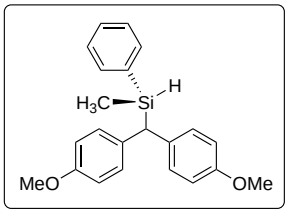


Synthesized using method F with diazo compound **2.20c** (0.20 mmol, 42 mg) and silane **2.1e** (122 mg, 1.00 mmol) to give a white solid in 45% yield (31.3 mg, 0.0900 mmol). Enantiomeric ratio was determined by HLPC after hydrolysis with a Daicel CHIRALPAK ® AS column (2% IPA/ hexanes), 1.0 mL/min. $t_R$ (**2.21ba**) = 13.7 min, $t_R$ (**2.21bb**) = 16.2 min, 81:19 er (Si-OH product). Absolute configuration was assigned to be (*S)* based on analogy to **2.26c**.

$^1$H NMR (600 MHz, $C_6D_6$) δ 7.41 – 7.36 (m, 2H), 7.17 (m, 2H), 7.15 – 7.09 (m, 5H), 6.78 (d, *J* = 8.6 Hz, 2H), 6.73 (d, *J* = 8.7 Hz, 2H), 4.96 (p, *J* = 3.6 Hz, 1H), 3.72 (d, *J* = 3.9 Hz, 1H), 3.31 (s, 3H), 3.27 (s, 3H), 0.29 (d, *J* = 3.7 Hz, 3H). $^{13}$C NMR (101 MHz, $CDCl_3$) δ 157.6, 157.5, 135.1, 135.0, 134.8, 134.7, 129.9, 129.8, 129.56, 127.8, 114.0, 113.9, 55.4, 55.3, 40.9, -5.8. Did not ionize using ESI, MALDI or APCI.

Racemic Standard for **2.21b**:

**<Chromatogram>**

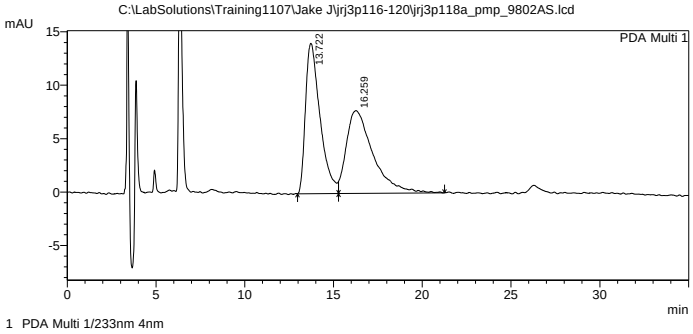


1 PDA Multi 1/233nm 4nm

**< Peak Table >**

PeakTable C:\LabSolutions\Training1107\Jake J\jrj3p116-120\jrj3p118a_pmp_9802AS.lcd

PDA Ch1 233nm 4nm

| Peak# | Ret. Time | Area | Height | Area % | Height % |
|---|---|---|---|---|---|
| 1 | 13.722 | 805317 | 14077 | 49.974 | 64.499 |
| 2 | 16.259 | 806151 | 7748 | 50.026 | 35.501 |
| Total | | 1611469 | 21826 | 100.000 | 100.000 |

Enantiomerically enriched (*S*) **2.21b** using *S*-TCPTTL:

**<Chromatogram>**

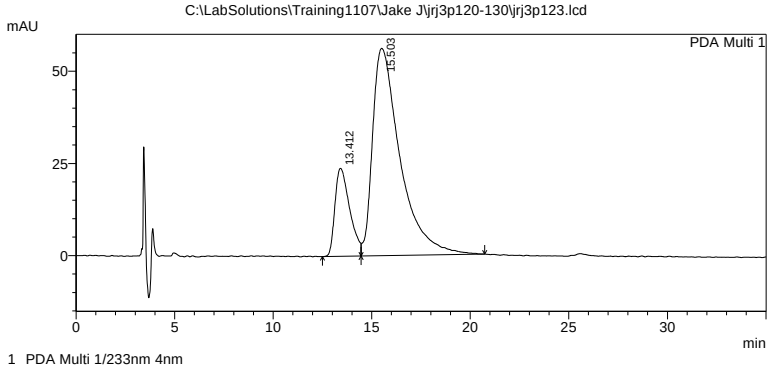


**< Peak Table >**

PeakTable C:\LabSolutions\Training1107\Jake J\jrj3p120-130\jrj3p123.lcd

PDA Ch1 233nm 4nm

| Peak# | Ret. Time | Area | Height | Area % | Height % |
|---|---|---|---|---|---|
| 1 | 13.412 | 1249142 | 23869 | 18.595 | 29.783 |
| 2 | 15.503 | 5468390 | 56276 | 81.405 | 70.217 |
| Total | | 6717532 | 80145 | 100.000 | 100.000 |

**(*S*)-(bis(4-chlorophenyl)methyl)(methyl)(phenyl)silane (2.21c)**

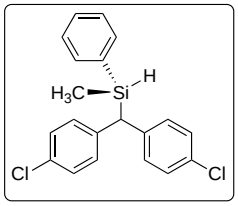


Synthesized using method F with diazo compound **2.20b** (0.200 mmol, 52.6 mg) and silane **2.1e** (122 mg, 1.00 mmol) to give a white solid in 91% yield (65.7 mg, 0.158 mmol). Enantiomeric ratio was determined by HLPC after hydrolysis with a Daicel CHIRALPAK ® OD-H column (2% IPA/ hexanes), 1.0 mL/min. $t_R$ (**2.21ca**) = 16.4 min, $t_R$ (**2.21cb**) = 18.0 min, 74:26 er (Si-OH product). Absolute configuration was assigned to be (*S, S)* based on analogy to **2.26c**.

$^1$H NMR (600 MHz, $CDCl_3$) δ 7.40 – 7.33 (m, 1H), 7.30 – 7.25 (m, 4H), 7.24 (d, *J* = 7.3 Hz, 2H), 7.18 (d, *J* = 7.3 Hz, 2H), 7.12 (d, *J* = 7.5 Hz, 2H), 7.05 (d, *J* = 7.5 Hz, 2H), 4.67 (p, *J* = 4.5, 4.1 Hz, 1H), 3.75 (d, *J* = 3.7 Hz, 1H), 0.30 (d, *J* = 2.8 Hz, 3H). $^{13}$C NMR (101 MHz, $CDCl_3$) δ 140.3, 140.0, 134.8, 133.7, 131.5, 131.4, 130.1, 130.0, 129.9, 128.7, 128.6, 127.9, 41.9, -6.2. $^{29}$Si NMR (79 MHz, $CDCl_3$) δ -10.8. MALDI *m/z* calc for $C_{20}H_{18}Cl_2Si$ $[M + Na]^+$ 379.045. Found 379.220.

Racemic Standard for **2.21c**:

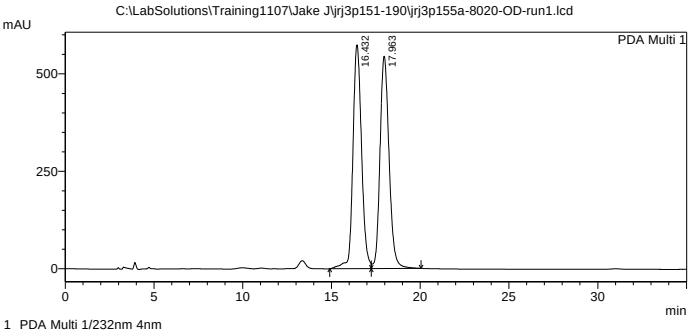


1 PDA Multi 1/232nm 4nm

**< Peak Table >**

PeakTable C:\LabSolutions\Training1107\Jake J\jrj3p151-190\jrj3p155a-8020-OD-run1.lcd

PDA Ch1 232nm 4nm

| Peak# | Ret. Time | Area | Height | Area % | Height % |
|---|---|---|---|---|---|
| 1 | 16.432 | 19469494 | 574519 | 50.125 | 51.331 |
| 2 | 17.963 | 19372708 | 544721 | 49.875 | 48.669 |
| Total | | 38842201 | 1119240 | 100.000 | 100.000 |

Enantiomerically enriched (*S*) **2.21c** using *S*-TCPTTL:

**<Chromatogram>**

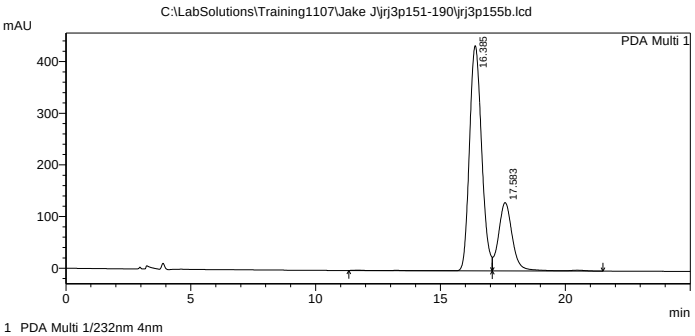


1 PDA Multi 1/232nm 4nm

**< Peak Table >**

PeakTable C:\LabSolutions\Training1107\Jake J\jrj3p151-190\jrj3p155b.lcd

PDA Ch1 232nm 4nm

| Peak# | Ret. Time | Area | Height | Area % | Height % |
|---|---|---|---|---|---|
| 1 | 16.385 | 14732848 | 435744 | 74.301 | 76.728 |
| 2 | 17.583 | 5095809 | 132161 | 25.699 | 23.272 |
| Total | | 19828657 | 567905 | 100.000 | 100.000 |

## (*S*)-benzhydryl(4-methoxyphenyl)(methyl)silane (2.21d)

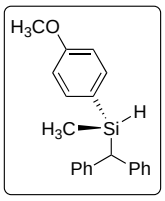


Synthesized using method F with diazo compound **2.20a** (0.200 mmol, 42.0 mg) and silane **2.19g** (152 mg, 1.00 mol) to give a white solid in 72% yield (45.9 mg, 0.144 mmol). Enantiomeric ratio was determined by HLPC after hydrolysis with a Daicel CHIRALPAK ® OD-H column (1% IPA/ hexanes), 1.0 mL/min. $t_R$ (**2.21da**) = 17.2, $t_R$ (**2.21db**) = 18.7, 50:50 er (Si-OH product). Absolute configuration was assigned to be (*S, S)* based on analogy to **2.26c**.

$^1$H NMR (600 MHz, $CDCl_3$) δ 7.31 – 7.08 (m, 13H), 6.81 (d, *J* = 8.5 Hz, 2H), 4.70 (p, *J* = 3.7 Hz, 1H), 3.79 (d, *J* = 1.6 Hz, 4H), 0.28 (d, *J* = 3.6 Hz, 3H).$^{13}$C NMR (151 MHz, $CDCl_3$) δ 160.7, 142.3, 142.0, 141.4, 136.8, 136.3, 129.0, 128.8, 125.4, 125.3, 113.5, 113.1, 55.7, 43.4, -7.3. $^{29}$Si NMR (79 MHz, $CDCl_3$) δ -11.6. MALDI *m/z* calc for $C_{21}H_{22}OSi$ $[M + H]^+$ 319.151. Found 319.245.

Racemic Standard for **2.21d**:

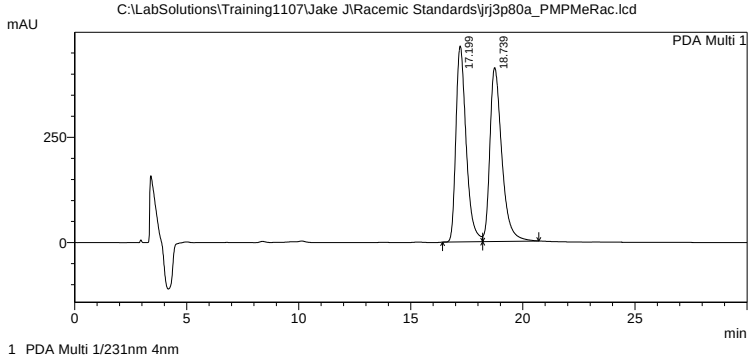


1 PDA Multi 1/231nm 4nm

**< Peak Table >**

PeakTable C:\LabSolutions\Training1107\Jake J\Racemic Standards\jrj3p80a_PMPMeRac.lcd

PDA Ch1 231nm 4nm

| Peak# | Ret. Time | Area | Height | Area % | Height % |
|---|---|---|---|---|---|
| 1 | 17.199 | 14775321 | 465125 | 49.202 | 52.976 |
| 2 | 18.739 | 15254421 | 412863 | 50.798 | 47.024 |
| Total | | 30029742 | 877988 | 100.000 | 100.000 |

HPLC trace of **2.21d** using *S*-TCPTTL:

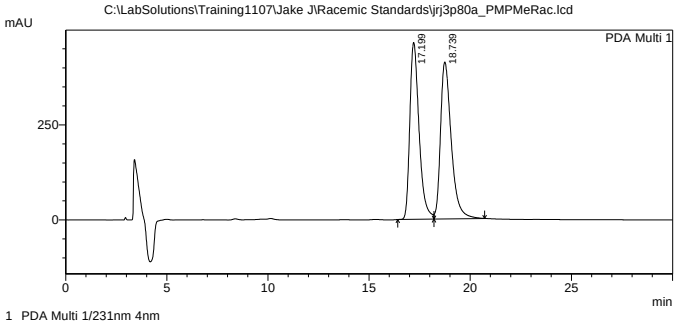


1 PDA Multi 1/231nm 4nm

**< Peak Table >**

PeakTable C:\LabSolutions\Training1107\Jake J\Racemic Standards\jrj3p80a_PMPMeRac.lcd

PDA Ch1 231nm 4nm

| Peak# | Ret. Time | Area | Height | Area % | Height % |
|---|---|---|---|---|---|
| 1 | 17.199 | 14775321 | 465125 | 49.202 | 52.976 |
| 2 | 18.739 | 15254421 | 412863 | 50.798 | 47.024 |
| Total | | 30029742 | 877988 | 100.000 | 100.000 |

## (*S*)-benzhydryl(4-methylphenyl)(methyl)silane (2.21e)

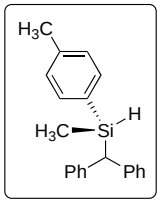


Synthesized using method F with diazo compound **2.20a** (38.8 mg, 0.200 mmol) and silane **2.19c** (136 mg, 1.00 mmol) to give a white solid in 76% yield (46.0 mg, 0.152 mmol). Enantiomeric ratio was determined by HLPC after hydrolysis with a Daicel CHIRALPAK ® AD-H column (2% IPA/ hexanes), 1.0 mL/min. $t_R$ (**2.21ea**) = 9.9 min, $t_R$ (**2.21eb**) = 10.7 min, 74:26 er (Si-OH product). Absolute configuration was assigned to be (*S)* based on analogy to **2.26c**.

$^1$H NMR (600 MHz, $CDCl_3$) δ 7.31 – 7.24 (m, 5H), 7.22 (dd, *J* = 8.8, 2.4 Hz, 5H), 7.20 – 7.12 (m, 2H), 7.11 (d, *J* = 7.5 Hz, 2H), 4.73 (p, *J* = 3.8 Hz, 1H), 3.83 (d, *J* = 3.9 Hz, 1H), 2.34 (s, 3H), 0.31 (d, *J* = 3.7 Hz, 3H).$^{13}$C NMR (151 MHz, $CDCl_3$) δ 142.4, 142.2, 139.5, 135.1, 131.0, 129.1, 129.0, 128.7, 128.6, 128.5, 125.5, 44.2, 22.1, -5.8. $^{29}$Si NMR (79 MHz, $CDCl_3$) δ -11.3. MALDI *m/z* calc for $C_{21}H_{22}Si$ $[M + H]^+$ 328.138. Found 325.207.

Racemic Standard for **2.21e**:

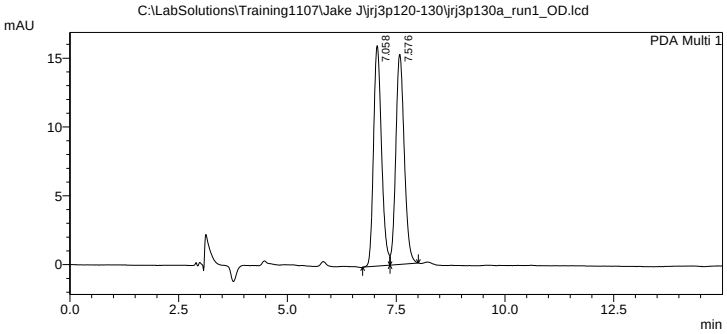


1 PDA Multi 1/254nm 4nm

**< Peak Table >**

PeakTable C:\LabSolutions\Training1107\Jake J\jrj3p120-130\jrj3p130a_run1_OD.lcd

PDA Ch1 254nm 4nm

| Peak# | Ret. Time | Area | Height | Area % | Height % |
|---|---|---|---|---|---|
| 1 | 7.058 | 205950 | 16014 | 49.944 | 51.207 |
| 2 | 7.576 | 206416 | 15259 | 50.056 | 48.793 |
| Total | | 412367 | 31273 | 100.000 | 100.000 |

Enantiomerically enriched (*S*) **2.21e** using *S*-TCPTTL:

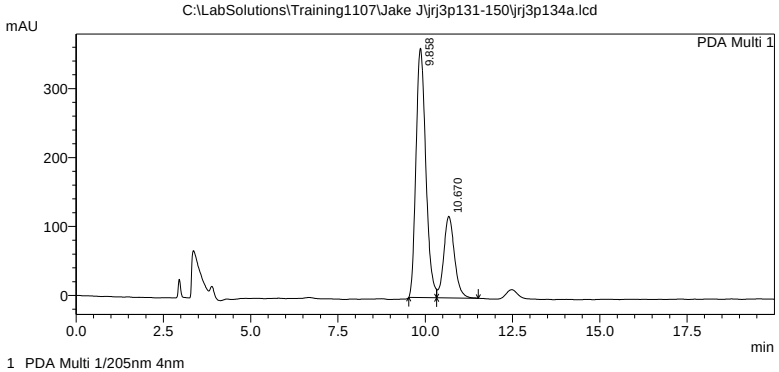


1 PDA Multi 1/205nm 4nm

**< Peak Table >**

PeakTable C:\LabSolutions\Training1107\Jake J\jrj3p131-150\jrj3p134a.lcd

PDA Ch1 205nm 4nm

| Peak# | Ret. Time | Area | Height | Area % | Height % |
|---|---|---|---|---|---|
| 1 | 9.858 | 7044481 | 361590 | 73.577 | 75.312 |
| 2 | 10.670 | 2529844 | 118530 | 26.423 | 24.688 |
| Total | | 9574324 | 480120 | 100.000 | 100.000 |

## (*S*)-benzhydryl(4-fluorophenyl)(methyl)silane (2.21f)

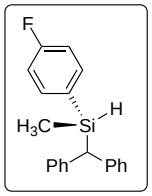


Synthesized using method F with diazo compound **2.20a** (38.8 mg, 0.200 mmol) and silane **2.19f** (140 mg, 1.00 mmol) to give a white solid in 66% yield (40.4 mg, 0.132 mmol). Enantiomeric ratio was determined by HLPC after hydrolysis with a Daicel CHIRALPAK ® AD-H column (2% IPA/ hexanes), 1.0 mL/min. $t_R$ (**2.21fa**) = 10.2 min, $t_R$ (**2.21fb**) = 12.9 min, 80:20 er (Si-OH product). Absolute configuration was assigned to be (*S)* based on analogy to **2.26c**.

$^1$H NMR (400 MHz, $CDCl_3$) δ 7.31 (dd, $J$ = 9.4, 5.8 Hz, 3H), 7.28 – 7.23 (m, 5H), 7.23 – 7.13 (m, 4H), 6.99 (t, $J$ = 8.7 Hz, 2H), 4.76 (p, $J$ = 3.9 Hz, 1H), 3.82 (d, $J$ = 3.9 Hz, 1H), 0.35 (d, $J$ = 3.6 Hz, 3H). $^{13}$C NMR (101 MHz, $CDCl_3$) δ 164.0 (d, $J_{CF}$ = 249.0 Hz), 141.9, 141.75, 136.8 (d, $J_{CCCF}$ = 7.4 Hz), 130.1 (d, $J_{CCCCF}$ = 3.9 Hz), 128.9, 128.8, 128.6, 128.4, 125.6, 125.6, 115.0 (d, $J_{CCF}$ = 19.8 Hz), 43.2, -5.9. $^{19}$F NMR (376 MHz, $CDCl_3$) δ -110.96. $^{29}$Si NMR (79 MHz, $CDCl_3$) δ -11.1. MALDI *m/z* calc for $C_{20}H_{19}FSi$ $[M + Na]^+$ 329.113. Found 329.158.

Racemic Standard for **2.21f**:

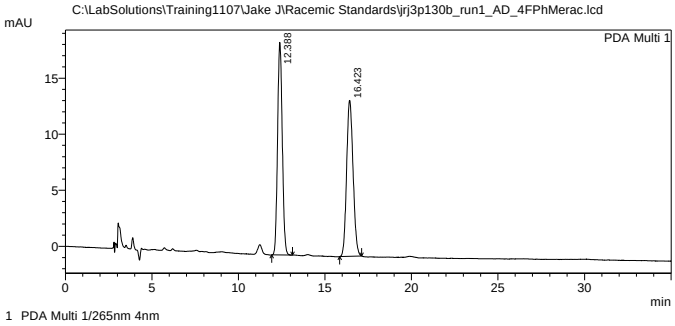


PeakTable C:\LabSolutions\Training1107\Jake J\Racemic Standards\jrj3p130b_run1_AD_4FPhMerac.lcd
PDA Ch1 265nm 4nm

| Peak# | Ret. Time | Area | Height | Area % | Height % |
|---|---|---|---|---|---|
| 1 | 12.388 | 358819 | 18961 | 49.906 | 57.700 |
| 2 | 16.423 | 360171 | 13901 | 50.094 | 42.300 |
| Total | | 718991 | 32862 | 100.000 | 100.000 |

Enantiomerically enriched (*S*) **2.21f** using *S*-TCPTTL:

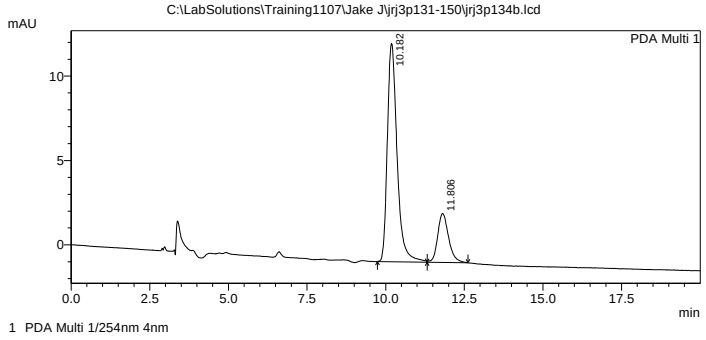


PeakTable C:\LabSolutions\Training1107\Jake J\jrj3p131-150\jrj3p134b.lcd
PDA Ch1 254nm 4nm

| Peak# | Ret. Time | Area | Height | Area % | Height % |
|---|---|---|---|---|---|
| 1 | 10.182 | 278783 | 12928 | 79.816 | 81.628 |
| 2 | 11.806 | 70500 | 2910 | 20.184 | 18.372 |
| Total | | 349283 | 15838 | 100.000 | 100.000 |

**(*S*)-benzhydryl(methyl)(naphthalen-2-yl)silane (2.21g)**

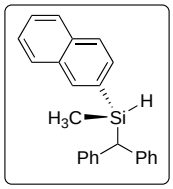


Synthesized according to the general procedure for enantioselective donor/donor insertion using **2.20a** (38.8 mg, 0.200 mmol) and silane **2.19d** (172 mg, 1.00 mmol) to give a white solid in 69% yield (0.158 mmol, 46.7 mg). Enantiomeric ratio was determined by HLPC after hydrolysis with a Daicel CHIRALPAK ® AD-H column (1% IPA/ hexanes), 1.0 mL/min. $t_R$ (**2.21ga**) = 19.5 min, $t_R$ (**2.21gb**) = 24.2 min, 82:18 er (Si-OH product). Absolute configuration was assigned to be (*S)* based on analogy to **2.26c**.

$^1$H NMR (600 MHz, $C_6D_6$)δ 7.86 (s, 1H), 7.61 – 7.49 (m, 3H), 7.33 (d, *J* = 8.1 Hz, 1H), 7.28 – 7.18 (m, 6H), 7.13 (t, *J* = 7.6 Hz, 2H), 7.04 (dt, *J* = 13.7, 7.4 Hz, 3H), 6.97 (t, *J* = 7.3 Hz, 1H), 5.04 (p, *J* = 3.6 Hz, 1H), 3.83 (d, *J* = 3.8 Hz, 1H), 0.32 (d, *J* = 3.6 Hz, 3H). $^{13}$C NMR (151 MHz, $CDCl_3$) δ 142.2, 142.0, 136.1, 134.0, 132.9, 132.3, 130.9, 129.1, 129.0, 128.66, 128.5, 128.2, 127.8, 127.0,

126.7, 126.0, 125.7, 125.6, 43.3, -5.7. $^{29}$Si NMR (119 MHz, $C_6D_6$) δ -10.9 MALDI *m/z* calc for $C_{24}H_{22}Si$ $[M + Na]^+$ 361.1383. Found 363.1318.

Racemic Standard for **2.21g**:

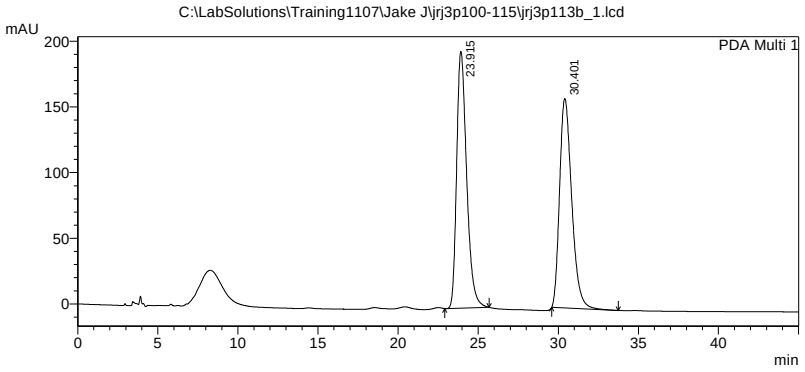


Enantiomerically enriched (*S*) **2.21g** using *S*-TCPTTL:

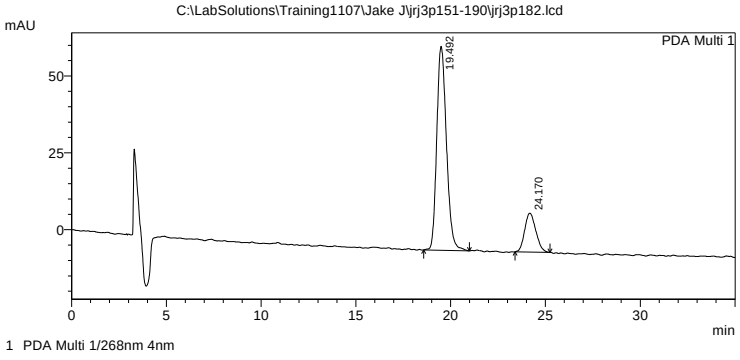


**< Peak Table >**

PeakTable C:\LabSolutions\Training1107\Jake J\jrj3p151-190\jrj3p182.lcd

PDA Ch1 268nm 4nm

| Peak# | Ret. Time | Area | Height | Area % | Height % |
|---|---|---|---|---|---|
| 1 | 19.492 | 2360689 | 66341 | 82.092 | 83.988 |
| 2 | 24.170 | 514989 | 12648 | 17.908 | 16.012 |
| Total | | 2875678 | 78989 | 100.000 | 100.000 |

**(*S*)-benzhydryl(methyl)(naphthalen-1-yl)silane (2.21h)**

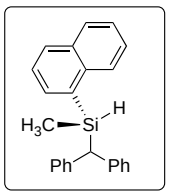


Synthesized using method F with diazo compound **2.20a** (38.8 mg, 0.200 mmol) and silane **2.19b** (172 mg, 1.00 mmol) to give a white solid in 60% yield (40.6 mg, 0.120 mmol). Enantiomeric ratio was determined by HLPC after hydrolysis with a Daicel CHIRALPAK ® AD-H column (1% IPA/ hexanes), 1.0 mL/min. $t_R$ (**2.21ha**) = 10.1 min, $t_R$ (**2.21hb**) = 11.2 min, 77:23 er (Si-OH product). Absolute configuration was assigned to be (*S, S)* based on analogy to **2.26c.**

$^1$H NMR (600 MHz, $C_6D_6$) δ 8.08 – 8.01 (m, 1H), 7.63 – 7.58 (m, 2H), 7.54 – 7.49 (m, 1H), 7.25 (m, 2H), 7.19 (d, *J* = 7.5 Hz, 4H), 7.14 (s, 1H), 7.09 (t, *J* = 7.6 Hz, 2H), 7.03 – 6.96 (m, 3H), 6.91 (t, *J* = 7.3 Hz, 1H), 5.33 (p, *J* = 3.6 Hz, 1H), 4.05 (d, *J* = 4.0 Hz, 1H), 0.36 (d, *J* = 3.7 Hz, 3H).$^{13}$C NMR (151 MHz, $CDCl_3$) δ 142.3, 142.2, 137.1, 135.2, 133.3, 133.3, 130.4, 129.0, 129.0, 128.6,

128.4, 127.8, 126.0, 125.6, 125.5, 125.1, 43.1, -5.0. $^{29}$Si NMR (79 MHz, $CDCl_3$) δ -15.6. MALDI *m/z* calc for $C_{24}H_{22}Si$ $[M + Na]^+$ 361.1383. Found 361.1446.

Racemic Standard for **2.21h**:

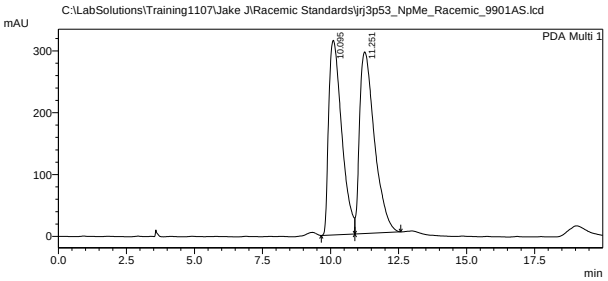


1 PDA Multi 1/284nm 4nm

**< Peak Table >**

PeakTable C:\LabSolutions\Training1107\Jake J\Racemic Standards\jrj3p53_NpMe_Racemic_9901AS.lcd

PDA Ch1 284nm 4nm

| Peak# | Ret. Time | Area | Height | Area % | Height % |
|---|---|---|---|---|---|
| 1 | 10.095 | 10468276 | 314759 | 48.236 | 51.733 |
| 2 | 11.251 | 11233883 | 293668 | 51.764 | 48.267 |
| Total | | 21702159 | 608427 | 100.000 | 100.000 |

Enantiomerically enriched (*S*) **2.21hh** using *S*-TCPTTL:

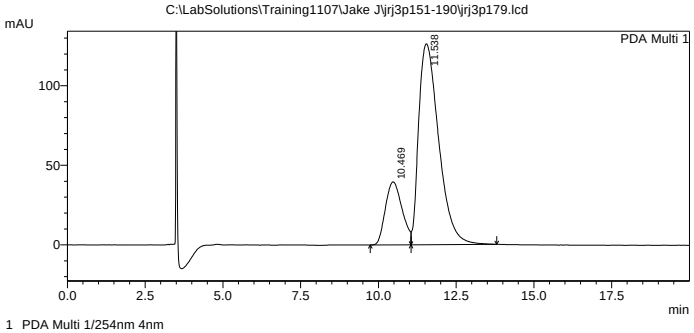


1 PDA Multi 1/254nm 4nm

**< Peak Table >**

PeakTable C:\LabSolutions\Training1107\Jake J\jrj3p151-190\jrj3p179.lcd

PDA Ch1 254nm 4nm

| Peak# | Ret. Time | Area | Height | Area % | Height % |
|---|---|---|---|---|---|
| 1 | 10.469 | 1482658 | 39621 | 20.760 | 23.884 |
| 2 | 11.538 | 5659377 | 126271 | 79.240 | 76.116 |
| Total | | 7142035 | 165892 | 100.000 | 100.000 |

**(*S*)-benzhydryl(2-methylphenyl)(methyl)silane (2.21i)**

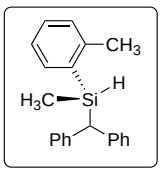


Synthesized using method F with diazo compound **2.20a** (38.8 mg, 0.200 mmol) and silane **2.19l** (136 mg, 1.00 mmol) to give a white solid in 55% yield (33.2 mg, 0.110 mmol). Enantiomeric ratio was determined by HLPC after hydrolysis with a Daicel CHIRALPAK ® OD-H column (1% IPA/ hexanes), 1.0 mL/min. $t_R$ (**2.21ia**) = 10.9 min, $t_R$ (**2.21ib**) = 12.6 min, 69:31 er (Si-OH product). Absolute configuration was assigned to be (*S, S)* based on analogy to **2.26c.**

$^1$H NMR (600 MHz, $CDCl_3$) δ 7.34 (m, 1H), 7.27 (m, 1H), 7.25 – 7.21 (m, 4H), 7.15 (m, 5H), 7.11 – 7.04 (m, 3H), 4.82 (p, *J* = 3.7 Hz, 1H), 3.86 (d, *J* = 4.3 Hz, 1H), 2.17 (s, 3H), 0.28 (d, *J* = 3.7 Hz, 3H). $^{13}$C NMR (151 MHz, $CDCl_3$) δ 144.3, 142.4, 142.3, 135.6, 133.8, 129.8, 129.7, 129.1,

128.8, 128.6, 128.4, 125.6, 125.5, 125.0, 43.2, 22.6, -5.4. $^{29}$Si NMR (119 MHz, $CDCl_3$) δ -13.7 MALDI *m/z* calc for $C_{21}H_{22}Si$ $[M + H]^+$ 328.138. Found 325.227.

Racemic Standard for **2.21i**:

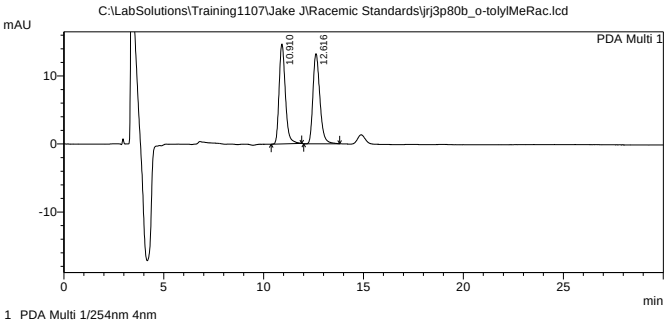


1 PDA Multi 1/254nm 4nm

**< Peak Table >**

PeakTable C:\LabSolutions\Training1107\Jake J\Racemic Standards\jrj3p80b_o-tolylMeRac.lcd

PDA Ch1 254nm 4nm

| Peak# | Ret. Time | Area | Height | Area % | Height % |
|---|---|---|---|---|---|
| 1 | 10.910 | 318494 | 14704 | 50.034 | 52.599 |
| 2 | 12.616 | 318058 | 13251 | 49.966 | 47.401 |
| Total | | 636552 | 27956 | 100.000 | 100.000 |

Enantiomerically enriched (*S*,*S*) **2.21i** using *S*-TCPTTL:

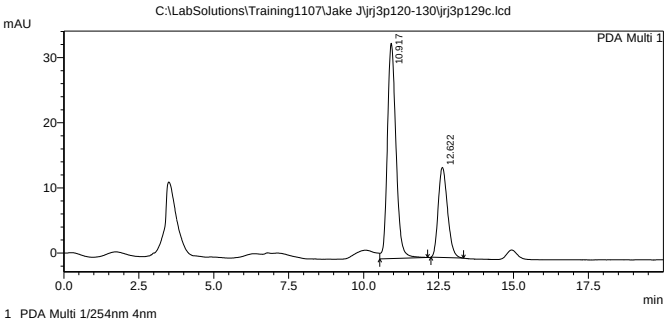


1 PDA Multi 1/254nm 4nm

**< Peak Table >**

PeakTable C:\LabSolutions\Training1107\Jake J\jrj3p120-130\jrj3p129c.lcd

PDA Ch1 254nm 4nm

| Peak# | Ret. Time | Area | Height | Area % | Height % |
|---|---|---|---|---|---|
| 1 | 10.917 | 660519 | 33039 | 68.790 | 70.490 |
| 2 | 12.622 | 299672 | 13831 | 31.210 | 29.510 |
| Total | | 960191 | 46870 | 100.000 | 100.000 |

**(*S*)-benzhydryl(mesityl)(methyl)silane (2.21j)**

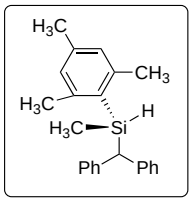


Synthesized using method F with diazo compound **2.20a** (38.8 mg, 0.200 mmol) and silane **2.19h** (164 mg, 1.00 mmol) to give a white solid in 64% yield (42.3 mg, 0.128 mmol). Enantiomeric ratio was determined by HLPC after hydrolysis with a Daicel CHIRALPAK ® OD-H column (2% IPA/ hexaness), 1.0 mL/min. $t_R$ (**2.21ja**) = 6.8 min, $t_R$ (**2.21jb**) = 8.6 min, 60:40 er (Si-OH product). Absolute configuration was assigned to be (*S)* based on analogy to **2.26c.**

$^1$H NMR (400 MHz, $CDCl_3$)δ 7.31 (m, 3H), 7.28 – 7.13 (m, 2H), 7.10 (d, *J* = 4.7 Hz, 4H), 7.04 (m, 1H), 6.75 (s, 2H), 4.94 (p, *J* = 4.3 Hz, 1H), 3.92 (d, *J* = 5.4 Hz, 1H), 2.24 (s, 9H), 0.29 (d, *J* = 4.0 Hz, 3H). $^{13}$C NMR (101 MHz, $CDCl_3$) δ 144.7, 142.7, 142.4, 139.4, 129.3, 129.1, 128.7, 128.6, 128.4, 128.3, 125.7, 125.3, 43.4, 24.1, 21.2, -3.7. $^{29}$Si NMR (79 MHz, $CDCl_3$) δ -18.0. MALDI *m/z* calc for $C_{23}H_{26}Si$ $[M + Na]^+$ 353.170. Found 353.248.

Racemic Standard for **2.21j**:

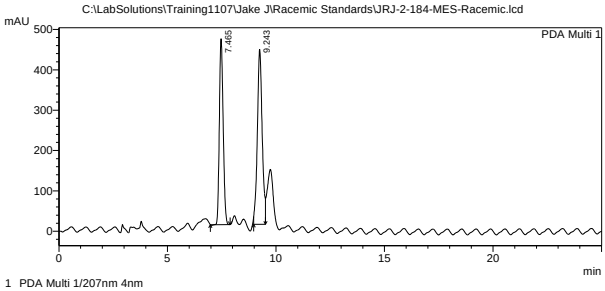


**< Peak Table >**

PeakTable C:\LabSolutions\Training1107\Jake J\Racemic Standards\JRJ-2-184-MES-Racemic.lcd

PDA Ch1 207nm 4nm

| Peak# | Ret. Time | Area | Height | Area % | Height % |
|---|---|---|---|---|---|
| 1 | 7.465 | 5633456 | 460567 | 45.645 | 51.548 |
| 2 | 9.243 | 6708400 | 432898 | 54.355 | 48.452 |
| Total | | 12341856 | 893465 | 100.000 | 100.000 |

Enantiomerically enriched (*S*) **2.21j** using *S*-TCPTTL:

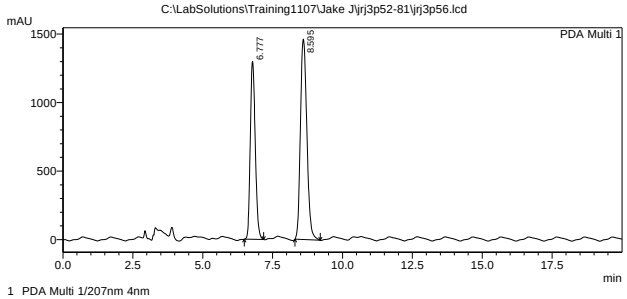


**< Peak Table >**

PeakTable C:\LabSolutions\Training1107\Jake J\jrj3p52-81\jrj3p56.lcd

PDA Ch1 207nm 4nm

| Peak# | Ret. Time | Area | Height | Area % | Height % |
|---|---|---|---|---|---|
| 1 | 6.777 | 16197961 | 1298528 | 40.801 | 47.019 |
| 2 | 8.595 | 23502137 | 1463158 | 59.199 | 52.981 |
| Total | | 39700098 | 2761686 | 100.000 | 100.000 |

**(*S*)-benzhydryl(isobutyl)(phenyl)silane (2.21k)**

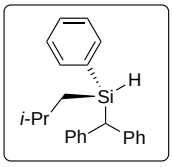


Synthesized using method F with diazo compound **2.20a** (388 mg, 1.00 mmol) and silane **2.19a** (820 mg, 5.00 mmol) to give a white solid in 45% yield (297 mg, 0.450 mmol). Enantiomeric ratio was determined by HLPC after hydrolysis with a Daicel CHIRALPAK ® OD-H column (1% IPA/ hexanes), 1.0 mL/min. $t_R$ (**2.21ka**) = 5.6 min, $t_R$ (**2.21kb**) = 6.2 min, 86:14 er (Si-OH product). Absolute configuration was assigned to be (*S, S)* based on analogy to **2.26c.**

$^1$H NMR (400 MHz, $CDCl_3$) δ 7.40 – 7.31 (m, 3H), 7.29 (d, *J* = 5.5 Hz, 6H), 7.25 – 7.15 (m, 5H), 7.12 (t, *J* = 6.8 Hz, 1H), 4.74 (h, *J* = 2.2 Hz, 1H), 3.86 (d, *J* = 3.9 Hz, 1H), 1.68 (dh, *J* = 12.5, 6.3 Hz, 1H), 0.93 (d, *J* = 5.9 Hz, 1H), 0.89 (d, *J* = 6.6 Hz, 6H), 0.80 (dd, *J* = 14.7, 7.7 Hz, 1H).$^{13}$C NMR (101 MHz, $CDCl_3$) δ 142.4, 142.2, 135.4, 134.3, 129.5, 129.1, 129.0, 128.6, 128.4, 127.8, 125.6, 125.4, 42.8, 26.1, 25.5, 25.2, 21.7. $^{29}$Si NMR (79 MHz, $CDCl_3$) δ -8.7. Did not ionize using ESI-MS or MALDI-TOF.

Racemic Standard for **2.21k**:

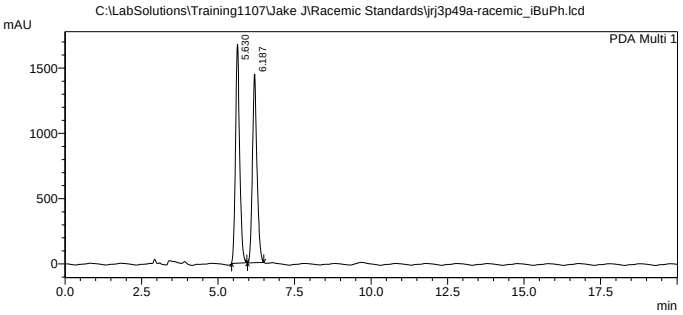


1 PDA Multi 1/195nm 4nm

**< Peak Table >**

PeakTable C:\LabSolutions\Training1107\Jake J\Racemic Standards\jrj3p49a-racemic_iBuPh.lcd

PDA Ch1 195nm 4nm

| Peak# | Ret. Time | Area | Height | Area % | Height % |
|---|---|---|---|---|---|
| 1 | 5.630 | 15800629 | 1676986 | 51.577 | 53.732 |
| 2 | 6.187 | 14834414 | 1444032 | 48.423 | 46.268 |
| Total | | 30635043 | 3121017 | 100.000 | 100.000 |

Enantiomerically enriched (*S*) **2.21k** using *S*-TCPTTL:

**<Chromatogram>**

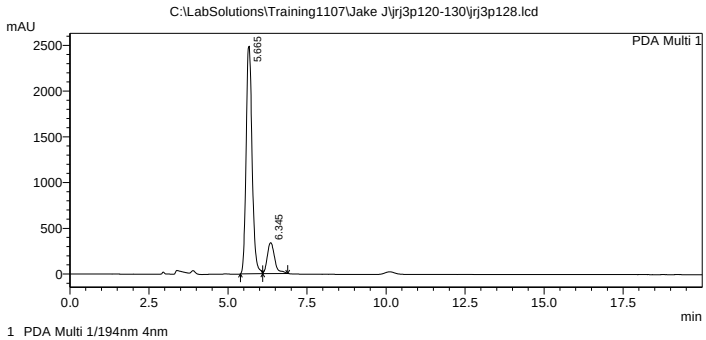


1 PDA Multi 1/194nm 4nm

**< Peak Table >**

PeakTable C:\LabSolutions\Training1107\Jake J\jrj3p120-130\jrj3p128.lcd

PDA Ch1 194nm 4nm

| Peak# | Ret. Time | Area | Height | Area % | Height % |
|---|---|---|---|---|---|
| 1 | 5.665 | 32779438 | 2487817 | 85.694 | 88.076 |
| 2 | 6.345 | 5472326 | 336794 | 14.306 | 11.924 |
| Total | | 38251764 | 2824612 | 100.000 | 100.000 |

## (*S*)-benzhydryl(isobutyl)(naphthalen-1-yl)silane (2.21l)

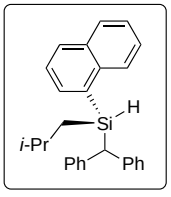


Synthesized using method F with diazo compound **2.20a** (38.8 mg, 0.200 mmol) and silane **2.19e** (214 mg, 1.00 mmol) to give a white solid in 60% yield (41.3 mg, 0.120 mmol). Enantiomeric ratio was determined by HLPC after hydrolysis with a Daicel CHIRALPAK ® AD-H column (1% IPA/ hexanes), 1.0 mL/min. $t_R$ (**2.21la**) = 10.9 min, $t_R$ **(2.21lb**) = 12.6 min, 82:18 er (Si-OH product). Absolute configuration was assigned to be (*S)* based on analogy to **2.26c**.

$^1$H NMR (600 MHz, $CDCl_3$) δ 7.92 (d, *J* = 8.3 Hz, 1H), 7.83 (dd, *J* = 8.1, 6.4 Hz, 2H), 7.59 (dd, *J* = 6.7, 1.2 Hz, 1H), 7.48 – 7.43 (m, 1H), 7.40 (ddd, *J* = 8.1, 6.8, 1.4 Hz, 1H), 7.36 (td, *J* = 7.3, 6.7, 1.2 Hz, 1H), 7.30 – 7.26 (m, 5H), 7.26 – 7.23 (m, 1H), 7.17 (ddd, *J* = 8.5, 5.1, 1.8 Hz, 1H), 7.09 (d, *J* = 6.8 Hz, 2H), 7.07-7.03 (m 2H), 7.00 (td, *J* = 6.9, 1.4 Hz, 1H), 5.11 (td, *J* = 5.0, 2.2 Hz, 1H),

4.04 (d, *J* = 4.5 Hz, 1H), 1.59 (ddt, *J* = 12.9, 7.7, 6.5 Hz, 1H), 1.03 (dt, *J* = 14.8, 5.8 Hz, 1H), 0.89 (dtd, *J* = 14.3, 7.1, 6.4, 2.3 Hz, 1H), 0.82 (t, *J* = 6.3 Hz, 7H). $^{13}$C NMR (151 MHz, $CDCl_3$) δ 142.4, 142.4, 137.3, 135.9, 133.3, 132.8, 130.3, 129.2, 129.0, 128.8, 128.6, 128.3, 127.9, 125.9, 125.7, 125.5, 125.3, 125.1, 41.4, 26.2, 25.5, 25.4, 22.5. $^{29}$Si NMR (79 MHz, $CDCl_3$) δ -9.5. MALDI *m/z* calc for $C_{27}H_{28}Si$ $[M - H]^+$ 379.1877. Found 379.220.

Racemic Standard for **2.21l**:

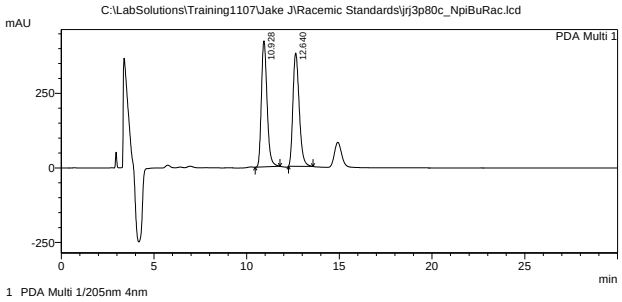


1 PDA Multi 1/205nm 4nm

**< Peak Table >**

PeakTable C:\LabSolutions\Training1107\Jake J\Racemic Standards\jrj3p80c_NpiBuRac.lcd

PDA Ch1 205nm 4nm

| Peak# | Ret. Time | Area | Height | Area % | Height % |
|---|---|---|---|---|---|
| 1 | 10.928 | 8992685 | 422849 | 50.155 | 52.701 |
| 2 | 12.640 | 8937207 | 379512 | 49.845 | 47.299 |
| Total | | 17929892 | 802361 | 100.000 | 100.000 |

Enantiomerically enriched (*S*) **2.21l** using *S*-TCPTTL:

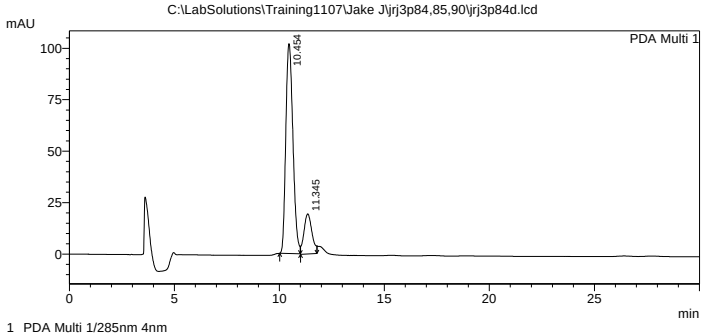


1 PDA Multi 1/285nm 4nm

**< Peak Table >**

PeakTable C:\LabSolutions\Training1107\Jake J\jrj3p84,85,90\jrj3p84d.lcd

PDA Ch1 285nm 4nm

| Peak# | Ret. Time | Area | Height | Area % | Height % |
|---|---|---|---|---|---|
| 1 | 10.454 | 2402971 | 101957 | 82.469 | 83.984 |
| 2 | 11.345 | 510822 | 19444 | 17.531 | 16.016 |
| Total | | 2913793 | 121400 | 100.000 | 100.000 |

**(*S*)-benzhydryl(neopentyl)(phenyl)silane (2.21m)**

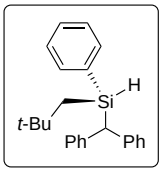


Synthesized using method F with diazo compound **2.20a** (38.8 mg, 0.200 mmol) and silane **2.19k** (178 mg, 1.00 mmol) to give a white solid in 60% yield (41.3 mg, 0.120 mmol). Enantiomeric ratio was determined by HLPC after hydrolysis with a Daicel CHIRALPAK ® AD-H column (1% IPA/ heptane), 1.0 mL/min. $t_R$ (**2.21ma**) = 10.6 min, $t_R$ (**2.21mb**) = 13.1 min, 50:50 er (Si-OH product). Absolute configuration was assigned to be (*S)* based on analogy to **5a**.

$^1$H NMR (400 MHz, $CDCl_3$) δ 7.37 – 7.30 (m, 3H), 7.30 – 7.21 (m, 6H), 7.18 (t, *J* = 6.8 Hz, 3H), 7.15 – 7.04 (m, 3H), 4.81 (t, *J* = 4.7 Hz, 1H), 3.80 (d, *J* = 4.0 Hz, 1H), 1.08 (dd, *J* = 14.7, 5.4 Hz, 1H), 0.93 (s, 1H), 0.89 (s, 9H). $^{13}$C NMR (101 MHz, $CDCl_3$) δ 142.4, 142.2, 135.4, 135.3, 129.4, 129.3, 128.9, 128.6, 128.3, 127.7, 125.6, 125.3, 43.3, 32.5, 30.6, 27.45. $^{29}$Si NMR (79 MHz, $CDCl_3$) δ -11.1. Did not ionize using ESI, MALDI or APCI.

Racemic Standard for **2.21m**:

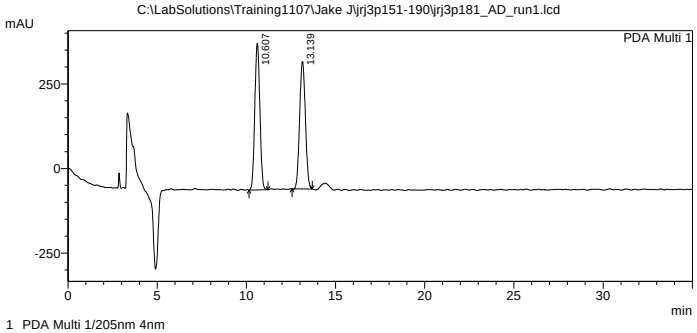


1 PDA Multi 1/205nm 4nm

**< Peak Table >**

PeakTable C:\LabSolutions\Training1107\Jake J\jrj3p151-190\jrj3p181_AD_run1.lcd

PDA Ch1 205nm 4nm

| Peak# | Ret. Time | Area | Height | Area % | Height % |
|---|---|---|---|---|---|
| 1 | 10.607 | 8549235 | 433259 | 50.265 | 53.471 |
| 2 | 13.139 | 8459167 | 377007 | 49.735 | 46.529 |
| Total | | 17008402 | 810266 | 100.000 | 100.000 |

Enantiomerically enriched (*S*) **2.21m** using *S*-TCPTTL:

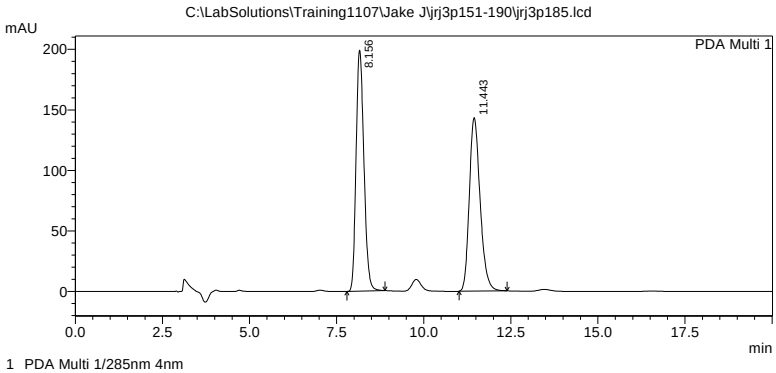


1 PDA Multi 1/285nm 4nm

**< Peak Table >**

PeakTable C:\LabSolutions\Training1107\Jake J\jrj3p151-190\jrj3p185.lcd

PDA Ch1 285nm 4nm

| Peak# | Ret. Time | Area | Height | Area % | Height % |
|---|---|---|---|---|---|
| 1 | 8.156 | 3118650 | 199177 | 50.230 | 58.155 |
| 2 | 11.443 | 3090035 | 143318 | 49.770 | 41.845 |
| Total | | 6208685 | 342495 | 100.000 | 100.000 |

**(*S*)-3-benzhydryl-1,1,1-triethyl-3-phenyldisiloxane (2.21n)**

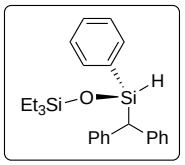


Synthesized using method F with diazo compound **2.20a** (38.8 mg, 0.200 mmol) and silane **2.19m** (238 mg, 1.00 mmol) to give a white solid in 60% yield (41.3 mg, 0.120 mmol). Enantiomeric ratio was determined by HLPC after hydrolysis with a Daicel CHIRALPAK ® AD-H column (2% IPA/ hexanes), 1.0 mL/min. $t_R$ (**2.21na**) = 9.5 min, $t_R$ (**2.21nb**) = 10.6 min, 61:39 er (Si-OH product). Absolute configuration was assigned to be (*S)* based on analogy to **2.26c**.

$^1$H NMR (600 MHz, $CDCl_3$) δ 7.37 – 7.31 (m, 1H), 7.31 – 7.25 (m, 8H), 7.25 – 7.20 (m, 3H), 7.20 – 7.09 (m, 3H), 5.30 (d, *J* = 2.6 Hz, 1H), 3.80 (d, *J* = 2.6 Hz, 1H), 0.80 (t, *J* = 8.0 Hz, 6H), 0.41 (q, *J* = 7.7 Hz, 6H). $^{13}$C NMR (101 MHz, $CDCl_3$) δ 141.1, 141.0, 135.5, 134.1, 130.0, 129.5, 129.1, 128.5, 128.5, 127.7, 125.7, 125.6, 44.4, 6.7, 6.0. $^{29}$Si NMR (79 MHz, $CDCl_3$) δ -14.5, -18.4/ Did not ionize using ESI, MALDI or APCI.

Racemic Standard for **2.21n**:

<Chromatogram>

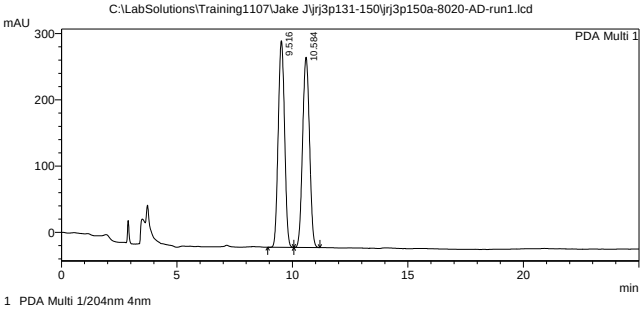


1 PDA Multi 1/204nm 4nm

< Peak Table >

PeakTable C:\LabSolutions\Training1107\Jake J\jrj3p131-150\jrj3p150a-8020-AD-run1.lcd

PDA Ch1 204nm 4nm

| Peak# | Ret. Time | Area | Height | Area % | Height % |
|---|---|---|---|---|---|
| 1 | 9.516 | 5973920 | 311973 | 49.931 | 52.058 |
| 2 | 10.584 | 5990388 | 287304 | 50.069 | 47.942 |
| Total | | 11964308 | 599277 | 100.000 | 100.000 |

Enantiomerically enriched (*S*) **2.21n** using *S*-TCPTTL:

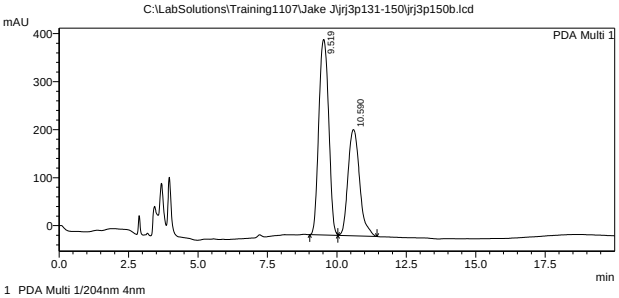


1 PDA Multi 1/204nm 4nm

< Peak Table >

PeakTable C:\LabSolutions\Training1107\Jake J\jrj3p131-150\jrj3p150b.lcd

PDA Ch1 204nm 4nm

| Peak# | Ret. Time | Area | Height | Area % | Height % |
|---|---|---|---|---|---|
| 1 | 9.519 | 10084552 | 407338 | 61.079 | 64.804 |
| 2 | 10.590 | 6426044 | 221227 | 38.921 | 35.196 |
| Total | | 16510595 | 628565 | 100.000 | 100.000 |

**(*S*)-benzhydryl(cyclohexyl)(phenyl)silane (2.21o)**

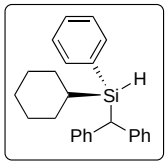


Synthesized using method F with diazo compound **2.20a** (38.8 mg, 0.200 mmol) and silane **2.19l** (190 mg, 1.00 mmol) to give a white solid in 77% yield (54.9 mg, 0.158 mmol). Enantiomeric ratio was determined by HLPC after hydrolysis with a Daicel CHIRALPAK ® AD-H column (2% IPA/ hexanes), 1.0 mL/min. $t_R$ (**2.21oa**) = 37.7 min, $t_R$ (**2.21ob**) = 42.6 min, 70:30 er (Si-OH product). Absolute configuration was assigned to be (*S)* based on analogy to **2.26c.**

$^1$H NMR (600 MHz, $CDCl_3$) δ 7.34 – 7.27 (m, 6H), 7.27 – 7.20 (m, 4H), 7.19 – 7.10 (m, 5H), 7.07 – 7.01 (m, 1H), 4.48 (dd, *J* = 4.5, 2.9 Hz, 1H), 3.96 (d, *J* = 4.4 Hz, 1H), 1.72 – 1.62 (m, 1H), 1.65 – 1.55 (m, 4H), 1.17 – 1.01 (m, 5H), 1.00 – 0.90 (m, 1H).NMR (151 MHz, $CDCl_3$) δ 142.6, 142.3, 135.8, 133.2, 129.4, 129.2, 129.0, 128.6, 128.4, 127.7, 125.7, 125.4, 40.5, 28.5, 28.1, 27.8, 26.8, 22.9. $^{29}$Si NMR (79 MHz, $CDCl_3$) δ -2.8. MALDI *m/z* calc for $C_{25}H_{28}Si$ $[M + Na]^+$ 379.185. Found 379.140.

Racemic Standard for **2.21o**:

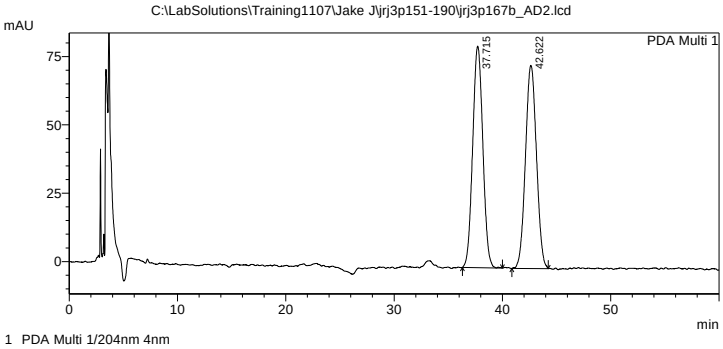


**< Peak Table >**

PeakTable C:\LabSolutions\Training1107\Jake J\jrj3p151-190\jrj3p167b_AD2.lcd

PDA Ch1 204nm 4nm

| Peak# | Ret. Time | Area | Height | Area % | Height % |
|---|---|---|---|---|---|
| 1 | 37.715 | 5281022 | 81077 | 50.124 | 52.165 |
| 2 | 42.622 | 5254858 | 74346 | 49.876 | 47.835 |
| Total | | 10535880 | 155423 | 100.000 | 100.000 |

Enantiomerically enriched (*S*) **2.21o** using *S*-TCPTTL:

<Chromatogram>

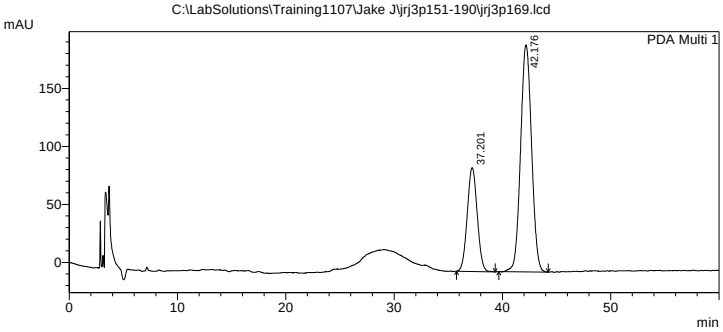


1 PDA Multi 1/204nm 4nm

< Peak Table >

PeakTable C:\LabSolutions\Training1107\Jake J\jrj3p151-190\jrj3p169.lcd

PDA Ch1 204nm 4nm

| Peak# | Ret. Time | Area | Height | Area % | Height % |
|---|---|---|---|---|---|
| 1 | 37.201 | 5726477 | 89443 | 29.288 | 31.364 |
| 2 | 42.176 | 13826155 | 195731 | 70.712 | 68.636 |
| Total | | 19552632 | 285174 | 100.000 | 100.000 |

**(*S*)-methyl(phenyl)((*S*)-phenyl(*o*-tolyl)methyl)silane (2.26a):**

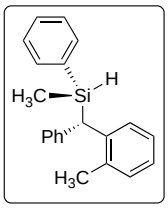

Synthesized using method G with diazo compound **2.20d** (1.00 g, 5.10 mmol) and silane **2.1e** (3.50 mL, 25.5 mmol) to give a clear oil in 89% yield (93:7 dr, 1.34 g, 4.5 mmol). Enantiomeric ratio was determined by HLPC after hydrolysis with a Daicel CHIRALPAK ® AD-H column (1% IPA/ heptane), 1.0 mL/min. $t_R$ (**2.26aa**) = 29.9 min, $t_R$ (**2.26ab**) = 32.1 min, $t_R$ (**2.26aa'**) = 45.3 min, $t_R$ (**2.26ab'**) = 53.3 min, 93:7 er (Si-OH product, **2.26ab**:**2.26ab'**). Absolute configuration was assigned to be (*S, S)* based on analogy to **2.26c** and **2.31a**.

$^1$H NMR (600 MHz, $CDCl_3$)) δ 7.45 – 7.04 (m, 14H), 4.72 (q, *J* = 3.6 Hz, 3H), 3.96 (d, *J* = 4.0 Hz, 1H), 2.21 (s, 3H), 0.33 (d, *J* = 3.6 Hz, 3H).$^{13}$C NMR (151 MHz, $CDCl_3$) δ 142.0, 140.5, 137.0, 135.1, 135.0, 139.0, 129.7, 129.6, 128.9, 128.3, 127.8, 126.1, 125.9, 125.2, 38.7, 20.3, -5.6. $^{29}$Si NMR (119 MHz, $CDCl_3$) δ -10.2. MALDI *m/z* calc for $C_{21}H_{22}Si$ $[M + H]^+$ 303.156. Found 303.154.

Racemic Standard for **2.26a**:

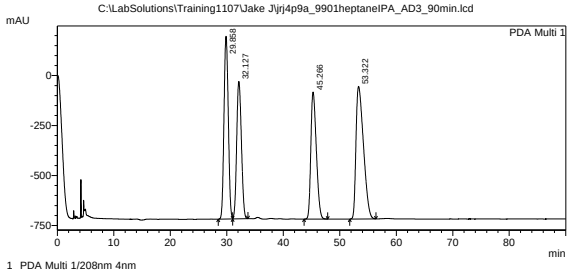


1 PDA Multi 1/208nm 4nm

< Peak Table >

PeakTable C:\LabSolutions\Training1107\Jake J\jrj4p9a_9901heptaneIPA_AD3_90min.lcd

PDA Ch1 208nm 4nm

| Peak# | Ret. Time | Area | Height | Area % | Height % |
|---|---|---|---|---|---|
| 1 | 29.858 | 48239523 | 914305 | 25.085 | 31.533 |
| 2 | 32.127 | 40004513 | 687079 | 20.802 | 23.696 |
| 3 | 45.266 | 42953904 | 635333 | 22.336 | 21.912 |
| 4 | 53.322 | 61108498 | 662816 | 31.777 | 22.859 |
| Total | | 192306438 | 2899533 | 100.000 | 100.000 |

Enantiomerically enriched (*S*,*S*) **2.26a** using *S*-TCPTTL:

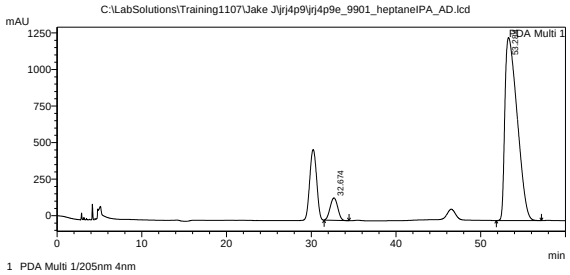


**< Peak Table >**

PeakTable C:\LabSolutions\Training1107\Jake J\jrj4p9\jrj4p9e_9901_heptaneIPA_AD.lcd

PDA Ch1 205nm 4nm

| Peak# | Ret. Time | Area | Height | Area % | Height % |
|---|---|---|---|---|---|
| 1 | 32.674 | 9589040 | 153329 | 7.062 | 10.913 |
| 2 | 53.284 | 126202061 | 1251634 | 92.938 | 89.087 |
| Total | | 135791101 | 1404963 | 100.000 | 100.000 |

Enantiomerically enriched (*R*,*R*) **2.26a** using *R*-TCPTTL:

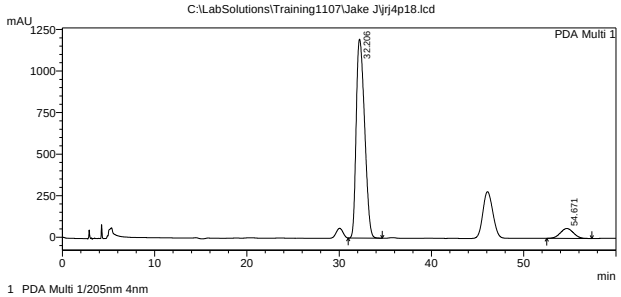


**< Peak Table >**

PeakTable C:\LabSolutions\Training1107\Jake J\jrj4p18.lcd

PDA Ch1 205nm 4nm

| Peak# | Ret. Time | Area | Height | Area % | Height % |
|---|---|---|---|---|---|
| 1 | 32.206 | 75751446 | 1197113 | 92.871 | 95.280 |
| 2 | 54.671 | 5815274 | 59299 | 7.129 | 4.720 |
| Total | | 81566720 | 1256412 | 100.000 | 100.000 |

**(*S*)-(4-fluorophenyl)(methyl)((*S*)-phenyl(*o*-tolyl)methyl)silane (2.26b):**

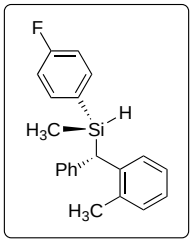


Synthesized using method F with diazo compound **2.20d** (42.0 mg, 0.200 mmol) and silane **2.19f** (140 mg, 1.00 mmol) to give an oil in 90% yield (57.7 mg, 0.180 mmol, 90:10 dr). Enantiomeric ratio was determined by HLPC after hydrolysis with a Daicel CHIRALPAK ® AD-H column (2% IPA/ hexanes), 1.0 mL/min. $t_R$ (**2.26ba**) = 36.0 min, $t_R$ (**2.26bb**) = 46.3 min, $t_R$ (**2.26ba'**) = 50.8 min, $t_R$ (**2.26bb'**) = 56.5 min, 61:39 er (Si-OH product, **2.26bb'**:**2.26bb**) Absolute configuration was assigned to be (*S, S*) based on analogy to **2.26c**.

$^1$H NMR (600 MHz, $CDCl_3$) δ 7.43 (dd, *J* = 7.6, 1.4 Hz, 1H), 7.30 – 7.23 (m, 2H), 7.23 – 7.15 (m, 4H), 7.15 – 7.05 (m, 4H), 7.01 – 6.94 (m, 2H), 4.76 (p, *J* = 3.7 Hz, 1H), 3.96 (d, *J* = 4.1 Hz, 1H), 2.24 (s, 3H), 0.37 (d, *J* = 3.7 Hz, 3H). $^{13}$C NMR (151 MHz, $CDCl_3$) δ 164.1 (d, $J_{CF}$ = 248.9 Hz), 141.8, 140.26, 137.0 (d, $J_{CCCF}$ = 7.5 Hz), 137.0, 130.9, 129.6, 128.9, 128.5, 128.4, 126.1, 126.0, 125.3, 115.0 (d, $J_{CCF}$ = 19.7 Hz), 38.8, 20.3, -5.5. $^{19}$F NMR (376 MHz, $CDCl_3$) δ -110.97. $^{29}$Si

NMR (76 MHz, $CDCl_3$) δ -10.9. MALDI *m/z* calc for $C_{21}H_{21}FSi$ $[M + Na]^+$ 343.129. Found 343.134.

Racemic Standard for **2.26b**:

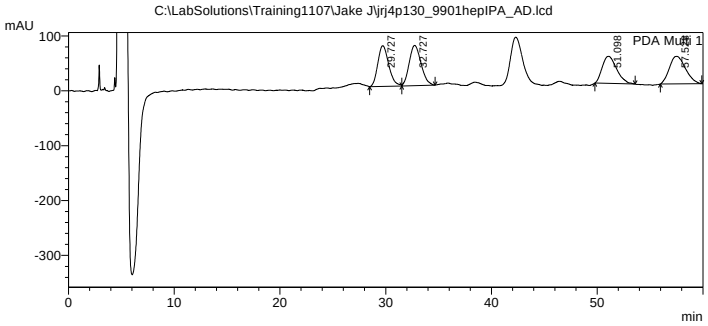


1 PDA Multi 1/203nm 4nm

**< Peak Table >**

PeakTable C:\LabSolutions\Training1107\Jake J\jrj4p130_9901hepIPA_AD.lcd

PDA Ch1 203nm 4nm

| Peak# | Ret. Time | Area | Height | Area % | Height % |
|---|---|---|---|---|---|
| 1 | 29.727 | 5340505 | 74092 | 25.353 | 29.986 |
| 2 | 32.727 | 5722663 | 73381 | 27.167 | 29.698 |
| 3 | 51.098 | 4693375 | 49413 | 22.281 | 19.998 |
| 4 | 57.528 | 5308366 | 50207 | 25.200 | 20.319 |
| Total | | 21064908 | 247094 | 100.000 | 100.000 |

Enantiomerically enriched (*S*,*S*) **2.26b** using *S*-TCPTTL:

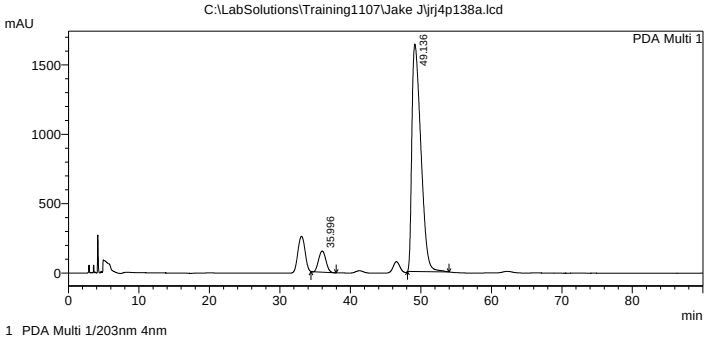


1 PDA Multi 1/203nm 4nm

**< Peak Table >**

PeakTable C:\LabSolutions\Training1107\Jake J\jrj4p138a.lcd

PDA Ch1 203nm 4nm

| Peak# | Ret. Time | Area | Height | Area % | Height % |
|---|---|---|---|---|---|
| 1 | 35.996 | 10899260 | 152350 | 6.957 | 8.501 |
| 2 | 49.136 | 145765515 | 1639890 | 93.043 | 91.499 |
| Total | | 156664775 | 1792240 | 100.000 | 100.000 |

Enantiomerically enriched (*R*,*R*) **2.26b** using *R*-TCPTTL:

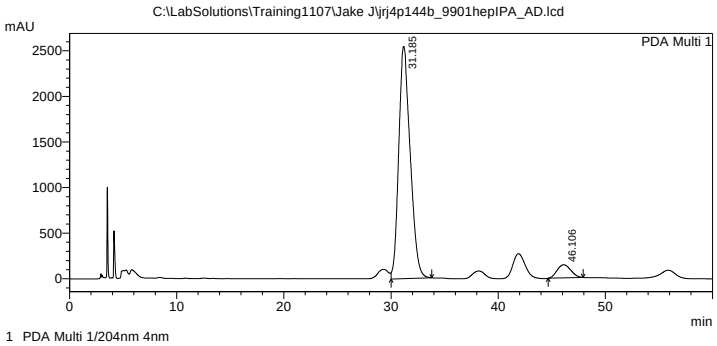


**< Peak Table >**

PeakTable C:\LabSolutions\Training1107\Jake J\jrj4p144b_9901hepIPA_AD.lcd

PDA Ch1 204nm 4nm

| Peak# | Ret. Time | Area | Height | Area % | Height % |
|---|---|---|---|---|---|
| 1 | 31.185 | 189219089 | 2547395 | 93.621 | 94.628 |
| 2 | 46.106 | 12893569 | 144617 | 6.379 | 5.372 |
| Total | | 202112657 | 2692012 | 100.000 | 100.000 |

**(*S*)-(4-methoxyphenyl)(methyl)((*S*)-phenyl(*o*-tolyl)methyl)silane (2.26c):**

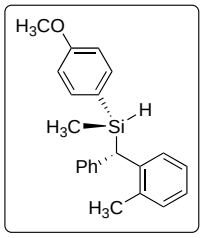


Synthesized using method F with diazo compound **2.20d** (42.0 mg, 0.200 mmol) and silane **2.19g** (152 mg, 1.00 mmol) to give a clear oil in 85% yield (56.5 mg, 0.170 mmol, 94:6 dr). Enantiomeric ratio was determined by HLPC after hydrolysis with a Daicel CHIRALPAK ® AD-H column (1% IPA/ heptane), 1.0 mL/min. $t_R$ (**2.26ca**) = 33.3 min, $t_R$ (**2.26cb**) = 37.5 min, $t_R$ (**2.26ca'**) = 47.5 min, $t_R$ (**2.26cb'**) = 56.3 min, 93.5:6.5 er (Si-OH product, **2.26cb'**:**2.26cb**). Absolute configuration was assigned to be (*S*,*S*) based Tamao-Fleming oxidation results and analogy to **2.31a.**

$^1$H NMR (400 MHz, $CDCl_3$) δ 7.39 (d, *J* = 7.6 Hz, 2H), 7.04-7.23 (m, 4H), 6.80 (d, *J* = 7.9 Hz, 1H), 4.73 – 4.67 (m, 1H), 3.93 (d, *J* = 3.7 Hz, 1H), 3.79 (s, 1H), 2.22 (s, 1H), 0.31 (d, *J* = 3.5 Hz, 3H). $^{13}$C NMR (151 MHz, $CDCl_3$) δ 160.9, 142.13, 140.7, 137.0, 136.6, 130.9, 129.7, 128.9, 128.3, 126.0, 125.9, 125.7, 125.2, 113.6, 55.2, 39.0, 20.4, -5.4. $^9$Si NMR (119 MHz, $CDCl_3$) δ -11.4. Did not ionize using ESI, MALDI or APCI.

Racemic Standard for **2.26c**:

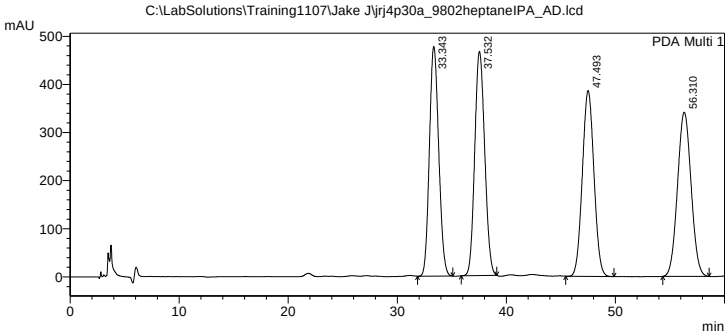


**< Peak Table >**

PeakTable C:\LabSolutions\Training1107\Jake J\jrj4p30a_9802heptaneIPA_AD.lcd

PDA Ch1 230nm 4nm

| Peak# | Ret. Time | Area | Height | Area % | Height % |
|---|---|---|---|---|---|
| 1 | 33.343 | 28394457 | 477248 | 24.430 | 28.566 |
| 2 | 37.532 | 29672263 | 466046 | 25.530 | 27.895 |
| 3 | 47.493 | 28590025 | 386124 | 24.598 | 23.111 |
| 4 | 56.310 | 29570529 | 341290 | 25.442 | 20.428 |
| Total | | 116227274 | 1670708 | 100.000 | 100.000 |

Enantiomerically enriched (*S*,*S*) **2.26c** using *S*-TCPTTL:

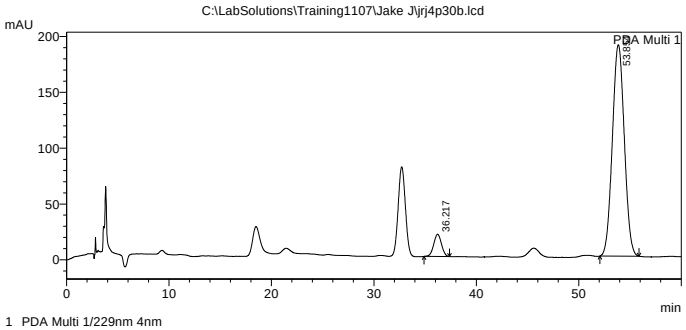


**< Peak Table >**

PDA Ch1 229nm 4nm

| Peak# | Ret. Time | Area | Height | Area % | Height % |
|---|---|---|---|---|---|
| 1 | 36.217 | 1055937 | 19918 | 6.437 | 9.516 |
| 2 | 53.854 | 15348653 | 189387 | 93.563 | 90.484 |
| Total | | 16404589 | 209306 | 100.000 | 100.000 |

Enantiomerically enriched (*R*,*R*) **2.26c** using *R*-TCPTTL:

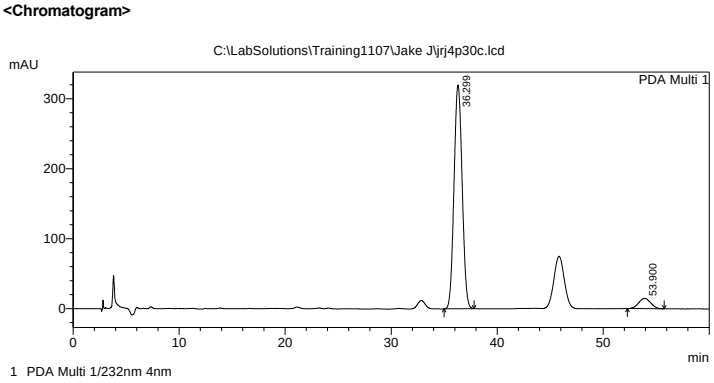


**< Peak Table >**

PeakTable C:\LabSolutions\Training1107\Jake J\jrj4p30c.lcd

PDA Ch1 232nm 4nm

| Peak# | Ret. Time | Area | Height | Area % | Height % |
|---|---|---|---|---|---|
| 1 | 36.299 | 17064389 | 319925 | 93.596 | 95.572 |
| 2 | 53.900 | 1167520 | 14823 | 6.404 | 4.428 |
| Total | | 18231909 | 334749 | 100.000 | 100.000 |

**(*S*)-methyl(naphthalen-2-yl)((*S*)-phenyl(*o*-tolyl)methyl)silane (2.26d):**

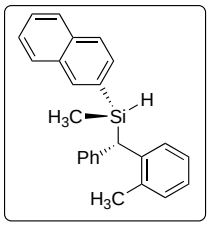


Synthesized using method F with diazo compound **2.20d** (42.0 mg, 0.200 mmol) and silane **2.19d** (172 mg, 1.00 mmol) to give a white solid in 95% yield (66.9 mg, 0.190 mmol, 91:9 dr). Enantiomeric ratio was determined by HLPC after hydrolysis with a Daicel CHIRALPAK ® AD-H column (1% IPA/ heptane), 1.0 mL/min. $t_R$ (**2.26da**) = 57.1 min, $t_R$ (**2.26db**) = 62.8 min, $t_R$ (**2.26da'**) = 86.4 min, $t_R$ (**2.26db'**) = 113.1 min, 92:8 er (Si-OH product, **2.26db'**:**2.26db**) Absolute configuration was assigned to be (*S, S*) based on analogy to **2.26c.**

$^1$H NMR (600 MHz, $CDCl_3$) δ 7.85 (m, 2H), 7.77 (dd, *J* = 12.3, 8.0 Hz, 2H), 7.55 – 7.48 (m, 3H), 7.35 (d, *J* = 8.1 Hz, 1H), 7.21 (td, *J* = 15.6, 14.8, 7.9 Hz, 4H), 7.17 – 7.09 (m, 4H), 4.93 (p, *J* = 3.8 Hz, 1H), 4.11 (d, *J* = 3.7 Hz, 1H), 2.29 (s, 3H), 0.48 (d, *J* = 3.5 Hz, 3H). $^{13}$C NMR (151 MHz, $CDCl_3$) δ 141.9, 140.5, 137.0, 136.2, 134.0, 132.9, 132.5, 131.0, 130.9, 129.7, 128.9, 128.4, 128.2, 127.8, 126.9, 126.7, 126.1, 126.0, 126.0, 125.3, 38.8, 20.4, -5.4. $^{29}$Si NMR (119 MHz, $CDCl_3$) δ -10.1. MALDI *m/z* calc for $C_{25}H_{24}Si$ $[M + Na]^+$ 375.154. Found 375.166.

Racemic Standard for **2.26d**:

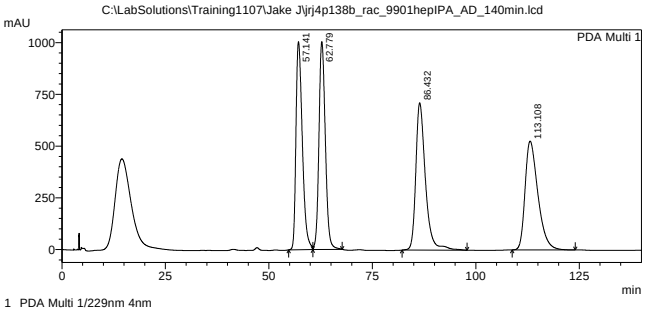


1 PDA Multi 1/229nm 4nm

**< Peak Table >**

PeakTable C:\LabSolutions\Training1107\Jake J\jrj4p138b_rac_9901hepIPA_AD_140min.lcd

PDA Ch1 229nm 4nm

| Peak# | Ret. Time | Area | Height | Area % | Height % |
|---|---|---|---|---|---|
| 1 | 57.141 | 107678104 | 1005424 | 24.285 | 30.955 |
| 2 | 62.779 | 107704834 | 1004970 | 24.291 | 30.941 |
| 3 | 86.432 | 115186832 | 711986 | 25.978 | 21.921 |
| 4 | 113.108 | 112830097 | 525615 | 25.447 | 16.183 |
| Total | | 443399867 | 3247994 | 100.000 | 100.000 |

Enantiomerically enriched (*S*,*S*) **2.26d** using *S*-TCPTTL:

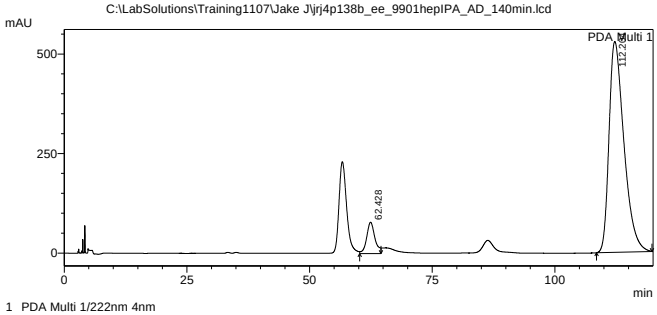


1 PDA Multi 1/222nm 4nm

**< Peak Table >**

PeakTable C:\LabSolutions\Training1107\Jake J\jrj4p138b_ee_9901hepIPA_AD_140min.lcd

PDA Ch1 222nm 4nm

| Peak# | Ret. Time | Area | Height | Area % | Height % |
|---|---|---|---|---|---|
| 1 | 62.428 | 9205162 | 78804 | 7.609 | 12.948 |
| 2 | 112.204 | 111770364 | 529829 | 92.391 | 87.052 |
| Total | | 120975526 | 608633 | 100.000 | 100.000 |

Enantiomerically enriched (*R*,*R*) **2.26d** using *R*-TCPTTL:

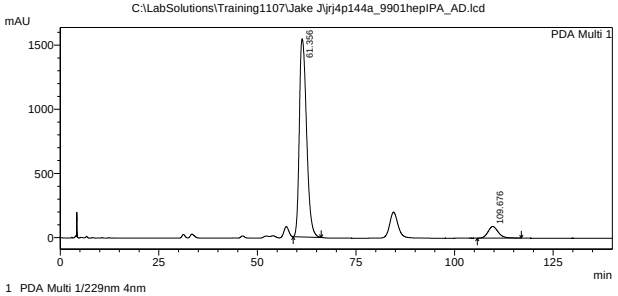


1 PDA Multi 1/229nm 4nm

**< Peak Table >**

PeakTable C:\LabSolutions\Training1107\Jake J\jrj4p144a_9901hepIPA_AD.lcd

PDA Ch1 229nm 4nm

| Peak# | Ret. Time | Area | Height | Area % | Height % |
|---|---|---|---|---|---|
| 1 | 61.356 | 196868375 | 1545840 | 92.289 | 94.460 |
| 2 | 109.676 | 16447848 | 90670 | 7.711 | 5.540 |
| Total | | 213316223 | 1636509 | 100.000 | 100.000 |

**(*S*)-methyl(naphthalen-1-yl)((*S*)-phenyl(*o*-tolyl)methyl)silane (2.26e):**

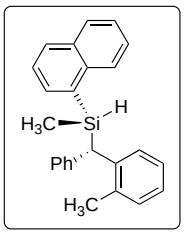

Synthesized using method F with diazo compound **2.20d** (0.200 mmol, 42.0 mg) and silane **2.19b** (172 mg, 1.00 mmol) to give a white solid in 55% yield (38.8 mg, 0.110 mmol, 82:18 dr). Enantiomeric ratio was determined by HLPC after hydrolysis with a Daicel CHIRALPAK ® AD-H column (2% IPA/ heptane), 1.0 mL/min. $t_R$ (**2.26ea**) = 23.9 min, $t_R$ (**2.26eb**) = 25.5 min, $t_R$ (**2.26ea'**) = 41.6 min, $t_R$ (**2.26eb'**) = 50.4 min, 92:8 er (Si-OH product, **2.26ea'**:**2.26ea**) Absolute configuration was assigned to be (*S, S*) based on analogy to **2.26c.**

$^1$H NMR (400 MHz, $CDCl_3$) δ 7.90 – 7.75 (m, 4H), 7.57 (d, *J* = 6.7 Hz, 1H), 7.53 – 7.38 (m, 3H), 7.34 (dt, *J* = 8.5, 4.5 Hz, 2H), 7.15 (t, *J* = 7.2 Hz, 2H), 7.08 (m, 2H), 7.02 (m, 1H), 6.95 (m,1H), 5.16 (p, *J* = 4.1 Hz, 1H), 4.23 (d, *J* = 4.5 Hz, 1H), 2.17 (s, 3H), 0.45 (d, *J* = 3.8 Hz, 3H). NMR (101 MHz, $CDCl_3$) δ 142.3, 14.0, 137.2, 136.9, 135.2, 133.5, 133.3, 130.9, 130.4, 129.8, 127.0, 128.7, 128.3, 127.7, 126.1, 126.0, 125.9, 125.6, 125.2, 125.1, 38.5, 20.3, -4.64.$^{29}$Si NMR (119 MHz, $CDCl_3$) δ -10.6. MALDI *m/z* calc for $C_{25}H_{24}Si$ $[M + Na]^+$ 375.154. Found 375.163.

Racemic Standard for **2.26e**:

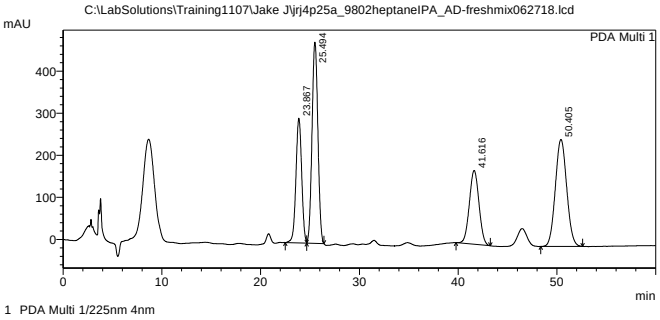


**< Peak Table >**

PeakTable C:\LabSolutions\Training1107\Jake J\jrj4p25a_9802heptaneIPA_AD-freshmix062718.lcd

PDA Ch1 225nm 4nm

| Peak# | Ret. Time | Area | Height | Area % | Height % |
|---|---|---|---|---|---|
| 1 | 23.867 | 11999034 | 296453 | 18.768 | 24.617 |
| 2 | 25.494 | 19735208 | 478133 | 30.868 | 39.703 |
| 3 | 41.616 | 11911651 | 175483 | 18.631 | 14.572 |
| 4 | 50.405 | 20288125 | 254205 | 31.733 | 21.109 |
| Total | | 63934018 | 1204274 | 100.000 | 100.000 |

Enantiomerically enriched (*S,S*) **2.26e** using *S*-TCPTTL:

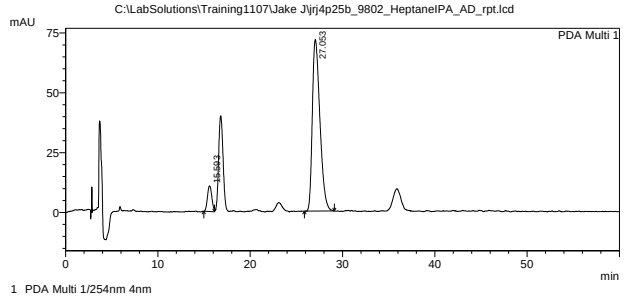


**< Peak Table >**

PeakTable C:\LabSolutions\Training1107\Jake J\jrj4p25b_9802_HeptaneIPA_AD_rpt.lcd

PDA Ch1 254nm 4nm

| Peak# | Ret. Time | Area | Height | Area % | Height % |
|---|---|---|---|---|---|
| 1 | 15.593 | 350639 | 10711 | 7.891 | 13.008 |
| 2 | 27.053 | 4093054 | 71632 | 92.109 | 86.992 |
| Total | | 4443693 | 82343 | 100.000 | 100.000 |

**(*S*)-(4-fluoronaphthalen-1-yl)(methyl)((*S*)-phenyl(*o*-tolyl)methyl)silane (2.26f):**

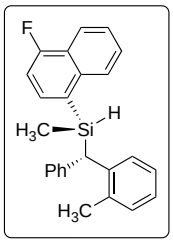

Synthesized using method F with diazo compound **2.20d** (0.200 mmol, 42.0 mg) and silane **2.19j** (190 mg, 1.00 mmol) to give a white solid in 66% yield (0.132 mmol, 48.9 mg, 84:16 dr. Enantiomeric ratio was determined by HLPC after hydrolysis with a Daicel CHIRALPAK ® AD-H column (2% IPA/ heptane), 1.0 mL/min. $t_R$ (**2.26fa**) = 35.0 min, $t_R$ (**2.26fb**) = 37.9 min, $t_R$ (**2.26fa'**) = 59.8 min, $t_R$ (**2.26fb'**) = 65.6 min, 92:8 er (Si-OH product, **2.26fa'**:**2.26fa**) Absolute configuration was assigned to be (*S, S*) based on analogy to **2.26c.**

$^1$H NMR (400 MHz, $CDCl_3$) δ 8.18 (d, *J* = 8.3 Hz, 1H), 7.94 (d, *J* = 8.5 Hz, 1H), 7.59 – 7.42 (m, 4H), 7.25 – 7.00 (m, 9H), 5.20 (q, *J* = 5.9, 4.0 Hz, 1H), 4.24 (d, *J* = 4.4 Hz, 1H), 2.23 (s, 3H), 0.52 (d, *J* = 3.5 Hz, 3H). $^{13}$C NMR (101 MHz, $CDCl_3$) δ 160.5 (d, $J_{CF}$ = 255.0 Hz), 140.2, 136.8, 135.2 (d, $J_{CCCF}$ = 8.3 Hz), 130.9, 129.66, 129.1 (d, $J_{CCCF}$ = 4.9 Hz), 128.7, 128.6, 128.4, 128.2, 127.4 (d, $J_{CCCF}$ = 3.2 Hz), 126.8, 126.0, 125.9, 125.8 (d, $J_{CCCCF}$ = 1.6 Hz), 125.1, 123.7 (d, $J_{CCF}$ = 15.0 Hz), 121.1 (d, $J_{CCCF}$ = 6.3 Hz), 108.9 (d, $J_{CCF}$= 18.5 Hz), 38.5, 20.2, -4.8. $^{19}$F NMR (376 MHz, $CDCl_3$) δ -120.35. $^{29}$Si NMR (76 MHz, $CDCl_3$) δ -12.7 MALDI *m/z* calc for $C_{25}H_{23}FSi$ $[M + H]^+$ 371.163. Found 371.151.

Racemic Standard for **2.26f**:

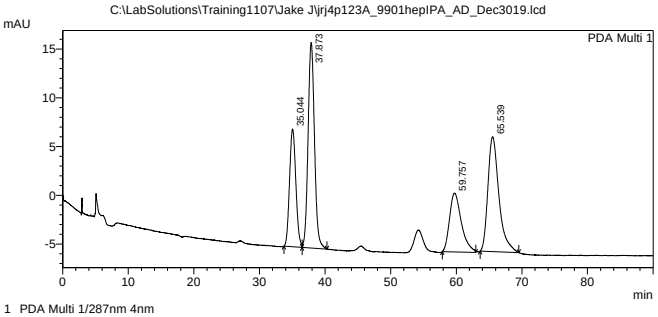


**< Peak Table >**

PeakTable C:\LabSolutions\Training1107\Jake J\jrj4p123A_9901hepIPA_AD_Dec3019.lcd
PDA Ch1 287nm 4nm

| Peak# | Ret. Time | Area | Height | Area % | Height % |
|---|---|---|---|---|---|
| 1 | 35.044 | 807448 | 12083 | 18.458 | 23.694 |
| 2 | 37.873 | 1433974 | 21093 | 32.780 | 41.363 |
| 3 | 59.757 | 756270 | 6031 | 17.288 | 11.826 |
| 4 | 65.539 | 1376912 | 11788 | 31.475 | 23.117 |
| Total | | 4374605 | 50995 | 100.000 | 100.000 |

Enantiomerically enriched (*S*,*S*) **2.26f** using *S*-TCPTTL:

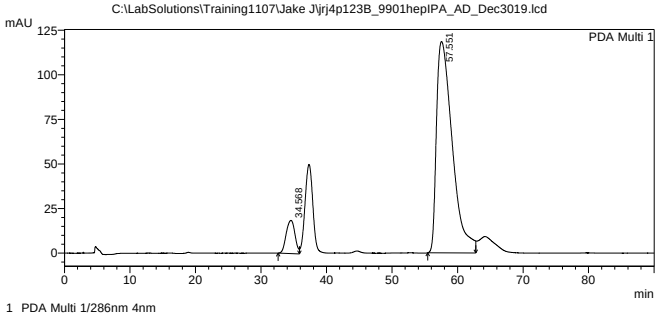


**< Peak Table >**

PeakTable C:\LabSolutions\Training1107\Jake J\jrj4p123B_9901hepIPA_AD_Dec3019.lcd

PDA Ch1 286nm 4nm

| Peak# | Ret. Time | Area | Height | Area % | Height % |
|---|---|---|---|---|---|
| 1 | 34.568 | 1735561 | 18627 | 8.022 | 13.578 |
| 2 | 57.551 | 19900422 | 118563 | 91.978 | 86.422 |
| Total | | 21635983 | 137190 | 100.000 | 100.000 |

**(*S*)-methyl(phenyl)((*S*)-phenyl(2-(trifluoromethyl)phenyl)methyl)silane (2.26g):**

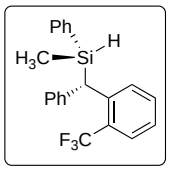


Synthesized using method F with diazo compound **2.20f** (0.200 mmol, 52.4 mg) and silane **2.1e** (122 mg, 1.00 mmol) to give a white solid in 93% yield (66.3 mg, 0.186 mmol, 98:2 dr, determined using $^{19}$F NMR). Enantiomeric ratio was determined by HLPC after hydrolysis with a Daicel CHIRALPAK ® AD-H column (2% IPA/ hexanes), 1.0 mL/min. $t_R$ (**2.26ga**) = 14.7 min, $t_R$ (**2.26gb**) = 15.7 min, $t_R$ (**2.26gb'**) = 23.4 min, $t_R$ (**2.26ga'**) = 26.6 min, 93:7 er (Si-OH product, **5cb'**:**5cb**) Absolute configuration was assigned to be (*S*, *S*) based on analogy to **2.26c.**

$^1$H NMR (600 MHz, $CDCl_3$) δ 7.63 (dd, *J* = 12.3, 7.9 Hz, 2H), 7.50 (t, *J* = 7.6 Hz, 1H), 7.34 (d, *J* = 7.1 Hz, 3H), 7.29 – 7.22 (m, 4H), 7.21 (d, *J* = 7.5 Hz, 2H), 7.17 (t, *J* = 7.6 Hz, 2H), 7.10 (t, *J* = 7.2 Hz, 1H), 4.76 (p, *J* = 4.0 Hz, 1H), 4.22 (d, *J* = 4.7 Hz, 1H), 0.20 (d, *J* = 3.7 Hz, 4H). $^{13}$C NMR (151 MHz, $CDCl_3$) δ 141.7,141.7, 141.4, 134.9, 134.3, 131.9, 131.4, 129.8, 128.8, 128.5, 128.5 (q, $J_{CCCF}$ = 7.0 Hz),128.3, 128.1 (q, $J_{CCF}$ = 36.0 Hz), 127.9, 126.4 (q, $J_{CCF}$ = 5.9 Hz, 125.8, 125.7, 124.8 (q, $J_{CF}$ = 274 Hz), 37.80, -5.80. $^{19}$F NMR (376 MHz, $CDCl_3$) δ -58.2. $^{29}$Si NMR (76 MHz, $CDCl_3$) δ -9.2. MALDI *m/z* calc for $C_{21}H_{19}F_3Si$ [M + Na]$^+$ 379.110. Found 379.100

Racemic Standard for **2.26g**:

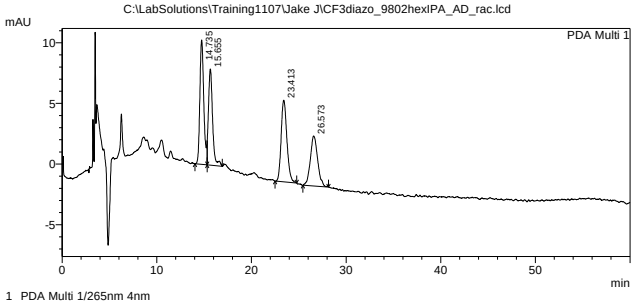


**< Peak Table >**

PeakTable C:\LabSolutions\Training1107\Jake J\CF3diazo_9802hexIPA_AD_rac.lcd

PDA Ch1 265nm 4nm

| Peak# | Ret. Time | Area | Height | Area % | Height % |
|---|---|---|---|---|---|
| 1 | 14.735 | 296985 | 10257 | 28.532 | 35.312 |
| 2 | 15.655 | 238179 | 7932 | 22.883 | 27.310 |
| 3 | 23.413 | 284555 | 6737 | 27.338 | 23.194 |
| 4 | 26.573 | 221156 | 4120 | 21.247 | 14.184 |
| Total | | 1040875 | 29046 | 100.000 | 100.000 |

Enantiomerically enriched (*S*,*S*) **2.26g** using *S*-TCPTTL:

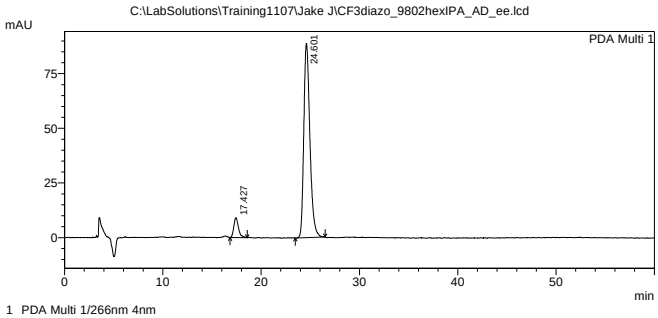


**< Peak Table >**

PeakTable C:\LabSolutions\Training1107\Jake J\CF3diazo_9802hexIPA_AD_ee.lcd

PDA Ch1 266nm 4nm

| Peak# | Ret. Time | Area | Height | Area % | Height % |
|---|---|---|---|---|---|
| 1 | 17.427 | 301249 | 9119 | 7.286 | 9.308 |
| 2 | 24.601 | 3833358 | 88855 | 92.714 | 90.692 |
| Total | | 4134607 | 97974 | 100.000 | 100.000 |

**(*S*)-((*S*)-(2-methoxyphenyl)(phenyl)methyl)(methyl)(phenyl)silane (2.26h):**

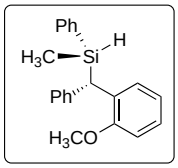


Synthesized using method F with diazo compound **2.20e** (48.9 mg, 0.200 mmol) and silane **2.1e** (122 mg, 1.00 mmol) to give a clear solid in 91% yield (58.0 mg, 0.182 mmol, 90:10 dr). Enantiomeric ratio was determined by HLPC after hydrolysis with a Daicel CHIRALPAK ® AD-H column (2% IPA/ hexanes), 1.0 mL/min. $t_R$ (**2.26ha**) = 26.6 min, $t_R$ (**2.26hb**) = 29.0 min, $t_R$ (**2.26ha'**) = 36.8 min, $t_R$ (**2.26hb'**) = 42.9 min, 95:5 er (Si-OH product, **2.26ha'**:**2.26ha**) Absolute configuration was assigned to be (*S, S*) based on analogy to **2.26c.**

$^1$H NMR (600 MHz, $CDCl_3$) δ 7.33 (d, *J* = 7.6 Hz, 2H), 7.30 (d, *J* = 7.2 Hz, 1H), 7.24 (dt, *J* = 11.6, 5.4 Hz, 3H), 7.19 – 7.11 (m, 5H), 7.09 – 7.05 (m, 1H), 6.88 (t, *J* = 7.4 Hz, 1H), 6.82 (d, *J* = 8.2 Hz, 1H), 4.70 – 4.66 (m, 1H), 4.26 (d, *J* = 3.5 Hz, 1H), 3.72 (s, 3H), 0.25 (d, *J* = 3.4 Hz, 3H). $^{13}$C NMR (151 MHz, $CDCl_3$) δ 156.9, 142.5, 136.0, 134.9, 131.0, 130.2, 129.3, 129.2, 128.3, 127.7, 126.8, 125.2, 120.7, 110.6, 55.3, 35.3, -5.7.$^{29}$Si NMR (76 MHz, $CDCl_3$) δ -12.5. ESI-MS *m/z* calc for $C_{21}H_{22}O_2Si$ (Si–OH) $[M - H]^-$ 333.1316. Found: 333.1304.

Racemic Standard for **2.26h**:

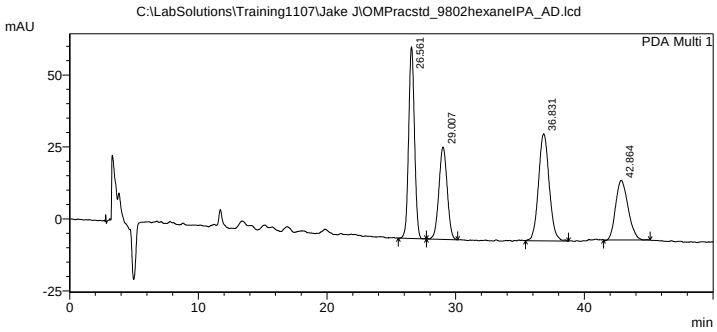


1 PDA Multi 1/273nm 4nm

**< Peak Table >**

PeakTable C:\LabSolutions\Training1107\Jake J\OMPracstd_9802hexaneIPA_AD.lcd

PDA Ch1 273nm 4nm

| Peak# | Ret. Time | Area | Height | Area % | Height % |
|---|---|---|---|---|---|
| 1 | 26.561 | 2108170 | 66513 | 29.761 | 42.517 |
| 2 | 29.007 | 1436247 | 32070 | 20.275 | 20.500 |
| 3 | 36.831 | 2148115 | 37141 | 30.325 | 23.741 |
| 4 | 42.864 | 1391142 | 20716 | 19.639 | 13.242 |
| Total | | 7083674 | 156439 | 100.000 | 100.000 |

Enantiomerically enriched (*S*,*S*) **2.26h** using *S*-TCPTTL:

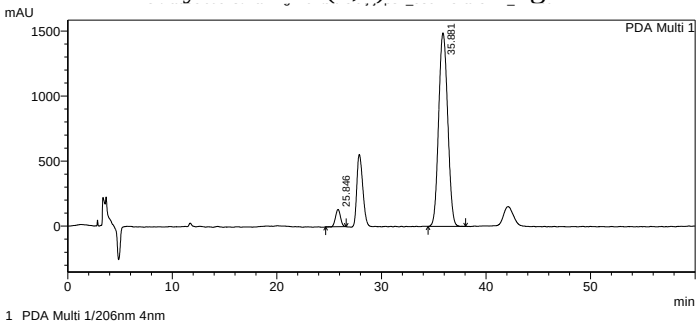


1 PDA Multi 1/206nm 4nm

**< Peak Table >**

PeakTable C:\LabSolutions\Training1107\Jake J\jrj4p84_9802hexaneIPA_AD.lcd

PDA Ch1 206nm 4nm

| Peak# | Ret. Time | Area | Height | Area % | Height % |
|---|---|---|---|---|---|
| 1 | 25.846 | 4372963 | 132933 | 4.655 | 8.202 |
| 2 | 35.881 | 89566615 | 1487798 | 95.345 | 91.798 |
| Total | | 93939577 | 1620731 | 100.000 | 100.000 |

Enantiomerically enriched (*R*,*R*) **2.26h** using *R*-TCPTTL:

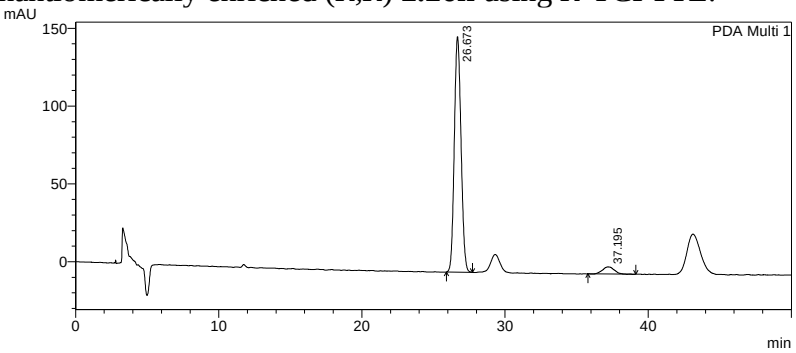


1 PDA Multi 1/274nm 4nm

**< Peak Table >**

PeakTable C:\LabSolutions\Training1107\Jake J\jrj4p87_9802HexIPA_AD.lcd

PDA Ch1 274nm 4nm

| Peak# | Ret. Time | Area | Height | Area % | Height % |
|---|---|---|---|---|---|
| 1 | 26.673 | 4936920 | 151331 | 95.059 | 97.064 |
| 2 | 37.195 | 256588 | 4577 | 4.941 | 2.936 |
| Total | | 5193508 | 155909 | 100.000 | 100.000 |

**(*S*)-((*S*)-(2-chlorophenyl)(4-methoxyphenyl)methyl)(methyl)(phenyl)silane (2.26i)**

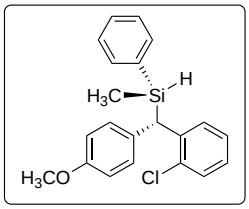


Synthesized using method F with diazo compound **2.20h** (52.0 mg, 0.200 mmol) and silane **2.1e** (122 mg, 1.00 mol) to give a white solid in 98% yield (69.0 mg, 0.196 mmol, 90:10 dr. Enantiomeric ratio was determined by HLPC after hydrolysis with a Daicel CHIRALPAK ® AD-H column (2% IPA/ heptane), 1.0 mL/min. $t_R$ (**2.26ia**) = 49.1 min, $t_R$ (**2.26ib**) = 52.5 min, $t_R$ (**2.26ia'**) = 55.0 min, $t_R$ (**2.26ib'**) = 87.0 min, 89:11 er (Si-OH product, **2.26ia'**:**2.26ia**) Absolute configuration was assigned to be (*S*, *S*) based on analogy to **2.26c.**

$^1$H NMR (600 MHz, $CDCl_3$) δ 7.39 (m, 5H), 7.31 (t, *J* = 7.2 Hz, 2H), 7.22 (t, *J* = 7.6 Hz, 1H), 7.16 (d, *J* = 8.2 Hz, 2H), 7.12 (t, *J* = 7.7 Hz, 1H), 6.78 (d, *J* = 8.4 Hz, 2H), 4.82 – 4.76 (m, 1H), 4.45 (d, *J* = 4.5 Hz, 1H), 3.76 (s, 3H), 0.38 (d, *J* = 3.4 Hz, 3H).$^{13}$C NMR (151 MHz, $CDCl_3$) δ 157.7, 140.7, 135.0, 134.6, 134.1, 133.3, 130.4, 130.3, 129.9, 129.7, 127.9, 127.0, 126.8, 113.9, 75.9, 53.2, 36.2, -5.2. $^{29}$Si NMR (79 MHz, $CDCl_3$) δ -11.34. MALDI *m/z* calc for $C_{21}H_{21}ClOSi$ $[M - H]^+$ 351.097. Found 351.083.

Racemic Standard for **2.26i**:

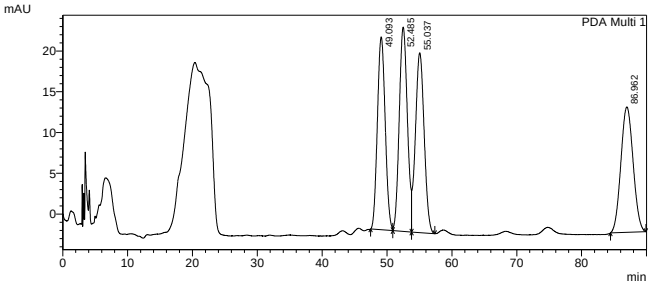


**< Peak Table >**

PeakTable C:\LabSolutions\Training1107\Jake J\jrj4p185a_9802hepIPA_ADonODvalve.lcd

PDA Ch1 233nm 4nm

| Peak# | Ret. Time | Area | Height | Area % | Height % |
|---|---|---|---|---|---|
| 1 | 49.093 | 1980775 | 23674 | 24.047 | 27.467 |
| 2 | 52.485 | 2179913 | 25065 | 26.465 | 29.081 |
| 3 | 55.037 | 2060887 | 22061 | 25.020 | 25.596 |
| 4 | 86.962 | 2015386 | 15391 | 24.468 | 17.857 |
| Total | | 8236960 | 86192 | 100.000 | 100.000 |

Enantiomerically enriched (*S*,*S*) **2.26i** using *S*-TCPTTL:

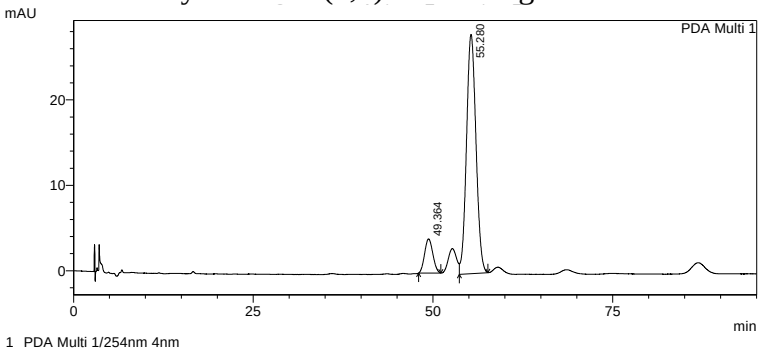


1 PDA Multi 1/254nm 4nm

**< Peak Table >**

PeakTable C:\LabSolutions\Training1107\Jake J\jrj4p185b_9802hepIPA_ADonODvalve.lcd

PDA Ch1 254nm 4nm

| Peak# | Ret. Time | Area | Height | Area % | Height % |
|---|---|---|---|---|---|
| 1 | 49.364 | 317147 | 3994 | 10.972 | 12.473 |
| 2 | 55.280 | 2573303 | 28030 | 89.028 | 87.527 |
| Total | | 2890450 | 32024 | 100.000 | 100.000 |

Enantiomerically enriched (*R*,*R*) **2.26i** using *R*-TCPTTL:

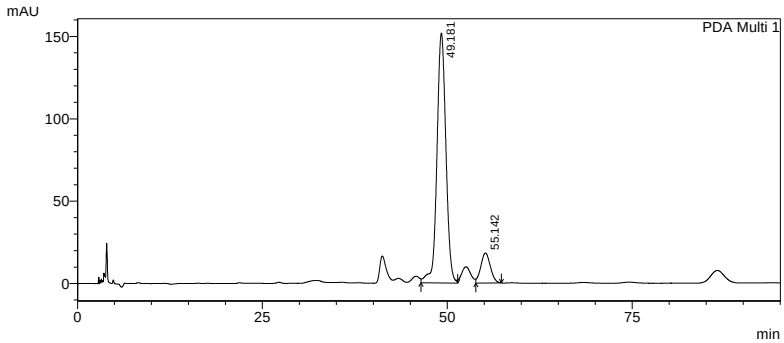


1 PDA Multi 1/233nm 4nm

**< Peak Table >**

PeakTable C:\LabSolutions\Training1107\Jake J\jrj4p185c_9802hepIPA_ADonODvalve.lcd

PDA Ch1 233nm 4nm

| Peak# | Ret. Time | Area | Height | Area % | Height % |
|---|---|---|---|---|---|
| 1 | 49.181 | 12792352 | 151676 | 88.662 | 89.256 |
| 2 | 55.142 | 1635909 | 18258 | 11.338 | 10.744 |
| Total | | 14428261 | 169934 | 100.000 | 100.000 |

**(*S*)-methyl((*S*)-naphthalen-1-yl(phenyl)methyl)(phenyl)silane (2.26j):**

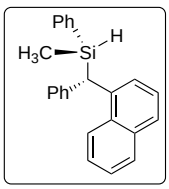


Synthesized using method F with diazo compound **2.20g** (48.9 mg, 0.200 mmol) and silane **2.1e** (122 mg, 1.00 mmol) to give a white solid in 78% yield (52.8 mg, 0.158 mmol, 85:15 dr). Enantiomeric ratio was determined by HLPC after hydrolysis with a Daicel CHIRALPAK ® AD-H column (2% IPA/ hexanes), 1.0 mL/min. $t_R$ (**2.26ja**) = 36.0 min, $t_R$ (**2.26ja'**) = 46.3 min, $t_R$ (**2.26jb**) = 50.8 min, $t_R$ (**2.26jb'**) = 56.5 min, 61:39 er (Si-OH product, **2.26ja**:**2.26ja'**) Absolute configuration was assigned to be (*S*, *S*) based on analogy to **2.26c.**

$^1$H NMR (600 MHz, $CDCl_3$) δ 8.12 – 8.05 (m, 1H), 7.82 – 7.78 (m, 1H), 7.70 (d, *J* = 8.3 Hz, 1H), 7.62 (d, *J* = 7.1 Hz, 3H), 7.46 – 7.36 (m, 3H), 7.35 – 7.29 (m, 2H), 7.27 – 7.16 (m, 1H), 7.11 (m, 3H), 7.08 – 7.00 (m, 1H), 4.83 (p, *J* = 3.2 Hz, 1H), 4.56 (d, *J* = 4.2 Hz, 1H), 0.33 (d, *J* = 3.6 Hz,

3H). $^{13}$C NMR (151 MHz, $CDCl_3$) δ 142.3, 138.2, 135.1, 134.5, 132.8, 129.7, 129.0, 128.7, 128.5, 128.4, 127.8, 127.4, 126.9, 126.0, 125.6, 125.4, 125.3, 124.2, 38.1, -5.4.$^{29}$Si NMR (119 MHz, $CDCl_3$) δ -10.0. Did not ionize using ESI, MALDI or APCI.

Racemic Standard for **2.26j**:

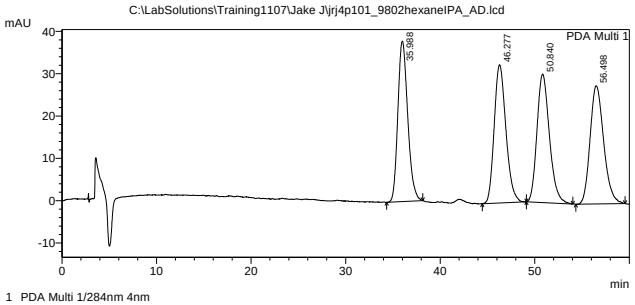


1 PDA Multi 1/284nm 4nm

**< Peak Table >**

PeakTable C:\LabSolutions\Training1107\Jake J\jrj4p101_9802hexaneIPA_AD.lcd

PDA Ch1 284nm 4nm

| Peak# | Ret. Time | Area | Height | Area % | Height % |
|---|---|---|---|---|---|
| 1 | 35.988 | 2750234 | 37927 | 24.688 | 29.426 |
| 2 | 46.277 | 2813267 | 32673 | 25.254 | 25.349 |
| 3 | 50.840 | 2789483 | 30380 | 25.041 | 23.570 |
| 4 | 56.498 | 2786868 | 27912 | 25.017 | 21.655 |
| Total | | 11139853 | 128892 | 100.000 | 100.000 |

Enantiomerically enriched (*S*,*S*) **2.26j** using *S*-TCPTTL:

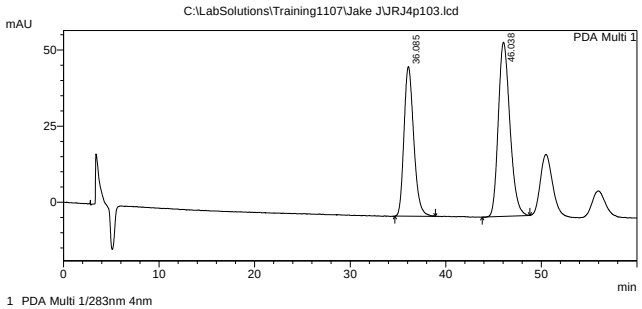


1 PDA Multi 1/283nm 4nm

**< Peak Table >**

PeakTable C:\LabSolutions\Training1107\Jake J\JRJ4p103.lcd

PDA Ch1 283nm 4nm

| Peak# | Ret. Time | Area | Height | Area % | Height % |
|---|---|---|---|---|---|
| 1 | 36.085 | 3479088 | 49147 | 41.817 | 46.219 |
| 2 | 46.038 | 4840630 | 57187 | 58.183 | 53.781 |
| Total | | 8319718 | 106334 | 100.000 | 100.000 |

Enantiomerically enriched (*R*,*R*) **2.26j** using *R*-TCPTTL:

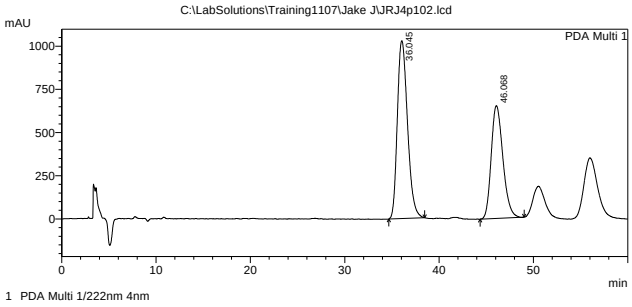


**< Peak Table >**

PeakTable C:\LabSolutions\Training1107\Jake J\JRJ4p102.lcd

PDA Ch1 222nm 4nm

| Peak# | Ret. Time | Area | Height | Area % | Height % |
|---|---|---|---|---|---|
| 1 | 36.045 | 76982519 | 1029081 | 57.866 | 61.189 |
| 2 | 46.068 | 56053744 | 652716 | 42.134 | 38.811 |
| Total | | 133036262 | 1681797 | 100.000 | 100.000 |

## Azines and functionalized insertion products:

### 1,2-bis(diphenylmethylene)hydrazine (2.22a):

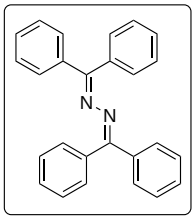

Spectrum matches previous report.[49]

$^1$H NMR (600 MHz, $CDCl_3$) δ 7.47 (d, *J* = 7.7 Hz, 4H), 7.39 (dt, *J* = 11.4, 6.5 Hz, 6H), 7.36 – 7.31 (m, 6H), 7.27 (t, *J* = 7.5 Hz, 4H).

### (1*E*,2*E*)-1,2-bis(phenyl(*o*-tolyl)methylene)hydrazine (2.22b):

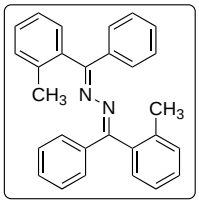

Observed and isolated during kinetics experiments as a yellow solid.

$^1$H NMR (600 MHz, $CDCl_3$) δ 7.37 (m, 4H), 7.29 (m, 6H), 7.22 (m, 6H), 2.23 (s, 6H). $^{13}$C NMR (151 MHz, $CDCl_3$) δ 137.8, 136.6, 130.3, 123.0, 129.9, 128.3, 128.3, 128.2, 128.0, 125.4, 20.2

**(*R*)-methyl(phenyl)((*S*)-phenyl(*o*-tolyl)methyl)silanol (2.29a):**

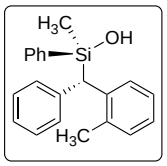


Synthesized using method K **2.26a** (100 mg, 0.330 mmol) to give a clear oil in 90% yield (94.5 mg, 0.300 mmol, 93:7 dr). Enantiomeric ratio was determined by HLPC with a Daicel CHIRALPAK ® AD-H column (1% IPA/ heptane), 1.0 mL/min. $t_R$ (**2.29a**) = 29.9 min, $t_R$ (**2.29b**) = 32.1 min, $t_R$ (**2.29a'**) = 45.3 min, $t_R$ (**2.29b'**) = 53.3 min, 93:7 er (**2.29b**:**2.29b'**). Absolute configuration was assigned to be (*R, S)* based on analogy to **2.26a**, and formed through inversion.[29]

$^1$H NMR (400 MHz, $C_6D_6$) δ 7.70 (d, *J* = 7.6 Hz, 1H), 7.36 (d, *J* = 7.9 Hz, 2H), 7.26 (d, *J* = 7.6 Hz, 2H), 7.12 – 7.06 (m, 5H), 7.05 – 6.88 (m, 4H), 3.96 (s, 1H), 2.03 (s, 3H), 1.57 (s, 1H), 0.29 (s, 1H). $^{13}$C NMR (151 MHz, $CDCl_3$) δ 141.3, 139.7, 137.1, 136.9, 134.0, 130.9, 130.0, 129.9, 129.0, 128.4, 127.8, 126.0, 125.9, 125.4, 41.6, 20.4, -1.6. $^{29}$Si NMR (79 MHz, $CDCl_3$) δ 1.66. MALDI *m/z* calc for $C_{22}H_{22}Si$ $[M + Na]^+$ 341.1332. Found 341.212.

Racemic Standard for **2.29a**:

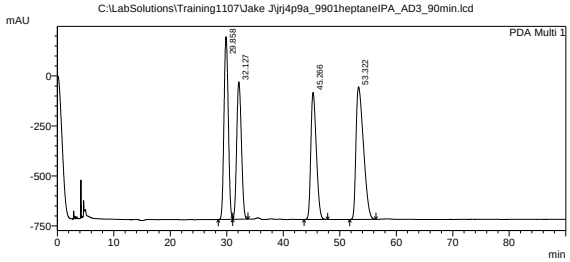


1 PDA Multi 1/208nm 4nm

**< Peak Table >**

PeakTable C:\LabSolutions\Training1107\Jake J\jrj4p9a_9901heptaneIPA_AD3_90min.lcd

PDA Ch1 208nm 4nm

| Peak# | Ret. Time | Area | Height | Area % | Height % |
|---|---|---|---|---|---|
| 1 | 29.858 | 48239523 | 914305 | 25.085 | 31.533 |
| 2 | 32.127 | 40004513 | 687079 | 20.802 | 23.696 |
| 3 | 45.266 | 42953904 | 635333 | 22.336 | 21.912 |
| 4 | 53.322 | 61108498 | 662816 | 31.777 | 22.859 |
| Total | | 192306438 | 2899533 | 100.000 | 100.000 |

Enantiomerically enriched (*S,S*) **2.29a** using *S*-TCPTTL:

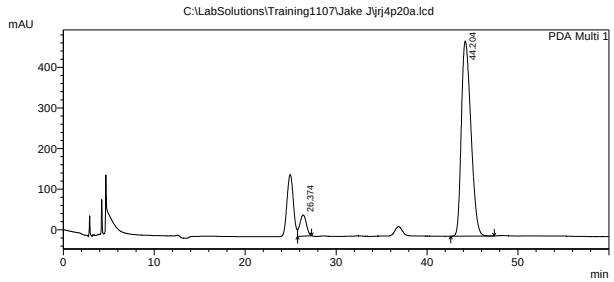


1 PDA Multi 1/204nm 4nm

**< Peak Table >**

PeakTable C:\LabSolutions\Training1107\Jake J\jrj4p20a.lcd

PDA Ch1 204nm 4nm

| Peak# | Ret. Time | Area | Height | Area % | Height % |
|---|---|---|---|---|---|
| 1 | 26.374 | 2588118 | 52218 | 6.858 | 9.805 |
| 2 | 44.204 | 35149381 | 480353 | 93.142 | 90.195 |
| Total | | 37737499 | 532571 | 100.000 | 100.000 |

**(*R*)-((*E*)-4-fluorostyryl)(methyl)(phenyl)((*S*)-phenyl(*o*-tolyl)methyl)silane (2.30a):**

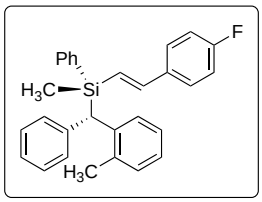


Synthesized using method L with **2.26a** (100 mg, 0.330 mmol) to give a clear oil in 62% yield (104.1 mg, 0.204 mmol, 85:15 **2.30a**:**2.30a'**, 93:7 dr). Absolute configuration was assigned to be (*R, S)* based on analogy to **2.26a** and assuming retention of configuration.[29] The E isomer was assigned based off *J* values of the alkene protons. Enantiomers could not separate using CSP-HPLC.

$^{1}$H NMR (600 MHz, $CDCl_3$) δ 7.41 – 7.32 (m, 6H), 7.29 (m 2H), 7.20 – 7.13 (m, 3H), 7.13 – 7.06 (m, 4H), 7.02 (m, 3H), 6.81 (d, *J* = 19.2 Hz, 1H), 6.50 (d, *J* = 19.2 Hz, 1H), 4.11 (s, 1H), 2.22 (s, 3H), 0.46 (s, 3H). $^{13}$C NMR (151 MHz, $CDCl_3$) δ 162.9 (d, $J_{CF}$ = 250.4 Hz), 145.8, 141.7, 140.5, 137.0, 136.8, 135.0, 130.9, 130.3, 129.4, 129.1, 128.9, 128.4, 128.3, 128.2, 127.8, 125.8 (d, $J_{CCCF}$ = 6.3 Hz), 125.1, 124.1 (d, $J_{CCCCF}$ = 2.3 Hz), 115.6 (d, $J_{CCF}$= 21.6 Hz), 40.1, 20.4, -3.9.MALDI *m/z* calc for $C_{29}H_{27}FSi$ $[M + H_3O]^+$ . 441.204. Found 441.158. $^{19}$F NMR (376 MHz, $CDCl_3$) δ -113.3. $^{29}$Si NMR (79 MHz, $CDCl_3$) δ -12.0.

**(1*S*,2*R*)-2-methyl-1,2-diphenyl-2,3-dihydro-1*H*-benzo[*c*]silole (2.31a):**

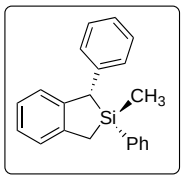


Synthesized using method J with **2.26a** (100 mg, 0.330 mmol) to give a clear oil in 90% yield (89.2 mg, 0.300 mmol, 90:10 dr). Absolute configuration was assigned to be (*S, S)* based on analogy to **2.26c**, and $^{1}$H NOESY experiments. Could not separate using CSP-HPLC.

$^{1}$H NMR (600 MHz, $CDCl_3$) δ 7.46 (d, *J* = 7.6 Hz, 1H), 7.32 – 7.20 (m, 1H), 7.19 – 7.12 (m, 4H), 7.08 (d, *J* = 7.6 Hz, 2H), 7.01 (d, *J* = 7.2 Hz, 1H), 6.75 (d, *J* = 8.4 Hz, 2H), 3.91 (s, 1H), 2.66 (d, *J* = 17.3 Hz, 1H), 2.34 (d, *J* = 17.3 Hz, 1H), 0.63 (s, 3H).$^{13}$C NMR (151 MHz, $CDCl_3$) δ 144.8, 142.9, 142.1, 134.5, 129.6, 129.0, 128.9, 128.1, 127.9, 127.6, 126.6, 124.3, 43.4, 18.9, -4.6. $^{29}$Si NMR (79 MHz, $CDCl_3$) δ 15.7. MALDI *m/z* calc for $C_{21}H_{20}Si$ $[M + Na]^+$ 323.123. Found 323.166.

**(*S*)-phenyl(*o*-tolyl)methanol (2.32a)**

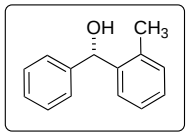


Synthesized using procedure I for Tamao-Fleming oxidation of **2.26c**. HPLC retention times match previously reported syntheses. Enantiomeric ratio was determined by HLPC with a Daicel CHIRALPAK ® OD-H column (2% IPA/ hexanes), 0.5 mL/min. $t_R$ (**2.32aa**) = 20.4 min, $t_R$ (**2.32ab**) = 21.6 min, 91.5:8.5 er. Absolute configuration was assigned to be (*S)* based on previous reports.[39]

$^{1}$H NMR (600 MHz, $CDCl_3$) δ 7.50 (d, *J* = 7.6 Hz, 1H), 7.31 (m, 4H), 7.27 – 7.21 (m, 2H), 7.19 (td, *J* = 7.4, 1.6 Hz, 1H), 7.13 (d, *J* = 7.3 Hz, 1H), 5.97 (s, 1H), 2.23 (s, 3H).

Racemic Standard:

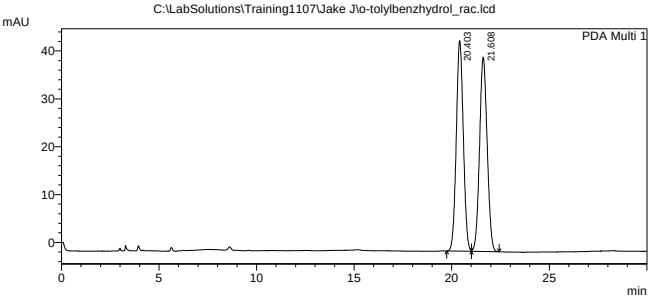


**< Peak Table >**

PeakTable C:\LabSolutions\Training1107\Jake J\o-tolylbenzhydrol_rac.lcd

PDA Ch1 254nm 4nm

| Peak# | Ret. Time | Area | Height | Area % | Height % |
|---|---|---|---|---|---|
| 1 | 20.403 | 1104154 | 43993 | 50.043 | 51.995 |
| 2 | 21.608 | 1102272 | 40617 | 49.957 | 48.005 |
| Total | | 2206427 | 84609 | 100.000 | 100.000 |

HPLC trace after Tamao-Fleming Oxidation of **2.32a**:

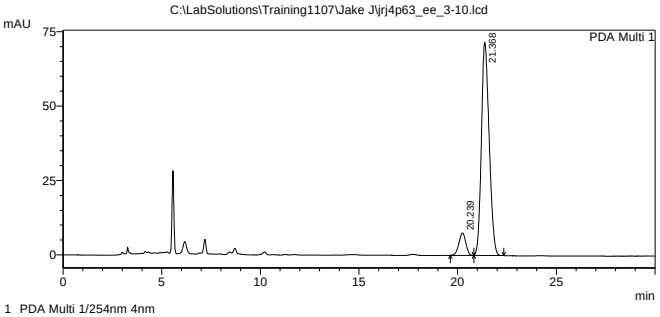


**< Peak Table >**

PeakTable C:\LabSolutions\Training1107\Jake J\jrj4p63_ee_3-10.lcd

PDA Ch1 254nm 4nm

| Peak# | Ret. Time | Area | Height | Area % | Height % |
|---|---|---|---|---|---|
| 1 | 20.239 | 183861 | 7514 | 8.569 | 9.489 |
| 2 | 21.368 | 1961798 | 71672 | 91.431 | 90.511 |
| Total | | 2145659 | 79186 | 100.000 | 100.000 |

## 2.12: References


(1) Diemoz, K. M. Design, Synthesis, and Investigation of Siloxanol Hydrogen-Bonding Catalysts and Chiral Silanol Ligands, University of California, Davis, 2018.

(2) Kelly, A. T. Synthesis of Siloxanol Containing Compounds and Studies Toward Enantioenriched Variants, University of California, Davis.

(3) Jagannathan, J. R.; Fettinger, J. C.; Shaw, J. T.; Franz, A. K. Enantioselective Si–H Insertion Reactions of Diarylcarbenes for the Synthesis of Silicon-Stereogenic Silanes. *J. Am. Chem. Soc.* **2020**, *142* (27), 11674–11679. https://doi.org/10.1021/jacs.0c04533.

(4) Xu, L.-W.; Li, L.; Lai, G.-Q.; Jiang, J.-X. The Recent Synthesis and Application of Silicon-Stereogenic Silanes: A Renewed and Significant Challenge in Asymmetric Synthesis. *Chem. Soc. Rev.* **2011**, *40* (3), 1777–1790. https://doi.org/10.1039/C0CS00037J.

(5) Doyle, M. P.; Duffy, R.; Ratnikov, M.; Zhou, L. Catalytic Carbene Insertion into C-H Bonds. *Chem. Rev.* **2010**, *110* (2), 704–724. https://doi.org/10.1021/cr900239n.

(6) Nakamura, E.; Yoshikai, N.; Yamanaka, M. Mechanism of C−H Bond Activation/C−C Bond Formation Reaction between Diazo Compound and Alkane Catalyzed by Dirhodium Tetracarboxylate. *J. Am. Chem. Soc.* **2002**, *124* (24), 7181–7192. https://doi.org/10.1021/ja017823o.

(7) Allred, A. L. Electronegativity Values from Thermochemical Data. *J. Inorg. Nucl. Chem.* **1961**, *17* (3), 215–221. https://doi.org/https://doi.org/10.1016/0022-1902(61)80142-5.
(8) Yasutomi, Y.; Suematsu, H.; Katsuki, T. Iridium(III)-Catalyzed Enantioselective Si−H Bond Insertion and Formation of an Enantioenriched Silicon Center. *J. Am. Chem. Soc.* **2010**, *132* (13), 4510–4511. https://doi.org/10.1021/ja100833h.
(9) Nakagawa, Y.; Chanthamath, S.; Fujisawa, I.; Shibatomi, K.; Iwasa, S. Ru(Ii)-Pheox-Catalyzed Si–H Insertion Reaction: Construction of Enantioenriched Carbon and Silicon Centers. *Chem. Commun.* **2017**, *53* (26), 3753–3756. https://doi.org/10.1039/C7CC01070B.
(10) Chanthamath, S.; Iwasa, S. Enantioselective Cyclopropanation of a Wide Variety of Olefins Catalyzed by Ru(II)–Pheox Complexes. *Acc. Chem. Res.* **2016**, *49* (10), 2080–2090. https://doi.org/10.1021/acs.accounts.6b00070.
(11) Doyle, M. P.; McKervey, M. A. 1938-; Ye, T. 1963-. *Modern Catalytic Methods for Organic Synthesis with Diazo Compounds : From Cyclopropanes to Ylides LK - Https://Melvyl.on.Worldcat.Org/Oclc/36767864*; Wiley: New York SE - xvii, 652 pages : illustrations ; 25 cm, 1998.
(12) Zhu, D.; Chen, L.; Fan, H.; Yao, Q.; Zhu, S. Recent Progress on Donor and Donor–Donor Carbenes. *Chem. Soc. Rev.* **2020**, *49* (3), 908–950. https://doi.org/10.1039/C9CS00542K.
(13) Vicente, R.; González, J.; Riesgo, L.; González, J.; López, L. A. Catalytic Generation of Zinc Carbenes from Alkynes: Zinc-Catalyzed Cyclopropanation and Si□H Bond Insertion Reactions. *Angew. Chemie Int. Ed.* **2012**, *51* (32), 8063–8067. https://doi.org/https://doi.org/10.1002/anie.201203914.
(14) Jia, M.; Ma, S. New Approaches to the Synthesis of Metal Carbenes. *Angew. Chemie Int. Ed.* **2016**, *55* (32), 9134–9166. https://doi.org/https://doi.org/10.1002/anie.201508119.
(15) Yue, X.; Shan, C.; Qi, X.; Luo, X.; Zhu, L.; Zhang, T.; Li, Y.; Li, Y.; Bai, R.; Lan, Y. Insights into Disilylation and Distannation: Sequence Influence and Ligand/Steric Effects on Pd-Catalyzed Difunctionalization of Carbenes. *Dalt. Trans.* **2018**, *47* (6), 1819–1826. https://doi.org/10.1039/C7DT04084A.
(16) Liu, Z.; Tan, H.; Fu, T.; Xia, Y.; Qiu, D.; Zhang, Y.; Wang, J. Pd(0)-Catalyzed Carbene Insertion into Si–Si and Sn–Sn Bonds. *J. Am. Chem. Soc.* **2015**, *137* (40), 12800–12803. https://doi.org/10.1021/jacs.5b09135.
(17) Qin, C.; Boyarskikh, V.; Hansen, J. H.; Hardcastle, K. I.; Musaev, D. G.; Davies, H. M. L. D2-Symmetric Dirhodium Catalyst Derived from a 1,2,2-Triarylcyclopropanecarboxylate Ligand: Design, Synthesis and Application. *J. Am. Chem. Soc.* **2011**, *133* (47), 19198–19204. https://doi.org/10.1021/ja2074104.
(18) Lamb, K. N.; Squitieri, R. A.; Chintala, S. R.; Kwong, A. J.; Balmond, E. I.; Soldi, C.; Dmitrenko, O.; Castiñeira Reis, M.; Chung, R.; Addison, J. B.; Fettinger, J. C.; Hein, J. E.; Tantillo, D. J.; Fox, J. M.; Shaw, J. T. Synthesis of Benzodihydrofurans by Asymmetric C−H Insertion Reactions of Donor/Donor Rhodium Carbenes. *Chem. – A Eur. J.* **2017**, *23* (49), 11843–11855. https://doi.org/10.1002/chem.201701630.
(19) Soldi, C.; Lamb, K. N.; Squitieri, R. A.; González-López, M.; Di Maso, M. J.; Shaw, J. T. Enantioselective Intramolecular C–H Insertion Reactions of Donor–Donor Metal Carbenoids. *J. Am. Chem. Soc.* **2014**, *136* (43), 15142–15145. https://doi.org/10.1021/ja508586t.
(20) Nickerson, L. A.; Bergstrom, B. D.; Gao, M.; Shiue, Y. S.; Laconsay, C. J.; Culberson, M. R.; Knauss, W. A.; Fettinger, J. C.; Tantillo, D. J.; Shaw, J. T. Enantioselective Synthesis of Isochromans and Tetrahydroisoquinolines by C-H Insertion of Donor/Donor Carbenes. *Chem. Sci.* **2020**, *11* (2), 494–498. https://doi.org/10.1039/c9sc05111b.
(21) Souza, L. W.; Squitieri, R. A.; Dimirjian, C. A.; Hodur, B. M.; Nickerson, L. A.; Penrod, C. N.; Cordova, J.; Fettinger, J. C.; Shaw, J. T. Enantioselective Synthesis of Indolines, Benzodihydrothiophenes, and Indanes by C−H Insertion of Donor/Donor Carbenes. *Angew. Chemie* **2018**, *130* (46), 15433–15436. https://doi.org/10.1002/ange.201809344.
(22) Diemoz, K. M.; Wilson, S. O.; Franz, A. K. Synthesis of Structurally Varied 1,3-Disiloxanediols

and Their Activity as Anion-Binding Catalysts. *Chemistry (Easton)*. **2016**, *22* (51), 18349–18353. https://doi.org/10.1002/chem.201604103.
(23) Kelly, A. T.; Franz, A. K. Metal-Free Synthesis of 1,3-Disiloxanediols and Aryl Siloxanols. *ACS Omega* **2019**, *4* (4), 6295–6300. https://doi.org/10.1021/acsomega.9b00121.
(24) Satoh, Y.; Igarashi, M.; Sato, K.; Shimada, S. Highly Selective Synthesis of Hydrosiloxanes by Au-Catalyzed Dehydrogenative Cross-Coupling Reaction of Silanols with Hydrosilanes. *ACS Catal.* **2017**, *7* (3), 1836–1840. https://doi.org/10.1021/acscatal.6b03560.
(25) Zheng, J.; Lin, J.-H.; Yu, L.-Y.; Wei, Y.; Zheng, X.; Xiao, J.-C. Cross-Coupling between Difluorocarbene and Carbene-Derived Intermediates Generated from Diazocompounds for the Synthesis of Gem-Difluoroolefins. *Org. Lett.* **2015**, *17* (24), 6150–6153. https://doi.org/10.1021/acs.orglett.5b03159.
(26) Zhu, D.; Ma, J.; Luo, K.; Fu, H.; Zhang, L.; Zhu, S. Enantioselective Intramolecular C−H Insertion of Donor and Donor/Donor Carbenes by a Nondiazo Approach. *Angew. Chemie Int. Ed.* **2016**, *55* (29), 8452–8456. https://doi.org/10.1002/anie.201604211.
(27) Bagheri, V.; Doyle, M. P.; Taunton, J.; Claxton, E. E. A New and General Synthesis of .Alpha.-Silyl Carbonyl Compounds by Silicon-Hydrogen Insertion from Transition Metal-Catalyzed Reactions of Diazo Esters and Diazo Ketones. *J. Org. Chem.* **1988**, *53* (26), 6158–6160. https://doi.org/10.1021/jo00261a045.
(28) Doyle, M. P.; High, K. G.; Bagheri, V.; Pieters, R.; Lewis, P. J.; Pearson, M. M. Rhodium(II) Perfluorobutyrate Catalyzed Silane Alcoholysis. A Highly Selective Route to Silyl Ethers. *J. Org. Chem.* **1990**, *55* (25), 6082–6086. https://doi.org/10.1021/jo00312a010.
(29) Corriu, R. J. P.; Guérin, C.; Moreau, J. J. E. Stereochemistry at Silicon. *Topics in Stereochemistry*. January 1, 1984, pp 43–198. https://doi.org/doi:10.1002/9780470147245.ch2.
(30) Keipour, H.; Carreras, V.; Ollevier, T. Recent Progress in the Catalytic Carbene Insertion Reactions into the Silicon-Hydrogen Bond. *Org Biomol Chem* **2017**, *15* (26), 5441–5456. https://doi.org/10.1039/c7ob00807d.
(31) Lee, M.; Ren, Z.; Musaev, D. G.; Davies, H. M. L. Rhodium-Stabilized Diarylcarbenes Behaving as Donor/Acceptor Carbenes. *ACS Catal.* **2020**, 6240–6247. https://doi.org/10.1021/acscatal.0c01131.
(32) Huang, M.-Y.; Yang, J.-M.; Zhao, Y.-T.; Zhu, S.-F. Rhodium-Catalyzed Si–H Bond Insertion Reactions Using Functionalized Alkynes as Carbene Precursors. *ACS Catal.* **2019**, *9* (6), 5353–5357. https://doi.org/10.1021/acscatal.9b01187.
(33) Landais, Y.; Parra-Rapado, L.; Planchenault, D.; Weber, V. Mechanism of Metal-Carbenoid Insertion into the Si–H Bond. *Tetrahedron Lett.* **1997**, *38* (2), 229–232. https://doi.org/https://doi.org/10.1016/S0040-4039(96)02285-X.
(34) Qu, Z.; Shi, W.; Wang, J. A Kinetic Study on the Pairwise Competition Reaction of α-Diazo Esters with Rhodium(II) Catalysts: Implication for the Mechanism of Rh(II)-Carbene Transfer. *J. Org. Chem.* **2001**, *66* (24), 8139–8144. https://doi.org/10.1021/jo0107352.
(35) Yang, L.-L.; Evans, D.; Xu, B.; Li, W.-T.; Li, M.-L.; Zhu, S.-F.; Houk, K. N.; Zhou, Q.-L. Enantioselective Diarylcarbene Insertion into Si–H Bonds Induced by Electronic Properties of the Carbenes. *J. Am. Chem. Soc.* **2020**, *142* (28), 12394–12399. https://doi.org/10.1021/jacs.0c04725.
(36) Igawa, K.; Tomooka, K. Chiral Silicon Molecules. *Organosilicon Chemistry*. November 11, 2019, pp 495–532. https://doi.org/doi:10.1002/9783527814787.ch14.
(37) Onopchenko, A.; Sabourin, E. T.; Beach, D. L. Vinyl- and Allylsilanes from the Rhodium(I)-Catalyzed Hydrosilylation of 1-Alkenes with Trialkylsilanes. *J. Org. Chem.* **1984**, *49* (18), 3389–3392. https://doi.org/10.1021/jo00192a030.
(38) Cheng, C.; Hartwig, J. F. Catalytic Silylation of Unactivated C–H Bonds. *Chem. Rev.* **2015**, *115* (17), 8946–8975. https://doi.org/10.1021/cr5006414.
(39) Touge, T.; Nara, H.; Fujiwhara, M.; Kayaki, Y.; Ikariya, T. Efficient Access to Chiral Benzhydrols via Asymmetric Transfer Hydrogenation of Unsymmetrical Benzophenones with Bifunctional Oxo-Tethered Ruthenium Catalysts. *J. Am. Chem. Soc.* **2016**, *138* (32), 10084–10087.

https://doi.org/10.1021/jacs.6b05738.
(40) Green, S. P.; Wheelhouse, K. M.; Payne, A. D.; Hallett, J. P.; Miller, P. W.; Bull, J. A. Thermal Stability and Explosive Hazard Assessment of Diazo Compounds and Diazo Transfer Reagents. *Org. Process Res. Dev.* **2020**, *24* (1), 67–84. https://doi.org/10.1021/acs.oprd.9b00422.
(41) Yasutomi, Y.; Suematsu, H.; Katsuki, T. Iridium(III)-Catalyzed Enantioselective Si−H Bond Insertion and Formation of an Enantioenriched Silicon Center. *J. Am. Chem. Soc.* **2010**, *132* (13), 4510–4511. https://doi.org/10.1021/ja100833h.
(42) Chen, J.; Chen, C.; Ji, C.; Lu, Z. Cobalt-Catalyzed Asymmetric Hydrogenation of 1,1-Diarylethenes. *Org. Lett.* **2016**, *18* (7), 1594–1597. https://doi.org/10.1021/acs.orglett.6b00453.
(43) Brown, E.; Chevalier, C.; Huet, F.; Le Grumelec, C.; Lézé, A.; Touet, J. Determination of the Enantiomeric Excesses of Chiral Acids by 19F NMR Studies of Their Esters Deriving from (R)-(+)-2-(Trifluoromethyl)Benzhydrol. *Tetrahedron: Asymmetry* **1994**, *5* (7), 1191–1194. https://doi.org/https://doi.org/10.1016/0957-4166(94)80154-1.
(44) Wu, C.; Hu, F.; Liu, Z.; Deng, G.; Ye, F.; Zhang, Y.; Wang, J. Cu(I)-Catalyzed Coupling of Diaryldiazomethanes with Terminal Alkynes: An Efficient Synthesis of Tri-Aryl-Substituted Allenes. *Tetrahedron*. 2015, pp 9196–9201. https://doi.org/10.1016/j.tet.2015.10.043.
(45) Cobo, A. A.; Armstrong, B. M.; Fettinger, J. C.; Franz, A. K. Catalytic Asymmetric Synthesis of Cyclopentene-Spirooxindoles Bearing Vinylsilanes Capable of Further Transformations. *Org. Lett.* **2019**, *21* (20), 8196–8200. https://doi.org/10.1021/acs.orglett.9b02852.
(46) Karmel, C.; Chen, Z.; Hartwig, J. F. Iridium-Catalyzed Silylation of C–H Bonds in Unactivated Arenes: A Sterically Encumbered Phenanthroline Ligand Accelerates Catalysis. *J. Am. Chem. Soc.* **2019**, *141* (17), 7063–7072. https://doi.org/10.1021/jacs.9b01972.
(47) Zhang, J.; Park, S.; Chang, S. Catalytic Access to Bridged Sila-N-Heterocycles from Piperidines via Cascade Sp3 and Sp2 C–Si Bond Formation. *J. Am. Chem. Soc.* **2018**, *140* (41), 13209–13213. https://doi.org/10.1021/jacs.8b08733.
(48) Koga, S.; Ueki, S.; Shimada, M.; Ishii, R.; Kurihara, Y.; Yamanoi, Y.; Yuasa, J.; Kawai, T.; Uchida, T. A.; Iwamura, M.; Nozaki, K.; Nishihara, H. Access to Chiral Silicon Centers for Application to Circularly Polarized Luminescence Materials. *J. Org. Chem.* **2017**, *82* (12), 6108–6117. https://doi.org/10.1021/acs.joc.7b00583.
(49) Lasri, J.; Aly, M. M.; Eltayeb, N. E.; Babgi, B. A. Synthesis of Symmetrical and Asymmetrical Azines from Hydrazones and/or Ferrocenecarboxaldehyde as Potential Antimicrobial–Antitumor Agents. *J. Mol. Struct.* **2018**, *1164*, 1–8. https://doi.org/https://doi.org/10.1016/j.molstruc.2018.03.030.

# Chapter 3: Studies of Carbene Insertion into Si–H Bonds of Silsesquioxane-based Silanes and Further Functionalizations*

## 3.1: Introduction

This chapter presents studies of rhodium-catalyzed carbene insertion into Si–H bonds of polyhedral oligomeric silsesquioxanes (POSSs). The Franz lab is interested in developing synthetic methodology to access functionalized silicon-containing nanomaterials. A previous lab member, Karina Targos, developed the methodology for carbene insertion into Si–H bonds of POSSs containing one and eight Si–H bonds.[1] My efforts focused on expanding the scope, synthesis of functionalized diazo compounds, and further transformations of insertion products. The results presented in this chapter were compiled in a manuscript and submitted.

POSSs have emerged as a versatile platform for the synthesis of functionalized materials. The inorganic siloxane core of POSSs, when incorporated into materials, has been noted to increase thermal and chemical stability compared to unmodified counterparts.[2,3] The organic groups on the siloxane scaffold promote solubilization of POSSs in organic solvents which enables facile processing and functionalization. Additionally, their discrete size and uniformity make them attractive platforms for design compared to silane-coated nanoparticles which are often synthesized in a distribution of sizes.[4] Cubic POSSs containing eight silicon atoms have been studied most extensively due to ease of synthesis.[5]

Several strategies have been applied to incorporate POSSs into materials with diverse applications (Figure 3.1).[6] POSSs blended with polymers have been shown to provide enhanced stiffness and stability and have been applied to low dielectric constant materials.[7] Alternative strategies focus on covalent linkages with the surrounding organic groups, which can be used to graft other molecules, polymers. Given the cubic shape, several different forms of connectivity can be accessed (Figure 3.1). Pendant connectivity of POSSs to a polymer has been used for solid-state batteries with increased thermal stability.[8] End-to-end connectivity of POSSs with a covalent linker has been used for hybrid-hydrogels for drug delivery systems.[9] Cross-linked structures of POSSs have been used for liquid crystal polymers for self-assembly.[10]

* Reproduced in part with permission from: J. R. Jagannathan, K. Targos, A. Franz, *Angew. Chemie Int. Ed.* **2021**, *n/a*, DOI: https://doi.org/10.1002/anie.202110417. Copyright 2021 John Wiley and Sons.

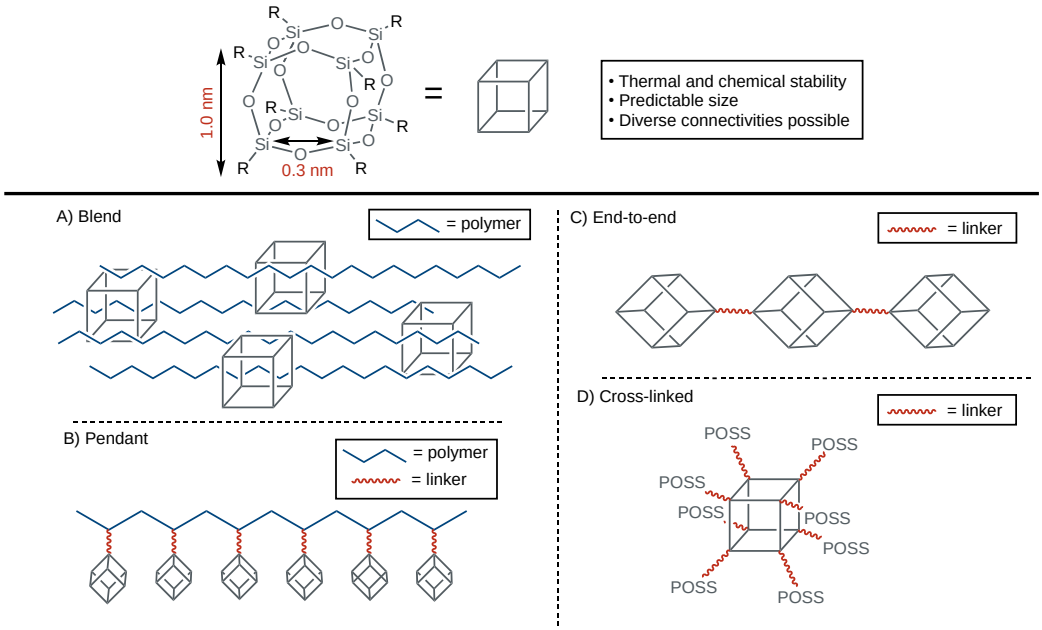


**Figure 3.1**. Methods to incorporate POSSs into materials include A) blends of POSSs and polymers, B) pendant connectivity to polymers, C) end-to-end connectivity of POSSs with covalent linkers, and D) cross-linked networks of POSSs with linkers.

Synthesis of POSSs with discrete, well-defined reactive sites is crucial for control of the microstructure of materials. The formation of the cubic siloxane core is substrate dependent and requires harsh conditions (Figure 3.2A). Alternative strategies are used to functionalize POSSs with the siloxane core assembled.[11] The state-of-the-art strategy is to derivatize POSSs with Si–H bonds using Si–C bond formation reactions (Figure 3.2B).[12] POSSs containing one, three, and eight Si–H bonds have been accessed in order to vary both the quantity and connectivity possible. POSSs **3.1a-c** are accessed from silanol-containing POSSs with the addition of chlorosilanes and base.[13]

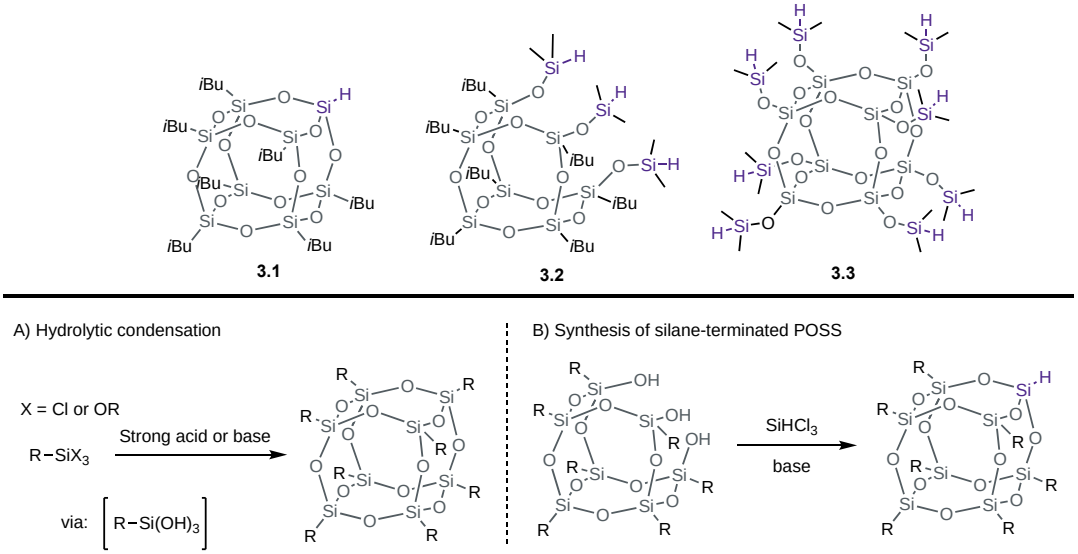


**Figure 3.2.** Strategies for synthesis of functionalized POSSs including A) hydrolytic condensation of alkoxy or chlorosilanes, B) synthesis of silane-containing POSSs.

Several Si–C bond formation reactions have been explored with POSSs to access functional materials (Figure 3.3).[14] Some challenges with POSS functionalization include the steric effects from the POSS cage or subsequent reactions with POSSs containing multiple Si–H bonds. Hydrosilylation of olefins is most commonly used in polymer science and materials science to functionalize POSSs because it is robust, scalable, and amenable to POSSs multiple Si–H bonds (Figure 3.3).[15] Additionally, Si–C arylation has been briefly explored to access aryl-alkyl POSSs.[16,17] However, with only two transformations known to form Si–C bonds with POSS-silanes, the scope of functionalized nanomaterials remains limited. Diversifying the applications of POSSs in materials science ultimately requires the development of new synthetic methods about the organic groups.

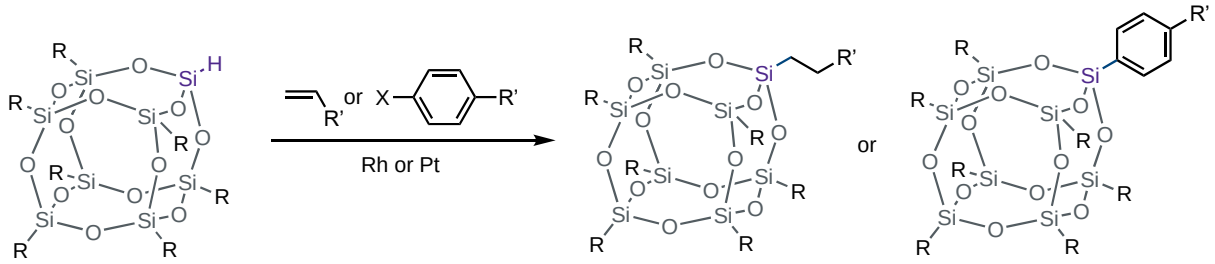


**Figure 3.3.** Strategies for synthesis of functionalized POSSs containing Si–H bonds.

Carbene insertion into Si–H bonds is an attractive transformation for POSS functionalization, given the potential for complex structures from simple building blocks.[18] Diazo compounds are versatile intermediates with the potential for convergent syntheses and have a rich

methodology to access architecturally diverse molecules.[19] A plethora of diazo compounds can be accessed in a single step from commercially available reagents. Carbene insertion can be stereoselective and several methods are known to produce carbon and silicon-centered chirality.[20,21] Several metals are known to catalyze carbene insertion into Si–H bonds, including Rh(II),[18] Cu(I),[22] Fe(II)[23] and Ag(I).[24]

Carbene insertion into Si–H bonds of small-molecule siloxanes has been demonstrated by Vincente and coworkers using Cu(I) catalysis with aryl(ester)diazo compounds (Figure 3.4).[22] Tetramine ligand **3.5** was found to limit dimerization of **3.4**, although slow addition of **3.4** was conducted for all entries. The authors showed that siloxy and bis-siloxy-containing siloxanes formed insertion products **3.6a** and **3.6b** in good yield (82% and 85%, respectively) using diazo compound **3.2** as the limiting reagent. Siloxanes with 2 Si–H bonds were reacted to produce single and double insertion products **3.6c** and **3.6d** in 95% and 79% yield, respectively, using the silane as the limiting reagent for **3.4d**. The double insertion product **3.4d** was isolated as a mixture of diastereomers. These results highlight that siloxanes are amenable to Si–H insertion reactions, and subsequent insertions are possible when using the diazo compound in excess.

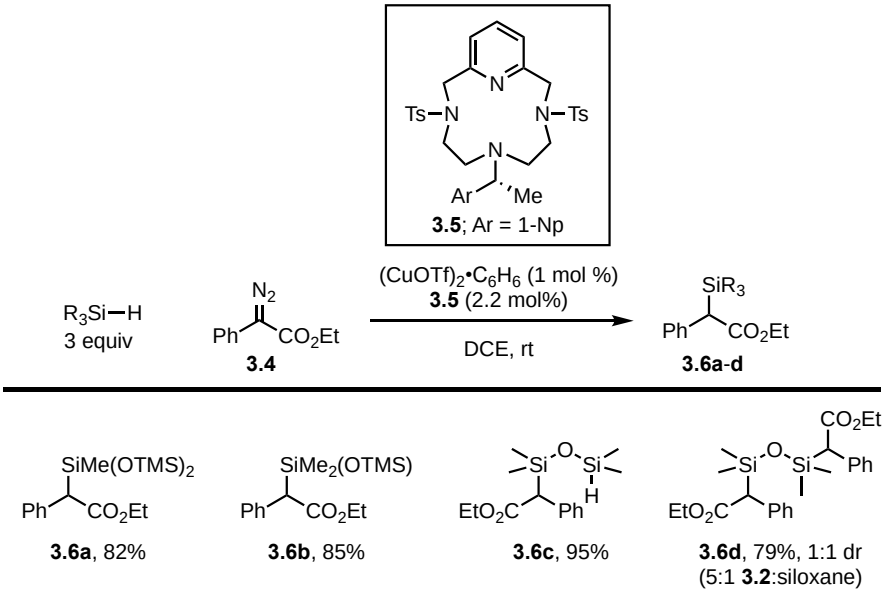


**Figure 3.4.** Vincente's Cu(I)-catalyzed carbene insertion into Si–H bonds using siloxanes.

A bottleneck in POSS functionalization is the number of transformations that have been demonstrated to form Si–C bonds with POSS-silanes. The success of carbene insertion into Si–H bonds of siloxanes inspired efforts to functionalized POSSs (Figure 3.5 A). Vincente's results highlight that siloxy substitution and multiple Si–H bonds are tolerated in the reaction with

modified conditions. Ultimately, we envisioned a study of carbene insertion into Si–H bonds of POSSs. POSSs with one, three and eight Si–H bonds (**3.2** and **3.3**) would be to be investigated. Aryl(ester) diazo compounds (**3.7**) serve as carbene precursors as they have ideal reactivity and two orthogonal functional handles for derivatization.[18] Selective insertions of POSS are predicated to occur with minimal competitive C–H insertion considering C–H bonds are less reactive to than Si–H bonds.[25] Additional transformations of insertion products (**3.8**) will be explored on both the aryl ring (to biaryl **3.9**) and ester (to amide **3.10**) to demonstrate precedent for inclusion into materials.

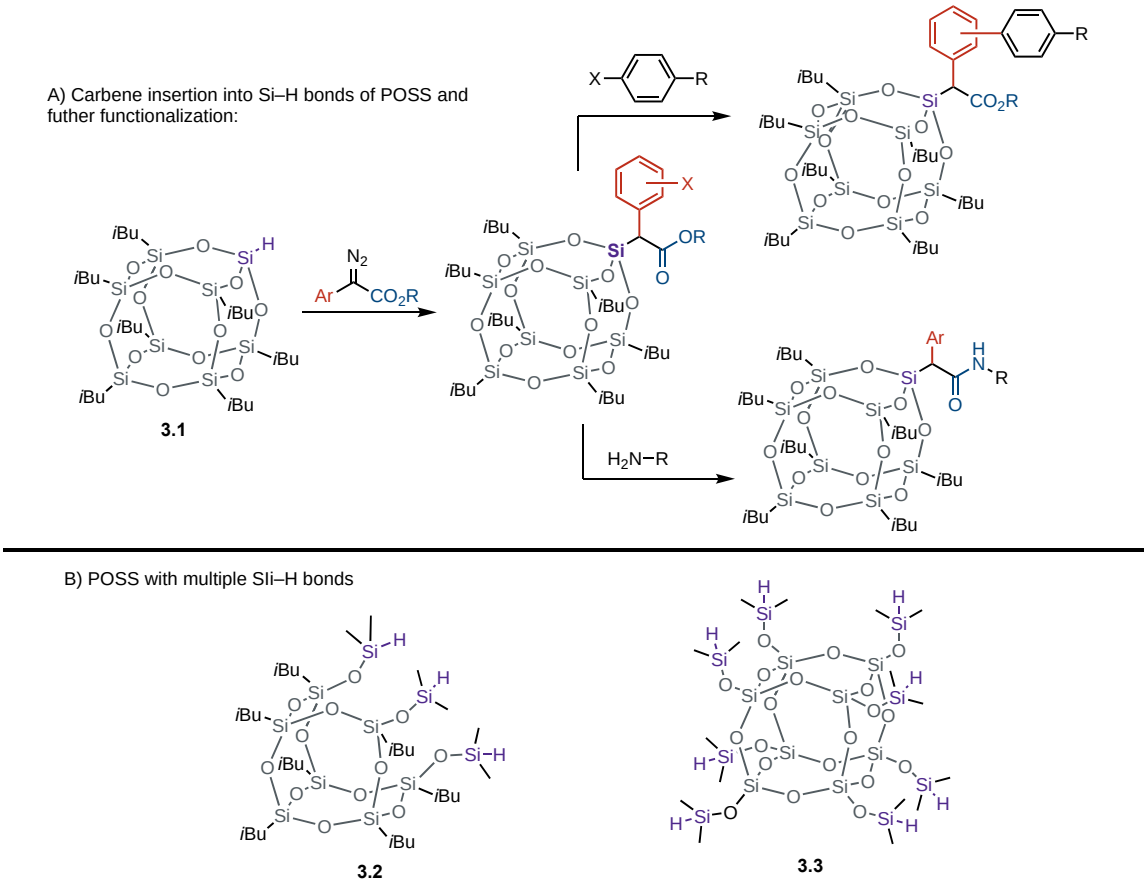


**Figure 3.5.** A) Project overview. B) POSS with multiple Si–H bonds to be explored.

## 3.2: Synthesis of Aryl(ester) Diazo Compounds

Aryl(ester) diazo compounds were synthesized to examine structure-activity relationships and install useful functionality for subsequent transformations. Diazo compounds utilized in this

work were synthesized from aryl acetic acid esters and tosyl azide as a diazo transfer reagent (Figure 3.6).[26] Using DBU as a base in MeCN, diazo compounds **3.7a-e** were synthesized in 50-95% yields. Diazo products ranged from oils to solids and decomposed at room temperature and were stored at -20 ˚C in the absence of light.

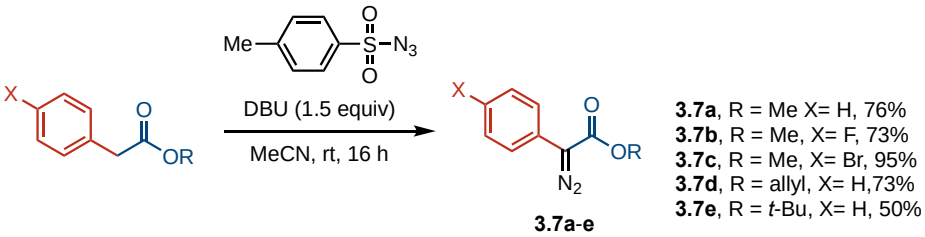


**Figure 3.6**. Synthesis of aryl(ester)diazo compounds.

## 3.3: Synthesis of POSS-silanes

POSSs with one, three, and eight Si–H bonds were studied to showcase the methodology (Figure 3.7). Additionally, there are varying ratios of C–H to Si–H bonds between POSSs, allowing for studies on competitive C–H insertion. POSSs **3.2** and **3.11** can be synthesized in one step from commercially available reagents and POSS **3.3** is available for purchase (at the time of this work) at Hybridplastics.com.

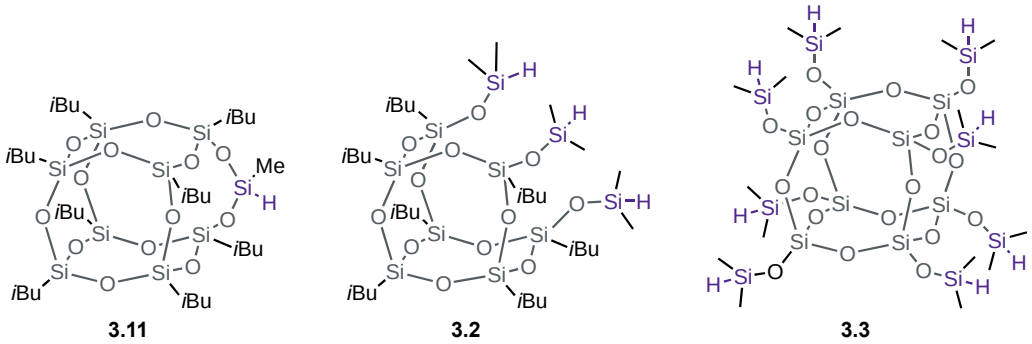


**Figure 3.7**. POSS-silanes studied in this chapter.

POSS **3.11** was synthesized by Karina Targos from POSS-diol **3.12** and dichloromethylsilane.[1] Using $Et_3N$ as the base, POSS **3.11** was isolated in 89% yield and the reaction could be performed on up to multi-gram scale (Figure 3.8). POSS **3.11** was found to be stable to air, moisture, and light for greater than 1 year. The Si–H bond is more readily accessible than previously studied POSSs with one Si–H bond,[27] which we expect to facilitate single carbene insertions with minimal competitive C–H insertion.

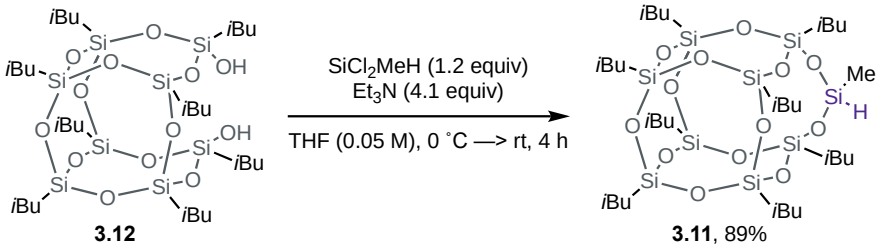


**Figure 3.8**. Synthesis of novel POSS **3.11**.

POSSs with three Si–H bonds are accessed from POSS-triols and chlorosilanes.[27] POSS **3.2** has been previously used for OLEDs,[27] three-dimensional emulsifiers,[28] and optical materials.[29] POSS **3.2** was synthesized from POSS-triol **3.13**, chlorodimethylsilane and Hünig's base in THF in 25% yield after trituration (Figure 3.9).

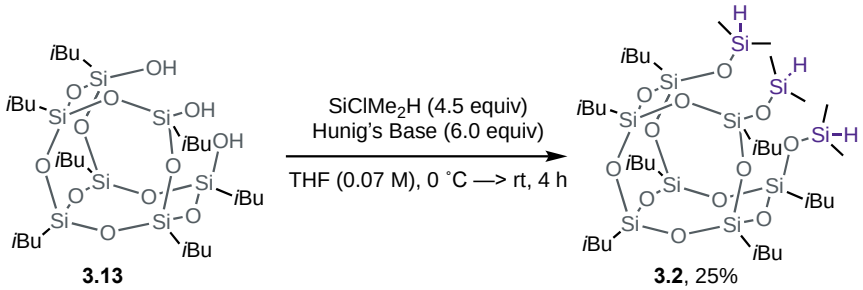


**Figure 3.9**. Synthesis of known POSS **3.2**.

## 3.4: Studies of Carbene insertion into Si–H bonds with POSS Containing One Si–H bond

Carbene insertion into the Si–H bond of **3.11** with **3.7a** was evaluated with metal catalysts (Table 3.1).[1] Optimization focused on Rh(II) and Cu(I) complexes as catalysts, using one equivalent of diazo compound **3.7a** in $CH_2Cl_2$. The addition of $MgSO_4$ is used to limit Si–H hydrolysis, which is known to occur with Rh(II) complexes.[30] The diazo compound was added over a period of one hour using a syringe pump to limit side reactions between diazo compounds.[18] Rh(II) sources provided superior reactivity to produce POSS **3.14a** (Table 3.1 entry 1-4), although incomplete Si–H conversion was observed. Several catalysts, including bis[rhodium(α,α,α′,α′-tetramethyl-1,3-benzenedipropionic acid)] ($Rh_2(esp)_2$), $Rh_2(Mes)_4$, and $Rh_2(OAc)_4$ provided similar reactivity, and ultimately $Rh_2(OAc)_4$ was chosen because it is commercially available. Increasing equivalents of diazo compound **3.7a** led to complete conversion of the Si–H bond of **3.11** and POSS **3.14a** was isolated in 75% yield (entry 7). Control experiments without $MgSO_4$ provide slightly reduced yields (Table 3.1 entry 8). Catalyst loading experiments highlight the

activity of $Rh_2(OAc)_4$ to produce **3.14a** down to 0.1 mol% loading (Table 3.1, entries 9-11). These conditions were applied to diazo compounds **3.7c**-**3.7e** to investigate which substitution patterns are tolerated in the reaction.

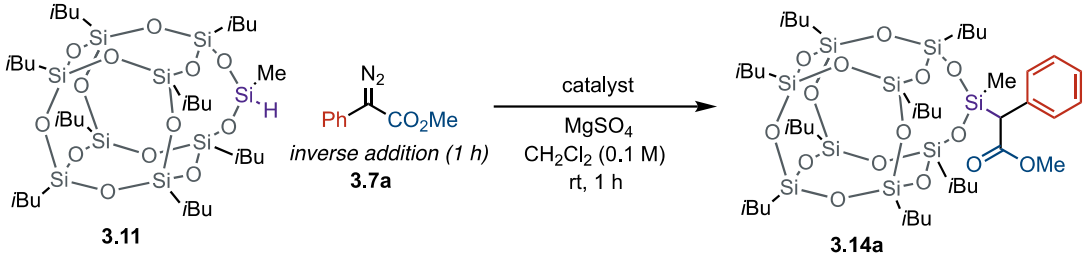


**Table 3.1.** Conditions tested for insertion of diazo compound **3.7a** into Si–H bond of POSS **3.11**.

| Entry | Catalyst (mol %) | **3.7a**: **3.11** | Si–H % Conversion | Yield **3.14a**[b] |
|---|---|---|---|---|
| 1 | $Rh_2(Mes)_4$ (1) | 1:1 | 46 | 43 |
| 2 | $Rh_2(TFA)_4$ (1) | 1:1 | 34 | 31 |
| 3 | $Rh_2(esp)_2$ (1) | 1:1 | 44 | 43 |
| 4 | $Cu(OTf)_2$ (10) | 2:1 | ND | 15 |
| 5 | $Cu[MeCN]_4PF_6$ (10) | 2:1 | ND | 22 |
| 6 | $Rh_2(OAc)_4$ (1) | 1:1 | 41 | 44 |
| 7 | $Rh_2(OAc)_4$ (1) | 2:1 | >95 | 85 (75[c]) |
| 8[d] | $Rh_2(OAc)_4$ (1) | 2:1 | >95 | 75 |
| 9 | $Rh_2(OAc)_4$ (0.5) | 2:1 | >95 | 84 |
| 10 | $Rh_2(OAc)_4$ (0.1) | 2:1 | >95 | 86 |
| 11 | $Rh_2(OAc)_4$ (0.01) | 2:1 | ND | 5 |

[a] Determined using $^1H$ NMR spectroscopy. [b] 0.1 mmol scale **3.11**, NMR yield using Ph-TMS as an internal standard. [c] Isolated yield. [d] No $MgSO_4$ added.

Diazo compounds containing aryl bromides, alkene functional handles, and labile protecting groups were studied with POSS **3.11** (Figure 3.9). POSS **3.11** was subjected to optimized conditions with diazo compounds **3.7c**-**3.7e** to produce **3.14b**-**3.14d** in 73-83% yield. Scaling the reaction to 1 mmol of POSS **3.11** (0.93 g) led to comparable yield using a 3-hour slow addition of diazo **3.7c** and **3.7e** (Figure 3.10). POSS compounds were found to be stable to air, light and moisture for weeks. Additional substrates were also explored by Karina Targos as part of a manuscript that was submitted.[1]

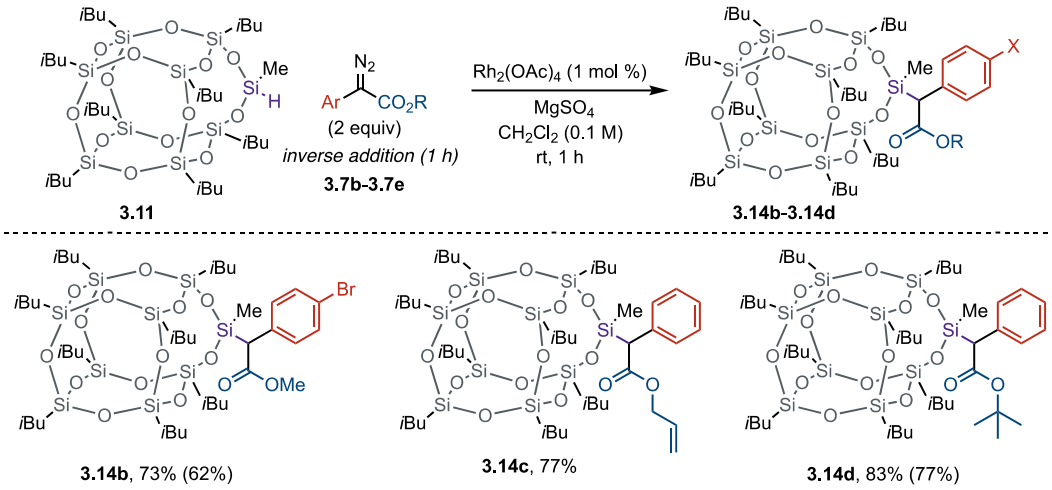


**Figure 3.10**. Scope of diazo compounds with valuable functionality. For reactions, 0.1 mmol of POSS **3.11** was used in $CH_2Cl_2$ (1 mL total). Yields in parenthesis indicate 1 mmol of POSS **3.11** (0.93 g) was used with a 3-hour slow addition of diazo compound in $CH_2Cl_2$ (10 mL total).

## 3.5: Studies of Carbene Insertion into Si–H Bonds with POSS Containing Three Si–H Bonds

POSS **3.2** with three Si–H bonds was subjected to optimized conditions to expand the POSS-silanes amenable with this method. A 3-hour slow addition of diazo compound was used for all trials. With diazo compound **3.7b** complete consumption of **3.2** was observed using two equivalents of diazo compound per Si–H bond (Figure 3.11). The product **3.15a** was isolated in 52% yield with alkene **3.16a** formed from diazo decomposition.[18] With one equivalent of diazo compound per Si–H bond, pure POSS **3.15a** was isolated in 45% yield. With diazo compound **3.7c** complete consumption of **3.2** was observed using two equivalents of diazo compound per Si–H bond (Figure 3.11). The product **3.15b** was isolated in 71% yield with alkene **3.16b** formed from diazo decomposition.[18] With one equivalent of diazo compound per Si–H bond, pure POSS **3.15b** was isolated in 49% yield. With diazo **3.7e** and **3.7a**, side products **3.16c** and **3.16d** were successfully separated by trituration and flash chromatography (Figure 3.11). Using two equivalents of a diazo compound, POSS **3.15c** and **3.15d** were isolated in 45% and 44% yield respectively.

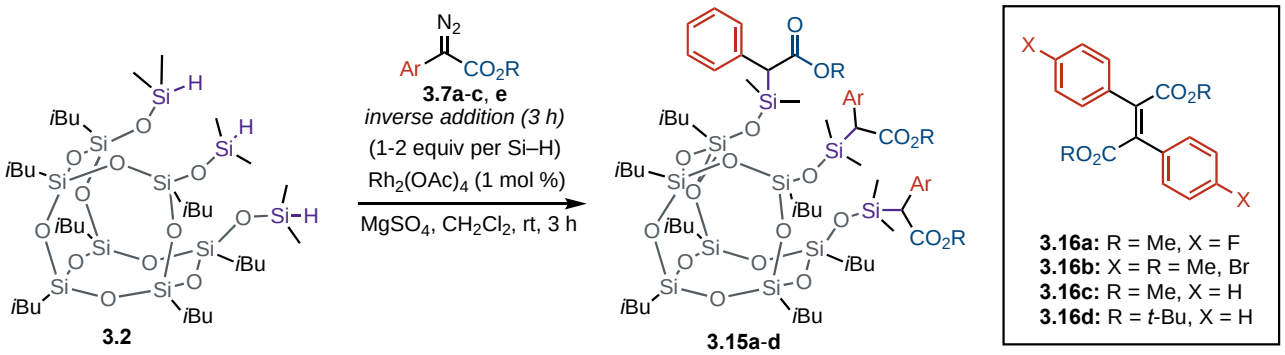


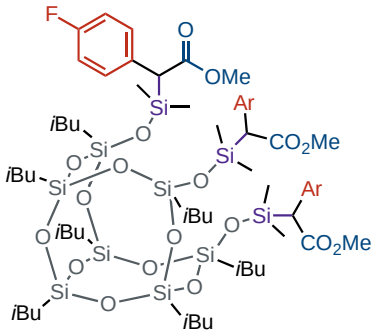

**3.15a**
(2:1 **3.7b**:Si–H); 52% (1:1 with **3.16a**)
(1:1 **3.7b**:Si–H); 45%

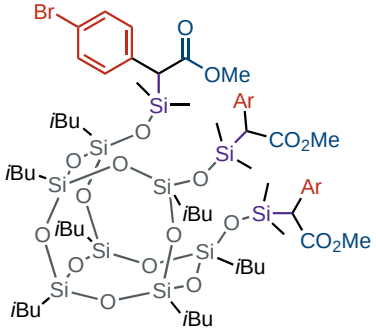

**3.15b**
(2:1 **3.7c**:Si–H) 71% (6:1 with **3.16b**)
(1:1 **3.7c**:Si–H) 49%

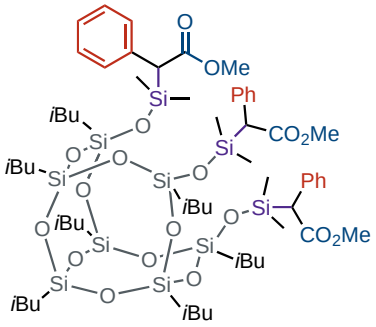

**3.15c**
(2:1 **3.7a**: Si–H); 45%

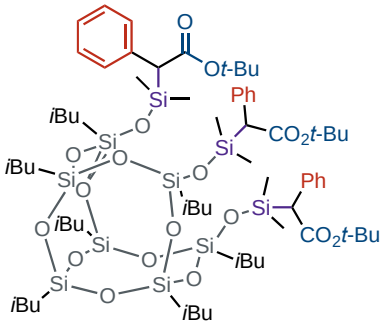

**3.15d**
(2:1 **3.7e**: Si–H); 45%

**Figure 3.11.** Carbene insertion into Si–H bonds of **3.2** using diazo compounds **3.7a-c** and **3.7e** and 0.1 mmol of POSS **3.2** was used for all trials in $CH_2Cl_2$ (1 mL total).

In general, reduced yields of products **3.15a-d** are attributed to several causes. Coelution of side products **3.16a-d** limits the total equivalents of a diazo compound that can be added in the reaction. Incomplete conversion of Si–H bonds was observed using one equivalent of diazo compound **3.7b** and **3.7c**. Additionally, it is noted that POSS **3.2** has 63 C–H bonds which compete with Si–H bonds despite higher reactivity.[25] I routinely observed products resulting from carbene

insertion into C–H bonds using $^{1}$H NMR spectroscopy. No evidence of diastereomers or diastereoselectivity was detected using $^{1}$H or $^{19}$F NMR spectroscopy for POSS **3.15a-d**.

## 3.6: Studies of Carbene Insertion into Si–H Bonds with POSS Containing Eight Si–H Bonds

POSS with eight Si–H bonds were examined to access global insertion products. POSS **3.3** has been used extensively to access materials for applications such as optoelectronic materials,[14] supramolecular dendritic networks,[31] and hybrid polymer inorganic nanocomposites.[32] Hydrosilylation is the typical transformation utilized for POSS **3.3**.

The optimization of carbene insertion into the Si–H bonds of **3.3** was completed by Karina Targos.[1] Initial conditions screened were performed using 1 mol % $Rh_2(OAc)_4$ in $CH_2Cl_2$ a 3-hour slow addition of diazo compound **3.7a**. Using five equivalents of **3.7a** relative to **3.3**, 50% conversion was observed but the yield could not accurately be determined. Using 8.5 equivalents of **3.7a**, POSS **3.17a** was synthesized in 31% yield and incomplete conversion was observed. Increasing to 10 equivalents of **3.7a** led to complete conversion of the Si–H bonds of **3.3** and POSS **3.17a** was isolated in 43% yield.

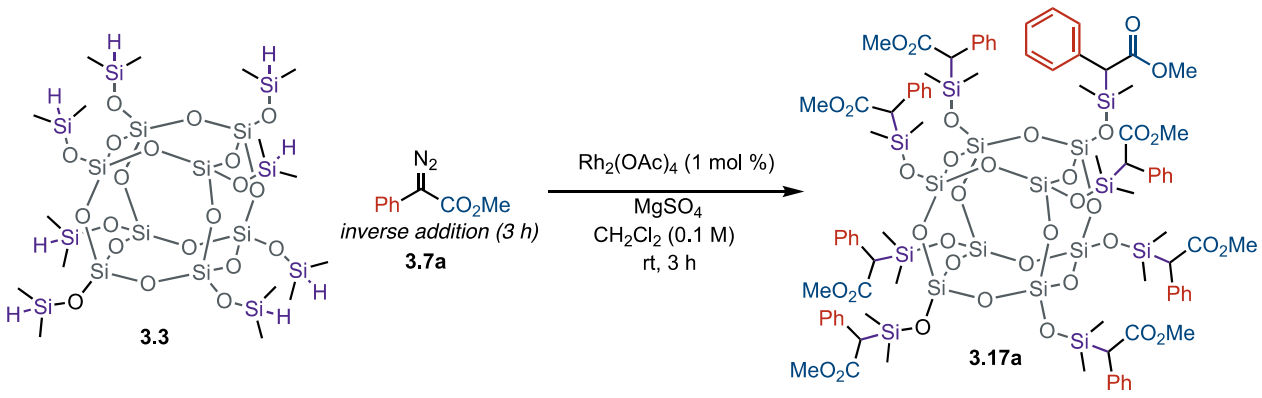


**Table 3.2.** Conditions tested for insertion of diazo compound **3.7a** into Si-H of POSS **3.3**.

| Entry | **3.7a**: **3.3** | Si–H % Conversion | Yield **3.17a**[b] |
|---|---|---|---|
| 1 | 5:1 | 50 | - |
| 2 | 8.5:1 | 83 | 31 |
| 3 | 10:1 | >95 | 43 (isolated) |

[a] Determined using $^{1}$H NMR spectroscopy. [b] 0.1 mmol **3.3**, NMR yield using Ph-TMS as an internal standard.

With diazo compound **3.7e**, optimized conditions were used to isolate POSS **3.17b** in 85% yield after flash chromatography (Figure 3.12). Karina Targos demonstrated several other substitutions on the aryl ring and found that electron-rich diazo compounds required higher

equivalents to access global insertion products. The reaction could also be scaled up to 1 mmol of **3.3** (1.01 g) with comparable yields.[1] No evidence of diastereomers or diastereoselectivity was detected using $^1$H NMR spectroscopy for POSS **3.17b**.

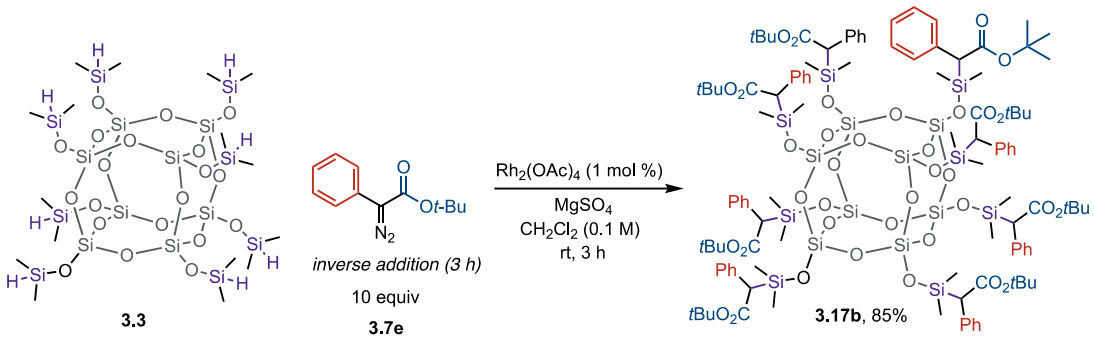


**Figure 3.12**. Carbene insertion into Si–H bonds of **3.3** using diazo compound **3.7e**.

## 3.7: Synthesis of Functionalized Diazo Compounds and Subsequent Carbene Insertion into Si–H Bonds with POSS 3.11

Diazo compounds with amides, photoswitches, fluorinated groups and BODIPY fluorophores were synthesized and reacted with POSS **3.11**. Novel diazo compounds containing fluorinated groups and BODIPY fluorophores were synthesized to showcase the versatility of the chemistry of diazo compounds.

### 3.7.1: Synthesis and Studies of Amide-containing Diazo Compounds

Amides are commonly found in POSS-based materials used for drug delivery,[33] wettable thermoplastics,[34] and photoswitch conjugates.[35] Demonstrating a successful transformation using an amide-containing diazo compound would allow for one-step access to POSS-amide products.

Diazo compound **3.20** was synthesized in two steps using a known procedure from phenylacetic acid **3.18.** Amide coupling conditions with chloro-*N*, *N*, *N'*, *N'*-tetramethylformamidinium hexafluorophosphate (TCFH) and *N*-methylaniline formed product **3.19**, which was isolated in 42% yield (Figure 3.13).[36] Diazo transfer using $TsN_3$ and DBU in MeCN at 35 ˚C formed diazo compound **3.20**, which was isolated in 10% yield. The starting material **3.19** was recovered in 85% yield based on initial moles. Formation of an enolate is needed to begin diazo transfer, so the reduced acidity of amides compared to esters may account for the rate discrepancy.[26]

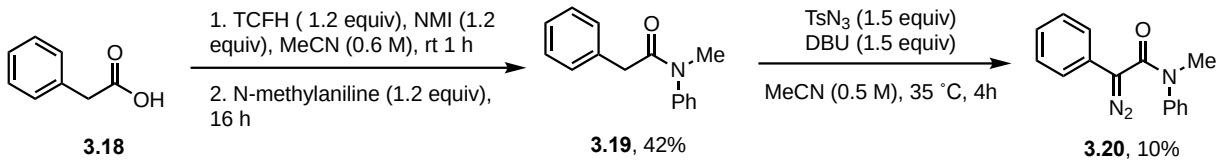


**Figure 3.13**. Synthesis of diazo compound **3.17**.

The reaction of diazo compound **3.20** was tested with POSS **3.11** using optimized conditions (2 equivalents **3.20**) with a 1-hour slow addition. Product **3.21** was observed in only 10% yield using $^{1}$H NMR spectroscopy. The major amide-containing product was **3.22**, isolated in 60% yield. Repeating the reaction using a 3-hour slow addition did not improve the yield of **3.21** and the major product was **3.22**. Previous reports with diazo compound **3.20** note the tendency to cyclize via intramolecular C–H insertion.[37,38] Despite the higher reactivity of Si–H bonds to C–H bonds,[39] the proximity due to an intramolecular C–H bond is more favorable. Substitution of the amide to methyl groups would limit intramolecular C–H insertion but limits scope of possible amide-containing POSSs.

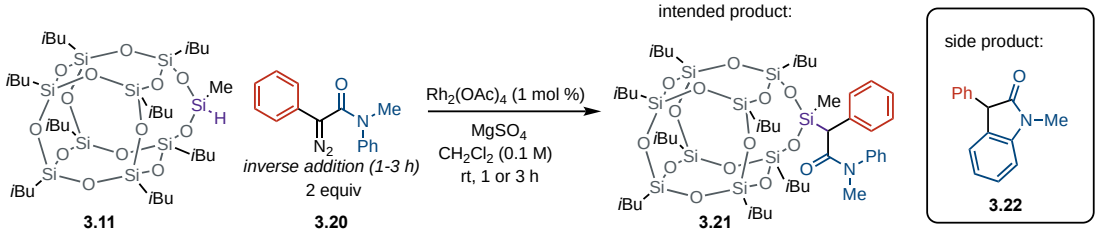


**Table 3.3.** Conditions for insertion of diazo compound **3.17** into Si–H bond of POSS **3.11**.

| Entry | Slow addition (h) | **3.20** conversion | Yield **3.21**[a] | Yield **3.22**[b] |
|---|---|---|---|---|
| 1 | 1 | >95% | 10 | 60 |
| 2 | 3 | >95% | 7 | 55 |

[a] 0.05 mmol **3.11**, NMR yield using Ph-TMS as an internal standard. [b] NMR yield using Ph-TMS as an internal standard.

Isatin-based diazo compound **3.25** was synthesized based on the hypothesis that competitive C–H insertion would not occur. Isatin-based diazo compound **3.25** was accessed from isatin (**3.23**) . Methylation in the presence of MeI and $K_2CO_3$ to formed **3.24** in 95% yield (Figure 3.14). Isatin **3.24** was subjected to hydrazone formation in the presence of tosylhydrazine in THF followed by aqueous NaOH to access diazo compound **3.25** in 45% yield.

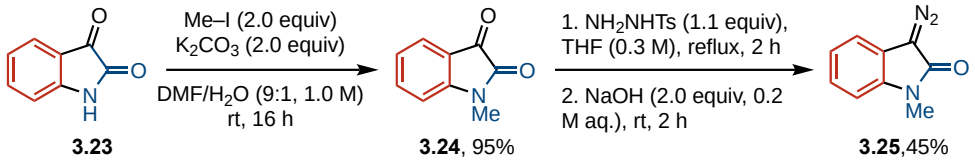


**Figure 3.14**. Synthesis of diazo compound **3.25**

Diazo compound **3.25** was subjected to optimized conditions with POSS **3.11** (2 equivalents of **3.25**) over a 1-hour slow addition (Figure 3.15). Diazo compound **3.25** was observed to build up in the flask during the slow addition, suggesting poor conversion; starting materials were recovered. Performing a slow addition for 3 hours led to recovery of POSS **3.11** and diazo compound **3.25** with no observable product (**3.26**) formation. A hypothesis for the poor reactivity observed can be explained with the resonance forms of the metal carbenoid intermediate **3.27** (Figure 3.15). Donation of electron density from the vinylogous nitrogen could stabilize the carbene, reducing reactivity.

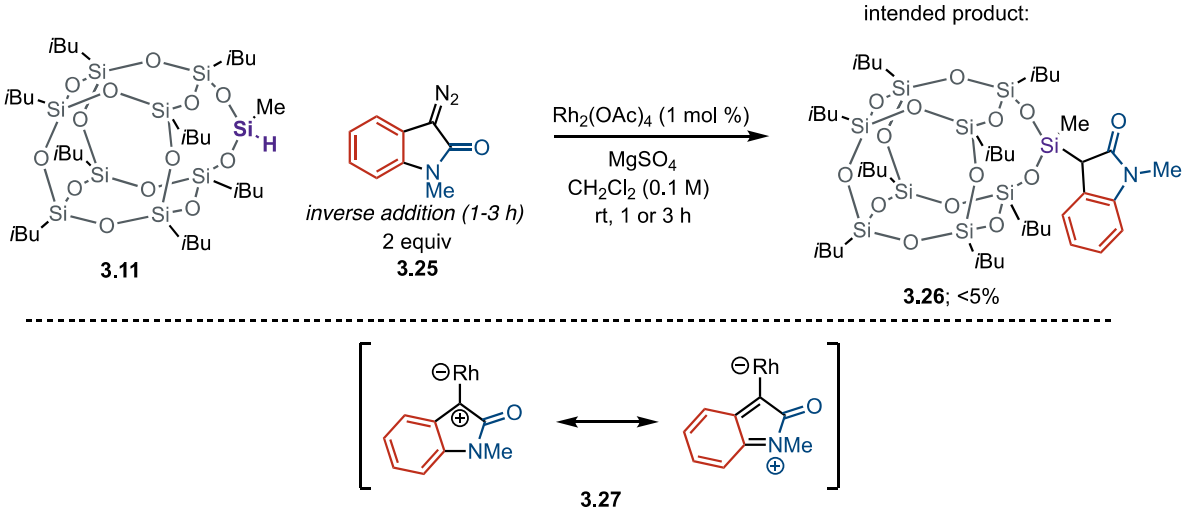


**Figure 3.15**. Studies of carbene insertion with diazo **3.25** and resonance forms of metal-carbenoid **3.27** formed with diazo **3.25.**

## 3.7.2: Synthesis and Studies of a Photoswitch-containing Diazo Compound

Photoswitches are molecules that absorb light and undergo reversible isomerization resulting in changes to the structure or properties of the molecule.[40] POSS-based photoswitches containing azobeneznes have been synthesized previoulsy and notable changes in isomerization half-life are observed compared to POSS-free counterparts.[41] Azobenzene-based diazo compounds were explored because several are known in the literature.

Diazo compound **3.34** was accessed using a previously reported procedure starting from glycine-methyl ester **3.31** and nitrosobenzene **3.28** (Figure 3.16).[42] Nitrosobenzene **3.28** was subjected to condensation conditions with aniline **3.29** in $CH_2Cl_2$/AcOH, forming azobenzene **3.30** in 85% yield. Glycine ester **3.31** was oxidized to methyldiazoacetate **3.32** using $NaNO_2$ at 0 ˚C. The diazo compound was quickly subjected to TFAA and pyridine to access coupling partner **3.33**, isolated in 47% yield over two steps. Cross-coupling of azobenzene **3.30** and diazo compound **3.33** in the presence of Pd(0) and base formed diazo compound **3.34** and was isolated in 60% yield.

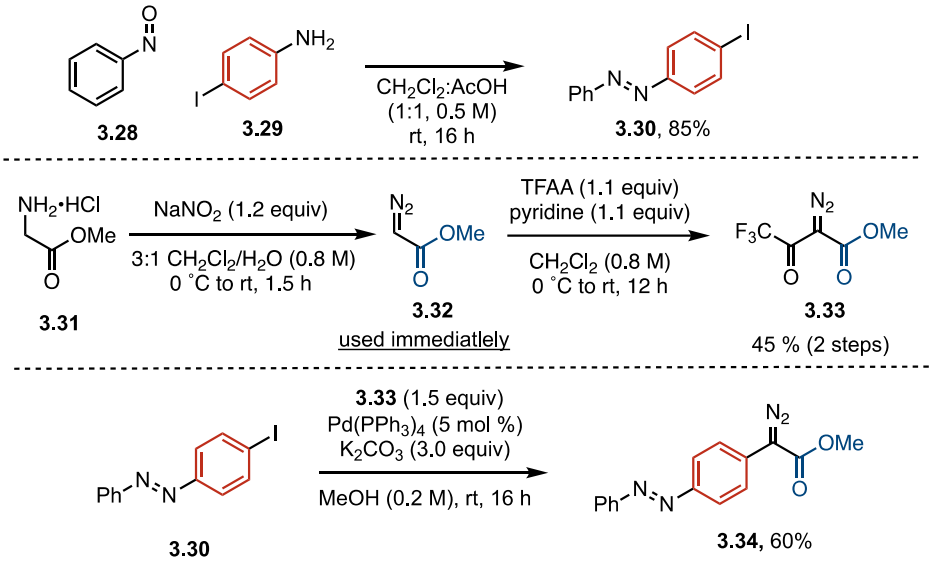


**Figure 3.16**. Synthesis of diazo compound **3.34**.

Diazo compound **3.34** was subjected to carbene insertion conditions with **3.11** using two equivalents of diazo compound. Several Rh(II) sources were screened, including $Rh_2(OAc)_4$, $Rh_2(TFA)_4$, and $Rh_2(esp)_2$. Full conversion of the diazo compound was observed by $^1H$ NMR and TLC analysis after 12 hours (Table 3.4, entries 1-3). For all sources screened, **3.35** was observed in less than 5% yield. Electron-donating effects from the azobenzene group are prposed to account for reduced reactivity towards Si–H insertion.[43]

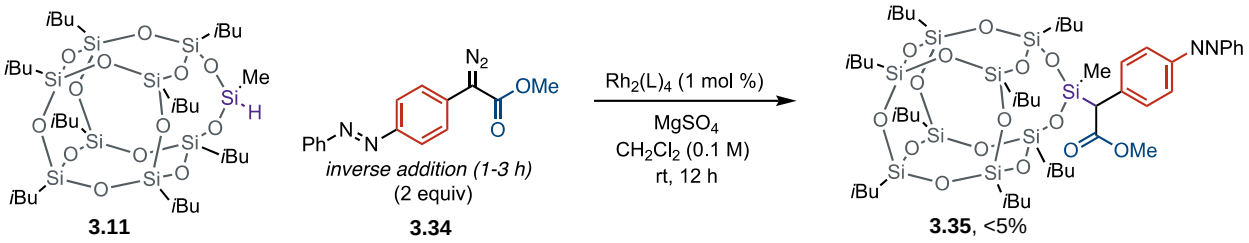


**3.11** **3.34** **3.35**, <5%

**Table 3.4.** Conditions for insertion of diazo compound **3.34** into Si–H bond of POSS **3.11.**

| Entry | Catalyst | **3.30** Conversion | Yield **3.31**[b] |
|---|---|---|---|
| 1 | $Rh_2(OAc)_4$ | >95 | 0 |
| 2 | $Rh_2(TFA)_4$ | >95 | 0 |
| 3 | $Rh_2(esp)_2$ | >95 | 0 |

[a]0.05 mmol **3.11** used, NMR yield using Ph-TMS as an internal standard.

### 3.7.3: Synthesis and Studies of a Novel BODIPY-containing Diazo Compound

Boron-dipyrromethene (BODIPY) is a commonly used fluorophore with applications in cellular imaging,[44] sensors[45] and mechanochromophoric materials.[46] BODIPY-based POSS compounds have been previously studied as photoemissive materials[47] and to probe POSS permeation in cellular membranes.[48] BODIPY-POSS compounds have been synthesized using Heck reactions from vinyl-containing POSSs, so carbene insertion provides a complementary route to access this functionality with a remaining ester for further functionalization. BODIPY-based diazo compounds such as **3.39** were unknown prior to this work. The BODIPY was placed at the 4-position of the aryl ring on the diazo compound to limit steric hinderance during the insertion process.

Diazo compound **3.39** was accessed using a convergent synthetic scheme similar to photoswitch **3.34** (Figure 3.17).[42] BODIPY **3.39** was accessed from benzoyl chloride **3.36** and pyrrole **3.37**, isolated in 14% yield over 2 steps. Cross-coupling of **3.33** and BODIPY **3.38** led to BODIPY **3.39** which was isolated in 73% yield.

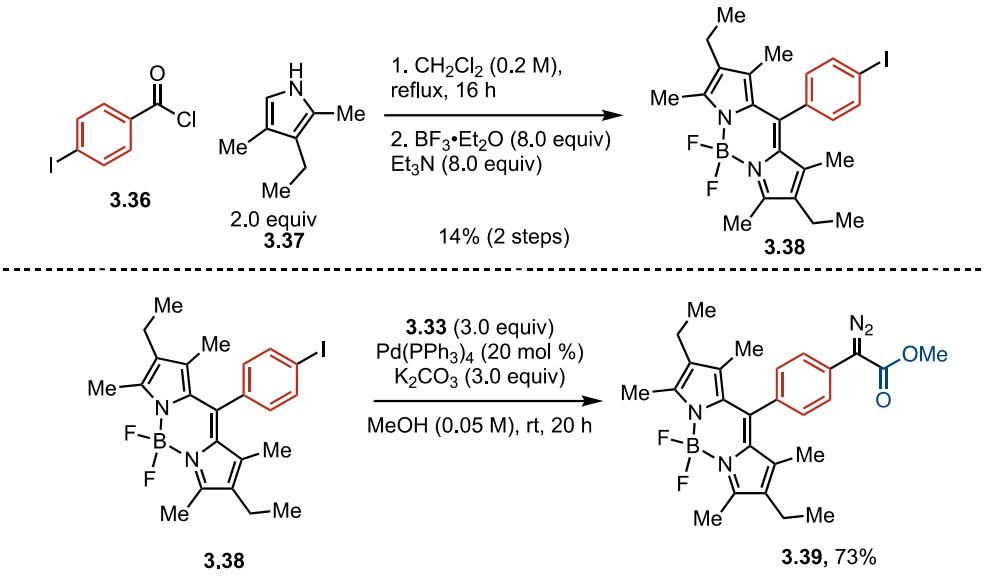


**Figure 3.17**: Synthesis of BODIPY-containing diazo compound **3.39**.

BODIPY-diazo compound **3.39** was reacted with POSS **3.11** using 1 mol % $Rh_2(OAc)_4$ to access insertion product **3.40** (Table 3.5). Diazo compound **3.39** proved unreactive with **3.11** using the diazo compound in excess, although complete conversion was observed using TLC and $^1$H NMR analysis (Table 3.5, entry 1). Competitive insertion into C–H bonds was observed using $^1$H NMR spectroscopy, suggesting steric effects are significant in limiting Si–H insertion. Extending the slow addition time to 6 or 12 hours did not increase the yield (Table 3.5, entries 2 and 3). With BODIPY **3.39** as the limiting reagent and 5 equivalents of POSS **3.11**, product **3.40** was isolated in 16% yield (entry 4). POSS **3.40** exhibits strong fluorescence at 545 nm with a 14 nm Stokes shift similar to previous BODIPYs (Figure 3.18).[49] Overall, diazo compound **3.39** undergoes carbene insertion processes, but the steric hinderance about POSS limits the yield of Si–H insertion.

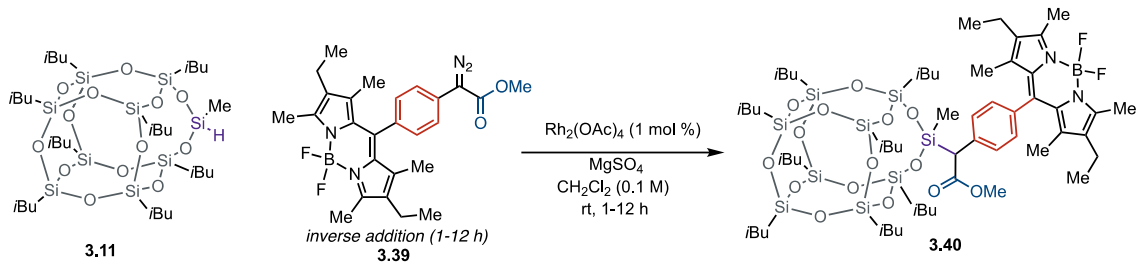


**Table 3.5.** Conditions for insertion of diazo compound **3.35** into Si–H bond of POSS **3.11**.

| Entry | **3.39** : **3.11** | Slow addition (h) | **3.39** Conversion[a] | Yield **3.40**[b] |
|---|---|---|---|---|
| 1 | 2:1 | 3 | >95 | 0 |
| 2 | 2:1 | 6 | >95 | 0 |
| 3 | 2:1 | 12 | >95 | 0 |
| 4 | 1:5 | 3 | >95 | 16 (isolated) |

[a] Determined using $^{1}$H NMR spectroscopy and TLC. [b] 0.05 mmol scale **3.39**, NMR yield using Ph-TMS as an internal standard.

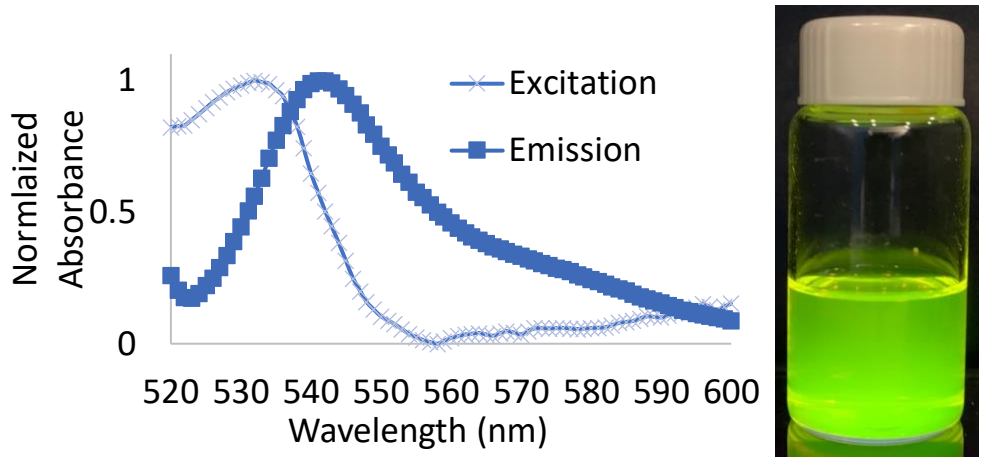


**Figure 3.18.** Normalized excitation and emission plots of POSS-BODIPY **3.40**. Data was collected at 3.1 x $10^{-7}$ M in EtOH to limit self-quenching.

## 3.7.4: Synthesis and Studies of a Novel Fluorinated Diazo Compound

Fluorinated groups on POSSs have shown promise for super-oleophobic coatings,[50] hydrophobic coatings,[51] and low-surface energy materials.[52] Previous methods to access fluorinated POSS include direct condensation of fluorinated alkoxysilanes,[50] hydrosilylation of fluorinated alkenes with POSS-silanes[51] and corner-capping of POSS-triols with fluorinated trichlorosilanes.[52] The use of carbene insertion into Si–H bonds to install fluorinated groups would provide a complementary route to methods that have been developed.

Fluorinated diazo compound **3.43** was accessed using diazo transfer from ester **3.42** (Figure 3.19). Alcohol **3.41** was subjected to esterification with phenylacetic acid **3.18** using TBTU in DMF, forming ester **3.42** which was isolated in 65% yield.[53] Ester **3.42** was subjected to diazo

transfer conditions using $TsN_3$ and DBU in MeCN, accessing diazo **3.43** which was isolated in 30% yield. Yields were typically low although total consumption of **3.42** was observed.

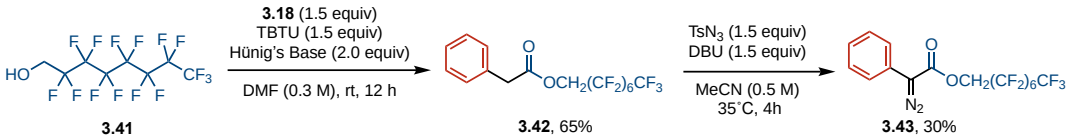


**Figure 3.19**. Synthesis of diazo compound **3.43**.

Fluorinated diazo compound **3.43** was tested with POSS **3.11** using 1 mol % $Rh_2OAc_4$ in $CH_2Cl_2$ with a 1-hour slow addition (Figure 3.20). The product **3.44** was observed in 25% yield and 30% conversion of POSS **3.11** using $^1H$ NMR spectroscopy. Extending the slow addition to 3 hours led to 70% conversion of the Si–H bond of **3.11**, and POSS **3.44** was isolated in 60% yield, comparable to yields from methyl ester-containing diazo compounds studied in this work.

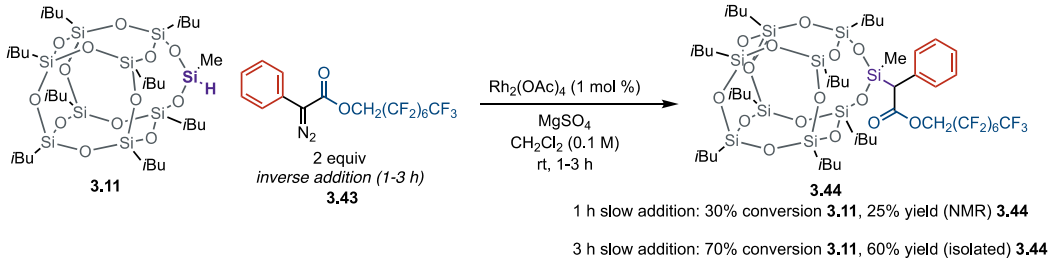


**Figure 3.20**. Carbene insertion into Si–H bond of POSS with diazo compound **3.43.**

## 3.8: Studies of Post-insertion Functionalization

### 3.8.1: Studies of Cross-coupling

Cross-coupling reactions of POSS compounds have been applied to the synthesis of OLEDs,[14] photovoltaics,[54] and heterogenous POSS-based catalysts.[55] To date, the majority of cross-coupling performed on POSS fall within Heck, Sonogashira, and Suzuki reactions.[14,56] Conditions that enable $sp^2$-$sp^2$ couplings with POSS **3.14b** would serve as precedent for potential inclusion into materials.

Heck coupling conditions were evaluated to functionalize POSS **3.14b**.[57] Heck coupling conditions with styrene and Hünig's base in DMF led to full conversion of starting material **3.14b** but no product formed (Table 3.6 entry 1).[58] Ester **3.46** was observed from C–Si cleavage. A reaction with P(*t*-Bu)$_3$ as the ligand formed no product, and no desilylation occurred (Table 3.6 entry 2). Palladium sources are suspected to have oxidized in all trials, but the results can serve as a control for POSS insertion products in the presence of a solubilized base. Previous examples of

Heck coupling used POSS with silicon-centers in more sterically demanding positions, so base hydrolysis (if that is the actual mechanism) would occur slowly compared to POSS **3.11**.[59] Another possibility could be Pd-catalyzed isomerization to the silyl-enol ether, and subsequent hydrolysis on work-up leading to separation of the aryl-ester moiety from POSS, which has been previously observed at elevated temperatures.[60] Using conditions reported by Fu,[61] no coupling occurred and partial desilylation of starting material was observed. (Table 3.6 entry 3). A repeated attempt using the same conditions led to full desilylation with no coupling product observed as determined by $^1$H NMR spectroscopy (Table 3.6 entry 4). A review of POSS-related literature noted cage rearrangements in the presence of solubilized bases even at room temperature.[62] Conditions where the base could be in a separate phase (i.e., aqueous phase) were investigated.

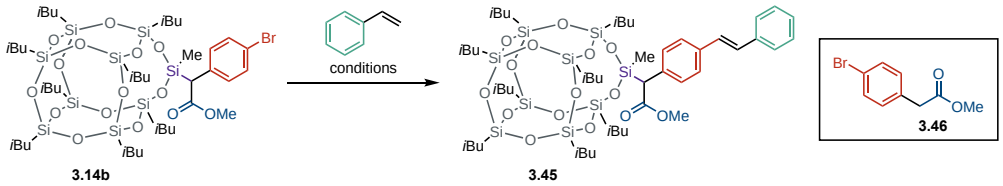


**Table 3.6.** Conditions tested for cross-coupling reactions with POSS **3.11b**.

| Entry [a] | Conditions | Solvent, Temp | C–Si cleavage (%)[b] | Yield **3.45**[b] |
|---|---|---|---|---|
| 1 | $Pd_2dba_3$, $PPh_3$, Hünig's base | DMF, 80˚C | Yes (>95%) | 0 |
| 2 | $PdOAc_2$, P(*t*-Bu)$_3$BF$_4$, $Cy_2MeN$ | THF, 50˚C | No | 0 |
| 3 | $Pd_2dba_3$, P(*t*-Bu)$_3$, $Cy_2MeN$ | 1,4-dioxane, rt | Yes (40%) | 0 |
| 4 | $Pd_2dba_3$, P(*t*-Bu)$_3$, $Cy_2MeN$ | 1,4-dioxane, rt | Yes (>95%) | 0 |

[a] 0.05 mmol scale, 1.5 equiv styrene 3 mol % Pd, 6 mol % ligand, 1.1 equiv base, 0.1 M, 16 h for all trials. [b] Determined using $^1$H NMR spectroscopy.

Suzuki couplings were investigated to test biphasic cross-coupling conditions.[63] Toluene was selected as the solvent given its low water solubility and $Na_2CO_3$ was selected as a base given the strong precedent. Using 4-fluorophenylboronic acid as a coupling partner with POSS **3.14b**, coupling product **3.47** formed in 37% yield analyzed by $^1$H NMR spectroscopy with partial cleavage of the C–Si bond (20%) (Figure 3.21). Biaryl-POSS **3.47** was isolated in 45% yield and

ester **3.48** was isolated in 35% yield. Hydrolysis is not entirely suppressed under these conditions. However, this result is a proof-of-concept that Suzuki couplings on POSS **3.47** yield isolable quantities of biaryl-products with a remaining methyl ester for further functionalization.

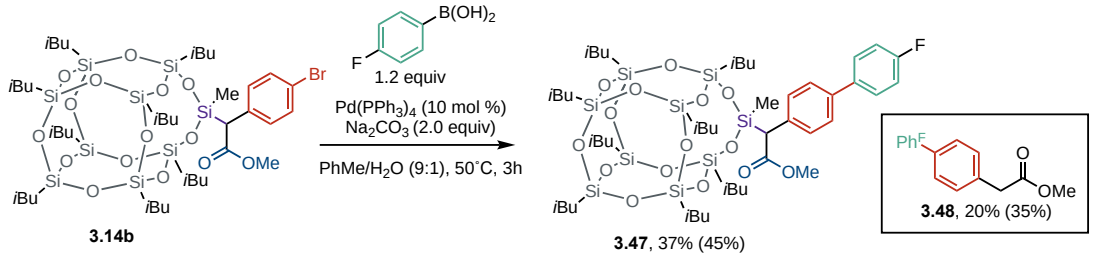


**Figure 3.21**. Suzuki coupling of POSS **3.15b** with 4-fluorophenylboronic acid, 0.1 mmol **3.15b,** NMR yield using Ph-TMS as an internal standard. Yields in parentheses are isolated.

## 3.8.2: Studies of Ester Deprotection:

To demonstrate the utility of the ester moiety, hydrolysis (i.e. deprotection) conditions were tested to access carboxylic acid-based POSS. POSS-based carboxylic acids have been reported previously.[64]

Conditions were tested with POSS **3.14a** containing a methyl ester. POSS **3.14a** was subjected to 10 equivalents of LiOH in THF/MeOH, leading to ester hydrolysis as well as C–Si hydrolysis after 16 h (Table 3.7, entry 1).[65] Reduced reaction times to 30 minutes and fewer equivalents of LiOH resulted in both ester and C–Si hydrolysis (Table 3.7, entry 2). Attempted acid-mediated hydrolysis using TFA resulted in recovery of starting material **3.14a**. Alternative ester substitutions were explored to investigate milder conditions.

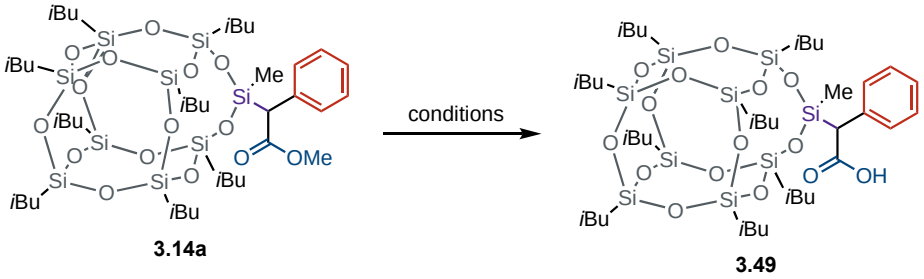


**3.14a** **3.49**

**Table 3.7.** Conditions tested for conversion to POSS acid **3.49**.

| Entry | Additive, Equiv | Solvent (M), Temp | Time (h) | Conversion (%)[a] | Yield **3.49**[b] |
|---|---|---|---|---|---|
| 1 | $LiOH•H_2O$ (20.0) | THF/MeOH (9:1, 0.1 M)[e], rt | 16 | >95 | 0 |
| 2 | $LiOH•H_2O$ (2.0) | THF/MeOH (9:1, 0.1 M)[e], rt | 0.5 | >95 | 0 |
| 3 | TFA (5.0) | $CH_2Cl_2$ (0.1 M)[e], rt | 0.5 | <5 | 0 |

[a] Determined using $^1$H NMR spectroscopy. [b] 0.1 mmol **3.11a**, NMR yield with Ph-TMS.

Deprotection of POSS **3.14d** with a *tert*-butyl ester was evaluated.[65] Thermal deprotection conditions in refluxing PhMe resulted in recovery of **3.14d** (Table 3.8, entry 1). Both $MgI_2$ and $I_2$ resulted in the consumption of **3.14d**, but no product **3.49** was observed (Table 3.8, entries 2 and 3). Several metal triflates in $CH_2Cl_2$ provided poor conversion after 16 h (Table 3.8, entries 3-5). Using five equivalents of $ZnBr_2$ in $CH_2Cl_2$, complete conversion of **3.11d** was observed using TLC and NMR spectroscopy. POSS **3.49** was isolated in 88% yield.[66]

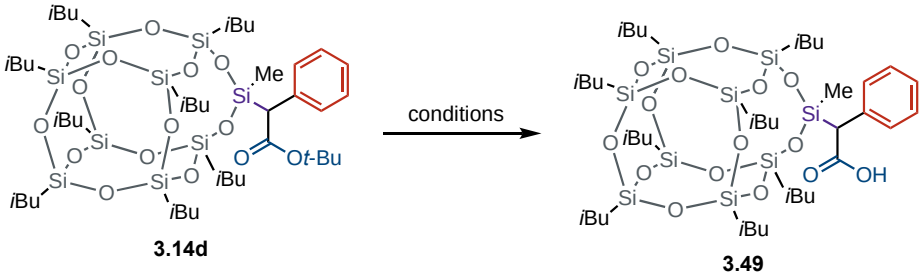


**3.14d** **3.49**

**Table 3.8.** Conditions tested for conversion to POSS acid **3.49**.

| Entry | Additive (Equiv) | Solvent (M), Temp | Conversions (%) | Yield **3.49**[d] |
|---|---|---|---|---|
| 1[a] | - | PhMe (0.1 M) , 110 ˚C | 0 | 0 |
| 2[b] | $MgI_2$ (1.5)[e] | PhMe (0.1 M), 110 ˚C | >95 | 0 |
| 3[a] | $I_2$ (1.0) | MeCN (0.1 M), 65 ˚C | >95 | 0 |
| 4[b] | $Sc(OTf)_3$ (0.1) | $CH_2Cl_2$ (0.1 M), rt | 10 | 0 |
| 5[b] | $La(OTf)_3$ (0.1) | $CH_2Cl_2$ (0.1 M), rt | 0 | 0 |
| 6[b] | $Fe(OTf)_2$ (0.1) | $CH_2Cl_2$ (0.1 M), rt | 0 | 0 |
| 7[a] | $ZnBr_2$ (5.0) | $CH_2Cl_2$ (0.1 M), rt | >95 | 88 (isolated) |

[a]0.1 mmol scale, 16 h. [b] 0.05 mmol scale, 16 h. [c] Determined using $^1$H NMR spectroscopy. [d] NMR yield using Ph-TMS as an internal standard. [e] Generated *in-situ* from $I_2$ and Mg(0) in $Et_2O$ for 2 h prior to use.

### 3.8.3: Studies of Amidation

Amidation is commonly used to prepare POSS-based hydrophilic dendrimers,[34] drug delivery systems,[33] and flame retardant materials.[67] These POSS are typically synthesized from POSS-based amines, so this method would allow for complementary syntheses. Amide-based diazo compounds are typically less reactive,[68] so amidation after Si–H insertion could circumvent reactivity issues.

Direct amidation from the methyl ester was examined to circumvent the requirement to isolate POSS-acid **3.49**. Catalytic DBU in PhMe for 16 h led to complete conversion of **3.14b**, but no product **3.50** was observed (Table 3.9, entry 1).[69] Stoichiometric Ti(O-*i*Pr)$_4$ in THF at 50˚C proved partially reactive, although no product **3.47** was observed (Table 3.9, entry 2). Lastly, LiHMDS-mediated amidation led to C–Si hydrolysis (Table 3.9, entry 3).[70] Given that all studies of direct amidation failed, conditions starting from POSS acid **3.49** were explored.

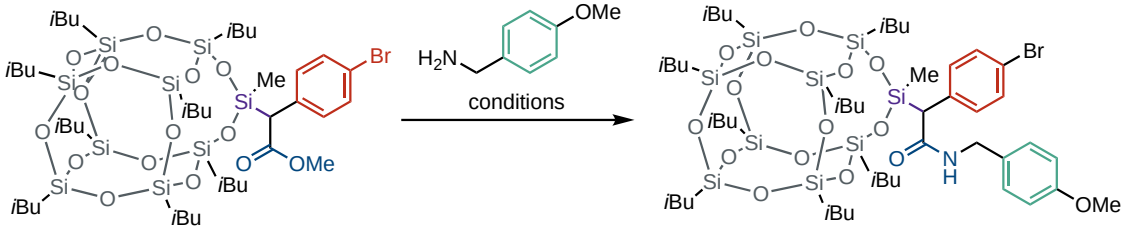


**3.14b** **3.50**

**Table 3.9.** Amidation conditions tested from ester **3.14b**.

| Entry | Additive (Equiv) | Solvent (M), Temp | Conversion[c] (%) | Yield **3.50**[b] |
|---|---|---|---|---|
| 1 | DBU (0.2) | PhMe (0.2 M), rt | >95 | 0 |
| 2 | Ti(O*i*-Pr)$_4$ (1.0), 4Å MS [a] | THF (0.6 M), 50 ˚C | 10 | 0 |
| 3 | LiHMDS (2.0) | PhMe (0.25 M), rt | >95 | 0 |

[a] 4A MS (0.5 g/mmol). [b] 0.05 mmol **3.14b**, NMR yield using Ph-TMS as an internal standard.

With POSS-acid **3.49** in hand, amide coupling conditions were tested. Conditions using oxalyl chloride followed by nucleophilic acyl substitution to form amide **3.51** resulted in C–Si cleavage (Table 3.10, entry 1). Conditions using EDC and HOBt, led to full conversion of the acid as determined by TLC and $^1$H NMR spectroscopy. When subjected to stirring with amine, C–Si cleavage was observed in addition to amide bond formation (Table 3.10, entry 2). Reduction of

reaction time (1 h and 0.2 h) led to similar results (Table 3.10, entries 3 and 4). Catalytic methods using boric acid or boronic acids led to C–Si cleavage as well (Table 3.10, entries 5 and 6).

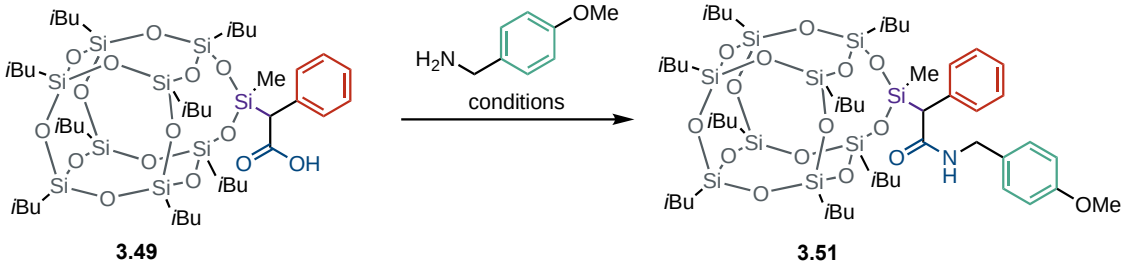


**Table 3.10.** Amidation conditions tested from acid **3.49**.

| Entry | Additive (Equiv) | Solvent (M), Temp | Time (h) | Conversion[a] (%) | C–Si hydrolysis (%)[a] | Yield **3.51**[b] |
|---|---|---|---|---|---|---|
| 1 | $(COCl)_2$ (1.2), DMF | $CH_2Cl_2$ (0.2 M), rt | 12 h | >95 | >95 | 0 |
| 2 | HOBt (1.2), EDC (1.2) | $CH_2Cl_2$ (0.1 M), rt | 12 h | >95 | >95 | 0 |
| 3 | HOBt (1.2), EDC (1.2) | $CH_2Cl_2$ (0.1 M), rt | 1 h | >95 | >95 | 0 |
| 4 | HOBt (1.2), EDC (1.2) | $CH_2Cl_2$ (0.1 M), rt | 0.2 | >95 | >95 | 0 |
| 5 | *p*-$CF_3PhB(OH)_2$ (0.2) | PhF (0.2 M), 80˚C | 16 h | >95 | >95 | 0 |
| 6 | $B(OH)_3$ (0.2) | PhF (0.2 M), 80˚C | 16 h | >95 | >95 | 0 |

[a] Determined using $^1H$ NMR spectroscopy [b] 0.05 mmol scale, 16 h, NMR yield using Ph-TMS as an internal standard. [c] 4Å MS (100 mg/0.1 mmol **3.49** added).

## 3.9: Conclusion

In conclusion, carbene insertion into Si–H bonds of POSS-silanes using diazo compounds as precursors has been demonstrated. Useful functionality, including aryl bromides, alkene functional handles, and labile protecting groups can be installed in good yield and purity. POSS

with one, three and eight Si–H bonds were reacted with diazo compounds to access functionalized POSS. POSS with three Si–H bonds yielded lower than other POSS studied due to competitive C–H insertion and coelution of side products. Diazo compounds containing fluorinated groups and BODIPY chromophores were synthesized and subsequently reacted to access novel functionalized POSS. Amide-containing diazo compounds were tested and all trials failed to produce insertion products. Synthetic transformations of insertion products including ester deprotection and Suzuki coupling were accomplished. However, all conditions for Heck couplings and amide couplings failed due competitive to C–Si cleavage. The results of this chapter in addition to the results from Karina Targos were compiled into a manuscript and submitted.

## 3.10 Experimental Procedures

### 3.10.1 General Information

See Chapter 1 and Chapter 2 experimental procedures (pages 64 and 132, respectively) for general information on synthesis, purification, and analysis.

For Chapter 3, Fluorescence data was collected using a Cary Eclipse Spectrometer in EtOH at 3.1 x $10^{-7}$ M in a 96-well plate to determine the proper dilution to limit quenching. Excitation and emission wavelengths were determined separately, and data was normalized on Microsoft Excel.

For Chapter 3, tetracyclo[9.5.1.1$^{3,9}$.1$^{5,15}$]octasiloxane-7,13-diol,1,3,5,7,9,11,13,15-octakis(2-methyl propyl) (diSilanolIsobutyl POSS) **3.13**, 1,3,5,7,9,11,14-heptaisobutyltricyclo[7.3.3.1$^{5,11}$]heptasiloxane-endo-3,7,14-triol (triSilanolIsobutyl POSS) **3.14** and octaSilane POSS (**3.3**) were purchased from Hybridplastics.com. Allyl-2-phenylacetate, *tert*-butyl-2-phenylacetate, and were synthesized from previous published procedures.[71,72] POSS **3.2** was synthesized from a previously reported procedure.[27] POSS compounds were named using the 9CI, ACI index.

### 3.10.2: Experimental Procedures

**Method A: Procedure for Preparation of POSS 3.11**

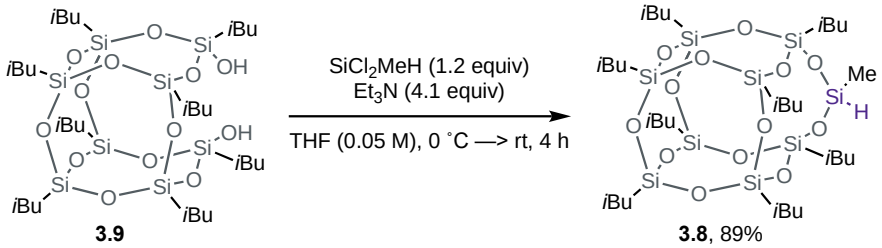


**3.9** **3.8**, 89%

In a flame-dried, Ar-charged 250-mL round-bottomed flask, a solution of POSS **3.9** (4.5 g, 5.0 mmol) and $Et_3N$ (5.65 mL, 40.5 mmol, 8.10 equiv) in THF (80 mL) was cooled to 0 °C and stirred for 10 min. A solution of methyldichlorosilane (0.63 mL, 6.0 mmol, 1.2 equiv) in THF (20 mL) was prepared under Ar atmosphere and added dropwise to the POSS-diol solution. A white solid immediately started to precipitate, and chlorosilane solution addition was temporarily halted if excessive gas formation clouded the reaction flask. After stirring at 0 °C for 1 h, the flask was removed from the bath and allowed to warm to room temperature. The flask stirred for an additional 3 h, then was quenched with sat. aq. $NaHCO_3$ (15 mL). Hexanes (15 mL) were added to the reaction flask, and the reaction mixture was filtered to remove solids. The organic layer was separated, dried with $MgSO_4$ for 10 min, and concentrated in vacuo. The crude product was purified via flash chromatography on silica gel, eluted with hexanes and dried under vacuum to afford POSS **3.11** as a colorless solid in 89% yield (4.20 g, 4.50 mmol). Characterization data can be found below.

**Method B: General Procedure for Carbene Insertion into POSS Silanes**

A 4-mL reaction vial equipped with a stir bar and $MgSO_4$ (56 mg/0.1 mmol) was heated under flame and dried under a high vacuum (<1 torr). After the vial was cooled to room temperature, it was purged with argon, followed by the addition of $Rh_2(OAc)_4$ (0.01 equiv) and the corresponding POSS. The vial was re-purged with argon, and solvent was added. The diazo compound was weighed into a separate flame-dried vial and solvent was added, then the solution was drawn into a syringe. Using a long needle, the syringe was placed on a syringe pump with the needle tip *in* the stirring solution of POSS and rhodium catalyst. The syringe pump was programmed to add the solution over a period of 1-3 h at room temperature. The mixture was stirred for 30 min after complete addition and subsequently filtered through silica gel using $CH_2Cl_2$ and evaporated under reduced pressure (rotary evaporator). The products were purified using flash

chromatography to furnish pure functionalized POSS compounds. For products **3.14a-d**, the crude material was dissolved in hexanes (10 mL) and filtered through celite to remove byproducts prior to flash chromatography. Specifics on mobile phase compositions are included in characterization entries.

**Method C: General Procedure for Gram-Scale Carbene Insertion into POSS Silanes**

A 50-mL round-bottomed flask equipped with a stir bar and $MgSO_4$ (560 mg) was heated in the oven for 24 h and cooled under high vacuum (>1 torr). After the flask cooled to room temperature, $Rh_2(OAc)_4$ (4.4 mg, 0.010 mmol) and POSS **3.11** (0.93 g, 1.0 mmol) or POSS **3.3** (1.01 g, 1.0 mmol) was added. The flask was purged with argon, followed by addition of $CH_2Cl_2$ (3.30 mL). The diazo compound was weighed into a separate flame-dried vial and $CH_2Cl_2$ was added (6.70 mL), then the solution was drawn into a 10-mL syringe. Using a long needle, the syringe was placed on a syringe pump with the needle tip *in* the stirring solution. The syringe pump was programmed to add the solution over a period of 3 h at room temperature.

The mixture was stirred for 30 min after complete addition and was subsequently filtered through silica gel using $CH_2Cl_2$ and evaporated under reduced pressure (rotary evaporator). The products were purified using flash chromatography to furnish pure POSS compounds.

**Method D: Procedure for Preparation of 3.42**

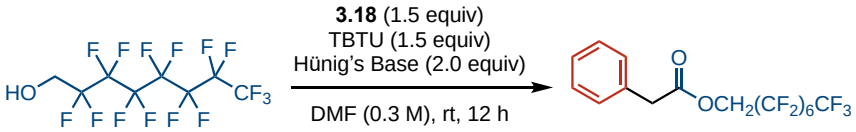


**3.41** **3.42**, 65%

In a flame-dried, Ar-charged 25-mL round-bottomed flask, phenylacetic acid **3.18** (0.326 g, 2.40 mmol, 1.50 equiv), 2-(1H-benzotriazole-1-yl)-1,1,3,3-tetramethylaminium tetrafluoroborate (TBTU, 0.960 g, 3.00 mmol, 1.50 equiv), Hünig's base (1.05 mL, 6.00 mmol, 2.00 equiv), and DMF (6.5 mL) were added and the flask stirred for 10 min. A solution of alcohol **3.41** (0.800 g, 2.00 mmol, 1.00 equiv) in DMF (1.5 mL) was prepared under an argon atmosphere and added dropwise to the solution of acid and the reaction stirred for 12 h at room temperature. After stirring, the reaction was diluted with $CH_2Cl_2$ (15 mL). The organic layer was washed with 5% HCl (2x 5 mL), saturated $NaHCO_3$ (2x 5 mL), and water (2x 5 mL). The organic layer was separated, dried with $MgSO_4$ for 10 min, and concentrated in vacuo. The crude product was

purified using flash chromatography (98:2 hexanes/EtOAc, dry loaded silica) to furnish **3.42** as an oil in 65% yield (0.728 g, 1.30 mmol). Characterization data can be found below.

**Method E: Procedure for the Synthesis of Diazo Compounds Using Diazo Transfer**

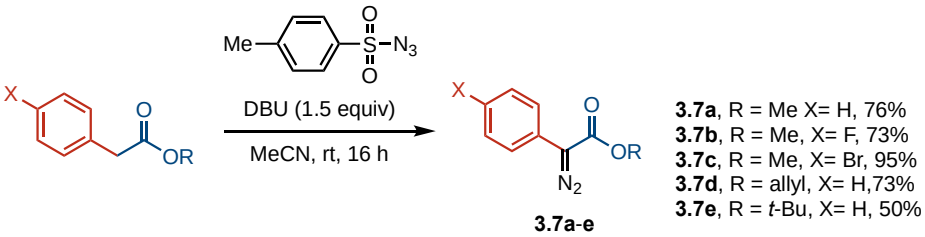


To a flame-dried, Ar-purged 25-mL round-bottomed flask charged with a stir bar, ester (1 equiv), tosyl azide (1.5 equiv) and MeCN (0.6 M) were added and stirred for 10 min. DBU (1.5 equiv) was added in a single portion with vigorous stirring and the reaction stirred at room temperature for 18 h. Upon complete consumption of the starting materials, the mixture was quenched with a sat. aq. solution of $NH_4Cl$ (5 mL), extracted with $CH_2Cl_2$ (3 × 30 mL), dried over $MgSO_4$, and concentrated under reduced pressure to afford a residue that was purified by flash chromatography (hexanes/EtOAc, dry loaded silica 100:0→98:2) to afford the respective diazo(aryl) acetates (**3.7a-e** and **3.43**). The products were obtained as orange-red oils or solids in variable yields (30-95%). The $^1H$ NMR spectra were compared to literature to confirm the formation of desired products.

**Method F: Synthesis of Diazo Compound 3.39**

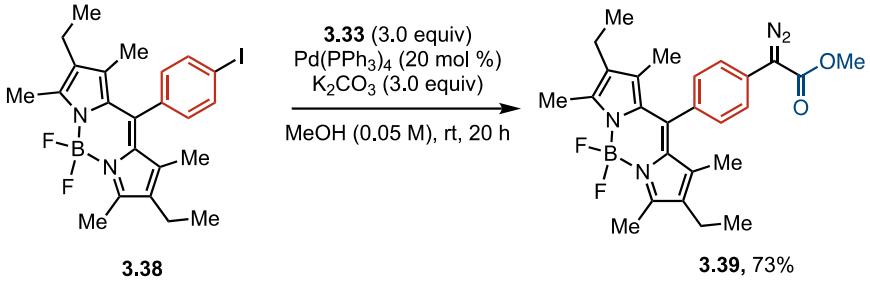


To a flame-dried, 8 mL vial with a stir bar and $K_2CO_3$ (0.083 g, 0.60 mmol, 3.0 equiv), BODIPY **3.38** (0.102 g, 0.200 mmol), methyl 2-diazo-4,4,4-trifluoro-3-oxobutanoate **3.33** (0.057 g, 0.30 mmol, 1.5 equiv), and anhydrous MeOH (4 mL) were added. The solution was purged with argon for 5 min to remove dissolved oxygen. Tetrakis(triphenylphosphine)palladium(0) (0.0462 g, 0.04 mmol, 0.2 equiv) was added in a single portion, and the reaction stirred at room temperature. After 12 h, methyl 2-diazo-4,4,4-trifluoro-3-oxobutanoate (0.057 g, 0.30 mmol, 1.5 equiv) was added in a second portion, and the reaction stirred for an additional 4 h. The reaction was diluted

with $CH_2Cl_2$ (5 mL) and filtered through celite. The residue was purified by flash chromatography (hexanes/EtOAc 100:0→90:10, dry loaded silica) to furnish **3.39** as an orange solid in 73% yield (0.0696 g, 0.145 mmol). Characterization data can be found below. Diazo **3.39** decomposed at room temperature and was stored at 4 ˚C.

**Method G: Procedure for Suzuki Cross-coupling**[73]

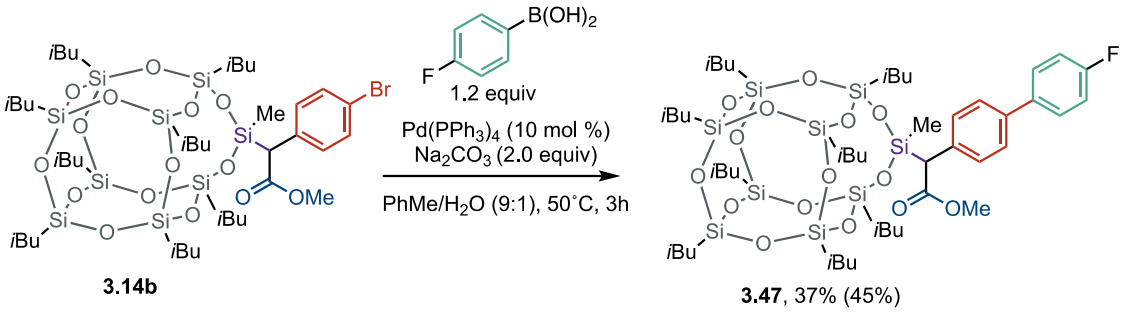


A 4-mL reaction vial equipped with a stir bar was purged with argon, followed by addition of POSS **3.14b** (101.0 mg, 0.100 mmol), $Na_2CO_3$ (22.0 mg, 0.200 mmol, 2.00 equiv,), 4-fluorophenylboronic acid (17.0 mg, 0.120 mmol, 1.20 equiv,), and $Pd(PPh_3)_4$ (11.6 mg, 0.0100 mmol, 0.100 equiv), and re-purged with argon. Toluene (0.90 mL), followed by deionized water (0.10 mL) were added, and the reaction was heated to 50 ˚C for 3 h. After cooling to room temperature, $CH_2Cl_2$ (5 mL) was added, followed by water (5 mL) and the organic layer was separated, dried with $MgSO_4$, and evaporated under reduced pressure (rotary evaporator). The crude product was purified by flash chromatography (hexanes/EtOAc (100/0 → 90/10), dry loaded silica) to furnish POSS **3.47** as a white solid in 45% yield (95% purity by $^{19}F$ NMR, 56.6 mg, 0.045 mmol).

**Method H: Procedure for Deprotection of POSS *tert*-Butyl Ester**[66]


A 4-mL reaction vial equipped with stir bar was purged with argon, followed by addition of POSS **3.14d** (112.0 mg, 0.1000 mmol) and $ZnBr_2$ (125.0 mg, 0.5000 mmol, 5.000 equiv). The vial was re-purged with argon, and $CH_2Cl_2$ was added (1.0 mL). The solution turned opaque and stirred at room temperature for 24 h. The reaction was quenched by the addition of water (5 mL) and

stirred for 1 h. $CH_2Cl_2$ (5 mL) was added, and the organic layer was separated, dried with $MgSO_4$, and evaporated under reduced pressure (rotary evaporator). The crude product was purified by flash chromatography (hexanes/EtOAc 97:3, dry loaded silica) to furnish POSS **3.49** as a white solid in 88% yield (93.8 mg, 0.09 mmol).

## 3.10.3: Characterization Entries

### Intermediates:

**_N_-methyl-_N_,2-diphenylacetamide (3.20)**

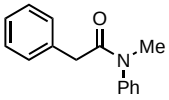


Synthesized using a known procedure[36] from phenyl acetic acid (0.675 g, 3.00 mmol), TCFH (1.01 g, 3.60 mmol, 1.20 equiv), NMI (0.28 mL, 3.6 mmol, 1.2 equiv), and *N*-methylaniline (0.39 mL, 3.6 mmol, 1.2 equiv) in MeCN (5 mL). Isolated in 65% yield (0.438g, 1.95 mmol). Spectrum matches previously reported data.[74]

$^1$H NMR (400 MHz, $CDCl_3$) δ 7.32-7.43 (m, 3H), 7.17-7.26 (m, 3H), 7.12 (d, J = 7.7 Hz, 2H), 7.05 (d, J = 7.2 Hz, 2H), 3.46 (s, 2H), 3.28 (s, 3H).

**N-methylisatin (3.24)**

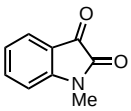


Synthesized from a known procedure[75] from isatin (0.294 g, 2.00 mmol), Me–I (0.187 g, 4.00 mmol, 2.00 equiv) and $K_2CO_3$ (0.552 g, 4.00 mmol, 2.00 equiv) in DMF/$H_2O$ (9:1, 4 mL). Isolated in 95% yield and spectrum matches with previous reports.[75]

$^1$H NMR (600 MHz, $CDCl_3$) δ 7.62 (t, *J* = 7.4 Hz, 2H), 7.19 – 7.09 (m, 1H), 6.90 (d, *J* = 7.9 Hz, 1H), 3.27 (s, 2H).

**(*E*)-1-(4-iodophenyl)-2-phenyldiazene (3.30)**

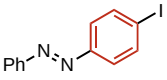


Synthesized using a known procedure[76] from nitrosobenzene (0.161g, 1.50 mmol), 4-iodoaniline (0.328g, 1.50 mmol, 1.00 equiv) in 1:1 $CH_2Cl_2$:AcOH (3 mL). Isolated in 85% yield and spectrum matches previous report.[76]

$^1$H NMR (400 MHz, $CDCl_3$) δ 7.98 – 7.91 (m, 2H), 7.91 – 7.85 (m, 2H), 7.71 – 7.63 (m, 2H), 7.59 – 7.47 (m, 2H).

**2,8-diethyl-5,5-difluoro-10-(4-iodophenyl)-1,3,7,9-tetramethyl-5*H*-4λ4,5λ4-dipyrrolo[1,2-*c*:2',1'-*f*][1,3,2]diazaborinine (3.38)**

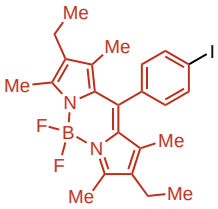


Synthesized using a known procedure[77] from 4-iodobenzoyl chloride (1.332 g, 5.000 mmol), 4-ethyl-2,6-dimethylpyrrole (1.34 mL, 5.00 mmol, 2.00 equiv), $BF_3$•$Et_2O$ (4.90 mL, 40.0 mmol, 8.00 equiv), and $Et_3N$ (5.57 mL, 40.0 mmol, 8.00 equiv) in $CH_2Cl_2$ (40 mL). Isolated in 14% yield. Spectra match with previous reports.[77]

$^1$H NMR (400 MHz, $CDCl_3$) δ 7.86 (d, *J* = 8.2 Hz, 2H), 7.07 (d, *J* = 8.1 Hz, 2H), 2.55 (s, 6H), 2.33 (q, *J* = 7.6 Hz, 4H), 1.34 (s, 6H), 1.01 (t, *J* = 7.5 Hz, 6H).

$^{19}$F NMR (376 MHz, $CDCl_3$) δ -145.80 (q, *J* = 33.0 Hz).

$^{11}$B NMR (128 MHz, $CDCl_3$) δ 0.80 (t, *J* = 33.5 Hz).

**2,2,3,3,4,4,5,5,6,6,7,7,8,8,8-pentadecafluorooctyl 2-phenylacetate (3.42)**

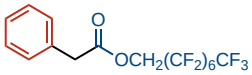


Synthesized using Procedure D in 65% yield.

$^1$H NMR (400 MHz, $CDCl_3$) δ 7.56 – 7.17 (m, 5H), 4.60 (t, *J* = 13.5 Hz, 2H), 3.73 (s, 2H).

$^{13}$C NMR (151 MHz, $CDCl_3$) δ 170.2, 132.8, 129.4, 128.9, 127.7, 59.9 (t, $J^3_{CF}$ = 27.4 Hz), 40.8.

$^{19}$F NMR (376 MHz, $CDCl_3$) δ -80.74 (3F), -119.42 (2F), -122.43 (4F), -122.68 (2F), -123.30 (2F), -126.08 (2F).

Orbitrap: exact mass calcd for $C_{16}H_9F_{15}O_2$ $[M + H]^+$, 519.0441; found: 519.0459.

**POSS silanes**

**Tricyclo[7.3.3.1$^{5,11}$]heptasiloxane, 3,7,14-tris[(dimethylsilyl)oxy]-1,3,5,7,9,11,14-heptakis(2-methylpropyl) (3.2)**

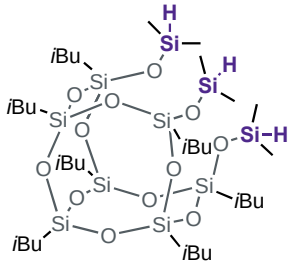

Synthesized using a known procedure[27] from POSS **3.10** (3.724 g, 4.000 mmol), chlorodimethylsilane (1.99 mL, 18.0 mmol, 4.50 equiv), and Hünig's base (4.18 mL, 24.0 mmol, 6.00 equiv) in THF (56 mL). The product was obtained as a white solid in 25 % yield (1.02 g, 1.05 mmol) after trituration in $CHCl_3$/MeOH (solvent: anti-solvent). Spectra match with previous report.[27]

$^1$H NMR (600 MHz, $CDCl_3$) δ 4.74 (h, *J* = 2.7 Hz, 3H), 1.84 (dh, *J* = 13.6, 6.7 Hz, 7H), 0.98 – 0.92 (m, 42H), 0.58 – 0.52 (m, 14H), 0.22 (t, *J* = 2.4 Hz, 18H).

$^{13}$C NMR (151 MHz, $CDCl_3$) δ 26.11, 26.01, 25.99, 25.78, 24.74, 24.21, 24.11, 24.03, 23.73, 22.58, 0.79.

$^{29}$Si NMR (79 MHz, $CDCl_3$[Cr(acac)$_3$] = 0.01 M) δ -5.46, -67.10, -67.66, -67.99

**Pentacyclo[9.7.1.1$^{3,9}$.1$^{5,17}$.1$^{7,13}$]nonasiloxane,13-methyl-1,3,5,7,9,11,15,17-octakis(2-methylpropyl) (3.11)**

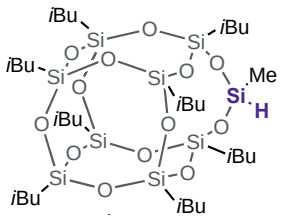

The product was synthesized according to procedure A section and was obtained as a white solid (4.36 g, 4.67 mmol, 93%).

$^1$H NMR (600 MHz, $CDCl_3$): δ 4.67 (s, 1H), 1.84 (m, 8H), 0.96 (d, *J* = 5.7 Hz, 48H), 0.58 (m, 16H), 0.18 (s, 3H).

$^{13}$C NMR (100 MHz, $CDCl_3$): δ 25.90, 25.87, 25.85, 25.8, 24.14, 24.07, 24.0, 23.6, 23.2, 23.1, 22.6, 0.7.

$^{29}$Si NMR ([Cr(acac)$_3$] = 0.01 M, 119 MHz, $CDCl_3$): δ -66.9, -68.2, -68.9, -69.1.

MALDI-TOF: exact mass calcd for $C_{33}H_{76}NaO_{13}Si_9$ $[M + Na]^+$, 955.311; found: 955.669.

**<u>Diazo compounds:</u>**

**Methyl Diazo(phenyl)acetate (3.7a)**

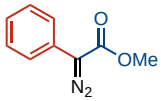

Procedure E was followed using p-toluenesulfonyl azide (4.828 g, 24.00 mmol) and methyl phenylacetate (2.30 mL, 16.0 mmol). The product was obtained as an orange-red oil (2.164 g, 12.23 mmol, 76%).[78]

$^1$H NMR (400 MHz, $CDCl_3$): δ 7.48 (d, *J* = 7.9 Hz, 2H), 7.38 (t, *J* = 7.8 Hz, 2H), 7.18 (t, *J* = 7.4 Hz, 1H), 3.86 (d, *J* = 1.5 Hz, 3H).

**Methyl Diazo(4-fluorophenyl)acetate (3.7b)**

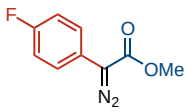


Procedure E was followed using p-toluenesulfonyl azide (4.82 g, 24.4 mmol) and methyl 2-(4-fluorophenyl)acetate (2.85 mL, 16.3 mmol). The product was obtained as a red-orange oil (2.31 g, 11.9 mmol, 73% yield).[78]

$^1$H NMR (400 MHz, $CDCl_3$): δ 7.46−7.42 (m, 2H), 7.11−7.07 (m, 2H), 3.86 (s, 3H) ppm.

$^{19}$F NMR (376 MHz, $CDCl_3$): δ -116.2 ppm.

**Methyl Diazo(4-bromophenyl)acetate (3.7c)**

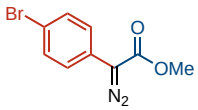


Procedure E was followed using p-toluenesulfonyl azide (3.00 g, 15.2 mmol) and methyl 2-(4-bromophenyl)acetate (2.05 mL, 10.1 mmol). The product was obtained as an orange solid (2.45 g, 9.60 mmol, 95% yield).[78]

$^1$H NMR (400 MHz, $CDCl_3$) δ 7.49 (d, *J* = 8.6 Hz, 2H), 7.36 (d, *J* = 7.2 Hz, 2H), 3.87 (s, 3H).

**Allyl-2-diazo-2-phenylacetate (3.7d)**

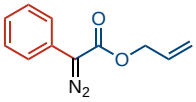


Procedure E was followed using p-toluenesulfonylazide (2.70 g, 13.7 mmol) and allyl 2-phenylacetate (1.58 mL, 9.10 mmol). The product was obtained as a red-orange oil (1.552 g, 7.670 mmol, 73%).[78]

$^1$H NMR (600 MHz, $CDCl_3$) δ 7.49 (d, *J* = 7.8 Hz, 2H), 7.39 (t, *J* = 6.9 Hz, 2H), 7.19 (t, *J* = 7.5 Hz, 1H), 5.98 (ddd, *J* = 16.1, 11.0, 6.3 Hz, 1H), 5.37 (d, *J* = 15.1 Hz, 1H), 5.28 (d, *J* = 9.8 Hz, 1H), 4.78 (d, *J* = 5.6 Hz, 2H).

***tert*-Butyl Diazophenylacetate (3.7e)**

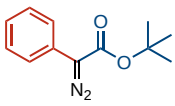

Procedure E was followed using p-toluenesulfonyl azide (1.97 g, 10.0 mmol) and *tert*butyl- 2-phenylacetate (1.29 g, 6.70 mmol). Product was obtained as a red-orange oil (0.732 g, 3.35 mmol, 50%).[71]

$^1$H NMR (600 MHz, $CDCl_3$) δ 7.47 (d, *J* = 7.4 Hz, 2H), 7.39 – 7.31 (m, 2H), 7.18 – 7.13 (m, 1H), 1.55 (s, 9H).

**2-diazo-*N*-methyl-*N*,2-diphenylacetamide (3.20)**

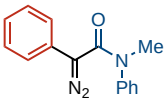


Procedure E using *N*-methyl-*N*,2-diphenylacetamide (1.71g, 7.6 mmol), tosyl azide (2.24 g, 11.4 mmol) and DBU (1.72 mL, 11.4 mmol) in MeCN (13 mL). The product was isolated as a yellow oil in 10% yield (0.178 g, 0. 76 mmol). Spectra match previous report. [79]

$^1$H NMR (400 MHz, $CDCl_3$) δ 7.42 – 7.08 (m, 10H), 3.44 (s, 3H).

**3-diazo-1-methylindolin-2-one (3.25)**

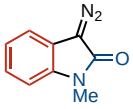


Synthesized using a previously published procedure from N-methylisatin (0.484g, 3.00 mmol) and tosylhydrazine (0.614g, 3.30 mmol) followed by basic workup and was accessed in 45% yield. Spectrum matches previous report.[37]

$^1$H NMR (400 MHz, $CDCl_3$) δ 7.23 (m, 2H), 7.11 (td, *J* = 7.6, 1.0 Hz, 1H), 6.98 – 6.91 (m, 1H), 3.36 (s, 1H).

**Methyl 2-diazo-4,4,4-trifluoro-3-oxobutanoate (3.33)**

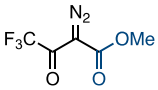


Synthesized using a known procedure[42] from methyldiazoacetate (1.05 mL, 10.0 mmol), TFAA (1.51 mL, 11.0 mmol, 1.10 equiv), pyridine (0.87 mL, 11 mmol, 1.1 equiv) in $CH_2Cl_2$ (14 mL). Isolated in 65% yield after bulb-to-bulb distillation (1.274 g, 6.5 mmol). Spectra match with previous report.[42]

$^1$H NMR (400 MHz, $CDCl_3$) δ 3.93. $^{19}$F NMR (376 MHz, $CDCl_3$) δ -73.94.

**Methyl-(*E*)-2-diazo-2-(4-(phenyldiazenyl)phenyl)acetate (3.34)**

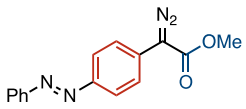

Synthesized using a previously reported procedure[42] from (*E*)-1-(4-iodophenyl)-2-phenyldiazene (0.150 g, 0.500 mmol), and methyl 2-diazo-4,4,4-trifluoro-3-oxobutanoate (0.118g, 0.750 mmol) in MeOH (3 mL) and was isolated in 60% yield (0.084g, 0.30 mmol) as an orange solid. Spectrum match with previous reports.[42]

$^{1}$H NMR (600 MHz, $CDCl_3$) δ 7.99 – 7.93 (m, 2H), 7.90 (d, *J* = 7.7 Hz, 2H), 7.67 – 7.61 (m, 2H), 7.51 (t, *J* = 7.4 Hz, 2H), 7.46 (t, *J* = 7.2 Hz, 1H), 3.89 (s, 3H).

**Methyl-2-diazo-2-(4-(2,8-diethyl-5,5-difluoro-1,3,7,9-tetramethyl-5*H*-4λ4,5λ4-dipyrrolo[1,2-*c*:2',1'-*f*][1,3,2]diazaborinin-10-yl)phenyl)acetate** (**3.39**)

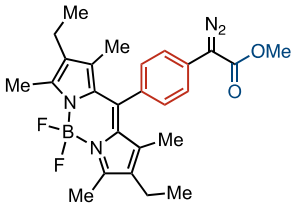

Synthesized using Procedure F and isolated in 73% yield.[42]

$^{1}$H NMR (600 MHz, $CDCl_3$) δ 7.63 (d, *J* = 8.4 Hz, 2H), 7.30 (d, *J* = 8.4 Hz, 2H), 3.90 (s, 3H), 2.53 (s, 6H), 2.30 (q, *J* = 7.6 Hz, 4H), 1.32 (s, 6H), 0.98 (t, *J* = 7.6 Hz,6H).

$^{13}$C NMR (151 MHz, cdcl$_3$) δ 165.48, 153.97, 139.61, 138.42, 133.66, 132.97, 130.83, 129.14, 126.60, 125.01, 51.06, 16.78, 14.77, 12.66, 12.05.

$^{19}$F NMR (376 MHz, $CDCl_3$) δ -145.80 (q, *J* = 33.0 Hz).

$^{11}$B NMR (128 MHz, $CDCl_3$) δ 0.80 (t, *J* = 33.5 Hz).

Orbitrap: exact mass calcd for $C_{26}H_{30}BF_2N_4O_2$ $[M + H]^+$, 479.2430; found: 479.2515.

**2,2,3,3,4,4,5,5,6,6,7,7,8,8,8-pentadecafluorooctyl 2-diazo-2-phenylacetate (3.43)**

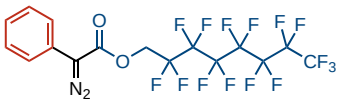

Procedure E was followed using p-toluenesulfonyl azide (0.172 g, 0.870 mmol) and **3.38** (0.303 g, 0.58 mmol). The product was obtained as a yellow solid (0.106 g, 0.17 mmol, 30%).

$^{1}$H NMR (400 MHz, $CDCl_3$) δ 7.47 (d, *J* = 7.7 Hz, 2H), 7.41 (t, *J* = 7.8 Hz, 2H), 7.28 – 7.18 (m, 1H), 4.78 (t, *J* = 13.2 Hz, 2H).

$^{13}$C NMR (151 MHz, $CDCl_3$) δ 163.2, 129.3, 124.6, 124.2, 59.7 (t, $J^3_{CF}$ = 27.6 Hz).

$^{19}$F NMR (376 MHz, $CDCl_3$) δ -80.81 (3F) -119.46 (2F), -121.98 (4F), -122.24 (2F), -123.33 (2F), -126.13 (2F).

Orbitrap: exact mass calcd for $C_{16}H_7F_{15}N_2O_2$ $[M - N_2 + H]^+$, 517.0279; found: 517.0308.

**Insertion Products**

***rac*-Pentacyclo[9.7.1.1$^{3,9}$.1$^{5,17}$.1$^{7,13}$]nonasiloxane,13-methyl-13-[2-(methyl-2-(4-bromophenyl)acetate)]-1,3,5,7,9,11,15,17-octakis(2-methylpropyl) (3.14b)**

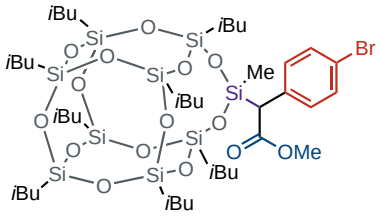


Procedure C was followed using 3 h slow addition of diazo compound **3.7c** (0.510 g, 2.00 mmol) in $CH_2Cl_2$ (6.70 mL) to POSS silane **3.11** (0.933 g, 1.00 mmol) in $CH_2Cl_2$ (3.30 mL). The product was obtained as a white solid using flash chromatography (100:0→98:2 hexanes/EtOAc, dry loaded silica) to furnish **3.14b** in 62% yield (0.719 g, 6.20 mmol).

$^1$H NMR (400 MHz, $CDCl_3$): δ 7.37 (d, *J* = 8.1 Hz, 2H), 7.24 (t, *J* = 7.0 Hz, 2H), 3.67 (s, 3H), 3.48 (s, 1H), 1.81 (m, 7H), 1.61 (m, 1H),0.96 (m, 42H), 0.86 (t, *J* = 6.7 Hz, 6H), 0.62 (d, *J* = 7.1 Hz, 2H), 0.56 (m, 10H), 0.47 (dd, *J* = 7.3, 2.4 Hz, 2H), 0.35 (d, *J* = 7.0 Hz, 2H), 0.23 (s, 3H).

$^{13}$C NMR (100 MHz, $CDCl_3$): δ 172.1, 134.6, 131.2, 130.9, 119.8, 51.8, 46.4, 26.0, 25.91, 25.88, 25.81, 25.78, 25.75, 25.73, 25.70, 24.1, 24.02, 23.95, 23.4, 23.22, 23.20, 23.11, 23.07, 22.5, -2.6.

$^{29}$Si NMR ([$Cr(acac)_3$] = 0.01 M, 79 MHz, $CDCl_3$): δ -34.4, -67.0, -68.8, -68.88, -68.94, -69.0, -69.1.

MALDI-TOF: exact mass calcd for $C_{42}H_{83}BrNaO_{15}Si_9$ $[M + Na]^+$, 1181.274; found: 1181.449.

***rac*-Pentacyclo[9.7.1.1$^{3,9}$.1$^{5,17}$.1$^{7,13}$]nonasiloxane,13-methyl-13-[2-(allyl-2-phenylacetate)]-1,3,5,7,9,11,15,17-octakis(2-methylpropyl) (3.14c)**

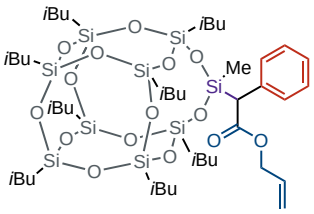


Procedure B was followed using 1 h slow addition of diazo compound **2.7e** (0.042 g, 0.20 mmol) in $CH_2Cl_2$ (0.67 mL) to POSS **3.11** (0.0934 g, 0.10 mmol) in $CH_2Cl_2$ (0.33 mL). The product was obtained as a white solid using flash chromatography (100:0→99:1 hexanes/EtOAc, dry loaded silica) to furnish **3.14c** in 77% yield (0.0852 g, 0.0770 mmol).

$^{1}$H NMR (600 MHz, $CDCl_3$) δ 7.34 (d, *J* = 7.6 Hz, 2H), 7.24 (d, *J* = 11.4 Hz, 2H), 7.16 (t, *J* = 7.4 Hz, 1H), 5.91 (ddt, *J* = 16.5, 10.9, 5.8 Hz, 1H), 5.29 (d, *J* = 17.1 Hz, 1H), 5.19 (d, *J* = 10.4 Hz, 1H), 4.62 (dd, *J* = 13.3, 5.8 Hz, 1H), 4.50 (dd, *J* = 13.3, 5.8 Hz, 1H), 3.52 (s, 1H), 1.96 – 1.69 (m, 6H), 1.57 (dd, *J* = 13.5, 6.8 Hz, 1H), 1.08 – 0.89 (m, 42H), 0.88 – 0.75 (m, 6H), 0.61 (d, *J* = 7.1 Hz, 2H), 0.55 (td, *J* = 9.7, 8.8, 4.4 Hz, 10H), 0.47 (t, *J* = 6.6 Hz, 2H), 0.28 (t, *J* = 6.8 Hz, 2H), 0.23 (s, 3H).

$^{13}$C NMR (100 MHz, $CDCl_3$) δ 171.4, 135.5, 132.7, 129.2, 128.2, 124.1, 118.2, 64.5, 47.1, 26.1, 26.0, 25.97, 25.94, 25.85, 25.81, 25.79, 25.73, 24.13, 24.11, 24.08, 24.06, 24.01, 23.94, 23.40, 23.28, 23.20, 23.14, 22.60, -1.93.

$^{29}$Si NMR (79 MHz, $CDCl_3$) δ -33.7, -66.9, -67.0, -68.8, -68.9, -69.0, -69.1, -69.2.

MALDI-TOF: exact mass calcd $C_{44}H_{86}O_{15}Si_9$ $[M + Na]^+$, 1129.378; found: 1129.338.

**_rac_-Pentacyclo[9.7.1.1$^{3,9}$.1$^{5,17}$.1$^{7,13}$]nonasiloxane,13-methyl-13-[2-(_tert_butyl-2-phenylacetate)]-1,3,5,7,9,11,15,17-octakis(2-methylpropyl) (3.14d)**

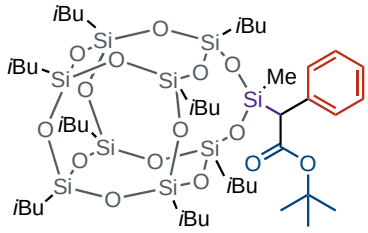


Procedure C was followed using 3 h slow addition of diazo compound **3.7e** (0.430 g, 2.00 mmol) in $CH_2Cl_2$ (6.70 mL) to POSS **3.11** (0.934 g, 1.00 mmol) in $CH_2Cl_2$ (3.30 mL). The product was obtained as a white solid using flash chromatography (100:0→99:1 hexanes/EtOAc, dry loaded silica) to furnish **3.14d** in 77% yield (0.865 g, 0.770 mmol).

$^{1}$H NMR (600 MHz, $CDCl_3$) δ 7.32 (d, *J* = 7.7 Hz, 2H), 7.27 – 7.21 (m, 2H), 7.15 (t, *J* = 7.4 Hz, 1H), 3.36 (s, 1H), 1.90 – 1.76 (m, 6H), 1.68 (m, 1H), 1.46 (s, 9H), 0.99 (m, 7H), 0.97 – 0.91 (m, 36H), 0.88 (m, 8H), 0.62 – 0.48 (m, 12H), 0.36 (m, 2H), 0.17 (s, 3H).

$^{13}$C NMR (100 MHz, $CDCl_3$) δ 171.1, 136.2, 129.4, 128.1, 125.8, 80.3, 48.2, 28.37, 26.06, 26.00, 25.98, 25.95, 25.93, 25.90, 25.86, 25.81, 25.78, 24.14, 24.08, 24.05, 24.02, 24.00, 23.53, 23.30, 23.21, 22.60, -1.9.

$^{29}$Si NMR ([$Cr(acac)_3$] = 0.01 M, 79 MHz, $CDCl_3$) δ -33.1, -67.1, -67.1, -68.8, -69.0, -69.1, -69.20, -69.25, -69.29.

MALDI-TOF: exact mass calcd $C_{45}H_{90}O_{15}Si_9$ $[M + Na]^+$, 1145.410; found: 1145.406.

***rac*-Tricyclo[7.3.3.1$^{5,11}$]heptasiloxane,3,7,14-tris[[dimethyl[2-[(methyl-2-phenylacetate)]oxy]propyl]silyl]oxy]-1,3,5,7,9,11,14-heptakis(2-methylpropyl) (3.15a)**

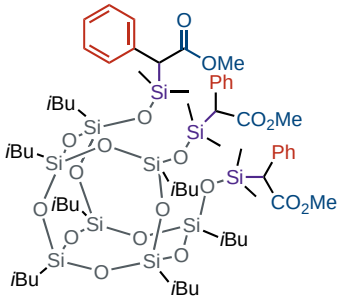

Procedure B was followed using 3 h slow addition of diazo compound **3.7a** (0.106 g, 0.600 mmol) in $CH_2Cl_2$ (0.8 mL) to POSS **3.2** (0.0965 g, 0.100 mmol) in $CH_2Cl_2$ (0.2 mL). The crude product was dissolved in hexanes (10 mL) and filtered to remove azine prior to flash chromatography. The product was obtained as a white solid using flash chromatography (97:3→95:5 hexanes/EtOAc, dry loaded silica) to furnish **3.15a** in 46% yield (0.0648 g, 0.460 mmol).

$^1$H NMR (400 MHz, $CDCl_3$) δ 7.36 (m, 6H), 7.27 (m, 6H), 7.23 – 7.13 (m, 3H), 3.67 (s, 9H), 3.55 (s, 3H), 1.92 – 1.67 (m, 7H), 1.08 – 0.90 (m, 42H), 0.58 (dt, *J* = 13.2, 6.7 Hz, 8H), 0.49 (d, *J* = 7.0 Hz, 6H), 0.24 (s, 9H), 0.14 (d, *J* = 2.4 Hz, 9H).

$^{13}$C NMR (100 MHz, $CDCl_3$) δ 172.50, 135.04, 128.29, 127.53, 125.06, 51.24, 47.17, 25.71, 25.66, 25.63, 25.35, 24.34, 23.68, 23.58, 23.54, 23.48, 23.45, 23.42, 22.07, -0.89, -0.93, -1.08.

$^{29}$Si NMR (79 MHz, $CDCl_3$) δ 4.66, 4.61, 4.54, -66.98, -67.01, -67.05, -67.07, -67.12, -67.18, -67.27.

MALDI-TOF: exact mass calcd for $C_{61}H_{108}O_{18}Si_{10}$ $[M + Na]^+$, 1431.513; found: 1431.492.

***rac*-Tricyclo[7.3.3.1$^{5,11}$]heptasiloxane,3,7,14-tris[[dimethyl[2-(methyl-2-(4-fluorophenyl)acetate)]oxy]propyl]silyl]oxy]-1,3,5,7,9,11,14-heptakis(2-methylpropyl) (3.15b)**

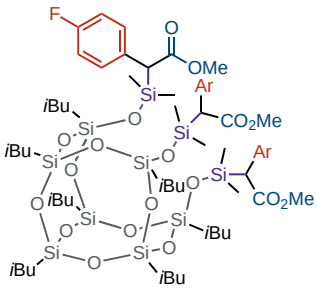

Procedure B was followed using 3 h slow addition of diazo compound **3.7b** (0.0591 g, 0.300 mmol) in $CH_2Cl_2$ (0.75 mL) to POSS **3.2** (0.0965 g, 0.100 mmol) in $CH_2Cl_2$ (0.25 mL). The product was obtained as a yellow solid using flash chromatography (97:3→95:5 hexanes/EtOAc, dry loaded silica) to furnish **3.15b** in 45% yield (0.0659 g, 0.450 mmol).

$^{1}$H NMR (600 MHz, $CDCl_3$) δ 7.30 (m, 6H), 6.95 (m, 6H), 3.66 (s, 9H), 3.50 (s, 3H), 1.81 (ddq, *J* = 17.1, 12.6, 6.5 Hz, 3H), 1.69 (h, *J* = 7.0 Hz, 4H), 1.00 – 0.87 (m, 42H), 0.55 (m, 8H), 0.45 (m, 6H), 0.21 – 0.17 (m, 9H), 0.15 – 0.10 (m, 9H).

$^{13}$C NMR (151 MHz, $CDCl_3$) δ 172.66, 161.26 (d, $^{1}J_{CF}$ = 244.0 Hz), 131.35 (d, $^{4}J_{CF}$ = 3.1 Hz), 129.92 (d, $^{3}J_{CF}$ = 7.2 Hz), 114.91 (d, $^{2}J_{CF}$ = 18.5 Hz), 51.52, 46.45, 25.91, 25.85, 25.83, 25.80, 25.55, 24.60, 24.57, 24.55, 23.94, 23.87, 23.83, 23.76, 23.67, 23.65, 23.62, -0.60, -0.64, -0.95, -0.97.

$^{19}$F NMR (376 MHz, $CDCl_3$) δ -117.75, -117.77, -117.78.

$^{29}$Si NMR (79 MHz, $CDCl_3$) δ 4.54, 4.48, 4.40, -66.77, -66.81, -66.85, -66.92, -66.99, -67.07, -67.22.

MALDI-TOF: exact mass calcd for $C_{61}H_{105}F_3O_{18}Si_{10}$ $[M + K]^+$, 1501.4569; found: 1501.4593.

**_rac_-Tricyclo[7.3.3.1$^{5,11}$]heptasiloxane,3,7,14-tris[[dimethyl[2-(methyl-2-(4-bromophenyl)acetate)])oxy]propyl]silyl]oxy]-1,3,5,7,9,11,14-heptakis(2-methylpropyl) (3.15c)**

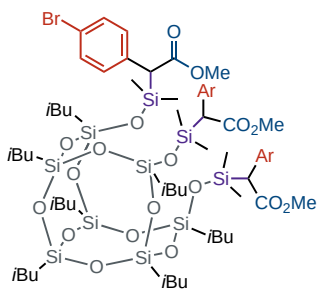


Procedure B was followed using 3 h slow addition of diazo compound **3.7c** (0.0772 g, 0.300 mmol) in $CH_2Cl_2$ (0.75 mL) to POSS **3.2** (0.0965 g, 0.100 mmol) in $CH_2Cl_2$ (0.25 mL). The crude product was dissolved in hexanes (10 mL) and filtered to remove azine prior to flash chromatography. The product was obtained as a white solid using flash chromatography (98:2→95:5 hexanes/EtOAc, dry loaded silica) to furnish **3.15c** in 49% yield (0.0801 g, 0.0490 mmol).

A separate trial using 3 h slow addition of diazo compound **2.7a** (0.0772 g, 0.600 mmol) in $CH_2Cl_2$ (0.75 mL) to POSS **3.2** (0.0965 g, 0.100 mmol) in $CH_2Cl_2$ (0.25 mL) after workup and flash chromatography yields POSS **3.15c** in 71% yield as a mixture (85% pure using $^{1}$H NMR spectroscopy) with diazo side-products.

$^{1}$H NMR (600 MHz, $CDCl_3$) δ 7.40 (m, 6H), 7.25 (m, 6H), 3.68 (s, 9H), 3.51 (s, 3H), 1.83 (m, 4H), 1.71 (m, 3H), 1.06 – 0.88 (m, 42H), 0.58 (m, 9H), 0.47 (m, 5H), 0.23 (overlapping singlets, 9H), 0.15 (overlapping singlets, 9H).

$^{13}$C NMR (151 MHz, $CDCl_3$) δ 172.44, 134.90, 131.33, 130.36, 119.79, 51.77, 46.99, 26.07, 25.99, 25.97, 25.71, 24.71, 24.68, 24.65, 24.10, 23.98, 23.91, 23.80, 23.77, 23.74, 22.38, -0.42, -0.46, -0.82, -0.85.

$^{29}$Si NMR (79 MHz, $CDCl_3$) δ 4.44, 4.38, 4.30, -66.71, -66.75, -66.80, -66.90, -66.98, -67.06, -67.21.

MALDI-TOF: exact mass calcd for $C_{61}H_{105}Br_3O_{18}Si_{10}$ $[M + K]^+$, 1683.218; found: 1683.215.

**_rac_-Tricyclo[7.3.3.1$^{5,11}$]heptasiloxane,3,7,14-tris[[dimethyl[2-(_tert_butyl-2-phenylacetate)oxy]propyl]silyl]oxy]-1,3,5,7,9,11,14-heptakis(2-methylpropyl) (3.15d)**

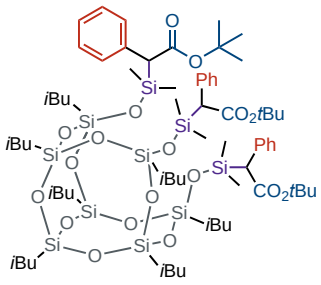


Procedure B was followed using 3 h slow addition of diazo compound **3.7e** (0.126 g, 0.600 mmol) in $CH_2Cl_2$ (0.80 mL) to POSS **3.2** (0.0935 g, 0.100 mmol) in $CH_2Cl_2$ (0.80 mL). The crude product was dissolved in hexanes (10 mL) and filtered to remove azine prior to flash chromatography. The product was obtained as a white solid using flash chromatography (97:3→95:5 hexanes/EtOAc, dry loaded celite) to furnish **3.15d** in 44% yield (0.0675 g, 0.0440 mmol).

$^1$H NMR (600 MHz, $CDCl_3$) δ 7.30 (d, $J$ = 7.9 Hz, 6H), 7.23 (t, $J$ = 5.0 Hz, 6H), 7.13 (d, $J$ = 7.7 Hz, 4H), 3.40 (s, 3H), 1.78 (h, 7.0 Hz, 4H), 1.64 (h, $J$ = 7.1 Hz, 3H), 1.46 (s, 27H), 0.99 – 0.79 (m, 42H), 0.51 (m, 8H), 0.37 (m, 6H), 0.29 – 0.20 (m, 9H), 0.15 (m, 9H).

$^{13}$C NMR (151 MHz, $CDCl_3$) δ 171.61, 135.89, 128.85, 128.15, 125.22, 80.35, 48.75, 28.39, 26.10, 26.06, 26.02, 25.72, 24.71, 24.66, 24.64, 24.59, 24.04, 24.02, 24.01, 23.91, 23.89, 23.87, 23.85, 23.82, 22.46, 0.36, 0.30, 0.25, -0.62, -0.71, -0.73, -0.80.

$^{29}$Si NMR (79 MHz, $CDCl_3$) δ 4.48, 4.35, 4.22, -66.98, -67.05, -67.14, -67.16, -67.31, -67.37, -67.42.

MALDI-TOF: exact mass calcd for $C_{96}H_{136}KO_{44}Si_{16}$ $[M + K]^+$, 1573.6268; found: 1573.6320.

**_rac_-Octa-2-( _tert_-butyl 2-phenylacetate)pentacyclo[9.5.1.1$^{3,9}$.1$^{5,15}$.1$^{7,13}$]octasiloxane (3.17a)**

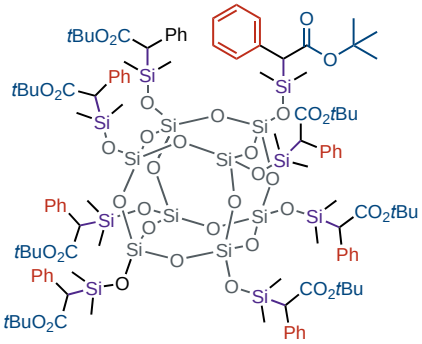

General procedure was followed using 2 h slow addition of diazo compound **3.7e** (0.218 g, 1.00 mmol) in $CH_2Cl_2$ (0.9 mL) to POSS **3.3** (0.1010 g, 0.1000 mmol) in $CH_2Cl_2$ (0.1 mL). The product was obtained as a white solid using flash chromatography (90:10→0:100 hexanes/EtOAc) to furnish **3.17a** in 85% yield (0.2159 g, 0.08500 mmol).

$^1$H NMR (600 MHz, $CDCl_3$) δ 7.30 – 7.27 (m, 16H), 7.22 (m, 16H), 7.13 (d, *J* = 7.6 Hz, 8H), 3.45 (s, 8H), 1.45 (s, 72H), 0.26 (s, 24H), 0.10 (m, 24H).

$^{13}$C NMR (151 MHz, $CDCl_3$) δ 171.19, 133.91, 128.61, 128.32, 124.96, 80.63, 47.07, 28.39, -0.58, -1.31.

$^{29}$Si NMR (([Cr(acac)$_3$] = 0.01 M 79 MHz, $CDCl_3$) δ 7.50, -110.11.

Orbitrap: exact mass calcd for $C_{112}H_{168}O_{36}Si_{16}$ $[M + NH_4]^+$, 2554.7962; found: 2554.7974.

## Functionalized Insertion Products

***rac*-Pentacyclo[9.7.1.1$^{3,9}$.1$^{5,17}$.1$^{7,13}$]nonasiloxane,13-methyl-13-[2-((methyl-2-(4-(2,8-diethyl-5,5-difluoro-1,3,7,9-tetramethyl-5*H*-4λ4,5λ4-dipyrrolo[1,2-*c*:2',1'-*f*][1,3,2]diazaborinin-10-yl)phenyl)acetate)]-1,3,5,7,9,11,15,17-octakis(2-methylpropyl) (3.40)**

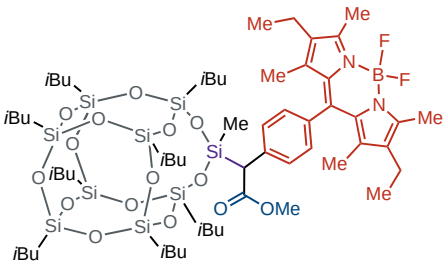

Procedure B was followed using 3 h slow addition of diazo compound **3.43** (0.0239 g, 0.0500 mmol) in $CH_2Cl_2$ (0.5 mL) to POSS silane **3.11** (0.230 g, 0.250 mmol) in $CH_2Cl_2$ (0.5 mL). The product was obtained as a red solid using preparative TLC (95:5 hexanes/EtOAc) to furnish **3.40** as a red solid in 16% yield (0.0114 g, 0.00800 mmol).

$^1$H NMR (400 MHz, $CDCl_3$) δ 7.54 (d, *J* = 7.9 Hz, 2H), 7.21 (d, *J* = 7.9 Hz, 2H), 3.74 (s, 3H), 3.65 (s, 1H), 2.55 (s, 6H), 2.32 (q, *J* = 7.5 Hz, 4H), 2.09 – 1.99 (m, 1H), 1.97 – 1.76 (m, 7H), 0.99 (dd, *J* = 10.1, 6.6 Hz, 58H), 0.77 – 0.47 (m, 18H), 0.13 (s, 3H).

$^{13}$C NMR (151 MHz, $CDCl_3$) δ 171.8, 153.2, 140.0, 138.1, 136.7, 133.3, 132.6, 130.8, 129.5, 128.1, 51.9, 46.8, 26.01, 25.97, 25.94, 25.92, 25.89, 25.83, 25.81, 25.79, 25.78, 24.18, 24.15, 24.11, 24.06, 24.01, 23.54, 23.52, 23.31, 23.18, 23.16, 22.57, 22.55, 17.2, 14.8, 12.0, -3.9.

$^{11}$B NMR (128 MHz, $CDCl_3$) δ 0.84 (t, *J* = 32.8 Hz).

$^{19}$F NMR (376 MHz, $CDCl_3$) δ -145.66 (q, *J* = 32.0 Hz).

IR (CCl4): 2962 $cm^{-1}$ (w), 2089 $cm^{-1}$ (s), 1707 $cm^{-1}$ (m), 1541 $cm^{-1}$ (s).

Fluorescence (EtOH, 3.1 x $10^{-7}$ M): ($l_{exc\ max}$ = 531 nm) $l_{em\ max}$ = 545 nm.

MALDI-TOF: exact mass calcd $C_{59}H_{105}BF_2N_2O_{15}Si_9$ $[M + H]^+$, 1383.558; found: 1383.548.

**_rac_-Pentacyclo[9.7.1.1$^{3,9}$.1$^{5,17}$.1$^{7,13}$]nonasiloxane,13-methyl-13-[2-((2,2,3,3,4,4,5,5,6,6,7,7,8,8,8-pentadecafluorooctyl)-2-phenylacetate)]-1,3,5,7,9,11,15,17-octakis(2-methylpropyl) (3.44)**

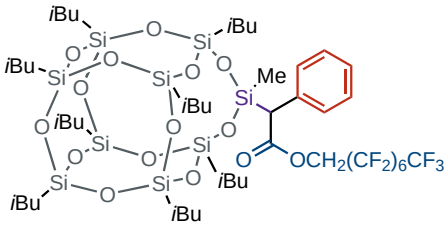

Procedure B was followed using 3 h slow addition of diazo compound **3.43** (0.0380 g, 0.0700 mmol) in $CH_2Cl_2$ (0.67 mL) to POSS **3.11** (0.0330 g, 0.0305 mmol) in $CH_2Cl_2$ (0.33 mL). The product was obtained as a white solid using flash chromatography (99.5:0.5 hexanes/EtOAc) to furnish **3.44** in 60% yield (0.0304 g, 0.0210 mmol).

$^1$H NMR (400 MHz, $CDCl_3$) δ 7.37 (d, *J* = 7.6 Hz, 2H), 7.33 – 7.26 (m, 3H), 7.22 (t, *J* = 7.2 Hz, 1H), 4.73 (q, *J* = 14.0 Hz, 1H), 4.46 (q, *J* = 13.7 Hz, 1H), 3.60 (s, 1H), 1.98 – 1.61 (m, 8H), 1.08

– 0.83 (m, 48H), 0.70 – 0.55 (m, 12H), 0.48 (dd, *J* = 7.1, 4.2 Hz, 2H), 0.38 (dd, *J* = 7.2, 2.6 Hz, 2H), 0.26 (s, 3H).

$^{13}$C NMR (151 MHz, $CDCl_3$) δ 170.7, 134.6, 129.2, 128.4, 126.4, 59.6 (t, *J* = 25.5 Hz), 46.6, 25.96, 25.92, 25.90, 25.88, 25.86, 25.82, 25.80, 25.78, 25.70, 24.11, 24.07, 24.05, 24.01, 23.98, 23.23, 23.18, 23.16, 23.11, 23.09, 22.57, -2.4.

$^{19}$F NMR (376 MHz, $CDCl_3$) δ -80.76 (3F), -119.38 (2F), -121.95 (4F), -122.71 (2F), -123.33 (2F), -126.09 (2F).

$^{29}$Si NMR (79 MHz, $CDCl_3$) δ -34.46, -66.97, -67.00, -68.67, -68.77, -68.83, -69.02, -69.07, -69.11.

MALDI-TOF: exact mass calcd $C_{49}H_{83}O_{15}Si_9$ $[M + Na]^+$, 1471.331; found: 1471.381.

**_rac_-Pentacyclo[9.7.1.1$^{3,9}$.1$^{5,17}$.1$^{7,13}$]nonasiloxane,13-methyl-13-2-[(methyl-2-(4'-fluoro-[1,1'-biphenyl]-4-yl)acetate)]-1,3,5,7,9,11,15,17-octakis(2-methylpropyl) (3.47)**

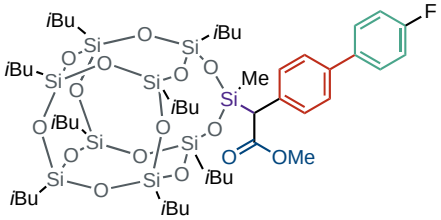


Synthesized using Procedure G. The product was obtained as a white solid in 45% yield (95% purity by $^{19}$F NMR) (0.0566 g, 0.0450 mmol).

$^{1}$H NMR (400 MHz, $CDCl_3$) δ 7.54 (m, 2H), 7.50 – 7.41 (m, 4H), 7.17 – 7.08 (m, 2H), 3.72 (s, 3H), 3.61 (s, 1H), 1.98 – 1.77 (m, 2H), 1.69 – 1.58 (m, 1H), 0.97 (m 42H), 0.84 (m, 2H), 0.67 (d, *J* = 7.0 Hz, 6H), 0.60 (m, 10H), 0.53 (m, 2H), 0.36 (m, 2H), 0.29 (s, 3H).

$^{13}$C NMR (100 MHz, $CDCl_3$) δ 172.45, 162.34 (d, $^{1}J_{CF}$ = 245.9 Hz), 137.21 (d, $^{4}J_{CF}$ = 3.3 Hz), 137.19, 134.69, 129.52, 128.42 (d, $^{3}J_{CF}$ = 7.9 Hz), 126.64, 115.54 (d, $^{2}J_{CF}$ = 21.4 Hz), 50.79, 46.52, 25.89, 25.86, 25.80, 25.76, 25.73, 25.71, 25.67, 25.65, 25.62, 24.02, 23.97, 23.95, 23.93, 23.91, 23.88, 23.81, 23.30, 23.27, 23.18, 23.14, 23.10, 23.04, 22.45, -2.70.

$^{19}$F NMR (376 MHz, $CDCl_3$) δ -116.27.

$^{29}$Si NMR (([$Cr(acac)_3$] = 0.01 M, 79 MHz, $CDCl_3$) δ -33.83, -66.93, -66.95, -68.80, -68.93, -69.01, -69.11.

MALDI-TOF: exact mass calcd for $C_{48}H_{87}FO_{15}Si_9$ $[M + K]^+$, 1213.3578; found: 1213.3599.

***rac*-Pentacyclo[9.7.1.1$^{3,9}$.1$^{5,17}$.1$^{7,13}$]nonasiloxane,13-methyl-13-2-[(2-phenylaceticacid)]-1,3,5,7,9,11,15,17-octakis(2-methylpropyl) (3.49)**

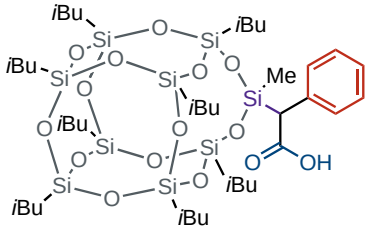


Synthesized using procedure H. The product was obtained as a white solid in 88% yield (95.9 mg, 0.0880 mmol).

$^{1}$H NMR (600 MHz, $CDCl_3$) δ 7.33 (d, *J* = 7.6 Hz, 2H), 7.24 (t, *J* = 8.1 Hz, 2H), 7.17 (t, *J* = 7.3 Hz, 1H), 3.53 (s, 1H), 1.84 (m, 6H), 1.73 (m, 1H), 1.56 (m, 1H), 0.99 (m, 6H), 0.94 (m, 32H), 0.88 (m, 6H), 0.84 – 0.75 (m, 6H), 0.62 (d, *J* = 7.0 Hz, 2H), 0.59 – 0.51 (m, 10H), 0.50 – 0.40 (m, 2H), 0.27 (s, 3H).

$^{13}$C NMR (151 MHz, $CDCl_3$) δ 176.9, 135.6, 131.2, 128.2, 126.1, 47.1, 26.0, 25.96, 25.95, 25.92, 25.91, 25.89, 25.85, 25.83, 25.81, 25.79, 25.76, 25.67, 24.12, 24.08, 24.05, 24.0, 23.9, 23.24, 23.22, 23.18, 23.2, 23.1, 23.1, 22.6, -2.5.

$^{29}$Si NMR ([$Cr(acac)_3$] = 0.01 M, 79 MHz, $CDCl_3$) δ -33.32, -66.46, -66.49, -68.25, -68.37, -68.40, -68.56, -68.64.

MALDI-TOF: exact mass calcd for $C_{41}H_{82}O_{15}Si_9$ $[M + K]^+$, 1105.321; found: 1105.316.

## 3.11 References


(1) Targos, K. Rh-Catalyzed Si-H Insertion Reactions of Diazoacetates for the Synthesis of Novel Organosiloxane Hybrid Nanomaterials Displaying Organic Functional Groups, University of California, Davis, 2019.

(2) Seidi, F.; Jouyandeh, M.; Taghizadeh, A.; Taghizadeh, M.; Habibzadeh, S.; Jin, Y.; Xiao, H.; Zarrintaj, P.; Saeb, M. R. Polyhedral Oligomeric Silsesquioxane/Epoxy Coatings: A Review. *Surf. Innov.* **2021**, *9* (1), 3–16. https://doi.org/10.1680/jsuin.20.00037.

(3) Weinhold, F.; West, R. Hyperconjugative Interactions in Permethylated Siloxanes and Ethers: The Nature of the SiO Bond. *J. Am. Chem. Soc.* **2013**, *135* (15), 5762–5767. https://doi.org/10.1021/ja312222k.

(4) Ahangaran, F.; Navarchian, A. H. Recent Advances in Chemical Surface Modification of Metal Oxide Nanoparticles with Silane Coupling Agents: A Review. *Adv. Colloid Interface Sci.* **2020**, *286*, 102298. https://doi.org/https://doi.org/10.1016/j.cis.2020.102298.

(5) Liu, S.; Guo, R.; Li, C.; Lu, C.; Yang, G.; Wang, F.; Nie, J.; Ma, C.; Gao, M. POSS Hybrid Hydrogels: A Brief Review of Synthesis, Properties and Applications. *Eur. Polym. J.* **2021**, *143*, 110180. https://doi.org/https://doi.org/10.1016/j.eurpolymj.2020.110180.

(6) Zhou, H.; Ye, Q.; Xu, J. Polyhedral Oligomeric Silsesquioxane-Based Hybrid Materials and Their Applications. *Mater. Chem. Front.* **2017**, *1* (2), 212–230. https://doi.org/10.1039/C6QM00062B.

(7) Sharma, B.; Verma, R.; Baur, C.; Bykova, J.; Mabry, J. M.; Smith, D. W. Ultra Low Dielectric, Self-Cleansing and Highly Oleophobic POSS-PFCP Aryl Ether Polymer Composites. *J. Mater. Chem. C* **2013**, *1* (43), 7222–7227. https://doi.org/10.1039/C3TC31161A.
(8) Kim, D.-G.; Shim, J.; Lee, J. H.; Kwon, S.-J.; Baik, J.-H.; Lee, J.-C. Preparation of Solid-State Composite Electrolytes Based on Organic/Inorganic Hybrid Star-Shaped Polymer and PEG-Functionalized POSS for All-Solid-State Lithium Battery Applications. *Polymer (Guildf).* **2013**, *54* (21), 5812–5820. https://doi.org/https://doi.org/10.1016/j.polymer.2013.08.049.
(9) Blanco, I. Polyhedral Oligomeric Silsesquioxanes (POSS)s in Medicine. *J. Nanomedicine* **2018**, *1* (1), 1–3. https://doi.org/10.33582/2578-8760/1002.
(10) Hou, P. P.; Gu, K. H.; Zhu, Y. F.; Zhang, Z. Y.; Wang, Q.; Pan, H. B.; Yang, S.; Shen, Z.; Fan, X. H. Synthesis and Sub-10 Nm Supramolecular Self-Assembly of a Nanohybrid with a Polynorbornene Main Chain and Side-Chain POSS Moieties. *RSC Adv.* **2015**, *5* (86), 70163–70171. https://doi.org/10.1039/c5ra12152c.
(11) Pescarmona, P. P.; Aprile, C.; Swaminathan, S. Silsesquioxanes and Their Use as Precursors for Catalysts and as Model Compounds. In *New and Future Developments in Catalysis*; 2013; pp 385–422. https://doi.org/10.1016/b978-0-444-53876-5.00018-0.
(12) Li, Y.; Dong, X.-H.; Zou, Y.; Wang, Z.; Yue, K.; Huang, M.; Liu, H.; Feng, X.; Lin, Z.; Zhang, W.; Zhang, W.-B.; Cheng, S. Z. D. Polyhedral Oligomeric Silsesquioxane Meets "Click" Chemistry: Rational Design and Facile Preparation of Functional Hybrid Materials. *Polymer (Guildf).* **2017**, *125*, 303–329. https://doi.org/https://doi.org/10.1016/j.polymer.2017.08.008.
(13) Mituła, K.; Dudziec, B.; Marciniec, B. Synthesis of Dialkenyl-Substituted Double-Decker Silsesquioxanes as Precursors for Linear Copolymeric Systems. *J. Inorg. Organomet. Polym. Mater.* **2018**, *28* (2), 500–507. https://doi.org/10.1007/s10904-017-0746-y.
(14) Dudziec, B.; Żak, P.; Marciniec, B. Synthetic Routes to Silsesquioxane-Based Systems as Photoactive Materials and Their Precursors. *Polymers (Basel).* **2019**, *11* (3), 504. https://doi.org/10.3390/polym11030504.
(15) Nakajima, Y.; Shimada, S. Hydrosilylation Reaction of Olefins: Recent Advances and Perspectives. *RSC Adv.* **2015**, *5* (26), 20603–20616. https://doi.org/10.1039/C4RA17281G.
(16) Imoto, H.; Wada, S.; Naka, K. Rh-Catalyzed Direct Arylation of a Polyhedral Oligomeric Silsesquioxane. *Dalt. Trans.* **2017**, *46* (19), 6168–6171. https://doi.org/10.1039/C7DT01106G.
(17) Imoto, H.; Wada, S.; Yumura, T.; Naka, K. Transition-Metal-Catalyzed Direct Arylation of Caged Silsesquioxanes: Substrate Scope and Mechanistic Study. *Eur. J. Inorg. Chem.* **2019**, *2019* (16), 2202–2207. https://doi.org/https://doi.org/10.1002/ejic.201900126.
(18) Keipour, H.; Carreras, V.; Ollevier, T. Recent Progress in the Catalytic Carbene Insertion Reactions into the Silicon-Hydrogen Bond. *Org Biomol Chem* **2017**, *15* (26), 5441–5456. https://doi.org/10.1039/c7ob00807d.
(19) Doyle, M. P.; McKervey, M. A. 1938-; Ye, T. 1963-. *Modern Catalytic Methods for Organic Synthesis with Diazo Compounds : From Cyclopropanes to Ylides LK - Https://Melvyl.on.Worldcat.Org/Oclc/36767864*; Wiley: New York SE - xvii, 652 pages : illustrations ; 25 cm, 1998.
(20) Dakin, L. A.; Schaus, S. E.; Jacobsen, E. N.; Panek, J. S. Carbenoid Insertions into the

Silicon–Hydrogen Bond Catalyzed by Chiral Copper (I) Schiff Base Complexes. *Tetrahedron Lett.* **1998**, *39* (49), 8947–8950. https://doi.org/https://doi.org/10.1016/S0040-4039(98)02013-9.

(21) Qu, Z.; Shi, W.; Wang, J. A Kinetic Study on the Pairwise Competition Reaction of α-Diazo Esters with Rhodium(II) Catalysts: Implication for the Mechanism of Rh(II)-Carbene Transfer. *J. Org. Chem.* **2001**, *66* (24), 8139–8144. https://doi.org/10.1021/jo0107352.

(22) Tseberlidis, G.; Caselli, A.; Vicente, R. Carbene XH Bond Insertions Catalyzed by Copper(I) Macrocyclic Pyridine-Containing Ligand (PcL) Complexes. *J. Organomet. Chem.* **2017**, *835*, 1–5. https://doi.org/https://doi.org/10.1016/j.jorganchem.2017.02.027.

(23) Keipour, H.; Ollevier, T. Iron-Catalyzed Carbene Insertion Reactions of α-Diazoesters into Si–H Bonds. *Org. Lett.* **2017**, *19* (21), 5736–5739. https://doi.org/10.1021/acs.orglett.7b02488.

(24) Liu, Z.; Li, Q.; Yang, Y.; Bi, X. Silver(i)-Promoted Insertion into X–H (X = Si, Sn, and Ge) Bonds with N-Nosylhydrazones. *Chem. Commun.* **2017**, *53* (16), 2503–2506. https://doi.org/10.1039/C6CC09650F.

(25) Davies, H. M. L.; Hansen, T.; Churchill, M. R. Catalytic Asymmetric C−H Activation of Alkanes and Tetrahydrofuran. *J. Am. Chem. Soc.* **2000**, *122* (13), 3063–3070. https://doi.org/10.1021/ja994136c.

(26) Ye, T.; McKervey, M. A. Organic Synthesis with .Alpha.-Diazo Carbonyl Compounds. *Chem. Rev.* **1994**, *94* (4), 1091–1160. https://doi.org/10.1021/cr00028a010.

(27) Imoto, H.; Ueda, Y.; Sato, Y.; Nakamura, M.; Mitamura, K.; Watase, S.; Naka, K. Corner- and Side-Opened Cage Silsesquioxanes: Structural Effects on the Materials Properties. *Eur. J. Inorg. Chem.* **2020**, *2020* (9), 737–742. https://doi.org/10.1002/ejic.201901182.

(28) Imoto, H.; Nakao, Y.; Nishizawa, N.; Fujii, S.; Nakamura, Y.; Naka, K. Tripodal Polyhedral Oligomeric Silsesquioxanes as a Novel Class of Three-Dimensional Emulsifiers. *Polym. J.* **2015**, *47* (9), 609–615. https://doi.org/10.1038/pj.2015.38.

(29) Yuasa, S.; Sato, Y.; Imoto, H.; Naka, K. Thermal Properties of Open-Cage Silsesquioxanes: The Effect of Substituents at the Corners and Opening Moieties. *Bull. Chem. Soc. Jpn.* **2018**, *92* (1), 127–132. https://doi.org/10.1246/bcsj.20180257.

(30) Doyle, M. P.; High, K. G.; Bagheri, V.; Pieters, R.; Lewis, P. J.; Pearson, M. M. Rhodium(II) Perfluorobutyrate Catalyzed Silane Alcoholysis. A Highly Selective Route to Silyl Ethers. *J. Org. Chem.* **1990**, *55* (25), 6082–6086. https://doi.org/10.1021/jo00312a010.

(31) Kolel-Veetil, M. K.; Dominguez, D. D.; Klug, C. A.; Keller, T. M. Hydrosilated Dendritic Networks of POSS Cores and Diacetylene Linkers. *Macromolecules* **2009**, *42* (12), 3992–4001. https://doi.org/10.1021/ma802392p.

(32) Kuo, S.-W.; Chang, F.-C. POSS Related Polymer Nanocomposites. *Prog. Polym. Sci.* **2011**, *36* (12), 1649–1696. https://doi.org/10.1016/j.progpolymsci.2011.05.002.

(33) John, Ł.; Malik, M.; Janeta, M.; Szafert, S. First Step towards a Model System of the Drug Delivery Network Based on Amide-POSS Nanocarriers. *RSC Adv.* **2017**, *7* (14), 8394–8401. https://doi.org/10.1039/C6RA26330E.

(34) Ogi, K.; Miyauchi, S.; Naka, K. Amphiphilic POSS-Core Dendrons for Optically Transparent Thermoplastic Films with Tunable Wettability. *Polym. J.* **2015**, *47* (3), 259–266. https://doi.org/10.1038/pj.2014.119.

(35) Kajiya, R.; Wada, H.; Kuroda, K.; Shimojima, A. Inorganicorganic Hybrid

Photomechanical Crystals of Azobenzene-Modified Polyhedral Oligomeric Silsesquioxane (POSS). *Chem. Lett.* **2020**, *49* (3), 327–329. https://doi.org/10.1246/cl.190926.

(36) Beutner, G. L.; Young, I. S.; Davies, M. L.; Hickey, M. R.; Park, H.; Stevens, J. M.; Ye, Q. TCFH–NMI: Direct Access to N-Acyl Imidazoliums for Challenging Amide Bond Formations. *Org. Lett.* **2018**, *20* (14), 4218–4222. https://doi.org/10.1021/acs.orglett.8b01591.

(37) Yamamoto, K.; Qureshi, Z.; Tsoung, J.; Pisella, G.; Lautens, M. Combining Ru-Catalyzed C–H Functionalization with Pd-Catalyzed Asymmetric Allylic Alkylation: Synthesis of 3-Allyl-3-Aryl Oxindole Derivatives from Aryl α-Diazoamides. *Org. Lett.* **2016**, *18* (19), 4954–4957. https://doi.org/10.1021/acs.orglett.6b02423.

(38) Dong, K.; Yan, B.; Chang, S.; Chi, Y.; Qiu, L.; Xu, X. Transition-Metal-Free Fluoroarylation of Diazoacetamides: A Complementary Approach to 3-Fluorooxindoles. *J. Org. Chem.* **2016**, *81* (15), 6887–6892. https://doi.org/10.1021/acs.joc.6b01286.

(39) Allred, A. L. Electronegativity Values from Thermochemical Data. *J. Inorg. Nucl. Chem.* **1961**, *17* (3), 215–221. https://doi.org/https://doi.org/10.1016/0022-1902(61)80142-5.

(40) Goulet-Hanssens, A.; Eisenreich, F.; Hecht, S. Enlightening Materials with Photoswitches. *Adv. Mater.* **2020**, *32* (20), 1905966. https://doi.org/https://doi.org/10.1002/adma.201905966.

(41) Ledin, P. A.; Tkachenko, I. M.; Xu, W.; Choi, I.; Shevchenko, V. V.; Tsukruk, V. V. Star-Shaped Molecules with Polyhedral Oligomeric Silsesquioxane Core and Azobenzene Dye Arms. *Langmuir* **2014**, *30* (29), 8856–8865. https://doi.org/10.1021/la501930e.

(42) Ye, F.; Wang, C.; Zhang, Y.; Wang, J. Synthesis of Aryldiazoacetates through Palladium(0)-Catalyzed Deacylative Cross-Coupling of Aryl Iodides with Acyldiazoacetates. *Angew. Chemie Int. Ed.* **2014**, *53* (43), 11625–11628. https://doi.org/https://doi.org/10.1002/anie.201407653.

(43) Hansch, C.; Leo, A.; Taft, R. W. A Survey of Hammett Substituent Constants and Resonance and Field Parameters. *Chem. Rev.* **1991**, *91* (2), 165–195. https://doi.org/10.1021/cr00002a004.

(44) Kowada, T.; Maeda, H.; Kikuchi, K. BODIPY-Based Probes for the Fluorescence Imaging of Biomolecules in Living Cells. *Chem. Soc. Rev.* **2015**, *44* (14), 4953–4972. https://doi.org/10.1039/C5CS00030K.

(45) Miao, W.; Yu, C.; Hao, E.; Jiao, L. Functionalized BODIPYs as Fluorescent Molecular Rotors for Viscosity Detection . *Frontiers in Chemistry* . 2019, p 825.

(46) Zhu, X.; Liu, R.; Li, Y.; Huang, H.; Wang, Q.; Wang, D.; Zhu, X.; Liu, S.; Zhu, H. An AIE-Active Boron-Difluoride Complex: Multi-Stimuli-Responsive Fluorescence and Application in Data Security Protection. *Chem. Commun.* **2014**, *50* (85), 12951–12954. https://doi.org/10.1039/C4CC05913A.

(47) Liras, M.; Pintado-Sierra, M.; Amat-Guerri, F.; Sastre, R. New BODIPY Chromophores Bound to Polyhedral Oligomeric Silsesquioxanes (POSS) with Improved Thermo- and Photostability. *J. Mater. Chem.* **2011**, *21* (34), 12803–12811. https://doi.org/10.1039/c1jm11261a.

(48) McCusker, C.; Carroll, J. B.; Rotello, V. M. Cationic Polyhedral Oligomeric Silsesquioxane (POSS) Units as Carriers for Drug Delivery Processes. *Chem. Commun.* **2005**, No. 8, 996–998. https://doi.org/10.1039/B416266H.

(49) Loudet, A.; Burgess, K. BODIPY Dyes and Their Derivatives: Syntheses and

Spectroscopic Properties. *Chem. Rev.* **2007**, *107* (11), 4891–4932. https://doi.org/10.1021/cr078381n.
(50) Tuteja, A.; Choi, W.; Mabry, J. M.; McKinley, G. H.; Cohen, R. E. Designing Super-Oleophobic Surfaces with Fluoroposs. *2007 AIChE Annu. Meet.* **2007**, No. December, 1618–1623.
(51) Tao, C.; Li, X.; Liu, B.; Zhang, K.; Zhao, Y.; Zhu, K.; Yuan, X. Highly Icephobic Properties on Slippery Surfaces Formed from Polysiloxane and Fluorinated POSS. *Prog. Org. Coatings* **2017**, *103*, 48–59. https://doi.org/https://doi.org/10.1016/j.porgcoat.2016.11.018.
(52) Chhatre, S. S.; Guardado, J. O.; Moore, B. M.; Haddad, T. S.; Mabry, J. M.; McKinley, G. H.; Cohen, R. E. Fluoroalkylated Silicon-Containing Surfaces-Estimation of Solid-Surface Energy. *ACS Appl. Mater. Interfaces* **2010**, *2* (12), 3544–3554. https://doi.org/10.1021/am100729j.
(53) Twibanire, J. K.; Grindley, T. B. Efficient and Controllably Selective Preparation of Esters Using Uronium-Based Coupling Agents. *Org. Lett.* **2011**, *13* (12), 2988–2991. https://doi.org/10.1021/ol201005s.
(54) Brick, C. M.; Ouchi, Y.; Chujo, Y.; Laine, R. M. Robust Polyaromatic Octasilsesquioxanes from Polybromophenylsilsesquioxanes, Br XOPS, via Suzuki Coupling. *Macromolecules* **2005**, *38* (11), 4661–4665. https://doi.org/10.1021/ma0501141.
(55) Ervithayasuporn, V.; Kwanplod, K.; Boonmak, J.; Youngme, S.; Sangtrirutnugul, P. Homogeneous and Heterogeneous Catalysts of Organopalladium Functionalized-Polyhedral Oligomeric Silsesquioxanes for Suzuki–Miyaura Reaction. *J. Catal.* **2015**, *332*, 62–69. https://doi.org/https://doi.org/10.1016/j.jcat.2015.09.014.
(56) Walczak, M.; Franczyk, A.; Dutkiewicz, M.; Marciniec, B. Synthesis of Bifunctional Silsesquioxanes (RSiMe2O)∼4(R′SiMe2O)∼4Si8O12 via Hydrosilylation of Alkenes. *Organometallics* **2019**, *38* (15), 3018–3024. https://doi.org/10.1021/acs.organomet.9b00350.
(57) Tunstall-Garcia, H.; Charles, B. L.; Evans, R. C. The Role of Polyhedral Oligomeric Silsesquioxanes in Optical Applications. *Adv. Photonics Res.* **2021**, *2* (6), 2000196. https://doi.org/https://doi.org/10.1002/adpr.202000196.
(58) Johansson Seechurn, C. C.; Kitching, M. O.; Colacot, T. J.; Snieckus, V. Palladium-Catalyzed Cross-Coupling: A Historical Contextual Perspective to the 2010 Nobel Prize. *Angew. Chemie, Int. Ed. English* **2012**, *51* (21), 5062–5085. https://doi.org/10.1002/anie.201107017.
(59) Li, Z.; Kong, J.; Wang, F.; He, C. Polyhedral Oligomeric Silsesquioxanes (POSSs): An Important Building Block for Organic Optoelectronic Materials. *J. Mater. Chem. C* **2017**, *5* (22), 5283–5298. https://doi.org/10.1039/c7tc01327b.
(60) Matsuda, I.; Sato, S.; Hattori, M.; Izumi, Y. Regio- and Stereodefined Synthesis of Trimethylsilyl Enol Ethers Resulted from the Isomerization of α-Trimethylsilyl Ketones. *Tetrahedron Lett.* **1985**, *26* (27), 3215–3218. https://doi.org/https://doi.org/10.1016/S0040-4039(00)98155-3.
(61) Littke, A. F.; Fu, G. C. A Versatile Catalyst for Heck Reactions of Aryl Chlorides and Aryl Bromides under Mild Conditions. *J. Am. Chem. Soc.* **2001**, *123* (29), 6989–7000. https://doi.org/10.1021/ja010988c.
(62) Rikowski, E.; Marsmann, H. C. Cage-Rearrangement of Silsesquioxanes. *Polyhedron*

**1997**, *16* (19), 3357–3361. https://doi.org/https://doi.org/10.1016/S0277-5387(97)00092-2.
(63) Lennox, A. J. J.; Lloyd-Jones, G. C. Selection of Boron Reagents for Suzuki–Miyaura Coupling. *Chem. Soc. Rev.* **2014**, *43* (1), 412–443. https://doi.org/10.1039/C3CS60197H.
(64) Shanmugan, S.; Cani, D.; Pescarmona, P. P. The Design and Synthesis of an Innovative Octacarboxy-Silsesquioxane Building Block. *Chem. Commun.* **2014**, *50* (75), 11008–11011. https://doi.org/10.1039/C4CC03756A.
(65) Protection for the Carboxyl Group. *Greene's Protective Groups in Organic Synthesis*. September 19, 2014, pp 686–836. https://doi.org/doi:10.1002/9781118905074.ch05.
(66) Wu, Y.; Limburg, D. C.; Wilkinson, D. E.; Vaal, M. J.; Hamilton, G. S. A Mild Deprotection Procedure for Tert-Butyl Esters and Tert-Butyl Ethers Using ZnBr2 in Methylene Chloride. *Tetrahedron Lett.* **2000**, *41* (16), 2847–2849. https://doi.org/https://doi.org/10.1016/S0040-4039(00)00300-2.
(67) Qu, L.; Sui, Y.; Zhang, C.; Li, P.; Dai, X.; Xu, B.; Fang, D. POSS-Functionalized Graphene Oxide Hybrids with Improved Dispersive and Smoke-Suppressive Properties for Epoxy Flame-Retardant Application. *Eur. Polym. J.* **2020**, *122*, 109383. https://doi.org/https://doi.org/10.1016/j.eurpolymj.2019.109383.
(68) Doyle, M. P.; Duffy, R.; Ratnikov, M.; Zhou, L. Catalytic Carbene Insertion into C-H Bonds. *Chem. Rev.* **2010**, *110* (2), 704–724. https://doi.org/10.1021/cr900239n.
(69) Price, K. E.; Larrivée-Aboussafy, C.; Lillie, B. M.; McLaughlin, R. W.; Mustakis, J.; Hettenbach, K. W.; Hawkins, J. M.; Vaidyanathan, R. Mild and Efficient DBU-Catalyzed Amidation of Cyanoacetates. *Org. Lett.* **2009**, *11* (9), 2003–2006. https://doi.org/10.1021/ol900435t.
(70) Li, G.; Ji, C. L.; Hong, X.; Szostak, M. Highly Chemoselective, Transition-Metal-Free Transamidation of Unactivated Amides and Direct Amidation of Alkyl Esters by N-C/O-C Cleavage. *J. Am. Chem. Soc.* **2019**, *141* (28), 11161–11172. https://doi.org/10.1021/jacs.9b04136.
(71) Lee, S. Il; Hwang, G.-S.; Ryu, D. H. Catalytic Enantioselective Carbon Insertion into the β-Vinyl C–H Bond of Cyclic Enones. *J. Am. Chem. Soc.* **2013**, *135* (19), 7126–7129. https://doi.org/10.1021/ja402873b.
(72) Thurow, S.; Fernandes, A. A. G.; Quevedo-Acosta, Y.; de Oliveira, M. F.; de Oliveira, M. G.; Jurberg, I. D. Preparation of Organic Nitrates from Aryldiazoacetates and Fe(NO3)3·9H2O. *Org. Lett.* **2019**, *21* (17), 6909–6913. https://doi.org/10.1021/acs.orglett.9b02522.
(73) Cobo, A. A.; Armstrong, B. M.; Fettinger, J. C.; Franz, A. K. Catalytic Asymmetric Synthesis of Cyclopentene-Spirooxindoles Bearing Vinylsilanes Capable of Further Transformations. *Org. Lett.* **2019**, *21* (20), 8196–8200. https://doi.org/10.1021/acs.orglett.9b02852.
(74) Franckevičius, V.; Cuthbertson, J. D.; Pickworth, M.; Pugh, D. S.; Taylor, R. J. K. Asymmetric Decarboxylative Allylation of Oxindoles. *Org. Lett.* **2011**, *13* (16), 4264–4267. https://doi.org/10.1021/ol201613a.
(75) Muthusamy, S.; Azhagan, D. Ring Opening Reaction of Furan with High Regio- and Diastereo-Selectivity via Controlled Addition of Isatin-Derived Diazoamides. *Tetrahedron Lett.* **2011**, *52* (50), 6732–6735. https://doi.org/https://doi.org/10.1016/j.tetlet.2011.10.004.
(76) Zhu, J. S.; Larach, J. M.; Tombari, R. J.; Gingrich, P. W.; Bode, S. R.; Tuck, J. R.;

Warren, H. T.; Son, J.-H.; Duim, W. C.; Fettinger, J. C.; Haddadin, M. J.; Tantillo, D. J.; Kurth, M. J.; Olson, D. E. A Redox Isomerization Strategy for Accessing Modular Azobenzene Photoswitches with Near Quantitative Bidirectional Photoconversion. *Org. Lett.* **2019**, *21* (21), 8765–8770. https://doi.org/10.1021/acs.orglett.9b03387.

(77) Haefele, A.; Zedde, C.; Retailleau, P.; Ulrich, G.; Ziessel, R. Boron Asymmetry in a BODIPY Derivative. *Org. Lett.* **2010**, *12* (8), 1672–1675. https://doi.org/10.1021/ol100109j.

(78) Keipour, H.; Jalba, A.; Delage-Laurin, L.; Ollevier, T. Copper-Catalyzed Carbenoid Insertion Reactions of α-Diazoesters and α-Diazoketones into Si–H and S–H Bonds. *J. Org. Chem.* **2017**, *82* (6), 3000–3010. https://doi.org/10.1021/acs.joc.6b02998.

(79) Chow, S.; Green, A. I.; Arter, C.; Liver, S.; Leggott, A.; Trask, L.; Karageorgis, G.; Warriner, S.; Nelson, A. Efficient Approaches for the Synthesis of Diverse α-Diazo Amides. *Synth.* **2020**, *52* (11), 1695–1706. https://doi.org/10.1055/s-0039-1690905.